Mirams, Gary R. (2008) Subcellular phenomena in colorectal cancer. PhD thesis, University of Nottingham.

Subcellular Phenomena in Colorectal Cancer

Gary R. Mirams, MMath

Thesis submitted to The University of Nottingham

for the degree of Doctor of Philosophy

May, 2008

Abstract

The Wnt signalling pathway is involved in stem cell maintenance, differentiation and tissue development, and in so doing plays a key role in controlling the homeostasis of colorectal crypts. In response to an external Wnt stimulus, the intracellular levels of the protein β-catenin are regulated by the proteins which make up the Wnt signalling pathway. Abnormalities in the Wnt signalling pathway have been implicated in the initiation of colorectal and other cancers.

In this thesis we analyse and simplify existing models of the Wnt signalling pathway, formulate models for Wnt's control of the cell cycle in a single cell, and incorporate these into a multiscale model to describe how Wnt may control the patterns of proliferation in a colorectal crypt.

A systematic asymptotic analysis of an existing ODE-based model of the Wnt signalling pathway is undertaken, highlighting the operation of different pathway components over three different timescales. Guided by this analysis we derive a simplified model which is shown to retain the essential behaviour of the Wnt pathway, recreating the accumulation and degradation of β-catenin. We utilise our simple model by coupling it to a model of the cell cycle. Our findings agree well with the observed patterns of proliferation in healthy colon crypts. Furthermore, the model clarifies a mechanism by which common colorectal cancer mutations may cause elevated β-catenin and Cyclin D levels, leading to uncontrolled cell proliferation and thereby initiating colorectal cancer.

A second model for the influence of the Wnt pathway on the cell cycle is constructed to incorporate the results of a recent set of knockout experiments. This model reproduces the healthy proliferation observed in crypts and additionally recreates the results of knockout experiments by additionally including the influence of Myc and CDK4 on the cell cycle. Analysis of this model leads us to suggest novel drug targets that may reverse the effects of an early mutation in the Wnt pathway.

We have helped to build a flexible software environment for cell-based simulations of healthy and cancerous tissues. We discuss the software engineering approach that we have used to develop this environment, and its suitability for scientific computing. We then use this software to perform multiscale simulations with subcellular Wnt signalling models inside individual cells, the cells forming an epithelial crypt tissue. We have used the multiscale model to compare the effect of different subcellular models on crypt dynamics and predicting the distribution of β-catenin throughout the crypt. We assess the extent to which a common experiment reveals the actual dynamics of a crypt and finally explain some recent mitochondrial-DNA experiments in terms of cell dynamics.

Contents

List of Figures

List of Tables

Acknowledgements

First and foremost I would like to thank my supervisors Helen and John, who have exhibited an extraordinary amount of patience over the last three years. My thanks also to the Integrative Biology team — my partner-in-crime Alex, t'other Alex, Ellie, Philip, Ozzy and Pras for making it such fun to work on the project; to Joe Pitt-Francis, Jon Cooper and Dave Parkin without whom it would have been impossible to get Chaste to work at all; and to Dave Gavaghan for his boundless enthusiasm whenever we were tempted to give it up as a bad job.

I'd also like to thank the postgrads who have inhabited Pope C9, particularly Duncan, Hannah, Rob, Sabine and Simon, who along with Ollie and Reuben, have caused plenty of welcome distractions and tea breaks over the years.

Finally I'd like to thank my Mum and Dad, family and friends who have helped me along throughout.

CHAPTER 1

Literature Review

1.1 Introduction

COLORECTAL cancer or bowel cancer (CRC) is one of the most widespread malignancies in the western world and is rapidly becoming a leading cause of cancer mortality worldwide. In 2004 CRC accounted for 13% of cancers in the UK, making it second only to lung cancer in terms of mortality rate[1] and the most common cancer to cause death in non-smokers. The lifetime risk of developing CRC in the UK population is 5%, and the risk rises dramatically with age. Incidence rates also vary by a factor of 20 times across the world, suggesting that there is a strong link with environmental and dietary factors (Fodde *et al.*, 2001).

The intestine contains a series of pits or crypts, lined by a monolayer of epithelial cells (see Figure 1.1). The earliest signs of cancer are aberrant crypt foci, these growths affecting only a few crypts. The next stage in tumour progression is abnormal and disordered growth, or dysplasia. Dysplastic aberrant crypt foci may develop into polyps — benign tumour masses that protrude from the epithelium. Some polyps retain normal cell architecture and morphology, whereas others have abnormalities in inter- and intra-cellular organisation. Abnormal polyps are called adenomatous polyps or adenomas. Most people aged 70 or above will have developed at least one colorectal adenoma, but it will usually be asymptomatic. The next stage of cancer progression is when adenomas develop into adenocarcinomas, aggressive tumours (Fodde *et al.*, 2001).

Metastasis is the process by which cancer cells break away from a tumour and spread around the body, usually in the bloodstream, to cause secondary tumours elsewhere. CRC is usually only diagnosed when adenocarcinomas have developed, but there is an excellent prognosis for cases caught before metastasis, surgery and chemo/radiotherapy being quite effective. However the likelihood of

---

[1] http://info.cancerresearchuk.org/cancerstats/

successful treatment following metastases is much lower. For this reason, the detection of CRC is as important a research area as its treatment. Fearon & Vogelstein (1990) proposed that accumulation of mutations in certain genes corresponded to the stages in development of colorectal cancer, as the early mutations were almost always in components of the Wnt signalling pathway.

In this thesis we investigate the link between Wnt signalling and cell proliferation, by building mathematical models of the Wnt signalling pathway and its influence on the cell cycle. We introduce such subcellular models into a cell-based model of a colorectal crypt to establish whether Wnt signalling is sufficient to cause the observed patterns of proliferation in the intestine, and further establish how populations harbouring mutations might establish themselves.

In section 1.2 of this literature review we introduce the physiology of colorectal crypts, describing how they function under normal circumstances and introducing the cells involved. In section 1.3 we describe the cell cycle, the process by which cells replicate, and review mathematical models of the cell cycle. In section 1.4 we focus on the Wnt signalling pathway and explain its intimate involvement in CRC. Finally, in section 1.5, we consider the effect of mutations on the crypts, explaining how they are thought to lead to CRC initiation.

1.2 Colorectal Crypts

The intestine is characterised by a large number of regularly spaced crypts which provide a large surface area for absorption of water and nutrients. These crypts were first identified in 1688 by Marcello Malpighi but are named after Johann Nathanael Lieberkühn who described them in 1745. In this thesis the *crypts of Lieberkühn* will be referred to simply as *crypts*. Figure 1.1 shows the crypts in the small and large intestine. In the small intestine small crypts are surrounded by larger villi — finger-like protrusions out from the surface of the epithelium. In the large intestine (colon and rectum) crypts are larger and there are no villi present; in this thesis we focus on the crypts of the large intestine which are more prone to cancer. The crypts are usually non-branching, tightly packed cylindrical tubes which are evenly distributed and parallel.

1.2.1 Cell Types

In the intestine epithelial stem cells, located at the base of each crypt, generate four cell lineages (Moore & Lemischka, 2006):

- enterocytes, which secrete hydrolases (enzymes for hydrolysis reactions) and absorb nutrients;
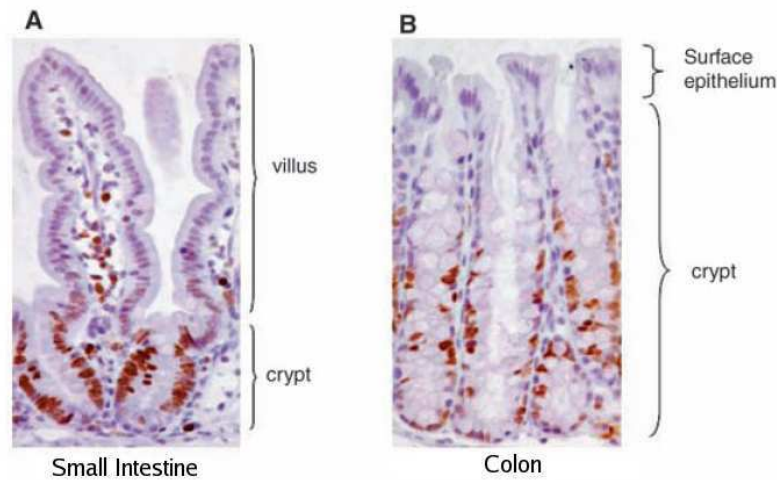
Figure 1.1: A. The small intestine crypts and villi. B. The colorectal crypts. Proliferating cells are stained brown. From Fig. 2a) and 2b) Radtke & Clevers, SCIENCE 307:1904-1909 (3/25/2005). Reprinted with permission from AAAS.

- goblet cells (most abundant), which secrete a protective mucous lining;

- enteroendocrine cells (rare), which secrete hormones including serotonine and secretin;

- Paneth cells (found only at the bottom of small intestinal crypts), which secrete antimicrobial peptides and enzymes (Porter *et al.*, 2002).

The first three cell types are generated throughout both the small and large intestines, whilst Paneth cells are present only in the small intestine. The proliferating epithelial cells sit on a bed of fibroblasts and mesenchyme (connective tissue). Studying the interactions between epithelial cells and fibroblasts is becoming more of a focus for research as there is increasing evidence that mutations in fibroblasts can precede crypt carcinoma development (Bhowmick & Neilson, 2004): epithelial cells are certainly dependent on fibroblasts for growth and differentiation signals.

1.2.2 Crypt Dynamics

It is thought that the base of each colonic crypt contains a number of stem cells that divide and differentiate; proliferating *transit* or *progenitor* cells are found in the lower two-thirds of the crypt and quiescent (non-dividing) differentiated cells in the upper third (Sancho *et al.*, 2004), see Figure 1.1. Despite the crucial importance of stem cells in the dynamics of colorectal crypts the precise number of stem cells is unknown. Estimates range between 4 and 16, with up to 40 cells retaining the ability to become stem cells if needed (Marshman *et al.*, 2002).

Under normal physiological colonic conditions, the epithelial cells differentiate as they migrate from the base to the top of the crypt. Once at the top, they are thought to undergo apoptosis before being shed into the gut lumen. The number of dividing cells is balanced by the number being shed into the lumen at the top of the crypt and, in this way, the whole of the intestinal epithelium is renewed (over a period of 3–6 days in mice (Potten & Loeffler, 1987) and around 6 days in humans (Ross *et al.*, 2003)).

Only the 'immortal' stem cells (and, in the small intestine, Paneth cells which live for 20 days) escape the flow of cells from the bottom to the top of the crypts. There is a balance that the body must strike between renewing the epithelium before it is damaged by the contents of the gut (leading to infection) and renewing the epithelium too fast (using lots of energy and predisposing the crypts to hyper-proliferation). It is the mechanisms that regulate rapid cell proliferation and apoptosis (homoeostatic mechanisms) that are prone to causing cancer when mutations occur (Radtke & Clevers, 2005).

The earliest mutations which occur in CRC are almost always in components of the Wnt signalling pathway (Powell *et al.*, 1992), which is involved in the control of cell proliferation, differentiation and adhesion. The level of Wnt-pathway-target gene expression in a colorectal crypt is observed to be highest at the base of a crypt, where the stem cells are located, and to decrease towards the top (Gaspar & Fodde, 2004; Larsson, 2006). Before we discuss how the Wnt pathway influences the cell cycle we first describe the cell cycle itself.

1.3 Cell Cycle

The repeating sequence of events involved in cell-division is known as the cell cycle and is commonly split into four phases. During the S phase a copy of the cell's DNA is synthesised. There follows a gap phase (G_2) during which the cell grows. During the mitosis (M) phase the cell splits and forms two 'daughter' cells, which then enter a long gap phase (G_1) during which they grow sufficiently to synthesise their DNA and repeat the process (Figure 1.2). There is large variation in the duration of the G_1 phase between different tissues and cell types. While the durations of the different phases in human colorectal tissue are not known, they are on the order of hours. The full cell cycle lasts approximately 12 hours in the highly proliferating cells near the base of a crypt in the mouse small intestine (Meineke *et al.*, 2001).

In most tissues at any given time not all cells are actively proliferating: many appear to be quiescent. A new phase of the cell cycle, G_0, has been introduced to account for this behaviour. Whether G_0 is distinct from G_1 or simply a name for cells 'stuck' in G_1 is still under debate, but in any

case it provides a useful way of describing cells which do not appear to be proliferating. Under suitable external signals quiescent cells may return to G_1 after hours, days, months or even years (Alberts *et al.*, 2002), or they may undergo apoptosis (programmed cell death). Cells enter G_0 for a number of reasons, including lack of available materials or energy for replication, but usually because they are terminally-differentiated (Hutchinson & Glover, 1995), such as an epithelial cell at the top of a crypt.
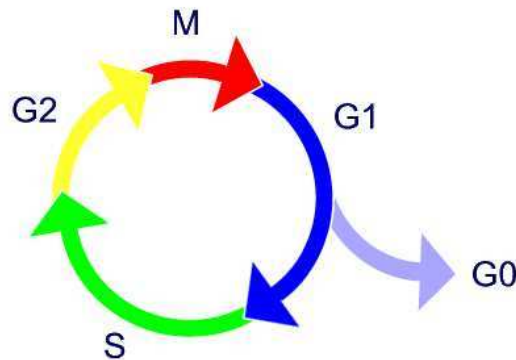
Figure 1.2: The phases of the cell cycle. G_0 Quiescence, G_1 Gap 1, S DNA Synthesis, G_2 Gap 2, M mitosis (DNA and cell division).

While progress through the cell cycle is known to be regulated by at least thirty different proteins, a small number of distinct 'checkpoints' have been identified. In order to pass through these checkpoints certain proteins must exceed threshold levels. For instance, the concentrations of the Cyclin family of proteins rise and fall as the cell cycle progresses. A map of all the known protein interactions involved in the cell cycle was created by Kohn (1999), which spanned four journal pages in fine print; many more interactions have now been identified and it is thought that still more remain to be documented. Any description of the cell cycle, in words or equations, therefore represents a dramatic simplification of the true events leading to replication of a cell.

1.3.1 Regulation by Cyclins

The role of cyclins in the cell cycle is of particular interest for us as Cyclin D has been identified as one of the targets of β-catenin promoted transcription in colorectal tissue (Tetsu & McCormick, 1999; Wang *et al.*, 2002a; Shtutman *et al.*, 1999). Cell-cycle control is regulated by interactions between cyclins, cyclin-dependent kinases (CDKs) and cyclin-dependent kinase inhibitors (CDKIs) (Kitazono *et al.*, 2005). Individual cyclins act by binding to their CDK partners at different stages

in the cell cycle. Of the many cyclins found to date, the following four have been identified as principal components of the cell cycle: Cyclins D and E are fundamental to G_1 and to the G_1/S transition, Cyclin A is active in the S phase and Cyclin B drives the G_2/M transition.

Cyclin D proteins are regulators of the G_1 phase of the cell cycle, binding to either CDK4 or CDK6 in response to mitogenic stimulation. A transcription factor E2F1 leads to the expression of proteins involved in the S phase of the cell cycle (Bracken *et al.*, 2004). It is degraded by retinoblastoma protein pRb. The Cyclin D/CDK complexes phosphorylate the retinoblastoma protein pRb, which is hyperphosphorylated by Cyclin E/CDK2, preventing its downregulation of E2F1 (Swat *et al.*, 2004); this leads to the accumulation of active E2F1 and the transcription of more Cyclin E and genes involved in S phase, such as Cyclin A (Sherr & Roberts, 1999). E2F1 is also a transcription factor for itself (Takahashi *et al.*, 2000).

The D-type cyclins (D1, D2 and D3) are generally expressed in response to extracellular growth factors (such as Wnt), resulting in cell proliferation under favourable conditions. The different D-type cyclins have structures which appear to be optimised for different tissue types, but each can form a complex with either CDK4 or CDK6. Recent findings in mice by Yang *et al.* (2006) suggest that Cyclin D2 is restricted to highly-proliferating areas of the crypt, whereas Cyclin D1 is expressed more widely throughout the crypt. The findings in Sansom *et al.* (2007) suggest that this is because Cyclin D2 is a transcriptional-target of β-catenin whilst Cyclin D1 is not (nuclear levels of β-catenin are high in highly-proliferating areas). While cell-cycle progression can occur in some tissues in the absence of Cyclin D (Kozar & Sicinski, 2005), the bulk of reports suggest that D-type cyclins are vital to the healthy operation of colorectal crypts (Tetsu & McCormick, 1999; Shtutman *et al.*, 1999; Rimerman *et al.*, 2000). Our use of the general term 'Cyclin D' represents all of the D-type cyclins present in the crypt.

In addition to the obvious role of Cyclin D in the G_1/S transition more subtle effects have been observed: Cyclin D1 can induce the differentiation of colon epithelial cells in mice (Hulit *et al.*, 2004), and E2F1 (whose levels are affected by Cyclin D) is important in epithelial morphogenesis (Ivanova *et al.*, 2005).

In section 1.3.3 we review existing mathematical models of the cell cycle, focussing on those that include Cyclin D. We are particularly interested in models that feature Cyclin D (so that they can easily be coupled to a model of the Wnt pathway) and which can reproduce two specific phenomena observed in the crypts: firstly, lack of Cyclin D can induce quiescence (Gemin *et al.*, 2005) and, secondly, reduction of Cyclin D levels can slow the onset of the G_1/S transition (Han *et al.*, 1999).

1.3.2   Regulation by c-Myc

c-Myc is an important target of the Wnt/β-catenin pathway (He *et al.*, 1998), which is responsible for many of Wnt's downstream effects. Sansom *et al.* (2005) showed that Cyclin D1 is not an immediate target of β-catenin following *APC* loss in the intestine, and suggested instead that the upregulation of Cyclin D2 and c-Myc is responsible for proliferation under a Wnt stimulus. Sansom *et al.* later showed that deletion of *c-Myc* and *APC* results in healthy colonic epithelium in mice (Sansom *et al.*, 2007), suggesting that *c-Myc* is an important target of β-catenin/TCF4 following a mutation in the Wnt pathway.

c-Myc is a protein which is heavily involved in deciding whether a cell should proliferate, differentiate or undergo apoptosis (Grandori *et al.*, 2000; Murphy *et al.*, 2005). c-Myc is almost always found in heterodimers with members of the Mad-Max family of proteins. Myc/Max proteins stimulate the transcription of many different genes, whilst Myc/Mad complexes repress transcription (Dang *et al.*, 1999). c-Myc is a known transcription factor for Cyclin D1, Cyclin D2, CDK4 and E2F1 (Hermeking *et al.*, 2000; Bouchard *et al.*, 1999; Adhikary & Eilers, 2005; ODonnell *et al.*, 2005). Miliani de Marval *et al.* (2004) showed that overexpression of c-Myc deregulates epithelial cells only when CDK4 is present.

c-Myc is a transcriptional repressor of p21 (a cyclin-dependent kinase inhibitor) (Wanzel *et al.*, 2003), and Liu *et al.* (2006b) showed that repressing p21 transcription is necessary for c-Myc to cause increased proliferation in the intestinal epithelium. c-Myc can also repress p21 by binding directly to it, preventing p21 from interacting with cyclins.

p21 forms a complex with Cyclin E/CDK2 and inhibits its function (Sherr & Roberts, 1999). In a role contradictory to its classification as a CDKI, p21 also forms a complex with Cyclin D/CDK4,6 activating it and allowing Cyclin D dependent phosphorylation of pRb (Weinberg & Denning, 2002). In addition, p21 can bind directly to E2F1 inhibiting its transcriptional activity (Dotto, 2000).

1.3.3   Mathematical Models of the Cell Cycle

There has been considerable effort invested in describing the proliferation of cells mathematically. Many different approaches have been taken; here we review some of these approaches.

Gyllenberg & Webb (1990) created a deterministic age-structured PDE model for a population of cells, in which the rate of cell division was age-dependent. Proliferating cells may become quiescent (and vice-versa), whilst only proliferating cells can grow and divide. In this way the evolution of a

population is tracked over time.

Pettet *et al.* (2001) formulated a spatially-structured PDE model of cell density, decomposing the tumour into populations of proliferating and quiescent cells whose densities could vary at different spatial positions in the tumour. The concentration of a diffusible nutrient governed the tumour's development since, as in Gyllenberg & Webb (1990), cells are segregated into proliferating and quiescent classes which respond differently to this nutrient. The proliferating cells divide and cause a population increase; this effect, and the directed movement of cells up spatial gradients of the nutrient, cause the tumour to grow. Assuming that quiescent cells are more motile than proliferating ones, a steady state is reached with an outer layer of quiescent cells (moving towards an external nutrient) followed by a layer of proliferating cells and another layer of quiescent cells forming a core. This model provides a possible explanation of tumours' internalisation of labelled cells and inert microspheres (Dorie *et al.*, 1982, 1986).

Basse *et al.* (2003) derived a DNA-content structured PDE model for the different phases of the cell cycle. A time delay was introduced into the governing equations as cells leave the G_1 phase, grow to double their DNA content (S phase) and enter G_2 a finite time later. The DNA content of a population of cells was determined numerically and favourably compared to flow cytometry experiments.

In each of the above models PDEs were used to model progress through the cell cycle in a large number of cells. Since we are interested in subcellular phenomena we will focus on models describing the protein interactions that drive a single cell through the cell cycle. These models are characterised by ODEs for the concentration of each of the proteins of interest and are formulated using the laws of mass-action and Michaelis-Menten kinetics.

Progress through the cell cycle is marked by changes in protein levels, and it is the interactions between different proteins that can form biochemical switches (Legewie *et al.*, 2005). Cell cycle 'checkpoints' are best explained as mathematical bifurcations: once a certain parameter (protein level) reaches a threshold value the system exhibits a new qualitative behaviour (passes through a checkpoint or bifurcates) (Csikasz-Nagy *et al.*, 2006).

Many cell-cycle models that account for the action of Cyclin D focus on the G_1/S transition, as it is believed that the durations of the S, G_2 and M phases are largely independent of Cyclin D, and their durations remain fairly constant throughout a tissue. Studying the G_1/S transition should therefore be sufficient to study the influence of Cyclin D on cell proliferation in the colon.

Some of the earliest cell-cycle models to incorporate Cyclin D were developed by Obeyesekere and

co-workers (Obeyesekere *et al.*, 1997; Obeyesekere & Zimmerman, 1999) and made predictions consistent with the observation that a cell becomes quiescent when growth-factor levels (Cyclin D transcription factors) are reduced. Aguda & Tang (1999) focussed their model on the G_1/S transition; simulations can complete the G_1/S transition in the absence of Cyclin D expression, so the model does not exhibit quiescence due to a lack of Cyclin D that we require.

Probably the best known protein-interaction model for the cell cycle is due to Tyson & Novak (2001), a more recent extension (Novak & Tyson, 2004) being tailored to mammalian cells. To stimulate production of Cyclin D and start the cell cycle Novak & Tyson included an early starter protein, whose concentration increases until it triggers the production of a delayed starter protein (DRG) which stimulates the production of Cyclin D. The concentration of DRG, denoted by [DRG], quickly reaches a stable level which it retains throughout further cell cycles.

In order to investigate the effect of reducing Cyclin D levels we have used a MatLab ODE solver (`ode15s`) to simulate the Novak & Tyson (2004) model, reducing the value of [DRG] in successive simulations. This leads to longer cell-cycle durations, with the undesirable side effect of cells growing to much greater, physically unrealistic, sizes (see Figure 1.3).

In the simulation presented in Figure 1.3 the size of the cells when they divide is much larger (by a factor of about 25) than that at which they normally divide. Figure 1.3 shows how each of the model variables evolve over five cell cycles. There are so many interactions being considered that it is extremely difficult to establish the precise relationship between Cyclin D expression and other cell-cycle variables. Removing Cyclin D from the system increased the cycle time but did not lead to quiescence. Because of its complexity and inability to reproduce the quiescence seen by Gemin *et al.* (2005), we have not utilised the Novak & Tyson (2004) model.

In chapter 3 we examine a deterministic ODE model developed by Swat *et al.* (2004) which focusses only on Cyclin D's role in the G_1/S transition, rather than all Cyclins and all phases of the cell cycle. The central components are the concentration of E2F1 (an indicator of the S phase), pRb (retinoblastoma protein), and Cyclin D; the model can exhibit both quiescence and slowing of the cell cycle in response to changes in Cyclin D levels.

1.4   Wnt Signalling

The components of the Wnt signalling pathway show a high degree of evolutionary conservation from *Drosophila* through to mammals (Nelson & Nusse, 2004), suggesting it is an important and
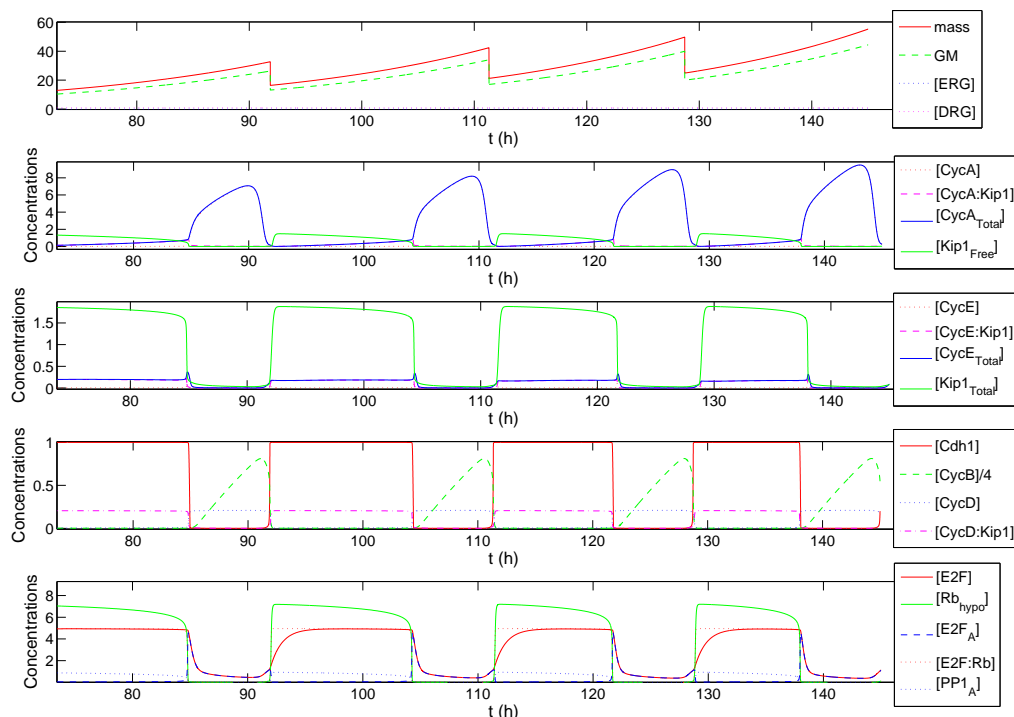
Figure 1.3: A simulation of the cell-cycle model developed by Novak & Tyson (2004) using the solver ode15s in MatLab, with the same equations and parameter values as Novak & Tyson (2004, Figure 2), subject to [DRG]=0.42. Novak & Tyson did not investigate such dependencies

fundamental pathway. Wnt signalling has long been implicated in colorectal cancer and is therefore thought to be important in maintaining the healthy crypt, with mutations leading to cancer initiation. We will describe the Wnt signalling pathway in some detail in this section. The roles of Wnt signalling are discussed in section 1.4.1; the action of the pathway's main downstream target, β-catenin, in section 1.4.2; the way in which β-catenin levels are regulated by Wnt in section 1.4.3; other downstream effects of Wnt in section 1.4.4; the way in which the Wnt pathway has been implicated in cancer in section 1.4.5; and mathematical models of Wnt signalling in section 1.4.6.

1.4.1 Functions of Wnt Signalling

The Wnt pathway is known to play a key role in stem cell maintenance (Reya & Clevers, 2005; Pinto & Clevers, 2005), cell-cell adhesion (Hinck *et al.*, 1994), cell-fate specification (cell differentiation) (Logan & Nusse, 2004), central-nervous-system patterning (Hall *et al.*, 2000) and tissue de-

velopment (Church & Francis-West, 2002; Nelson & Nusse, 2004). There are many different Wnt factor variants, 7 in *Drosophila* and at least 19 in humans, and these are numbered according to the order in which they were discovered, e.g. Wnt1, Wnt2 (Nusse, 2007).

A cell's response to Wnt signalling is believed to be mediated predominantly through β-catenin. The 'output' of the Wnt pathway is therefore considered to be the concentration and location of β-catenin (Fodde & Brabletz, 2007). When this protein forms a complex with T-Cell Factor (TCF) in the nucleus it activates the transcription of around 100 genes[2] which execute manifold functions. In the next section we discuss the different roles that β-catenin performs within the cell in more detail.

1.4.2 β-catenin

β-catenin is produced constitutively[3], encoded in humans by the gene *CTNNB1*, and is found as a monomer in the cytoplasm. Its levels are controlled by recruitment to a large multi-protein complex (referred to from now on as the *destruction complex*) which includes, amongst others, the proteins APC, Axin and GSK3β. The destruction complex phosphorylates β-catenin, labelling it for ubiquitination and hence for destruction by proteosomes (we examine this process more thoroughly in section 1.4.3). β-catenin cannot affect a cell's behaviour whilst remaining a monomer in the cytoplasm; the main sites at which β-catenin is thought to exert its influence are in the nucleus and at the cell membrane (Gavert & Ben-Zeév, 2007).

β-catenin in the nucleus

In the absence of β-catenin, T-cell factor (TCF)/lymphoid enhancer factor (LEF) DNA-bound transcription factors bind to transcriptional repressors such as Groucho and Carboxy-terminal binding protein (CtBP). When β-catenin enters the nucleus it dimerizes with TCFs to remove the repressors and activate the expression of Wnt target genes, such as Cyclin D (see section 1.3.1).

By preventing β-catenin from entering the nucleus, expression of target genes can be switched off (Cong *et al.*, 2003). Conversely, forcing β-catenin into the nucleus can activate target genes (Townsley *et al.*, 2004). Wnt signalling activity is therefore believed to be controlled by the amount of β-catenin in the nucleus. These levels, in turn, depend on the amount of β-catenin in the cytoplasm and its rates of nuclear import and export (Städeli *et al.*, 2006). A suprising number of Wnt pathway

---

[2]http://www.stanford.edu/~rnusse/pathways/targets.html
[3]i.e. continuously in all cells, under normal physiological conditions.

components appear in the nucleus (such as APC and Axin). APC has been shown to counteract β-catenin activation and methylation of Wnt target genes (Willert & Jones, 2006).

It is still unclear how β-catenin levels in the nucleus are regulated and how they relate to cytoplasmic levels. However, it is known that β-catenin levels in the nucleus are often much higher than those in the cytoplasm. Henderson (2000) states that APC acts as a nuclear chaperone for β-catenin, since APC contains two active nuclear export sequences and moves β-catenin from the nucleus to the cytoplasm. Xiong & Kotake (2006) agree that APC regulates β-catenin levels in the nucleus, but suggest that the mechanism is mainly due to APC binding to C-terminal Binding Protein (CtBP) on DNA promoter regions and preventing β-catenin's access to the sites. Krieghoff *et al.* (2006) suggest that TCF4 and BCL9 recruit β-catenin to the nucleus, but that there is no active export. They propose that the distribution of β-catenin is governed by the fact that it complexes with APC or Axin (which are large and move slowly) and therefore β-catenin is retained wherever they are present, creating a non-uniform distribution.

The level of β-catenin in cell nuclei has been observed to vary throughout the crypt, with the strongest presence in the cells near the base of the crypts. β-catenin and TCF have been shown to control the expression of EphB receptors in the crypt (Batlle *et al.*, 2002), and this could be one of the mechanisms by which β-catenin controls proliferation and differentiation patterns in the crypt (Gregorieff *et al.*, 2005). Interestingly, Kim *et al.* (2000) and Larsson (2006) showed that overexpression of β-catenin induces apoptosis independent of the involvement of major G1 cell-cycle regulators. However most research suggests that an excess of nuclear β-catenin leads to proliferation, whilst a deficit causes differentiation and cell-cycle arrest.

β-catenin at the cell membrane

At the cell membrane E-cadherin transmembrane proteins form dimers, the extra-cellular portions of which bind to other such dimers protruding from the surface of nearby cells to form *adherens junctions* at a rate which is Ca^{2+} dependent. On the inside of the cell membrane β-catenin and p120 bind to the cytoplasmic tail of E-cadherin (Hinck *et al.*, 1994; Lugli *et al.*, 2007). Once there, β-catenin forms a bridge to α-catenin, which in turn binds to the actin filaments of the cytoskeleton as shown in Figure 1.4.

Whilst sequestered at the cell membrane, β-catenin is unavailable for transcriptional activation of target genes in the nucleus (Harris & Peifer, 2005). Städeli *et al.* (2006) showed that the same (or at least overlapping) 'Arm repeats' within β-catenin are used to bind to the APC/Axin destruction complex (leading to β-catenin destruction), to TCF (leading to gene transcription) and to E-cadherin
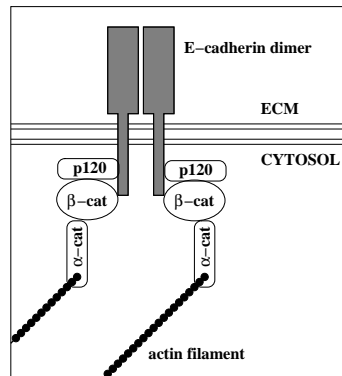
Figure 1.4: The role of β-catenin at an adherens junction. Bridging between E-cadherin and α-catenin, β-catenin is an essential component of the junction. In colorectal crypts these tight junctions form along the side of each cell, sealing them together. Reprinted from van Leeuwen *et al.* (2007), with permission from Elsevier.

(leading to adhesion). These are mutually exclusive binding partners, indicating that β-catenin must choose between degradation, transcription or adhesion. The overlapping binding regions are shown in Figure 1.5.
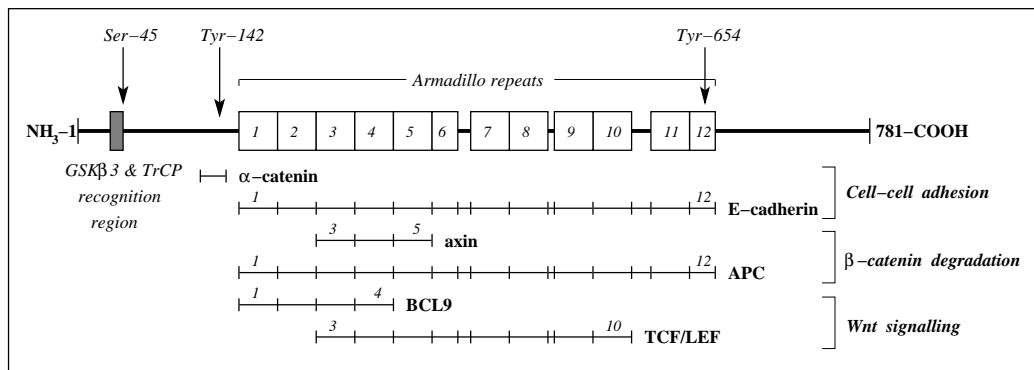
Figure 1.5: Human β-catenin (encoded by *CTNNB1*) is 781aa. Binding sites for the three main types of interaction are shown — adhesion, degradation and transcription. Binding of α-catenin and E-cadherin can be prevented by phosphorylation of Tyr^{142} and Tyr^{654} respectively. Ser^{45} must be phosphorylated by CKIα for canonical degradation to occur. Reprinted from van Leeuwen *et al.* (2007), with permission from Elsevier.

Kuphal & Behrens (2006) suggest that E-cadherin may modulate Wnt-dependent gene expression by regulating the availability of β-catenin. It is thought that Wnt signalling regulates both transcription and adhesion; a number of mechanisms have been suggested for these interactions. It is possible that the different Wnt proteins have different intracellular effects, for example Wnt11 seems to control adhesion of progenitor cells in crypt development (Ulrich *et al.*, 2005). Additionally β-

catenin is structurally altered only in the presence of Wnt (by an as yet unknown mechanism), so that its affinities for different binding partners change, altering the balance between transcription and adhesion (Harris & Peifer, 2005). This 'balance' has been modelled by van Leeuwen *et al.* (2007), and is discussed in section 1.4.6.

It is becoming clear that cell adhesion, motility and transcriptional Wnt signalling are inter-related, together forming a complex signalling pathway (Nelson & Nusse, 2004).

1.4.3   The Canonical or Wnt/β-catenin Pathway

Wnt proteins are released from cells into the extracellular space, and act as ligands which bind to receptors on the cell membrane, thereby stimulating the Wnt pathway of another cell. There are large numbers of extracellular Wnt inhibitors, for example Frps, WIFs, Dickkopf (Dkk), Kremen and Wise, as reviewed by Logan & Nusse (2004). Recently Ching & Nusse (2006) showed that Wntless/Evi is a transmembrane protein in Wnt-producing cells that facilitates Wnt secretion; knocking out Wntless/Evi halts Wnt secretion.

Of the large number of Wnt signalling pathway interactions, the 'canonical' pathway is widely accepted as the most important one for CRC (Ilyas, 2005) and a simplified version is presented in Figure 1.6. The canonical pathway can be described as either 'On' (with Wnt stimulation), or 'Off' (in its absence).

In this section we discuss the regulation of the canonical pathway (how it is turned 'On' and 'Off') and describe the roles of the various components.

Regulation

The destruction complex consists of the scaffold proteins[4] Axin and adenomatous polyposis coli (APC), the catalysts glycogen synthase kinase 3β (GSK3β) and casein kinase Iα (CKIα) which, along with several other proteins, phosphorylate β-catenin (Näthke, 2004). Phosphorylated β-catenin is ubiquitinated by β-transducin repeat containing protein (β-TrCP) and is subsequently destroyed by proteosomes: this is the main mechanism for controlling cytoplasmic levels of β-catenin.

To a lesser extent, β-catenin is degraded by a retinoid-X-receptor mechanism (Xiao *et al.*, 2003). Another novel pathway responds to p53 stimulation and involves a protein called Siah, which (with

---

[4]Scaffold proteins bind to both the substrate (in this case β-catenin) and enzymes (such as GSK3β), providing the correct binding and orientation for a reaction to take place.
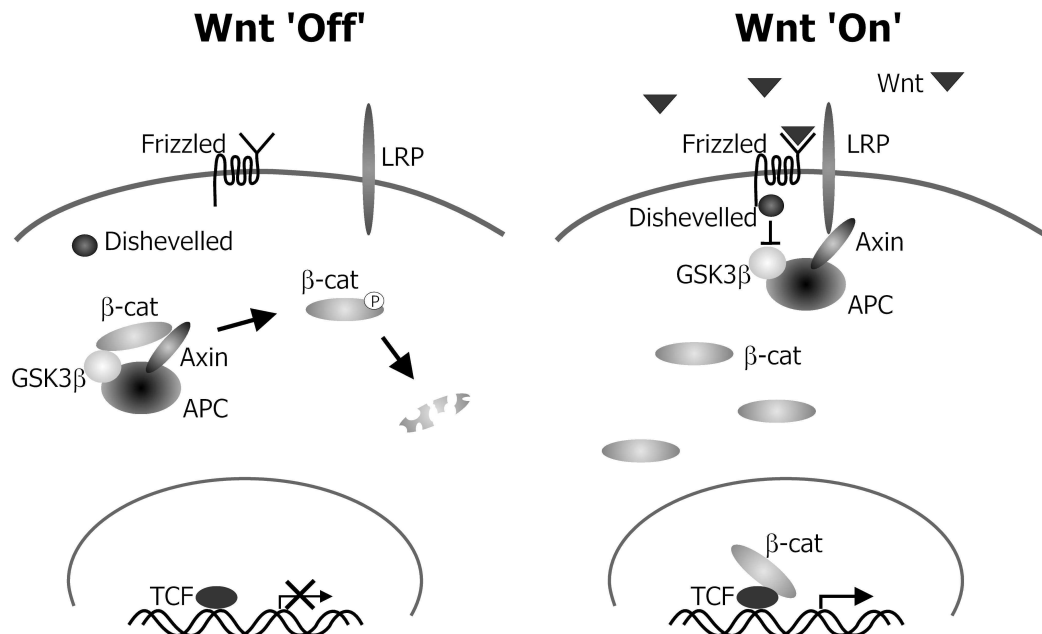
Figure 1.6: A simplified version of the canonical Wnt pathway. LEFT: In the absence of Wnt, β-catenin levels are regulated by a complex containing APC, Axin and GSK3β. Transcription of TCF target genes is suppressed by the presence of co-repressors. RIGHT: Wnt binds to Frizzled receptors and activates LRP, which subsequently binds to the Axin in the degradation complex. Dishevelled destabilises the degradation complex, allowing β-catenin to accumulate in the nucleus where it complexes with TCF and activates transcription.

APC) regulates β-catenin stability independently of GSK3β or Axin (Matsuzawa & Reed, 2001; Liu *et al.*, 2001): the role of APC in this pathway could be important when considering APC mutations.

Receptors

The first Wnt receptor was identified by Bhanot *et al.* (1996) as Frizzled (Fz), a seven-pass transmembrane protein (Fz passes across the membrane seven times, in a 'zig-zag' fashion). The human genome encodes 10 different Fz proteins. The canonical pathway also requires low-density-lipoprotein receptor related proteins 5 or 6 (LRP5 or LRP6) (Tamai *et al.*, 2000).

It is thought that Fz and LRP act as co-receptors for Wnt proteins. Wnt activates the pathway by physically joining, or facilitating the physical joining of, the two receptors on the outside of the cell. Reports suggest that physical interaction between Fz and LRP is sufficient to activate the canonical

pathway in the absence of Wnt (Cong *et al.*, 2004; Holmen *et al.*, 2005). Some of the non-canonical Wnt pathways (see section 1.4.4) do not require both Fz and LRP, for example the planar cell polarity pathway seems to depend only on Fz receptors (Wehrli *et al.*, 2000; Strutt, 2003).

Several Ser/Thr motifs in the cytoplasmic domain of LRP are phosphorylated: GSK3β has been shown to phosphorylate part of each motif, followed by CKIγ which phosphorylates the rest of the motif (Mao *et al.*, 2001; Nusse, 2005; Cadigan & Liu, 2006); Wnt stimulation promotes phosphorylation at these sites within 10-15 minutes (Davidson *et al.*, 2005; Zeng *et al.*, 2005). Axin is inactivated (perhaps simply by being attached to LRP, or perhaps by being labelled for degradation) and can no longer form part of an active destruction complex, leading to activation of the Wnt pathway. Interestingly, here GSK3β switches the Wnt pathway 'On', whereas further downstream, as part of the destruction complex, GSK3β maintains the 'Off' state (see Figure 1.6).

LRP levels are regulated by the Dickkopf (Dkk) and Wise families of proteins (He *et al.*, 2004). Dkk proteins are thought to prevent the formation of Fz/LRP complexes, and therefore regulate only the canonical Wnt pathway. Other extracellular factors (sFRP (Jones & Jomary, 2002), Wif (Hsieh *et al.*, 1999), Cerberus (Piccolo *et al.*, 1999), Coco (Bell *et al.*, 2003)) can inhibit all Wnt pathways.

Upon Wnt stimulation, Dishevelled (Dvl1, 2 and 3 in mammals) is recruited from the cytoplasm to Fz receptors and phosphorylated by PAR-1 and CKIε. The action of phosphorylated Dishevelled is unclear, although it appears to bind to Axin (Kishida *et al.*, 2001) and, in addition, forms a complex with (or facilitates the formation of a complex between) Frat1 and GSK3β, thereby inhibiting the activity of GSK3β (Reya & Clevers, 2005). Before the function of GSK3β in phosphorylating LRP was known, it was observed that GSK3β was localised to the Fz receptor area when a Wnt stimulus was present. Initially this was thought to be due to Dishevelled removing GSK3β from the destruction complex and sequestering it to the membrane; more recent results suggest that this behaviour could be explained by its role in LRP-phosphorylation (He *et al.*, 2004).

It is now thought that the main role of Dishevelled is to recruit Axin to the cell membrane. He *et al.* (2004) proposed three hypotheses to explain this. The first theory is that Fz recruits Dsh and LRP recruits Axin, bringing them into close proximity for inhibition or degradation. The second explanation is that Dishevelled and Axin interact in the cytoplasm, and vesicles transport them to Fz/LRP together. The third scenario is that Dishevelled inhibits Axin at the Fz receptor, and LRP independently inhibits Axin, both processes being necessary for downregulation of the canonical pathway. However, Zeng *et al.* (2008) have recently demonstrated that Dishevelled recruits an Axin/GSK3β complex to the membrane and hence to close proximity to LRP; GSK3β phosphorylates LRP, which

in turn sequesters further Axin/GSK3β complexes, preventing the formation of destruction complexes. Again we observe both a positive and a negative role for regulatory components of the Wnt pathway, suggesting an 'On' and 'Off' state may be overly simplistic.

CKIα and GSK3β

In addition to phosphorylating LRP, GSK3β's classical role is as the phosphorylatory subunit of the destruction complex. The first action of GSK3β in the destruction complex is to bind to Axin, then to stabilise the complex by phosphorylating both Axin and APC. GSK3β only has binding sites for Axin and cannot physically associate with either APC or β-catenin (Sakanaka *et al.*, 1998).

CKIα physically binds to β-catenin (Bustos *et al.*, 2006) and phosphorylates β-catenin at Ser^{45}, GSK3β can then sequentially phosphorylate the remaining target residues of Thr^{41}, Ser^{37} and Ser^{33}. β-catenin is then released back into the cytoplasm and ubiquitinated by β-TrCP and ubiquitin enzymes, labelling it for destruction by the proteosomes. All four residues must be successfully phosphorylated for ubiquitination to occur. For example, a mutation altering the amino acid at β-catenin residue 45 could leave β-catenin immune to degradation via the destruction complex, whilst, in all probability, maintaining its ability to promote transcription in the nucleus.

Upon stimulation of the canonical pathway, phosphorylated Dishevelled causes the formation of a Frat1/GSK3β complex which inhibits the activity of GSK3β (Kishida *et al.*, 2001). Surprisingly Sierra *et al.* (2006) found GSK3β in the nucleus acting as a co-repressor with β-TrCP on the *c-Myc* promoter region (one of the β-catenin target genes); until recently these proteins were thought to act only in the cytoplasm. Inoki *et al.* (2006) found that Wnt controls cell growth by activating the mTOR pathway, via inhibition of GSK3β; this could lead to regulation of translation through mTOR and regulation of transcription through β-catenin.

Another suprising finding is the involvement of GSK3β with Cyclin D1. Diehl *et al.* (1998) show that GSK3β phosphorylates Cyclin D1 at Thr^{286} significantly increasing its degradation rate. They also showed that GSK3β localises to the nucleus during S phase and causes the nuclear export of Cyclin D1. Salinas (2007) has recently reviewed the roles of GSK3β in the canonical Wnt pathway, and its influence on the microtubule skeleton in the cell.

Axin

Axin was identified by Zeng *et al.* (1997) and named because it is an **axi**s **n**egative regulator of embryonic axis formation, i.e. overexpression of Axin inhibits axis formation in embryos. It is still

not understood how Wnt and Axin are involved in establishing a tissue axis.

Axin forms the central scaffold of the destruction complex, binding to β-catenin, APC, GSK3β, CKIα and protein phosphatase 2A (PP2A). Axin has recently been recognised as the chief regulator of the canonical pathway (Tolwinski & Wieschaus, 2004), being present in a much lower concentration than other components of the destruction complex (Lee *et al.*, 2003).

As discussed above, upon Wnt stimulation Axin is recruited to the cell membrane by Dishevelled and inactivated by LRP and/or Dishevelled (Schwarz-Romond *et al.*, 2007); this prevents the formation of the destruction complex in the cytoplasm, as the active unit GSK3β must bind to both APC and Axin in order to phosphorylate β-catenin (Sakanaka *et al.*, 1998).

Jho *et al.* (2002), Leung *et al.* (2002) and Lustig *et al.* (2002) found that the *Axin* paralog[5] *Axin2* is a Wnt target gene, whereas Axin is expressed constitutively. Axin2 is believed to have the same binding sites and behaviour as Axin (Behrens *et al.*, 1998), and could therefore act as part of a negative feedback loop, limiting the intensity of a Wnt signal response.

Adenomatous Polyposis Coli (APC)

APC is a large scaffold protein (APC 2843aa, APC2 2303aa) which forms a scaffold for the destruction complex. APC was identified as a part of the Wnt signalling pathway by Papkoff *et al.* (1996), and plays a key role in regulating crypt fission (Wasan *et al.*, 1998). It is commonly held that APC binds to Axin and β-catenin, facilitating the formation of the destruction complex which phosphorylates β-catenin (Näthke, 2004; Senda *et al.*, 2007). However Takacs *et al.* (2008) have observed that APC can also reduce Axin levels (through an as yet unknown mechanism), this process upregulates β-catenin levels, so APC is another component which could both positively and negatively regulate the pathway.

The central region of APC is responsible for binding β-catenin through seven 20aa repeats (activated by phosphorylation of APC by GSK3β) and three 15aa repeats (constitutively active) (Rubinfeld *et al.*, 1993). The third 20aa repeat is the tightest binding site for β-catenin (Liu *et al.*, 2006a), and indeed most APC mutants in CRC have lost this repeat. The central region also includes three Ser-Ala-Met-Pro (SAMP) repeats which bind Axin. APC cannot form an active destruction complex in the absence of Axin as the conformation of the complex is not correct (Bienz & Clevers, 2000). Phosphatase 2A (PP2A) is a regulatory subunit of the destruction complex which also binds

---

[5]A paralog is a duplicated gene in a genome, which may have occurred due to replication errors. Paralogs can often mutate without changing the behaviour of the original gene and therefore usually exhibit similar but not identical behaviour (such as the Cyclin D family discussed in section 1.3.1).
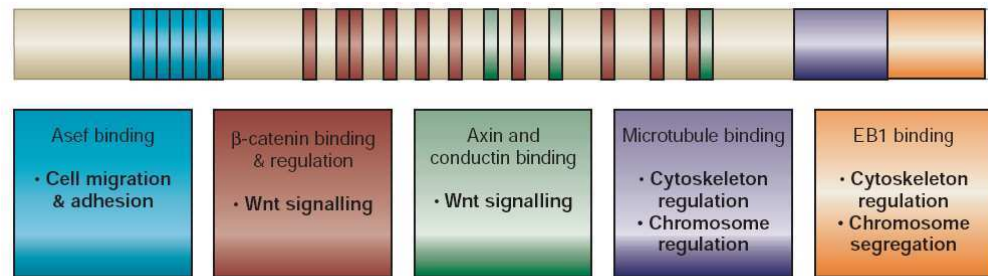
Figure 1.7: The many functions of APC. Schematic representation of the APC protein, showing regions that interact with other proteins, and the proposed functional significance of these interactions. Reprinted from Fodde *et al.* (2003) by permission from Macmillan Publishers Ltd: Nature Cell Biology 5:190-192, copyright (2003).

APC in this central region.

Penman *et al.* (2005) showed that full-length APC exists in two distinct soluble complexes, the fully assembled destruction complex, which cannot interact with microtubules, and a smaller complex (possibly APC monomers) which can. Before folding, proteins are linear chains of ordered amino acids with an N-terminal and a C-terminal end. The N-terminal and central regions of APC are highly conserved between species; there is more variation in the C-terminal end where new binding partners have been discovered (Näthke, 2005). The last 170 amino acids can bind to EB1, a small microtubule-tip-binding protein. This enables APC to bind to the 'plus' (advancing) ends of microtubules, tubes made up of proteins that provide a supportive cytoskeleton for the cell (and a network for active transport) (Aoki & Taketo, 2007).

APC is often found at the leading edge of migrating cells, perhaps stabilising microtubules; this recruitment also involves GSK3β (Mogensen *et al.*, 2002; Etienne-Manneville *et al.*, 2003) which may be regulating the action of APC. Zumbrunn *et al.* (2001) suggest that binding of APC to microtubules is decreased under GSK3β phosphorylation, in contrast to phosphorylation in the destruction complex which facilitates β-catenin binding.

During mitosis, APC localises to kinetochores (protein structures which assemble on chromosomes in order to separate the copies), which is consistent with its localisation to microtubule plus ends. In addition, APC has been detected at centrosomes (the main microtubule organising centres, usually found at the nuclear membrane) and mitotic spindles (fibres linking kinetochores to centrosomes during cell division — the 'ropes' pulling chromosome pairs apart) (Kaplan *et al.*, 2001). APC is therefore very important in the M phase of the cell cycle and APC mutations are often associated

with aneuploidy[6] in human gut tissue, suggesting that healthy APC is necessary to ensure the separation of the chromosomes works smoothly and chromosomes are not lost (a cell undergoing anaphase can be seen in Figure 1.8).
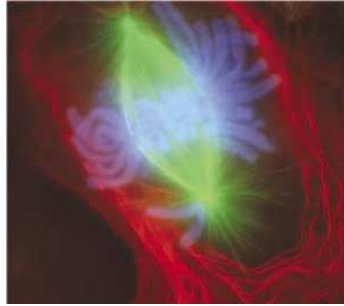
Figure 1.8: The separation of the chromosomes during anaphase. Chromosomes are stained blue, mitotic spindles are green, and the cell membrane is red. The centrosomes (where APC has been detected) are where the mitotic spindles converge and kinetochores (again containing APC) are where the spindles attach to the chromosomes (C.L. Rieder, public domain http://www.wadsworth.org/bms/SCBlinks/web_mit2/HOME.HTM).

APC-stimulated guanine nucleotide exchange factor (Asef) also binds to this busy central region of APC (see Figure 1.7). Asef stimulates actin polymerisation through the action of Rho proteins and F-actin. Actin fibres are the other main components of the cytoskeleton, binding to cadherins and again providing an active transport network. Overexpression of APC can lead to long cellular protrusions, as actin fibres over-polymerise and extend the cell membrane (Näthke, 2005). In addition KAP3 binds to APC in the same region as Asef. Since KAP3 is a linker protein for kinesins (motor proteins that travel along the microtubules), this may facilitate active transport of APC around the cell.

To add further intricacy, Chen *et al.* (2006) showed that the microtubule-actin cross linking factor (MACF1) is associated with the destruction complex in the absence of Wnt stimulation, and may aid the movement of Axin to the LRP receptors upon Wnt stimulation.

We have seen that cytoskeletal regulation is involved in intestinal cell migration, proliferation and differentiation; the role of APC in these mechanisms is yet another method by which the Wnt pathway can influence the behaviour of the cell (Hanson & Miller, 2005).

There is certainly shuttling of APC between the nucleus and the cytoplasm. In one study, APC was even reported to be concentrated in the nucleus (Zhang *et al.*, 2001), although most colorectal cell line studies find little APC in cell nuclei. As discussed earlier, APC contains nuclear export

---

[6]Aneuploidy is a condition in which the number of chromosomes is abnormal due to extra or missing chromosomes.

sequences (NESs), suggesting the need for nuclear-import activity. Nuclear import appears to be mediated by the Arm repeats, possibly in the same way that β-importin (which also contains Arm repeats) binds to nucleoporins to access the nucleus (Bienz, 2002).

Xiong & Kotake (2006) showed that one method of APC nuclear-export was via the CRM1 receptor on the nuclear membrane. APC possesses CRM1 nuclear export sequences, with at least two at the N-terminal and three at the C-terminal end. There is also evidence that APC acts as a chaperone, binding to β-catenin and carrying it in and out of the nucleus (Xiong & Kotake, 2006). APC-independent β-catenin shuttling also occurs, but it is not known whether this is influenced by Wnt signalling (Eleftheriou *et al.*, 2001).

APC and C-terminal Binding Protein (CtBP) act as repressors on TCF activation sites, providing another function for APC in the nucleus (Hamada & Bienz, 2004). Sierra *et al.* (2006) showed that APC, β-TrCP and CtBP transiently bind to β-catenin/TCF promoted genes as repressors, before stable binding of TLE-1 and HDAC1 corepressors. Nuclear CtBP binds to wild-type APC but not some CRC mutants, suggesting a mechanism for increased Wnt target gene expression that is independent of β-catenin levels. Thus, in healthy cells, APC directly represses activation of Wnt target genes and facilitates the degradation of β-catenin; APC performs neither of these functions in CRC cells.

Other components

As we saw in section 1.4.2, β-catenin interacts with TCF inside the nucleus. TCF is normally present in the nucleus, bound to DNA promoter regions[7] with other proteins which inhibit its activity (co-repressors). When β-catenin accumulates in the nucleus (in response to a Wnt signal) it displaces the co-repressors and acts as a co-factor with TCF and the transcription of TCF target-genes takes place. When the proteins ICAT and Duplin are present target gene expression is inhibited, as these proteins bind directly to β-catenin, in competition with TCF (Tago *et al.*, 2000; Kobayashi *et al.*, 2002).

TCF is modified in many different ways: phosphorylation of TCF inhibits its binding to β-catenin, as does acetylation; while sumoylation[8] of TCF activates transcription (Kikuchi *et al.*, 2006). How these modifications are regulated, and whether they are Wnt-dependent, is not clear; however the

---

[7]TCF has a high affinity for the DNA sequence (A/T)(A/T)CAA(A/T)GG and is found on promoter regions with this sequence.

[8]Addition of a *S*mall *U*biquitin related *Mo*difier protein, which usually extends the lifetime of a protein and may also target it for active transport

phosphorylation of TCF may occur in response to Wnt5a (Ca^{2+}) signalling (Ishitani *et al.*, 2003).

In this review of the canonical pathway we have focused only on the major components. RNAi screens suggest that over 200 genes are involved in Wnt signalling (Fearon & Cadigan, 2005; DasGupta *et al.*, 2005) and have established it as one of the most intricate signalling pathways.

1.4.4   Non-Canonical Wnt Pathways

Wnt research has traditionally been concerned with the canonical pathway. However much research is now directed at non-canonical pathways — those that do not involve β-catenin (for a review, see Veeman *et al.* (2003)). Few, if any, pathways are completely independent; it is almost inevitable that pathways share components, or are at least influenced by the downstream gene expression associated with other pathways; this suggests that Wnt signalling will have far reaching effects on a cell's behaviour.

Wnts are believed to be involved in pathways as diverse as: calcium (Ca^{2+}) signalling, via the action of Dishevelled (Sheldahl *et al.*, 2003); the *Drosophila* planar cell polarity (PCP) pathway, also via the action of Dishevelled (Axelrod *et al.*, 1998); tissue separation between the germ layers in embryonic development, via the action of Frizzled (Winklbauer *et al.*, 2001); the fibroblast growth factor (FGF) Snail pathway leading to E-cadherin regulation, via the action of GSK3β (Katoh & Katoh, in press); and cardiogenesis in the case of Wnt11 (Eisenberg & Eisenberg, 1999).

Wnt shares some of its components with the Hedgehog signalling pathway, namely CKIs and GSK3β (Taipale & Beachy, 2001) , and with the Notch signalling pathway (Nakamura *et al.*, 2007). Correct operation of both pathways is thought to be essential for stem-cell maintenance, normal epithelial renewal and patterning in the crypts (van den Brink & Hardwick, 2006). Akiyoshi *et al.* (2006) provide evidence that activation of the Hedgehog pathway antagonises the Wnt pathway in colorectal cancer cells, although the reason for this is not clear. There is growing evidence that non-canonical Wnt pathways can play an important role in colorectal cancer initiation (Kikuchi & Yamamoto, 2008).

Non-canonical Wnt pathways can also antagonise the canonical pathway (Topol *et al.*, 2003), and different Wnt factors may activate different Wnt pathways. For example, Wnt11 represses the canonical pathway (Wnt1, Wnt3, Wnt3a but not Wnt7 or Wnt7b) possibly due to competition for Frizzled receptors (Maye *et al.*, 2004). Similarly Wnt5a inhibits the canonical pathway, possibly by causing the phosphorylation of TCF (Weidinger & Moon, 2003).

1.4.5   Wnt Pathway in tumourigenesis

By linking mutations with stages in the progression of colorectal cancer, Fearon & Vogelstein (1990) suggested a genetic model for colorectal cancer progression. As more was discovered about the action of the various proteins it became clear that the first mutation in colorectal cancer was almost always in one of the components of the canonical Wnt pathway (Powell *et al.*, 1992; Morin *et al.*, 1997; Giles *et al.*, 2003). There are many reviews devoted to the role of Wnt signalling in cancer initiation, such as Behrens *et al.* (1996), Polakis (2000), Logan & Nusse (2004), Sancho *et al.* (2004), Bafico *et al.* (2004) and Reya & Clevers (2005). Before discussing the most common mutations in CRC we will first explain how mutations can occur.

Mutations

Each time the DNA in a cell is replicated (during the S phase of the cell cycle) mistakes can be made. DNA repair mechanisms are in place so most of these mistakes are rectified before S phase ends. For example, mismatch repair proteins look for nucleotides that do not conform to the usual A-T/C-G pairings and then use the original DNA strand as a template to repair the damage. But there are still mistakes, leading to a basic-level 'background' mutation rate. This mutation rate can increase if a random mutation occurs in critical genes, for example a mismatch repair gene. However, this is not believed to be the case in the majority of cancers (Tomlinson & Bodmer, 1999).

Mutations which occur during the lifespan of an organism and are not inherited are called somatic mutations. Their effect is varied. Most DNA does not encode genes, and is referred to as 'junk' DNA; this is useful at the end of chromosomes and in other vulnerable regions of the DNA, because mutations here have no effect. Even inside a coding region of DNA most mutations result in a harmless change of a nucleotide. Because of the way codons translate to amino acids this may not change the amino acid residue in question. On the other hand if a 'stop' codon is accidentally encoded this leads to premature truncation of the protein, which generally means it loses some binding sites and functions (a *truncation* mutation). Insertion and deletion mutations can also occur, usually in large repeated regions of the DNA as the replication machinery can easily 'slip'. The mutation rates for cancerous colorectal crypt cells are usually the same as the rates in healthy cells (Wang *et al.*, 2002b; Araten *et al.*, 2005), suggesting that DNA repair mechanisms are not usually mutated and the high turnover of cells in a crypt is the main reason for the prevalence of cancers here.

Approximately 20% of colorectal cancer cases arise as a result of inherited gene mutations (Lynch & de la Chapelle, 2003). One of the best defined cancer syndromes is familial adenoma-

tous polyposis (FAP). FAP causes large numbers of benign adenomatous polyps (precursor lesions of colorectal cancer) to arise in the colon and rectum (Bienz & Clevers, 2000), with some invariably progressing into invasive and eventually metastatic cancers. APC is the gene which, when mutated, causes FAP. Additionally most sporadic (non-hereditary) colorectal tumours arise due to APC mutations (Nagase & Nakamura, 1993). Another familial syndrome is hereditary non-polyposis colorectal cancer (HNPCC). HNPCC is associated with mutations in mismatch repair (MMR) genes and can cause colorectal cancer at the age of 40–45, without the usual warning of polyps lining the gut. Microsatellites are genomic regions where short DNA sequences or single nucleotides are repeated, and replication machinery is prone to mistakes; MMR genes ensure that these repeated sections of DNA are carefully lined up and repaired. Microsatellite instability occurs when these sections are not controlled carefully and can elongate or contract during DNA replication, leading to mutations in proteins such as β-catenin (Mirabelli-Primdahl et $al.$, 1999).

We will use a model of Wnt signalling to study the impact of both APC and β-catenin mutations in chapter 3; here we examine the effect of these mutations on the proteins' interactions.

APC Mutations

FAP patients have a mutation in one of their two APC alleles (a 'single-hit' or $APC^{+/-}$); the progression to colorectal cancer coincides with a mutation in the other allele (a 'double-hit' or $APC^{-/-}$). Models of cancerous crypts already exist (Komarova & Wang, 2004) and are reviewed in section 1.5.2. Since none of these models provides a direct explanation of why APC mutations cause uncontrolled proliferation, we now examine the effect of a mutation in APC more closely.

Aberrant Wnt signalling is fundamental to the initiation of CRC — around 80% of human CRC tumours possess an $APC^{-/-}$ mutation (Rowan et $al.$, 2000). These mutations render APC unable to bind to the other components, preventing the formation of an active destruction complex (Rowan et $al.$, 2000; Albuquerque et $al.$, 2002) and so β-catenin levels rise. Roughly a further 12% of CRC tumours possess a single-hit β-catenin mutation (Samowitz et $al.$, 1999; Ilyas, 2005): the β-catenin mutation is in one copy of the gene only (β-catenin$^{+/-}$). Half of the β-catenin produced is immune to degradation by the destruction complex, and retains its ability to promote transcription of target genes in the nucleus.

Knocking out Cyclin D1 in 'Min mice' (Multiple intestinal neoplasia — i.e. mice with FAP) results in fewer tumours (Hulit et $al.$, 2004), indicating that at least some of the tumourigenic effects of an $APC^{+/-}$ mutation are dependent on the presence of Cyclin D1.

There are mutation *hotspots* in APC, areas of the gene in which mutations are regularly observed. As it is thought that mutations occur randomly throughout the genome, there must be selection for cells that harbour mutations in the hotspot region of APC (Nagase & Nakamura, 1993). Lüchtenborg *et al.* (2004) detected mutations in the main APC hotspot, between codons 1286 – 1513, in 72% of CRC patients, truncating APC mutations accounting for just over half of these.

Albuquerque *et al.* (2002) have suggested that there is a minimum level of APC required for tumour initiation and β-catenin levels should not be too high. Cells completely devoid of APC can replicate but do not persist in a population indefinitely. Albuquerque *et al.* (2002) also observed an interdependence between the two hits (as did Rowan *et al.* (2000)): if the first hit knocked out APC completely then the second was usually a truncating mutation, and vice-versa. The truncation mutations commonly lead to the loss of most of the ARM repeats, removing APC's ability to bind to β-catenin and some of the components of the destruction complex. Most truncating mutations have lost the third 20aa repeat (see Figure 1.7), which is the tightest binding site for β-catenin (Liu *et al.*, 2006a). Thus the functional effect of APC mutations is to lose the ability to bind β-catenin; APC cannot disappear altogether or the cell becomes inviable in the long-term.

Kawasaki *et al.* (2003) showed that truncated APC, through the Asef pathway, leads to increased cell migration. It has also been shown that truncated APC can form a destruction complex that does not bind Axin and therefore cannot phosphorylate β-catenin (Penman *et al.*, 2005). Schneikert *et al.* (2007) recently showed that truncated APC regulates the transcriptional activity of β-catenin in a cell-cycle-dependent manner, which may lead to important feedback in future models of aberrant Wnt signalling. Whilst Bortlík *et al.* (2006) suggest that not as many mutations are truncating as was previously thought. It is possible to have double APC mutations, where neither is truncating, yet still form an adenoma.

Further intricacies in the behaviour of APC are emerging continually. For example, Yang *et al.* (2006) suggest that mutant APC acts to halt the ubiquitination or degradation of β-catenin, rather than its phosphorylation. Expression of full length (wild-type) APC in $APC^{-/-}$ colon cancer cells causes β-catenin to translocate from the nucleus and cytoplasm to the cell periphery, leading to an increase in E-cadherin expression and hence causing stronger cell-cell adhesion. Putting these formerly cancerous cells back into mice does not lead to tumour formation (Faux *et al.*, 2004).

β-catenin Mutations

Up to 12% of small adenomas possess β-catenin mutations instead of $APC^{-/-}$ mutations (Samowitz *et al.*, 1999). These mutations are commonly in the residues that would ordinarily

be phosphorylated by the destruction complex, and regulate β-catenin levels (e.g. Ser^{45}). However only 2.4% of large adenomas, and 1.4% of invasive cancers, carry such *β-catenin* mutations (Samowitz *et al.*, 1999). These findings suggest that adenoma development is promoted more strongly by *APC* mutations than by *β-catenin* mutations, even though mutations in both lead to an accumulation of β-catenin in the nucleus. This suggests that APC must have additional tumourigenic effects, perhaps through its action on the cytoskeleton, in cell adhesion and/or in mitosis.

Other Mutations

Of tumours exhibiting mismatch repair mutations, almost a quarter have mutations in *Axin2* rather than *APC* or *β-catenin*. However, this still accounts for only a small percentage of all tumours (Liu *et al.*, 2000) and few colorectal cancers are initiated by a mutation in a gene other than *APC* or *β-catenin*. Hadjihannas *et al.* (2006) showed that overexpression of Axin2 could lead to chromosomal instability. Axin2 could be upregulated as it is a target of Wnt signalling (Jho *et al.*, 2002; Leung *et al.*, 2002) or because it has a mutation which prevents its interaction with LRP.

Mutations that are associated with the progression of CRC are shown in Figure 1.9. All of the mutations discussed above are acquired during the earliest stages of colorectal cancer initiation, and further mutations must occur for progression to clinical cancer. Figure 1.9 shows the progression for the two forms of genetic instability that commonly contribute to CRC: chromosomal instability (CIN) and microsatellite instability (MIN). The familial syndrome FAP and *APC* mutations tend to cause CIN tumours, whilst HNPCC and *β-catenin* mutations usually lead to MIN tumours. CIN is characterised by losing chromosomes — reasons that *APC* mutations could cause this are discussed above. Approximately 15% of sporadic tumours are characterised by MIN and approximately 85% by CIN (Sancho *et al.*, 2004).

Despite the likelihood of a double-hit in *APC* being much lower than the likelihood of a single-hit in *β-catenin* we observe far more colorectal cancers with the double-hit in *APC*. For this reason a cell harbouring the *APC* mutations must be more likely to form a cancer than a cell with a single *β-catenin* mutation. We will see in our model of chapter 3 that this discrepancy cannot be due to the effect of the mutation on β-catenin levels, but APC mutations must be selected due to some of their other effects on the cell, such as their role in regulation of division as discussed in section 1.4.3.

The direction of our work is to link models of subcellular processes, such as Wnt signalling and the cell cycle, with models of an entire crypt and, in the future, tissues made up of many crypts. We will now discuss some of the existing models of Wnt signalling.
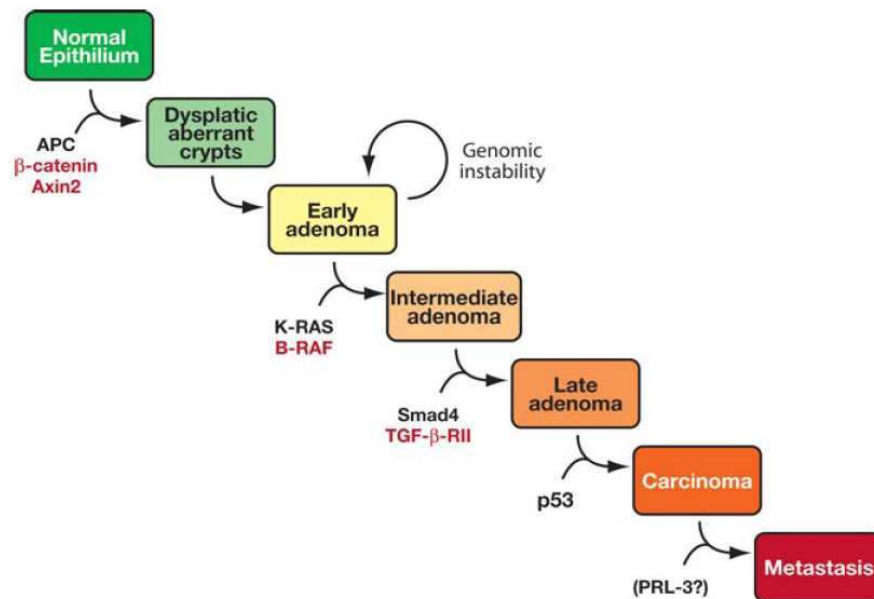
Figure 1.9: Correlation between CRC progression and the accumulation of genetic alterations according to Fearon & Vogelstein (1990). The genetic alterations frequently found in CIN tumors are depicted in black; genetic alterations more common in MIN tumours are depicted in red. Reprinted, with permission, from the Annual Review of Cell and Developmental Biology, Volume 20, ©2004 by Annual Reviews www.annualreviews.org.

1.4.6   Mathematical Models of Wnt Signalling

The Wnt pathway has been the subject of little mathematical modelling to date, due in part to its complexity and a lack of quantitative experimental data. However in 2003 Lee *et al.* published a detailed ODE-based model which replicated experimental results extremely well and significantly changed the way in which the Wnt pathway was thought to operate (Tolwinski & Wieschaus, 2004). The model accounts for Wnt's control over the formation of the destruction complex and the subsequent phosphorylation of β-catenin. One of its major strengths was the first-hand gathering of the necessary kinetic data. Lee's coworkers have expanded on the mathematical methods they originally presented in a further paper (Kruger & Heinrich, 2004). An asymptotic analysis of this model is presented in Chapter 2.

Van Leeuwen *et al.* (2007) developed a different model to investigate the interaction between β-catenin's roles in adhesion and transcription. There are two main hypotheses — either β-catenin's fate is determined by competition for binding partners or it undergoes a conformational change

which favours transcription. The authors formulated an ODE-based model distinguishing between the different pools of β-catenin, before presenting model simulations. The results of most of the *in silico* experiments suggest that the second hypothesis (β-catenin undergoes a conformational change) better explains some of the experimental data.

Cho *et al.* (2006) studied the effect of APC mutations on the Wnt pathway by extending the Lee *et al.* (2003) model to incorporate APC mutants with varying affinity for β-catenin. They suggest that APC mutants are selected because of the effect they have on β-catenin levels. They assume more β-catenin degradation sites are lost in more highly truncated APC mutants, and simulate the level of β-catenin that therefore accumulates. Cho *et al.* incorporated the Axin2 feedback loop into their model, a feature not included in the Lee *et al.* (2003) model. Weaknesses of the Cho *et al.* (2006) model include the fact that the probability of the different mutants occurring was not taken into account, neither was the fact that cancers carry two different mutated copies of the APC gene and therefore two different mutant 'versions' of the APC protein. As we saw in section 1.4.5, it is highly unlikely that both mutations are functionally the same. Cho *et al.* conclude that mutations are not selected on the basis of maximal levels of β-catenin expression, but rather on an 'optimal' level of β-catenin expression. We explain in more detail how the Cho *et al.* (2006) model differs from the Lee *et al.* (2003) model in Chapter 2.

Recently two articles have used the Cho *et al.* model to investigate further features of the Wnt/β-catenin pathway. In Kim *et al.* (2007), Cho *et al.*'s Wnt signalling model is coupled to a model of the ERK pathway and crosstalk between the two pathways was found to create a positive feedback loop, increasing the levels of β-catenin/TCF transcription factor. Wawra *et al.* (2007) have introduced a time-delay into Cho *et al.*'s model to account for the time taken to transcribe and translate Axin2; they also introduced a new source of negative feedback, assuming that one of the β-catenin/TCF target genes has a product which inhibits the action of Dishevelled. The authors showed that oscillations in β-catenin levels may arise as a result of the time delays involved.

1.5 Cancerous Crypt Dynamics

Gene mutations can cause the rate of cell proliferation in the crypts to exceed the rate of cell loss, leading to a net increase in cell number. We term a crypt exhibiting this behaviour (as a result of mutations rather than healthy growth) a *cancerous crypt*. We may also term an individual cell *cancerous* if the usual controls on, for example, cell proliferation and apoptosis are not functioning normally. Aberrant dysplastic crypts can be seen in Figure 1.10.

1.5.1 Observed Dynamics

The location in the crypt where the first mutation occurred is not usually known; cases can be made for "bottom-up" (a mutation occurs in the stem cell pool and propagates up the crypt) and "top-down" (a mutation occurs in a cell above the base and spreads down the crypt) expansion of the cancerous cells (Shih *et al.*, 2001; Leedham & Wright, 2007). The series of panels presented in Figure 1.10 show mutant cells which are proliferating throughout the crypt, whereas their healthy counterparts stop proliferating at some distance up the crypt.
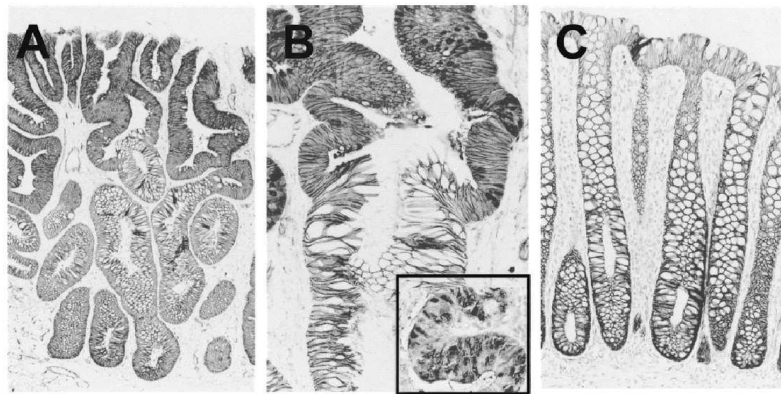
Figure 1.10: Cells stained for β-catenin expression in small adenomas (A and B) and healthy colonic epithelium (C). In A and B, dysplasia can be seen, with crypts beginning to branch and buckle. β-catenin is highly expressed and distributed throughout the top of the crypts, where it is found in the nucleus, cytoplasm and membrane. Staining for β-catenin is less intense in the normal-appearing epithelium at the bottom of the crypts of both A and B, where it is confined to the membranes. The staining pattern at the bottom of these adenomatous crypts is similar to that observed in normal colonic epithelium (C). Reproduced from Shih *et al.* (2001). Copyright (2001) National Academy of Sciences, U.S.A.

Once homeostasis in the crypt is lost, cells increase in number and an adenoma, or small polyp, forms. Crypts undergo increased crypt fission (splitting to form a new crypt), perhaps as a result of mechanical 'buckling' of the tissue. Further mutations (see Figure 1.9), can cause the formation of adenomas (polyps protruding into the gut) and, later, carcinomas — aggressive tumours (Bienz & Clevers, 2000).

1.5.2   Mathematical Models of Colorectal Crypts and Cancer

Mathematical modelling of tumour growth and mutations began in the 1970s, and was instrumental in explaining how cancer initiates (Knudson, 1971) and tumours grow (Greenspan, 1972). Van Leeuwen *et al.* (2006) provide a comprehensive review of models for normal colorectal physiology and CRC; here we briefly describe the theoretical approaches that have been undertaken. Models for colon crypts have tended to be stochastic population-based, compartmental or individual-cell-based spatial (2D grid and 2D lattice-free) models.

Stochastic population-based Models

Stochastic models are a natural approach for modelling mutations, which, by their very nature, are random occurrences. Komarova and colleagues have produced a series of models to examine the population genetics of colorectal cells (Komarova & Wang, 2004; Nowak *et al.*, 2004; Komarova & Cheng, 2006). They have found, perhaps counter-intuitively, that it is unlikely that a double-hit occurs in a stem cell. It is more likely that a single hit occurs in a stem cell and the second hit in a transit cell (as there are many more transit cells than stem cells dividing, though they usually leave the crypt before they acquire two mutations). In Komarova & Cheng (2006) the authors suggest that, given a similar probability of mutation in stem and normal cells, the likelihood of acquiring two mutations falls as the number of stem cells at the base of a crypt increases (since each lineage undergoes fewer divisions in a certain period of time).

The way in which a stem cell divides remains unknown. In 1997 Loeffler *et al.* developed a compartmental stochastic model to study the different alternatives: assuming that stem cells can divide symmetrically and give rise to two stem cells; asymmetrically to one stem cell and one differentiated cell; or symmetrically to two differentiated cells. When the phenotype of the daughter cell is assumed to be stochastic, the model generates results which appear to replicate the observed slow spread of monoclonality (eventually all cells are clones/descendants of one original cell) throughout the crypt .

Spatially-averaged lumped-parameter Models

These models consist of compartments representing all of the cells throughout a spatial location, with separate variables for different cell populations (with usually one 'lumped-parameter' representing the different behaviours of separate cell types), with ODEs describing the exchange of cells from one 'compartment' to another. Tomlinson & Bodmer (1995) used this approach to create simple models

for populations of stem cells, semi-differentiated cells, fully differentiated cells and dying cells. They predict that the failure of programmed cell death in stem cells is sufficient for tumourigenesis but, more interestingly, they also predict that tumourigenesis can occur when semi-differentiated cells acquire a mutation which prevents programmed cell death. D'Onofrio & Tomlinson (2007) extended Tomlinson & Bodmer's (1995) model to account for fluctuations in parameter values (such as death rates). This "generally makes exponential growth of a tumour more likely" and can lead to a long plateau of cell numbers, mimicking equilibrium, before exponential growth starts. If this happens in vivo then it may be impossible to predict when an apparently stable tumour may start to grow rapidly. Johnston *et al.* (2007) have also extended Tomlinson & Bodmer's (1995) model to allow for asynchronous cell-division.

Boman *et al.* (2001) developed a compartmental approach to study how the numbers of stem cells, transit cells (in each of the stages of the cell cycle), differentiated cells, terminally differentiated cells and apoptotic cells within a crypt change over time. They showed that the size of a crypt population is very sensitive to stem cell proliferation rates, and suggest that this validates the hypothesis that stem cell mutations are responsible for CRC initiation. Michor *et al.* (2005) used a similar approach to study genetic instability by modelling the number of cells harbouring different types of mutation, with a CIN mutation making further mutations more likely. They suggest that the presence of one or two CIN (Chromosomal Instability) genes in the entire genome may mean that colorectal cancer is likely to be instigated and accelerated by CIN mutations.

Cell-based Models

Individual cell-based models treat each biological cell as a discrete entity. Rather than taking a continuum approach for one or more variables, discrete values for the variables are contained within separate cells. Cell-based models for avascular tumours are reviewed in Drasdo & Hoehme (2003); here we briefly describe some models of this type which have been applied to colorectal crypts.

3D crypts have been represented by 2D grid models, with the crypt 'rolled out' along its axis and periodic boundary conditions imposed. Loeffler *et al.* (1986, 1988) proposed the first such models, consisting of 'squares' representing individual cells, with cells around the circumference of the crypt on the 'x-axis' and cells along the crypt axis on the 'y-axis'. Stem cells are held at the bottom of the crypt and cells are removed from the top to represent sloughing. These models were used to explain how cell proliferation may vary within a crypt to produce the turnover and distribution observed. The main weakness of models of this type is due to the fixed grid structure. For example, in order to insert a new daughter cell an entire column of cells must be moved upwards, breaking the contacts

between a large number of cells, when studying the effects of variable cell-cell adhesion or the lateral spread of populations around the crypt such models become unrealistic.

To overcome these problems Meineke *et al.* (2001) developed a 2D lattice-free model, in which cells are attached by spring-like attractive and repulsive forces. This model appears to reproduce the experimentally-observed cell migration in a crypt. We will describe this model in depth in Chapters 5 & 6. When the cells in a lattice-based model are moving up the crypt with a fixed velocity at each 'y' coordinate then such lattice-free models will exhibit the same behaviour as a lattice-based model.

Drasdo & Loeffler (2001) formulated a lattice free cell-based model for crypt fission. They start with a 1D 'line' of cells arranged into a 2D vertical section of a crypt. Forces on each cell include elastic bonds between neighbouring cells, a bending force when the curvature of the cells is too great, a force acting on the bottom of the crypt (ensuring it spreads upwards rather than downwards) and a force keeping the crypt orifice in position. In healthy cells a crypt keeps its shape whilst cells migrate up the crypt. If mutant cells with faster cell cycles and reduced Young's modulus values are introduced then crypt buckling and fission is observed.

Studies of marked cells have shown that epidermal cells proliferate in 'mosaic' clusters of between 20–350 cells in size (Asplund *et al.*, 2001). This suggests small pockets of stem cells maintain a larger group of surrounding cells. One of these epidermal 'clusters' is analogous to an epithelial colorectal crypt — the difference being the 3D surface on which the cells lie. Savill & Sherratt (2003) modelled these clusters on epidermal monolayers by adapting an earlier Cellular Potts Model (CPM) (see Graner & Glazier, 1992; Glazier & Graner, 1993) to investigate the effects of cell-cell signalling on differentiation. A CPM moves cells in order to minimise their 'surface energies', which can be any functions of interest, such as surface area for a given volume. Savill & Sherratt results suggest that stem cells must adhere to one another much more strongly than they do to differentiated cells and that regulation of differentiation is the main mechanism for controlling cluster size. If Savill & Sherratt's conclusions are correct, it is also probable that regulation of differentiation plays a key role in controlling crypt length.

1.6   Thesis Structure

We perform a multiple-timescale analysis of a detailed model for the Wnt signalling pathway proposed by Lee *et al.* (2003) in chapter 2, and show how it may be reduced to a single ODE describing the evolution of β-catenin levels. In chapter 3 we investigate how Wnt signalling might affect the

cell cycle in the colorectal crypts, by using a variation of the simple Wnt-signalling model derived in chapter 2. We use the simple model to predict the effect mutations in the Wnt pathway have on the level of β-catenin. We then use this level of β-catenin as an input into an existing cell-cycle model, as β-catenin is a transcription factor for Cyclin D.

Recent experiments by Sansom *et al.* (2007) suggest that c-Myc is the most important downstream target of aberrant Wnt signalling; a double APC and c-Myc knockout reverts the effects of an APC knockout. The model of chapter 3 cannot reproduce this effect, as c-Myc is not represented in the model. In chapter 4 we develop a more detailed model to describe the influence of β-catenin on the cell cycle, by modelling the amount of c-Myc and Cyclin D:CDK4 complex available to trigger the cell cycle.

We introduce the **C**ancer, **H**eart **A**nd **S**oft **T**issue **E**nvironment program (CHASTE) and describe its development and implementation for simulations of the Meineke *et al.* (2001) crypt-dynamics model in chapter 5. We extend the model due to Meineke *et al.* (2001), present experimental data on crypt-dynamics, and compare them to the results of CHASTE simulations in chapter 6. The thesis ends in chapter 7 with a discussion of our findings and suggestions for future work.

CHAPTER 2

Wnt Signalling Models

2.1 Introduction

I_N section 1.4.5 we saw that studying the Wnt pathway is fundamental to understanding the initiation of colorectal cancer. The model developed by Lee *et al.* in (2003) is probably the most detailed theoretical description of Wnt signalling to date, with experimental data matching its predictions very closely. In this chapter we analyse Lee *et al.*'s model, characterising its behaviour on different timescales. This analysis reveals that changes in the 'output' of the Wnt pathway (i.e. changes in β-catenin levels) occur over a long timescale and we exploit this result to reduce the full model to a simpler system.

The remainder of this chapter is organised as follows: in section 2.2 we present Lee *et al.*'s model, recasting it in terms of nondimensional variables, before presenting typical numerical results. Guided by these simulations we proceed in section 2.3 with an asymptotic analysis of the governing equations, thereby identifying which components of the pathway are active on different timescales and using these results to reduce the model to a simpler one, which retains the key features of the full model. In section 2.4 we perform a similar analysis on the Cho *et al.*'s extension to the original model (Cho *et al.*, 2006). The chapter concludes in section 2.5 with a summary of our findings and suggestions for future work.

2.2   The Lee *et al.* (2003) Wnt Signalling Model

2.2.1   Model Formulation

In this section we introduce the deterministic model of the Wnt signalling pathway that was developed by Lee *et al.* (2003) and formulated as a system of coupled ODEs. Known interactions between the 'core components' of the canonical pathway are included, the core components being: Wnt, Dishevelled, GSK3β, APC, Axin, β-catenin and TCF. As we saw in section 1.4.3, many more proteins influence the Wnt pathway, but the above components are all essential to its operation. A schematic diagram of the biochemical interactions is shown in Figure 2.1.

β-catenin is known to localise to both the cell membrane and the nucleus (Harris & Peifer, 2005; Städeli *et al.*, 2006). A system of partial differential equations (PDEs) could be used to model these spatial effects. However the mechanisms by which these processes are regulated are, as yet, poorly understood and remain very difficult to model. Lee *et al.* consider the cytoplasmic levels of the pathway components, as the destruction complex is thought to act only in the cytoplasm. The proteins are assumed to be well-mixed, so a system of time-dependent ordinary differential equations (ODEs) for the concentrations of each component is formulated. Lee *et al.*'s model consists of 15 ODEs, one for each protein or protein complex shown in Figure 2.1. Some reactions are known to proceed more rapidly than others, so they make rapid equilibrium approximations to the relevant ODEs, in order to simplify the governing equations. This process is discussed in detail in a supplementary paper (Kruger & Heinrich, 2004).

In formulating their model Lee *et al.* assume that Axin and β-catenin are the only components that degrade. In more detail, β-catenin is assumed to be labelled for degradation in the 'destruction core cycle' and also is degraded in its free un-complexed form, albeit at a lower rate than destruction-complex-dependent degradation (the 'non-Axin dependent proteolysis' in Figure 2.1). Axin is assumed to degrade only from its free state. The levels of Dishevelled, GSK3β, APC and TCF have not been observed to vary as the Wnt pathway operates, so these components are assumed to be conserved (produced and degraded at the same rates), and are labelled Dsh^0, GSK^0, APC^0 and TCF^0 respectively. Using these approximations Lee *et al.* reduced their system of 15 ODEs to 7 ODEs which we present below. For clarity we use the same notation as Lee *et al.* to represent the
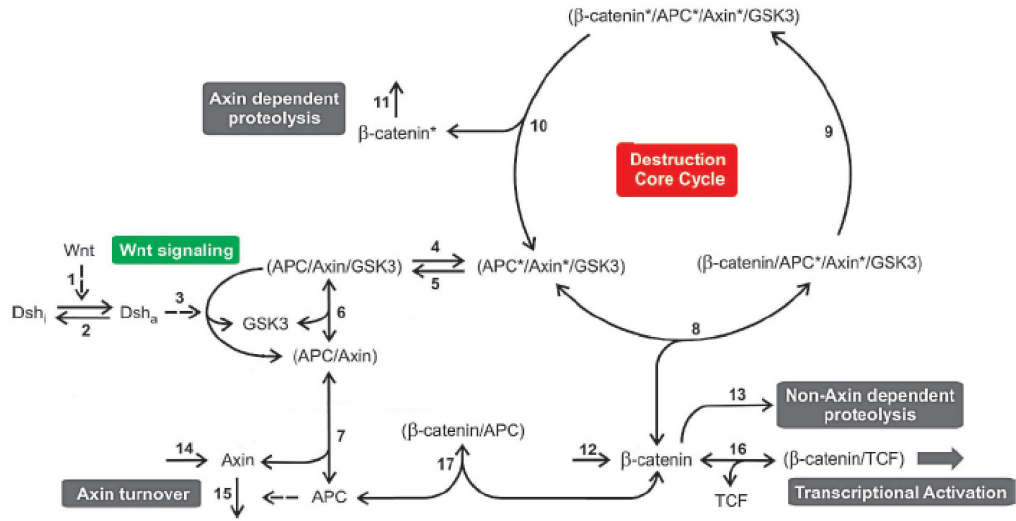
Figure 2.1: The reaction steps of the Wnt pathway, protein complexes being denoted by the names of their components. Phosphorylated components are marked by an asterisk. Single-headed solid arrows characterise reactions taking place only in the indicated direction. Double-headed arrows denote binding equilibria. The broken arrows indicate that the components mediate, but do not participate in, the reaction scheme. The irreversible reactions 2, 4, 5, 9-11, and 13 are unimolecular, and reactions 6, 7, 8, 16, and 17 are reversible binding steps. (Reproduced from Lee *et al.*, 2003, Figure 1.)

model variables, namely the concentrations of

$$X_2(t) \qquad \text{Dishevelled,}$$

$$X_3(t) \qquad \text{Destruction Complex (active),}$$

$$X_4(t) \qquad \text{Destruction Complex (inactive),}$$

$$X_9(t) \qquad \text{Destruction Complex (binding } \beta\text{-}catenin),$$

$$X_{10}(t) \qquad \beta\text{-Catenin (phosphorylated),}$$

$$X_{11}(t) \qquad \beta\text{-Catenin (free),}$$

$$X_{12}(t) \qquad \text{Axin (free),}$$

in units of nM.

In terms of X_2, X_3, X_4, X_9, X_{10}, X_{11} and X_{12}, with reaction constants numbered according to

Figure 2.1, the governing equations can be written as:

$$\frac{\mathrm{d}X_2}{\mathrm{d}t} = k_1 W(Dsh^0 - X_2) - k_2 X_2, \tag{2.1}$$

$$\frac{\mathrm{d}X_4}{\mathrm{d}t} = -(k_3 X_2 + k_4 + k_{-6})X_4 + k_5 X_3 + k_6 GSK^0 \frac{K_{17} X_{12} APC^0}{K_7(K_{17} + X_{11})}, \tag{2.2}$$

$$\frac{\mathrm{d}X_9}{\mathrm{d}t} = K_8 k_9 \frac{X_3}{K_8} \frac{X_{11}}{K_8} - k_{10} X_9, \tag{2.3}$$

$$\frac{\mathrm{d}X_{10}}{\mathrm{d}t} = k_{10} X_9 - k_{11} X_{10}, \tag{2.4}$$

$$\frac{\mathrm{d}X_{12}}{\mathrm{d}t} = \left(k_3 X_2 X_4 - \frac{k_6 GSK^0 APC^0 K_{17} X_{12}}{K_7(K_{17} + X_{11})} + k_{-6} X_4 + v_{14} - k_{15} X_{12} + \right.$$
$$\left. \frac{\mathrm{d}X_{11}}{\mathrm{d}t}\left(\frac{APC^0 K_{17} X_{12}}{K_7(K_{17} + X_{11})^2} \right) \right) \bigg/ \left(1 + \frac{APC^0 K_{17}}{K_7(K_{17} + X_{11})} \right), \tag{2.5}$$

whilst

$$\frac{\mathrm{d}X_3}{\mathrm{d}t} = \left(k_4 X_4 - k_5 X_3 - k_9 X_{11}\frac{X_3}{K_8} + k_{10} X_9 - \frac{1}{1 + \frac{K_8}{X_3}}\left(v_{12} - \left(k_9 \frac{X_3}{K_8} + k_{13} \right) X_{11} \right) \right)$$
$$\bigg/ \left(1 + \left(1 - \frac{1}{1 + \frac{K_8}{X_3}} \right) \frac{X_{11}}{K_8} \right), \tag{2.6}$$

$$\frac{\mathrm{d}X_{11}}{\mathrm{d}t} = \left(k_4 X_4 - k_5 X_3 - k_9 X_{11}\frac{X_3}{K_8} + k_{10} X_9 - \left(\frac{K_8}{X_{11}} + 1 \right)\left(v_{12} - \left(k_9 \frac{X_3}{K_8} + k_{13} \right) X_{11} \right) \right)$$
$$\bigg/ \left(\frac{X_3}{K_8} - \left(\frac{K_8}{X_{11}} + 1 \right)\left(1 + \frac{X_3}{K_8} + \frac{TCF^0 K_{16}}{(K_{16} + X_{11})^2} + \frac{APC^0 K_{17}}{(K_{17} + X_{11})^2} \right) \right), \tag{2.7}$$

where W is a nondimensional forcing term representing the extracellular Wnt concentration. The k's are mass-action rate constants, K's are Michaelis-Menten dissociation constants, and Dsh^0, GSK^0, APC^0 and TCF^0 are the total amounts of these proteins, as discussed earlier. We remark that the ODE for X_{10} decouples from the rest of the system: X_{10} appears only in equation (2.4). This is to be expected since X_{10} is the concentration of free phosphorylated β-catenin which has left the destruction complex and is awaiting ubiquitination and subsequent degradation by proteosomes; as such it can no longer participate in transcription in the nucleus (see Figure 2.1). For this reason we omit X_{10} henceforward.

Lee *et al.* performed *in-vitro* experiments on *Xenopus* egg extracts to estimate the system parameters. They then ran a numerical sensitivity analysis of these equations to find the most important parameters, i.e. the parameters in which small fluctuations caused the largest change in the β-catenin concentration. Lee *et al.* then went back and performed further *in-vitro* experiments to measure these parameters as directly and accurately as possible, and the resulting parameter values are stated in Table 2.2.

The resulting model is then used to predict the result of altering core component concentrations, with the model's cytoplasmic levels of β-catenin matching experiment very convincingly in a number of different scenarios (Lee *et al.*, 2003, Figure 2). The model suggested that the Wnt pathway is most sensitive to fluctuations in $Axin^0$, the total amount of Axin in a cell. Since Axin was found to be present at a much lower concentration than APC (0.02nM as opposed to 100nM), it was proposed that Axin is the limiting factor (and therefore acts as the major regulatory protein) for destruction complex formation. Previously it had been thought that APC must be the most important protein in destruction complex control, as it is the most commonly mutated protein in colorectal cancers (Rowan *et al.*, 2000).

While Lee *et al.* did not perform a systematic non-dimensionalisation of their model, they were able to estimate some of the system parameters. In the following sections we perform a systematic non-dimensionalisation and asymptotic analysis of Lee *et al.*'s model, in order to gain more insight into the processes controlling the levels of β-catenin within a cell.

2.2.2   Model Nondimensionalisation

Equations (2.1)–(2.7) appeared in Lee *et al.* (2003), what follows is our extended analysis of their model. We rescale the model equations by first introducing the nondimensional variables and scalings shown in Table 2.1. Time is scaled such that $t' = k_5 t$ denotes the nondimensional time, chosen because $1/k_5$ is a characteristic timescale for inactivation of the destruction complex, and so we expect it to be an important timescale for the activation of the Wnt pathway.

β-catenin is scaled with K_{16}, the dissociation constant for β-catenin/TCF. Free Axin and all the complexes containing Axin are scaled with v_{14}/k_5 which, we will see later, is the concentration of Axin produced if the system is at equilibrium. Introducing these scalings into equations (2.1)–(2.7) gives the following system of nondimensional equations:

Table 2.1: Model variables and nondimensionalisation scalings

Nondimensional Variable		Scaling	Lee Model Variable	Protein/Complex Description	Lee Model (Figure 2.1) Protein/Complex Notation
$V(t')$	$=$	$\dfrac{1}{Dsh^0}$	X_2	Dishevelled	Dsh_a
$B_a(t')$	$=$	$\dfrac{1}{K_{16}}$	X_{11}	β-catenin (active)	β-catenin
$D_a(t')$	$=$	$\dfrac{k_5}{v_{14}}$	X_3	Destruction Complex (active)	(APC*/Axin*/GSK3)
$D_b(t')$	$=$	$\dfrac{k_5}{v_{14}}$	X_9	Destruction Complex (bound)	(β-catenin*/APC*/Axin*/GSK3)
$D_i(t')$	$=$	$\dfrac{k_5}{v_{14}}$	X_4	Destruction Complex (inactive)	(APC/Axin/GSK3)
$X(t')$	$=$	$\dfrac{k_5}{v_{14}}$	X_{12}	Axin	Axin

$$\frac{\mathrm{d}V}{\mathrm{d}t'} = k_1'W(1-V) - k_2'V, \tag{2.8}$$

$$\frac{\mathrm{d}D_i}{\mathrm{d}t'} = -(k_3'V + k_4' + k_{-6}')D_i + D_a + k_6'\frac{X}{1+K_{16}'B_a}, \tag{2.9}$$

$$\frac{\mathrm{d}D_b}{\mathrm{d}t'} = k_9'B_aD_a - k_{10}'D_b, \tag{2.10}$$

$$\frac{\mathrm{d}X}{\mathrm{d}t'} = \left((k_3'V + k_{-6}')D_i - \left(\frac{k_6'}{(1+K_{16}'B_a)} + k_{15}'\right)X + 1\right.$$
$$\left. + K_{16}'\frac{\mathrm{d}B_a}{\mathrm{d}t'}\frac{K_7'X}{(1+K_{16}'B_a)^2}\right) \bigg/ \left(1 + \frac{K_7'}{(1+K_{16}'B_a)}\right), \tag{2.11}$$

$$\frac{\mathrm{d}D_a}{\mathrm{d}t'} = \left(\left(k_4'D_i - D_a - (k_9'D_aB_a - k_{10}'D_b)\right) - \right.$$
$$\frac{D_aK_8'\left(v_{12}' - k_{14}'D_aB_a - k_{13}'B_a\right)}{1 + k_6'v_{14}'D_a + \frac{TCF^{0'}}{(1+B_a)^2} + \frac{APC^{0'}}{(1+K_{16}'B_a)^2}}\right)$$
$$\bigg/ \left(1 + K_8'B_a - \frac{v_{14}'K_8'B_aD_a}{1 + k_6'v_{14}'D_a + \frac{TCF^{0'}}{(1+B_a)^2} + \frac{APC^{0'}}{(1+K_{16}'B_a)^2}}\right), \tag{2.12}$$

$$\begin{aligned}
\frac{\mathrm{d}B_a}{\mathrm{d}t'} &= \left(\frac{v'_{14}}{K'_8}\Big(k'_4 D_i - D_a - (k'_9 D_a B_a - k'_{10}D_b)\Big) - \right. \\
&\quad \left. \frac{1 + K'_8 B_a}{K'_8 B_a}\Big(v'_{12} - k'_{14}D_a B_a - k'_{13}B_a\Big) \right) \bigg/ \\
&\quad \left(v'_{14}D_a - \frac{1 + K'_8 B_a}{K'_8 B_a}\left(1 + k'_6 v'_{14}D_a + \frac{TCF^{0'}}{(1 + B_a)^2} + \frac{APC^{0'}}{(1 + K'_{16}B_a)^2}\right) \right), \quad (2.13)
\end{aligned}$$

where nondimensional parameters are denoted by primes and their values are shown in Table 2.2.

2.2.3 Numerical Simulations

The results from a numerical simulation of equations (2.8)-(2.13), where a Wnt stimulus is applied between $t' = 0$ and $t' = 300$, are presented in Figure 2.2, and were generated using the numerical stiff ODE solver routine *ode15s* in MatLab. The protein levels are initially given by their steady states in the absence of a Wnt stimulus ($W = 0$), and parameter values are as per Lee *et al.* (2003) (see Table 2.2). The sudden introduction of Wnt leads to a disabling of the destruction complex and a gradual build up of β-catenin. Once the Wnt stimulus is removed the destruction complex is reactivated and β-catenin is degraded until it returns to its original levels. We note that following Wnt stimulation different species respond over markedly different timescales. For example, V (Dishevelled) rapidly evolves to a new steady state value at $t' = 2$, whilst B_a (β-catenin) is still increasing at $t' = 200$. By $t' = 300$ all variables have attained their steady state values. We then remove the Wnt stimulus and the proteins return to their original Wnt-free steady states, again over different timescales.

In the next section we explain how to exploit the fact that the non-dimensional parameters in (2.8)-(2.13) vary markedly in magnitude (see Table 2.2) in order to simplify the model equations.

2.3 Model Analysis

2.3.1 Reduction of Model

The numerical simulation in Figure 2.2 and the variation in the dimensionless parameter estimates in Table 2.2 suggest that processes occur over at least two distinct timescales (it will turn out that there are in fact three distinct timescales). To understand such a complicated model it is therefore necessary to examine the behaviour of each equation on each of the different timescales.

We introduce $\varepsilon = k'_{13} = k_{13}/k_5 = 1.93 \times 10^{-3}$; this small parameter measures the ratio of the rate

Table 2.2: Parameter values from Lee *et al.* (2003) and our nondimensionalised parameters

Dimensional Parameter	Estimate (dimensional)	Units	Non-dimensional Parameter	Estimate (dimensionless)	Scaled Non-dimensional Parameter	Estimate (dimensionless)
Dsh^0	100.0	nM	—	—	—	—
APC^0	100.0	nM	$APC^{0'} = APC^0/K_{17}$	$8.3{\times}10^{-2}$	$\widehat{APC}^0 = \varepsilon^{-1}APC^{0'}$	43.01
TCF^0	15.0	nM	$TCF^{0'} = TCF^0/K_{16}$	0.50	$\widehat{TCF}^0 = \varepsilon^0 TCF^{0'}$	0.50
GSK^0	50.0	nM	—	—	—	—
K_7	50.0	nM	$K_7' = APC^0/K_7$	2.00	$\hat{K}_7 = \varepsilon^0 K_7'$	2.00
K_8	120.0	nM	$K_8' = K_{16}/K_8$	0.25	$\hat{K}_8 = \varepsilon^0 K_8'$	0.25
K_{16}	30.0	nM	$K_{16}' = K_{16}/K_{17}$	$2.5{\times}10^{-2}$	$\hat{K}_{16} = \varepsilon^{-1} K_{16}'$	12.95
K_{17}	1200.0	nM	—	—	—	—
K_{18}	10.0	nM	$K_{18}' = K_{16}/K18$	3.0	$\hat{K}_{18} = \varepsilon^0 K_{18}'$	3.0
k_1	0.182	min^{-1}	$k_1' = k_1/k_5$	1.37	$\hat{k}_1 = \varepsilon^0 k_1'$	1.37
k_2	1.82×10^{-2}	min^{-1}	$k_2' = k_2/k_5$	0.137	$\hat{k}_2 = \varepsilon^0 k_2'$	0.137
k_3	5.0×10^{-2}	nM^{-1} min^{-1}	$k_3' = Dsh^0 k_3/k_5$	0.376	$\hat{k}_3 = \varepsilon^0 k_3'$	0.376
k_4	0.267	min^{-1}	$k_4' = k_4/k_5$	2.01	$\hat{k}_4 = \varepsilon^0 k_4'$	2.01
k_5	0.133	min^{-1}	—	—	—	—
k_6	9.09×10^{-2}	nM^{-1} min^{-1}	$k_6' = \frac{k_6 GSK^0 APC^0}{(K_7 k_5)}$	68.4	$\hat{k}_6 = \varepsilon^0 k_6'$	68.4
k_{-6}	0.909	min^{-1}	$k_{-6}' = k_{-6}/k_5$	6.84	$\hat{k}_{-6} = \varepsilon^0 k_{-6}'$	6.84
k_9	206.0	min^{-1}	$k_9' = k_9 K_{16}/(k_5 K_8)$	387.25	$\hat{k}_9 = \varepsilon^1 k_9'$	0.75
k_{10}	206.0	min^{-1}	$k_{10}' = k_{10}/k_5$	1549	$\hat{k}_{10} = \varepsilon^1 k_{10}'$	2.99
k_{11}	0.417	min^{-1}	$k_{11}' = k_{11}/k_5$	3.14	$\hat{k}_{11} = \varepsilon^0 k_{11}'$	3.14
k_{13}	2.57×10^{-4}	min^{-1}	$k_{13}' = k_{13}/k_5$	1.93×10^{-3}	$\varepsilon = k_{13}'$	—
k_{15}	0.167	min^{-1}	$k_{15}' = k_{15}/k_5$	1.26	$\hat{k}_{15} = \varepsilon^0 k_{15}'$	1.26
k_{18}	1.0×10^{-6}	min^{-1}	$k_{18}' = k_{18} K_{16}/v_{14}$	0.365	$\hat{k}_{18} = \varepsilon^0 k_{18}'$	0.365
k_{18b}	1.0×10^{-4}	nM min^{-1}	$k_{18b}' = k_{18b} K_{16}/(v_{14} K_{18})$	3.65	$\hat{k}_{18b} = \varepsilon^0 k_{18b}'$	3.65
v_{12}	0.423	nM min^{-1}	$v_{12}' = v_{12}/(k_5 K_{16})$	0.106	$\hat{v}_{12} = \varepsilon^{-1} v_{12}'$	54.92
v_{14}	8.22×10^{-5}	nM min^{-1}	$v_{14}' = v_{14}/(k_5 K_8)$	5.15×10^{-6}	$\hat{v}_{14} = \varepsilon^{-2} v_{14}'$	1.38
			$k_{14}' = k_9 v_{14}'/k_5$	7.98×10^{-3}	$\hat{k}_{14} = \varepsilon^{-1} k_{14}'$	4.13
			W	1.00	$\hat{W} = \varepsilon^0 W$	1.00
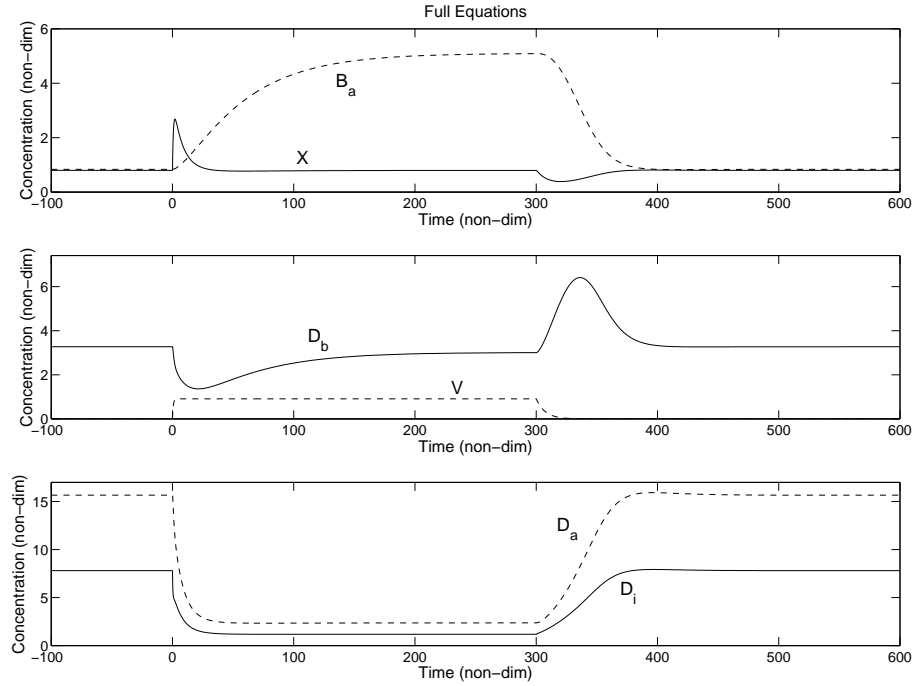
Figure 2.2: A simulation of equations (2.8)-(2.13), for which the Wnt stimulus, W, is increased suddenly from 0 to 1 at time $t = 0$ and removed at $t = 300$. Top: solid line X (Axin), dashed line B_a (β-catenin). Middle: solid line D_b (destruction complex bound to β-catenin), dashed line V (active Dishevelled). Bottom: solid line D_i (inactive destruction complex), dashed line D_a (active destruction complex). Parameter values can be found in Table 2.2 and the initial conditions are the steady states for $W = 0$, shown in Table 2.3.

at which β-catenin is degraded in a destruction-complex-independent manner compared to the rate at which the destruction complex becomes inactive. Guided by Lee *et al.*'s parameter estimates (see Table 2.2) we rescale the dimensionless parameters by multiplying them by appropriate powers of ε so that they are $O(1)$ (this process cannot of course be done unambiguously). In our system each equation must be capable of displaying a steady state on each timescale, so that for example $\hat{k}_6$ is chosen to be equal to $\varepsilon^0 k_6'$ instead of $\varepsilon^1 k_6'$ to avoid an unrealistic exponential increase in D_b on an $O(\varepsilon)$ timescale (equation (2.16)). The transformed parameters are denoted by ˆ's and their values are shown in the last column of Table 2.2. Under these parameter transformations, and dropping

Table 2.3: Initial conditions for the Lee *et al.* (2003) Wnt Signalling Model, for dimensional and nondimensional variables. These values are referred to in Lee *et al.* (2003) as the 'reference state', the steady state in the absence of Wnt signalling ($W = 0$).

Nondimensional			Dimensional		
Variable		Value	Variable		Value	Units
$V(0)$	$=$	0	$X_2(0)$	$=$	0	nM
$B_a(0)$	$=$	0.836	$X_{11}(0)$	$=$	25.1	nM
$D_a(0)$	$=$	15.7	$X_3(0)$	$=$	4.83×10^{-3}	nM
$D_b(0)$	$=$	3.27	$X_9(0)$	$=$	2.02×10^{-3}	nM
$D_i(0)$	$=$	7.80	$X_4(0)$	$=$	4.83×10^{-3}	nM
$X(0)$	$=$	0.796	$X_{12}(0)$	$=$	4.93×10^{-3}	nM

the primes on time t for ease of notation, equations (2.8)-(2.13) become

$$\frac{\mathrm{d}V}{\mathrm{d}t} = \hat{k}_1 W(1-V) - \hat{k}_2 V, \tag{2.14}$$

$$\frac{\mathrm{d}D_i}{\mathrm{d}t} = -(\hat{k}_3 V + \hat{k}_4 + \hat{k}_{-6})D_i + D_a + \hat{k}_6 \frac{X}{1 + \varepsilon \hat{K}_{16} B_a}, \tag{2.15}$$

$$\frac{\mathrm{d}D_b}{\mathrm{d}t} = \varepsilon^{-1}\left(\hat{k}_9 B_a D_a - \hat{k}_{10} D_b\right), \tag{2.16}$$

$$\frac{\mathrm{d}X}{\mathrm{d}t} = \left((\hat{k}_3 V + \hat{k}_{-6})D_i - \left(\frac{\hat{k}_6}{(1 + \varepsilon \hat{K}_{16} B_a)} + \hat{k}_{15}\right)X + 1 \right.$$
$$\left. + \varepsilon \hat{K}_{16} \frac{\mathrm{d}B_a}{\mathrm{d}t} \frac{\hat{K}_7 X}{(1 + \varepsilon \hat{K}_{16} B_a)^2}\right) \Bigg/ \left(1 + \frac{\hat{K}_7}{(1 + \varepsilon \hat{K}_{16} B_a)}\right), \tag{2.17}$$

$$\frac{\mathrm{d}D_a}{\mathrm{d}t} = \left(\left(\hat{k}_4 D_i - D_a - \frac{1}{\varepsilon}(\hat{k}_9 D_a B_a - \hat{k}_{10} D_b)\right) - \right.$$
$$\frac{\varepsilon D_a K_8' \left(\hat{v}_{12} - \hat{k}_{14} D_a B_a - B_a\right)}{1 + \varepsilon^2 \hat{k}_6 \hat{v}_{14} D_a + \frac{\widehat{TCF}^0}{(1+B_a)^2} + \frac{\varepsilon \widehat{APC}^0}{(1+\varepsilon \hat{K}_{16} B_a)^2}}\right)$$
$$\Bigg/ \left(1 + \hat{K}_8 B_a - \frac{\varepsilon^2 \hat{v}_{14} \hat{K}_8 B_a D_a}{1 + \varepsilon^2 \hat{k}_6 \hat{v}_{14} D_a + \frac{\widehat{TCF}^0}{(1+B_a)^2} + \frac{\varepsilon \widehat{APC}^0}{(1+\varepsilon \hat{K}_{16} B_a)^2}}\right), \tag{2.18}$$

$$\frac{\mathrm{d}B_a}{\mathrm{d}t} = \left(\varepsilon^2 \frac{\hat{v}_{14}}{\hat{K}_8}\left(\hat{k}_4 D_i - D_a - \frac{1}{\varepsilon}(\hat{k}_9 D_a B_a - \hat{k}_{10} D_b)\right) - \right.$$
$$\varepsilon\left(\frac{1 + \hat{K}_8 B_a}{\hat{K}_8 B_a}\right)\left(\hat{v}_{12} - \hat{k}_{14} D_a B_a - B_a\right)\Bigg/$$
$$\left(\varepsilon^2 \hat{v}_{14} D_a - \frac{1 + \hat{K}_8 B_a}{\hat{K}_8 B_a}\left(1 + \varepsilon^2 \hat{k}_6 \hat{v}_{14} D_a + \frac{\widehat{TCF}^0}{(1+B_a)^2} + \frac{\varepsilon \widehat{APC}^0}{(1+\varepsilon \hat{K}_{16} B_a)^2}\right)\right). \tag{2.19}$$

Rearranged in powers of ε equations (2.18) and (2.19) read

$$\frac{\mathrm{d}D_a}{\mathrm{d}t} = -\frac{1}{\varepsilon}\frac{\left(\hat{k}_9 D_a B_a - \hat{k}_{10}D_b\right)}{1+\hat{K}_8 B_a} + \frac{\hat{k}_4 D_i - D_a}{1+\hat{K}_8 B_a} + O(\varepsilon).$$

$$\frac{\mathrm{d}B_a}{\mathrm{d}t} = \varepsilon\left(\left(\hat{v}_{12} - \hat{k}_{14}D_a B_a - B_a\right) - \frac{\hat{v}_{14}B_a}{1+\hat{K}_8 B_a}\left(\hat{k}_9 D_a B_a - \hat{k}_{10}D_b\right) + O(\varepsilon)\right)$$
$$\bigg/\left(1 + \frac{\widehat{TCF}^0}{(1+B_a)^2} + O(\varepsilon)\right).$$

Since $\widehat{TCF}^0 = 0.5$ and numerical simulations show that $B_a > 1$, then $\widehat{TCF}^0/(1+B_a)^2 < \frac{1}{8}$, so we treat the grouping $\widehat{TCF}^0/(1+B_a)^2$ as small relative to 1, as a result the ODE for B_a can be simplified to read

$$\frac{\mathrm{d}B_a}{\mathrm{d}t} = \varepsilon\left(\left(\hat{v}_{12} - \hat{k}_{14}D_a B_a - B_a\right) - \frac{\hat{v}_{14}B_a}{1+\hat{K}_8 B_a}\left(\hat{k}_9 D_a B_a - \hat{k}_{10}D_b\right)\right) + O(\varepsilon^2). \tag{2.20}$$

Using (2.20) in equation (2.17) we find that

$$\frac{\mathrm{d}X}{\mathrm{d}t} = \left(\left(\hat{k}_3 V + \hat{k}_{-6}\right)D_i - \left(\hat{k}_6 + \hat{k}_{15}\right)X + 1\right)\bigg/\left(1 + \hat{K}_7\right) + O(\varepsilon). \tag{2.21}$$

Combining the above results and retaining only the dominant terms, our reduced model can be written

$$\frac{\mathrm{d}V}{\mathrm{d}t} = \hat{k}_1\hat{W}(1-V) - \hat{k}_2 V, \tag{2.22}$$

$$\frac{\mathrm{d}D_i}{\mathrm{d}t} = -(\hat{k}_3 V + \hat{k}_4 + \hat{k}_{-6})D_i + D_a + \hat{k}_6 X, \tag{2.23}$$

$$\varepsilon\frac{\mathrm{d}D_b}{\mathrm{d}t} = \hat{k}_9 D_a B_a - \hat{k}_{10}D_b, \tag{2.24}$$

$$\frac{\mathrm{d}X}{\mathrm{d}t} = \frac{\left(\hat{k}_3 V + \hat{k}_{-6}\right)D_i - \left(\hat{k}_6 + \hat{k}_{15}\right)X + 1}{1 + \hat{K}_7}, \tag{2.25}$$

$$\frac{\mathrm{d}D_a}{\mathrm{d}t} = -\frac{1}{\varepsilon}\frac{\left(\hat{k}_9 D_a B_a - \hat{k}_{10}D_b\right)}{1+\hat{K}_8 B_a} + \frac{\hat{k}_4 D_i - D_a}{1+\hat{K}_8 B_a}, \tag{2.26}$$

$$\frac{1}{\varepsilon}\frac{\mathrm{d}B_a}{\mathrm{d}t} = \left(\hat{v}_{12} - \hat{k}_{14}D_a B_a - B_a\right) - \frac{\hat{v}_{14}B_a}{1+\hat{K}_8 B_a}\left(\hat{k}_9 D_a B_a - \hat{k}_{10}D_b\right). \tag{2.27}$$

We note that equation (2.22) decouples from equations (2.23) – (2.27) and admits an analytic solution for V when there is a constant Wnt stimulus (i.e. $W(t) = \hat{W}$, constant):

$$V(t) = \frac{\hat{k}_1\hat{W}}{\hat{k}_1\hat{W} + \hat{k}_2} + \frac{-\hat{k}_1\hat{W} + (\hat{k}_1\hat{W} + \hat{k}_2)V_0}{\hat{k}_1\hat{W} + \hat{k}_2}e^{-(\hat{k}_1\hat{W}+\hat{k}_2)t} \longrightarrow \frac{\hat{k}_1\hat{W}}{\hat{k}_1\hat{W} + \hat{k}_2} \quad \text{as} \quad t \to \infty.$$

We note further that equations (2.24) and (2.27) have time derivatives that are multiplied by orders of ε. This suggests that the system has processes that operate on different timescales, and is consistent with the sudden spikes and slow accumulations shown in Figure 2.2. In the next section we analyse the system's behaviour on the different $O(\varepsilon^n)$ timescales.

2.3.2   Asymptotic Analysis

As revealed in the previous section, equations (2.22)–(2.27) operate on distinct timescales. This situation can arise if some reactions happen faster than others, but also when proteins at a low concentration (such as the destruction complex) act on populations of proteins at high concentrations (such as β-catenin). We might therefore expect the destruction complex concentration to change more quickly than the β-catenin concentration.

We will analyse the model on short, medium and long timescales, for which $t = O(\varepsilon)$, $t = O(1)$ and $t = O(\varepsilon^{-1})$ respectively, since these timescales appear on the left-hand side of equations (2.22)–(2.27) and appear to give a complete description of the $\varepsilon \to 0$ asymptotic behaviour. In each case asymptotic expansions in powers of ε are sought for the dependent variables and used to simplify the governing equations. We will explain why the different timescales appear and their physical significance. We consider the situation shown in Figure 2.2 where a Wnt stimulus is applied to a system which is initially at its Wnt-free equilibrium.

Short Timescale, $t = O(\varepsilon)$: the phosphorylation of bound β-catenin

Noting from equation (2.24) that the shortest timescale is $O(\varepsilon)$, we now introduce a new timescale, $\tau = t/\varepsilon$. We seek solutions on this short timescale that are regular power series expansions in ε so that, for example

$$V(\tau) = V_0(\tau) + \varepsilon V_1(\tau) + \varepsilon^2 V_2(\tau) + \dots$$

Firstly we substitute this approximation into equation (2.22) to give

$$\frac{\mathrm{d}}{\mathrm{d}\tau}(V_0 + \varepsilon V_1) \;\; = \;\; \varepsilon\left(k_1' W\left(1 - V_0 - \varepsilon V_1\right) - k_2' V_0 - \varepsilon k_2' V_1\right).$$

Equating coefficients of $O(\varepsilon^n)$ gives

$$\begin{aligned}
\frac{\mathrm{d}V_0}{\mathrm{d}\tau} &= 0, \\
\frac{\mathrm{d}V_1}{\mathrm{d}\tau} &= k_1' W(1 - V_0) - k_2' V_0.
\end{aligned} \tag{2.28}$$

We find that in all cases the leading order behaviour captures the necessary system dynamics and the correction terms are not important. So $V_0(\tau) = constant = V(0)$ and we have a linear ODE for $V_1(\tau)$. Applying the same procedure to equations (2.23)-(2.27) it is straightforward to show that

$$\frac{\mathrm{d}D_{i0}}{\mathrm{d}\tau} = 0, \quad \frac{\mathrm{d}X_0}{\mathrm{d}\tau} = 0, \quad \frac{\mathrm{d}B_{a0}}{\mathrm{d}\tau} = 0, \tag{2.29}$$
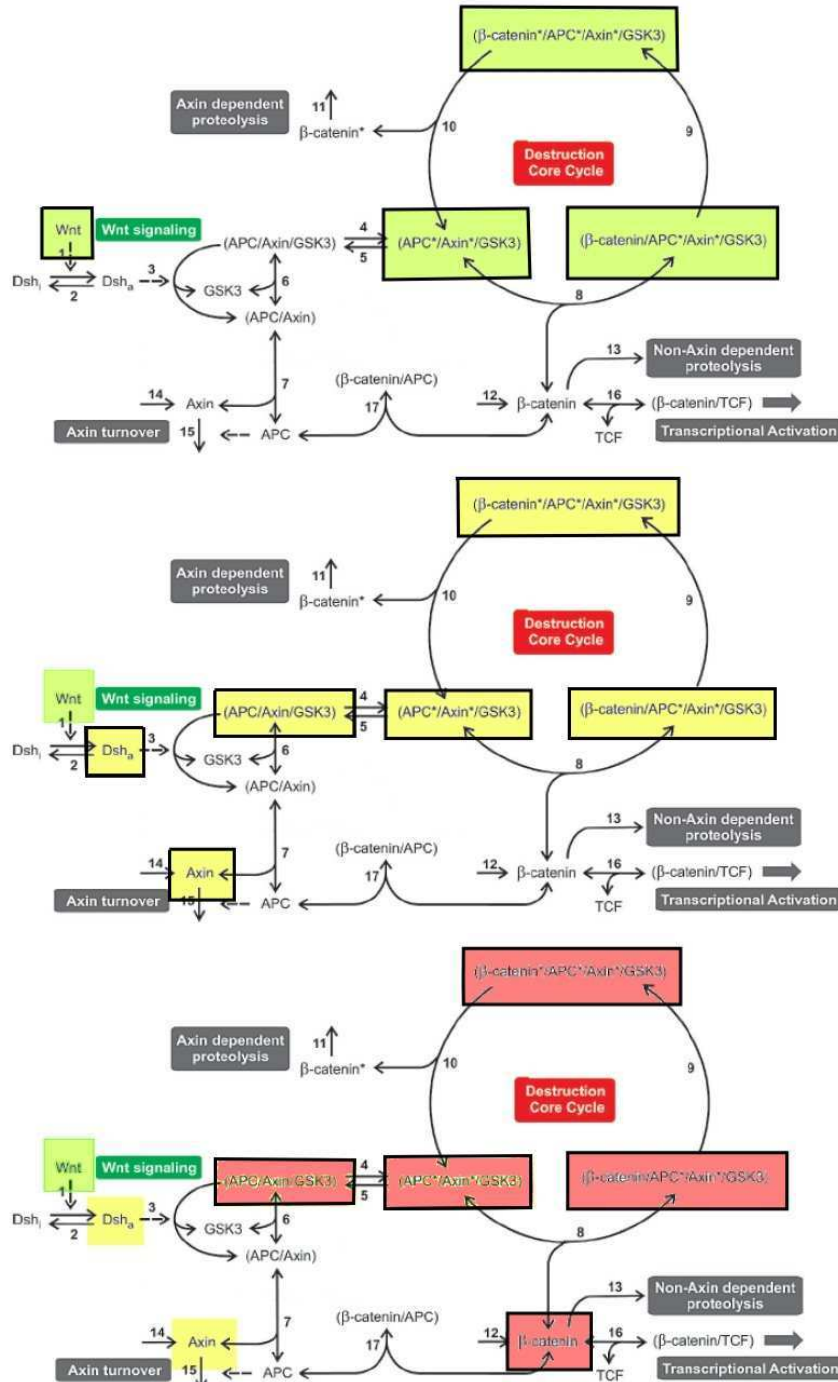
Figure 2.3: Components of the signalling pathway which vary over short (top), medium (middle) and long (bottom) timescales. The active components on each timescale are highlighted with bold borders. The schematic is based upon Figure 2.1, which is adapted from Lee *et al.* (2003, Figure 1).

$$\frac{\mathrm{d}D_{a0}}{\mathrm{d}\tau} = -\left(\hat{k}_9 B_{a0} D_{a0} - \hat{k}_{10} D_{b0}\right)\Big/\left(1 + \hat{K}_8 B_{a0}\right), \tag{2.30}$$

$$\frac{\mathrm{d}D_{b0}}{\mathrm{d}\tau} = \left(\hat{k}_9 B_{a0} D_{a0} - \hat{k}_{10} D_{b0}\right). \tag{2.31}$$

Noting that $B_{a0} = B_a(0)$, equations (2.30) and (2.31) can be solved analytically to give the solutions

$$D_{a0}(\tau) = \alpha e^{-\gamma\tau} + \mu, \tag{2.32}$$

$$D_{b0}(\tau) = \zeta e^{-\gamma\tau} + \eta, \tag{2.33}$$

where

$$\gamma = \frac{\phi}{1 + \hat{K}_8 B_a(0)},$$

$$\alpha = \frac{\hat{k}_9 D_a(0) B_a(0) - \hat{k}_{10} D_b(0)}{\phi},$$

$$\mu = \hat{k}_{10} \frac{D_a(0) + \hat{K}_8 D_a(0) B_a(0) + D_b(0)}{\phi},$$

$$\zeta = \frac{\hat{k}_{10} \hat{K}_8 B_a(0) D_b(0) - \hat{k}_9 D_a(0) B_a(0) + \hat{k}_{10} D_b(0) - \hat{k}_9 \hat{K}_8 D_a(0) B_a(0)^2}{\phi},$$

$$\eta = \frac{\hat{k}_9}{\hat{k}_{10}} B_a(0)\mu,$$

$$\phi = \hat{k}_{10} + \hat{k}_9 B_a(0) + \hat{k}_{10} \hat{K}_8 B_a(0).$$

Using equations (2.32) and (2.33) it is straightforward to see that, on this short timescale, D_a and D_b evolve from their initial conditions $D_a(0)$ and $D_b(0)$ to limiting values (D_{a0}^{∞} and D_{b0}^{∞}) which are related as follows

$$D_{b0}^{\infty} = \frac{\hat{k}_9}{\hat{k}_{10}} B_a(0) D_{a0}^{\infty},$$

Once D_a and D_b reach this equilibrium no other processes occur until $t = O(1)$, with the other variables retaining their initial conditions.

From equations (2.32) and (2.33) we deduce that the values of the steady state solutions depend upon the initial concentrations and the concentration of active β-catenin, B_a (which does not vary on this timescale, equation (2.29)). The dominant biological processes occurring on this fast timescale therefore involve only D_a and D_b, the active destruction complex and the β-catenin bound destruction complex, i.e. the components of the 'destruction core cycle' (see top schematic of Figure 2.3). The characteristic reaction for this timescale is therefore the phosphorylation (and release) of β-catenin by the destruction complex; the 'destruction core cycle' settles into an equilibrium faster than any of the other components change (either the amount of destruction complex in the core cycle or the amount of free β-catenin). Note that the 'destruction core cycle' consists of three components. Lee *et al.*'s (2003) model employs only two equations for these three components since they assumed

that β-catenin/APC*/Axin*/GSK3β quickly reached an equilibrium value. We will see in the next section that this approximation could also have been made for D_b without affecting the behaviour of the system.

In Figures 2.4 and 2.5 we introduce a Wnt stimulus into a pathway which has achieved equilibrium (defined in Table 2.3). Although reactions between D_a and D_b are happening on the short timescale, they are, as yet, independent of Wnt signalling since Dishevelled, V, does not become activated on this timescale (equation (2.28)), and no downstream components of the pathway can be affected. D_a and D_b therefore remain at their initial values. We compare the predicted steady concentrations with the numerical solutions of the full equations (2.8)-(2.13) in Figures 2.4 and 2.5. The short time approximations of the variables are in good agreement with the numerical solutions of the full model until time $t = O(1)$; in the next section we consider the system's behaviour for $t = O(1)$.

Intermediate Timescale, $t = O(1)$: formation of active destruction complex

As before, we seek model solutions that are regular power series expansions in ε, so that, for example

$$V(t) = V_0(t) + \varepsilon V_1(t) + \varepsilon^2 V_2(t) + \dots$$

Substituting into equation (2.22) and equating coefficients of ε gives

$$\frac{\mathrm{d}V_0}{\mathrm{d}t} = \hat{k}_1 \hat{W}(1 - V_0) - \hat{k}_2 V_0,$$

while substitution into equations (2.23)–(2.27) produces the following set of leading order equations for times $t = O(1)$

$$B_{a0}(t) = B_a(0), \tag{2.34}$$

$$D_{b0}(t) = \frac{\hat{k}_9}{\hat{k}_{10}} B_a(0) D_{a0}(t), \tag{2.35}$$

$$\frac{\mathrm{d}V_0}{\mathrm{d}t} = \hat{k}_1 \hat{W}(1 - V_0) - \hat{k}_2 V_0, \tag{2.36}$$

$$\frac{\mathrm{d}D_{a0}}{\mathrm{d}t} = \left(\hat{k}_4 D_{i0} - D_{a0} \right) \Big/ \left(1 + \hat{K}_8 B_a(0) + \frac{\hat{k}_9}{\hat{k}_{10}} B_a(0) \right), \tag{2.37}$$

$$\frac{\mathrm{d}D_{i0}}{\mathrm{d}t} = -(\hat{k}_3 V_0 + \hat{k}_4 + \hat{k}_{-6}) D_{i0} + D_{a0} + \hat{k}_6 X_0, \tag{2.38}$$

$$\frac{\mathrm{d}X_0}{\mathrm{d}t} = \left(\hat{k}_3 V_0 D_{i0} + \hat{k}_{-6} D_{i0} + 1 - \hat{k}_{15} X_0 - \hat{k}_6 X_0 \right) \Big/ \left(1 + \hat{K}_7 \right). \tag{2.39}$$

At this intermediate timescale B_a is still constant; we have an algebraic expression for D_b and four ODEs to describe the intermediate timescale behaviour. Plots of numerical solutions to equations
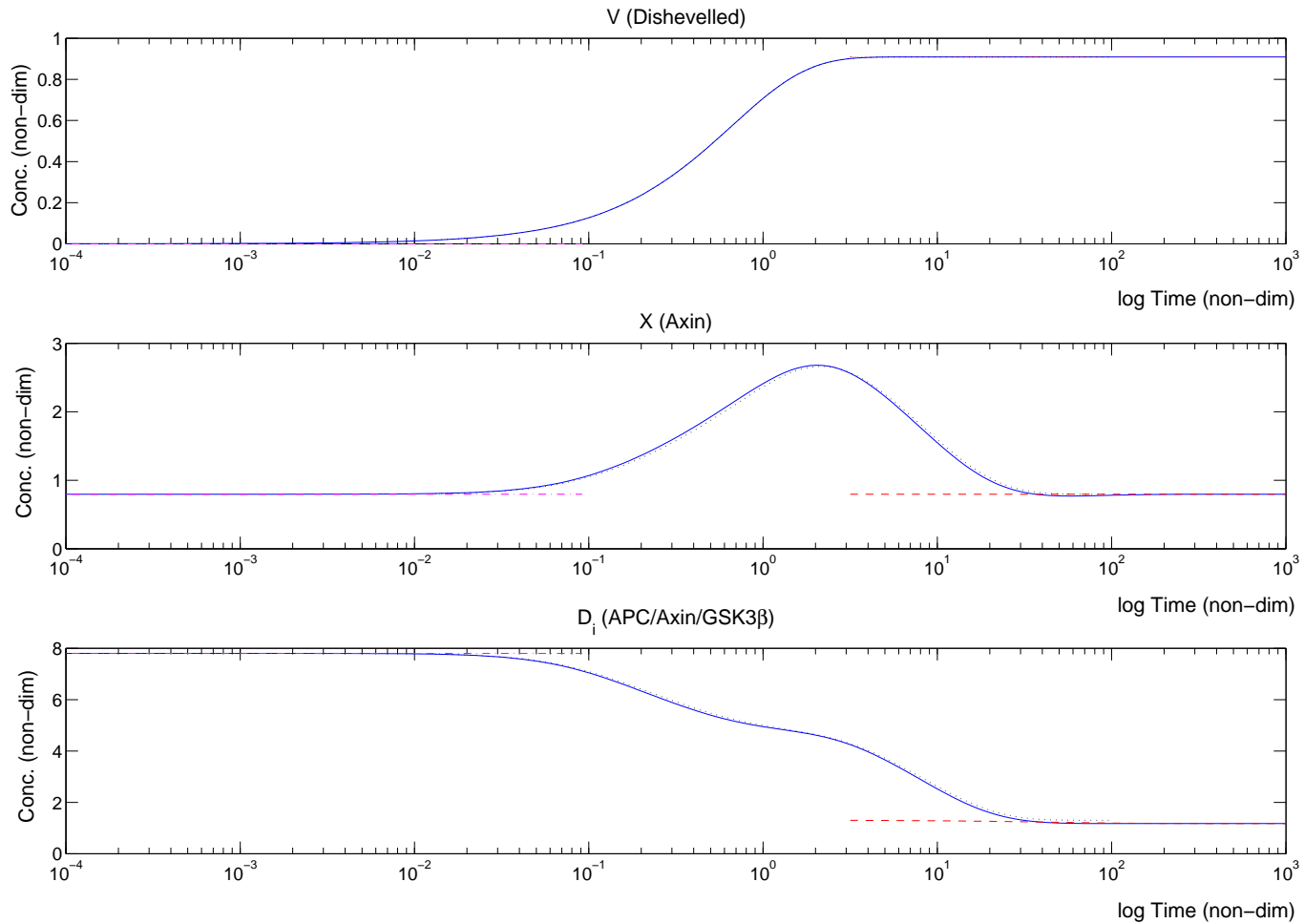
Figure 2.4: Model reaction to a sudden Wnt stimulus ($W = 1$) introduced into a system in equilibrium ($W = 0$) at $t = 0$. Numerical simulations of equations (2.8)–(2.13) are shown with a solid line. Short, medium and long time approximations are shown with dash-dotted, dotted and dashed lines respectively. There is good agreement between the approximations and numerical solutions at all timescales. Parameter values can be found in Table 2.2.
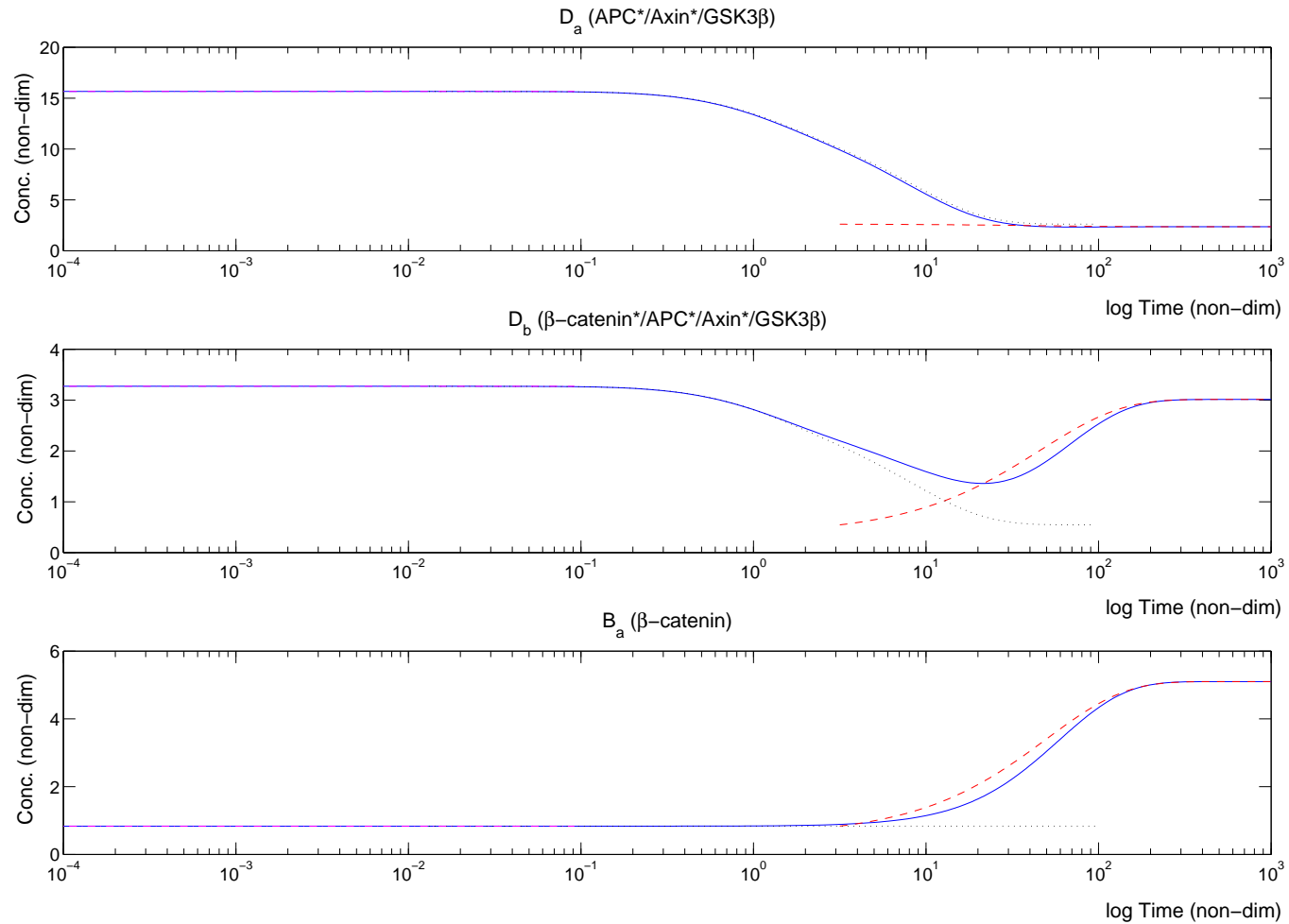
Figure 2.5: Model reaction to a sudden Wnt stimulus ($W = 1$) introduced into a system in equilibrium ($W = 0$) at $t = 0$. Numerical simulations of equations (2.8)–(2.13) are shown with a solid line. Short, medium and long time approximations are shown with dash-dotted, dotted and dashed lines respectively. There is good agreement between the approximations and numerical solutions at all timescales. Parameter values can be found in Table 2.2.

(2.36)–(2.39) are shown in Figures 2.4 and 2.5 and the results compare well with solutions of the original equations (2.8)–(2.13).

The Wnt stimulus now affects most of the pathway; we highlight components that change on this intermediate timescale in yellow in the middle schematic of Figure 2.3. Dishevelled is activated and lowers the level of the destruction complex (in all its forms) causing Axin levels to build up. We examine these processes in more detail below. The interpretation of equations (2.34)–(2.39) is aided by studying Figures 2.3, 2.4 and 2.5.

As we see in Figure 2.1, the initial response to a Wnt signal is in equation (2.36) as Dishevelled is the only protein directly activated by Wnt, and so V_0 (active Dishevelled protein) rises. The increase in V_0 leads to more of the inactive destruction complex (D_i =APC/Axin/GSK3β) being decomposed into GSK3β and APC/Axin (the first term in equation (2.38)). At the same time the level of free Axin (X) rises (the first term in equation (2.39)) as Lee *et al.* made a rapid equilibrium approximation for the $APC/Axin \rightleftharpoons APC + Axin$ reaction. The level of Axin (X) reaches a maximum at approximately the same time as V reaches its new steady state.

Equation (2.37) shows how the level of active destruction complex (D_a) falls as a result of the reduction of inactive complex (D_i), since the system moves to restore the equilibrium

$$(\text{APC/Axin/GSK3}\beta) \rightleftharpoons (\text{APC*/Axin*/GSK3}\beta).$$
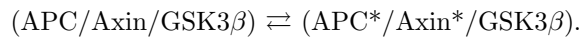
Equation (2.35) is a rapid equilibrium approximation for the reactions happening on the fast timescale (equations (2.32) and (2.33)) and states that the level of bound destruction complex D_b (phosphorylating β-catenin) will be proportional to the level of active destruction complex (D_a) and active β-catenin (B_a, which is not changing over this timescale). Therefore the level of bound destruction complex, D_b, falls in line with the level of active destruction complex, D_a. Note that the 'destruction core cycle' reactions occur on the faster timescale ($t = O(\varepsilon)$), but their 'equilibrium' values are now changing because D_a is evolving over this intermediate timescale, as a result of the fall in D_i.

As the level of Axin quickly reaches a maximum, the decomposition of D_i is slowed (equation (2.38)). The free pool of Axin then more slowly reduces ($\hat{k}_{15} \approx 1$ as opposed to $\hat{k}_6 \approx 70$) to its steady state value, whilst the inactive and active destruction complex levels also gradually re-adjust to this new level of Axin.

The characteristic reaction for this intermediate timescale is therefore the inactivation of the destruction complex. Note that B_a, the level of free β-catenin, still does not change (equation (2.34)): it evolves over an even longer timescale, which we examine in the next section.

Long Timescale, $t = O(\varepsilon^{-1})$: degradation of free β-catenin

Equation (2.27) suggests that the longest timescale of interest is of $O(\varepsilon^{-1})$. In terms of this long timescale $T = \varepsilon t$ equations (2.22)–(2.27) become

$$\varepsilon \frac{\mathrm{d}V}{\mathrm{d}T} = \hat{k}_1 \hat{W}(1-V) - \hat{k}_2 V, \tag{2.40}$$

$$\varepsilon \frac{\mathrm{d}D_i}{\mathrm{d}T} = -(\hat{k}_3 V + \hat{k}_4 + \hat{k}_{-6})D_i + D_a + \hat{k}_6 \frac{X}{1 + K'_{16}B_a}, \tag{2.41}$$

$$\varepsilon^2 \frac{\mathrm{d}D_b}{\mathrm{d}T} = \hat{k}_9 D_a B_a - \hat{k}_{10} D_b, \tag{2.42}$$

$$\varepsilon \frac{\mathrm{d}X}{\mathrm{d}T} = \left((\hat{k}_3 V + \hat{k}_{-6})D_i - \left(\frac{\hat{k}_6}{(1 + \varepsilon \hat{K}_{16}B_a)} + \hat{k}_{15} \right) X + 1 \right)$$
$$\left/ \left(1 + \frac{\hat{K}_7}{(1 + \varepsilon \hat{K}_{16}B_a)} \right), \right. \tag{2.43}$$

$$\varepsilon^2 \frac{\mathrm{d}D_a}{\mathrm{d}T} = \frac{\varepsilon(\hat{k}_4 D_i - D_a) - (\hat{k}_9 D_a B_a - \hat{k}_{10} D_b)}{1 + \hat{K}_8 B_a}, \tag{2.44}$$

$$\frac{\mathrm{d}B_a}{\mathrm{d}T} = \left(\hat{v}_{12} - \hat{k}_{14}D_a B_a - B_a \right) - \frac{\hat{v}_{14}B_a}{1 + \hat{K}_8 B_a} \left(\hat{k}_9 D_a B_a - \hat{k}_{10} D_b \right). \tag{2.45}$$

Assuming that the dependent variables can be expanded as regular power series in ε and equating to zero coefficients of $O(1)$ in equation (2.40) we obtain the following relationship between $V_0(T)$ and the applied Wnt stimulus $W(T)$:

$$V_0(T) = \frac{\hat{k}_1 W(T)}{\hat{k}_1 W(T) + \hat{k}_2}.$$

Similarly equations (2.41)–(2.45) give rise to the following equations for the leading-order behaviour on the long timescale:

$$X_0(T) = \frac{1}{\hat{k}_{15}}, \tag{2.46}$$

$$V_0(T) = \frac{\hat{k}_1 W(T)}{\hat{k}_1 W(T) + \hat{k}_2}, \tag{2.47}$$

$$D_{i0}(T) = \frac{X_0(T)\hat{k}_6}{\left(\hat{k}_3 V_0(T) + \hat{k}_{-6} \right)\left(1 + K'_{16}B_{a0}(T) \right)}, \tag{2.48}$$

$$D_{a0}(T) = \hat{k}_4 D_{i0}(T), \tag{2.49}$$

$$D_{b0}(T) = \frac{\hat{k}_9}{\hat{k}_{10}} D_{a0}(T)B_{a0}(T), \tag{2.50}$$

$$\frac{\mathrm{d}}{\mathrm{d}T} B_{a0}(T) = \hat{v}_{12} - \left(\hat{k}_{14}D_{a0}(T) + 1 \right) B_{a0}(T). \tag{2.51}$$

The components of the pathway that vary on the long timescale are highlighted on the bottom schematic of Figure 2.3; over this long timescale only the level of free β-catenin (B_a) and the level of

destruction-complex-bound β-catenin (D_b) vary. In Figures 2.4 and 2.5 we show the good agreement between the approximate solutions and those of the full system (equations (2.8)–(2.13)).

On the intermediate timescale we saw how destruction complex levels were controlled by the introduction of Wnt via the action of Dishevelled. On this timescale the level of destruction complex controls the rate at which β-catenin is degraded, whereas Axin (X) has already evolved to a steady level that is independent of Wnt signalling (equation (2.46)). In contrast, the final levels of D_i and D_a depend, via V, on the Wnt signal strength (see equations (2.48) and (2.49)).

Under an increased Wnt stimulus the level of active β-catenin, B_a, increases because there is less active destruction complex, D_a, present for its degradation (equation (2.51)). Interestingly, and perhaps counter-intuitively, the level of bound destruction complex, D_b, increases over this timescale, having decreased over the intermediate timescale (see Figure 2.5). In fact, on medium and long timescales D_b is proportional to both the levels of active destruction complex and active β-catenin (equation (2.35) and (2.50)). For this reason, the level of D_b falls as active destruction complex is removed, and rises again as β-catenin builds up. At the steady state, however, there is a slightly lower level of D_b when the Wnt signal is active, and much lower levels of D_a and D_i. It is simply the case that any destruction complex that is present will quickly bind to free β-catenin, as there is so much more β-catenin around.

The characteristic reaction for this long timescale is therefore the degradation of free β-catenin, which is surprising given that the characteristic reaction for the fastest timescale was the action of the 'destruction core cycle'. The reason this can happen is the disparity between the low levels of destruction complex and the high levels of β-catenin.

If we are interested in the levels of β-catenin produced in response to a Wnt signal then there is no need to consider the action of Wnt on shorter timescales; the long timescale analysis captures the dynamics of β-catenin. In the above sections we analysed the behaviour of the Lee *et al.* (2003) model on different timescales and have found that only one ODE is relevant at such long times. In the next section we consider how this single ODE performs as a simpler Wnt signalling model.

2.3.3   Reduction to a simpler Wnt signalling model

We have seen that the accumulation of active β-catenin occurs only on a long timescale. Since active β-catenin is the major downstream target of the Wnt pathway, it is often the only protein of interest to those studying the pathway. In this regard equation (2.51), a single ODE, describes the output of the whole signalling pathway. In terms of the original dimensional variables, equation (2.51) takes

the form

$$\frac{\mathrm{d}X_{11}}{\mathrm{d}t} = v_{12} - \left(a\big(W(t)\big)\frac{K_{17}}{K_{17} + X_{11}(t)} + k_{13}\right)X_{11}(t),\tag{2.52}$$

where

$$a\big(W(t)\big) = \frac{k_4 k_6 k_9 v_{14} GSK^0 APC^0}{k_5 k_{15} K_7 K_8}\left(\frac{k_1 W(t) + k_2}{(k_1 k_3 Dsh^0 + k_1 k_{-6})W(t) + k_2 k_{-6}}\right).\tag{2.53}$$

with all parameter values as given by Lee *et al.* (2003) (see Table 2.2). Note that $a\big(W(t)\big)$ has a Michaelis-Menten type dependence on $W(t)$, meaning that β-catenin levels can increase in response to a Wnt stimulus, but the rate reaches a saturation point with increasing Wnt.

A comparison of the steady states of equation (2.52) with those of the original system of equations (2.1)–(2.7) is shown in Figure 2.6. The reduced model behaves in exactly the same way as the full model at low Wnt stimulus and follows the same trend as Wnt levels are increased. The equilibrium β-catenin concentration at a high Wnt stimulus associated with the reduced model is slightly lower than that for the full model (137 nM versus 153 nM for the parameter values chosen). This error propagates from the approximations made for B_a in the reduction of equation (2.19) to equation (2.27).

We have used the estimates for parameter values in equation (2.52) for the model which we subsequently formulate from first principles in chapter 3, compare with equation (3.7).

We subject the reduced model to the same transient Wnt stimulus as Lee *et al.* (2003, Figure 6) to determine how well the transient (rather than steady-state) behaviour has been preserved. A Wnt stimulus of $W = e^{-t/20}$ is applied to a system resting at a steady state with $W(0) = 0$; the results are presented in Figure 2.7. We observe the same behaviour, although for the reduced model the response peaks slightly earlier than for the full model as we have essentially said that most reactions reach equilibrium instantly.

Often of interest to biologists and modellers is the level of β-catenin/TCF complex, as the main downstream transcription factor of the Wnt pathway (Pinto & Clevers, 2005). Lee *et al.* denote [β-catenin/TCF] as X_{14} and use the equilibrium condition

$$X_{14} = \frac{TCF^0 X_{11}}{K_{16} + X_{11}}.\tag{2.54}$$

Equation (2.54) could be used together with equation (2.52) to form a simpler model than Lee *et al.* (2003) for predicting the transcription factor response to Wnt signalling.
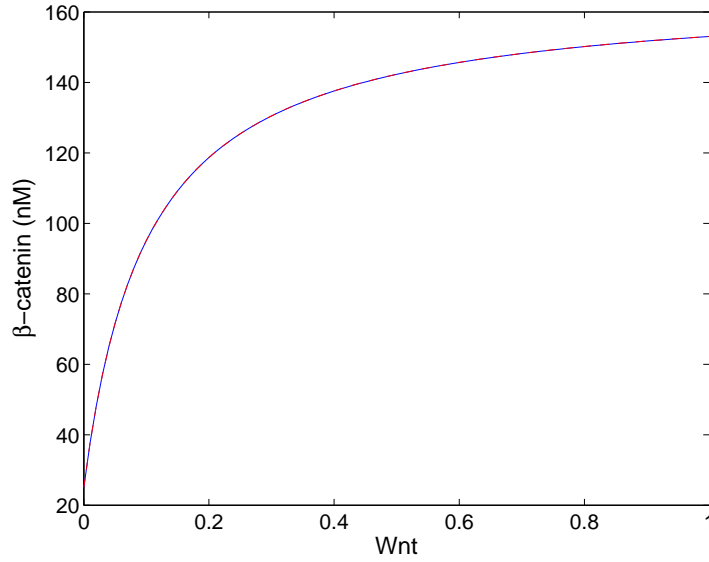
Figure 2.6: Diagram showing how the steady state level of β-catenin changes as the magnitude of the applied Wnt stimulus varies. Solid line for the full model (equations (2.1) – (2.7)) and dashed line for the reduced model (equation (2.52)), the lines are indistinguishable. Parameter values: see Table 2.2.
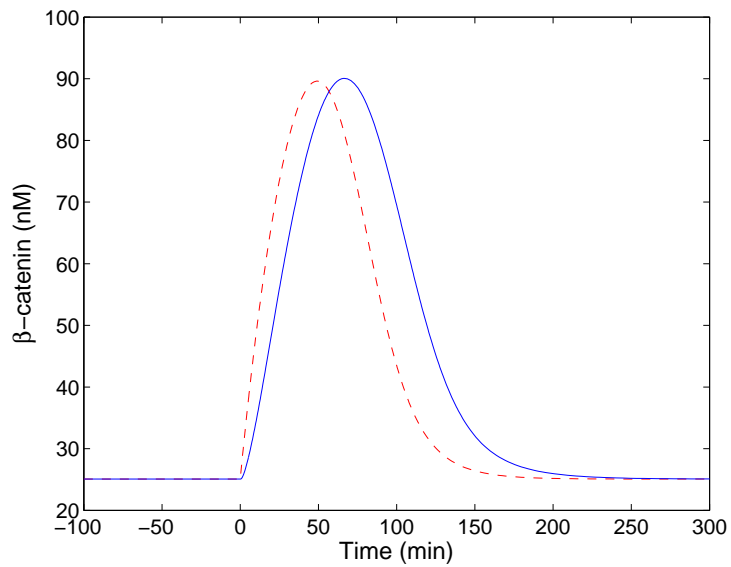
Figure 2.7: Diagram showing the response of β-catenin to a transient Wnt stimulus ($W = e^{-t/20}$, introduced into a system at steady state with $W = 0$ at $t = 0$). Solid line for the full model (equations (2.1) – (2.7)) and dashed line for the reduced model (equation (2.52)). Parameter values: as per Table 2.2.

2.4 Axin Feedback

2.4.1 Formulation of the Model

Cho *et al.* (2006) adapted the Lee *et al.* (2003) model to include Axin2 production in response to β-catenin/TCF transcription (Jho *et al.*, 2002). The model, including this feedback, has been used in further articles (Wawra *et al.*, 2007; Kim *et al.*, 2007). In this section we examine how such feedback changes our analysis of the pathway.

An additional production term of the form $k_{18}(X_{11} + X_{14})$ was introduced into equation (2.5) by Cho *et al.* (2006) to model Axin2 produced in response to β-catenin/TCF. We will conduct our previous analysis on the model as proposed by Cho *et al.* (2006). Including this feedback into equation (2.5) gives

$$
\begin{aligned}
\frac{\mathrm{d}X_{12}}{\mathrm{d}t} &= \left(k_3 X_2 X_4 - \frac{k_6 GSK^0 APC^0 K_{17} X_{12}}{K_7(K_{17} + X_{11})} + k_{-6} X_4 + v_{14} - k_{15} X_{12} + \right. \\
&\quad \left. k_{18} \left(X_{11} + \frac{TCF^0 X_{11}}{K_{16} + X_{11}} \right) + \frac{\mathrm{d}X_{11}}{\mathrm{d}t} \left(\frac{APC^0 K_{17} X_{12}}{K_7(K_{17} + X_{11})^2} \right) \right) \\
&\quad \left/ \left(1 + \frac{APC^0 K_{17}}{K_7(K_{17} + X_{11})} \right) \right. .
\end{aligned}
\tag{2.55}
$$

2.4.2 Reduction of Model

When the new feedback term is included, the non-dimensional form of equation (2.17) becomes

$$
\begin{aligned}
\frac{\mathrm{d}X}{\mathrm{d}t} &= \left((\hat{k}_3 V + \hat{k}_{-6}) D_i - \left(\frac{\hat{k}_6}{(1 + \varepsilon \hat{K}_{16} B_a)} + \hat{k}_{15} \right) X + 1 + \hat{k}_{18} \left(1 + \frac{\widehat{TCF}^0}{1 + B_a} \right) B_a \right. \\
&\quad \left. + \varepsilon \hat{K}_{16} \frac{\mathrm{d}B_a}{\mathrm{d}t} \frac{\hat{K}_7 X}{(1 + \varepsilon \hat{K}_{16} B_a)^2} \right) \left/ \left(1 + \frac{\hat{K}_7}{(1 + \varepsilon \hat{K}_{16} B_a)} \right) \right. .
\end{aligned}
\tag{2.56}
$$

To compare the overall behaviour of the system when equation (2.56) is substituted in place of equation (2.17) we solve the equations numerically, and the results are shown in Figure 2.8. Notice that we use the same initial conditions as in Figure 2.2, and a small adjustment to the system's new steady state for $-100 < t' < 0$ can be seen. When comparing Figures 2.2 and 2.8 the main differences are that more Axin (X) is produced, more destruction complex becomes activated (D_a) and the level of β-catenin is therefore reduced. This effect is small in the absence of a Wnt stimulation ($-100 < t' < 0$), but marked when Wnt is introduced ($0 < t' < 300$), roughly halving the steady state level of B_a.
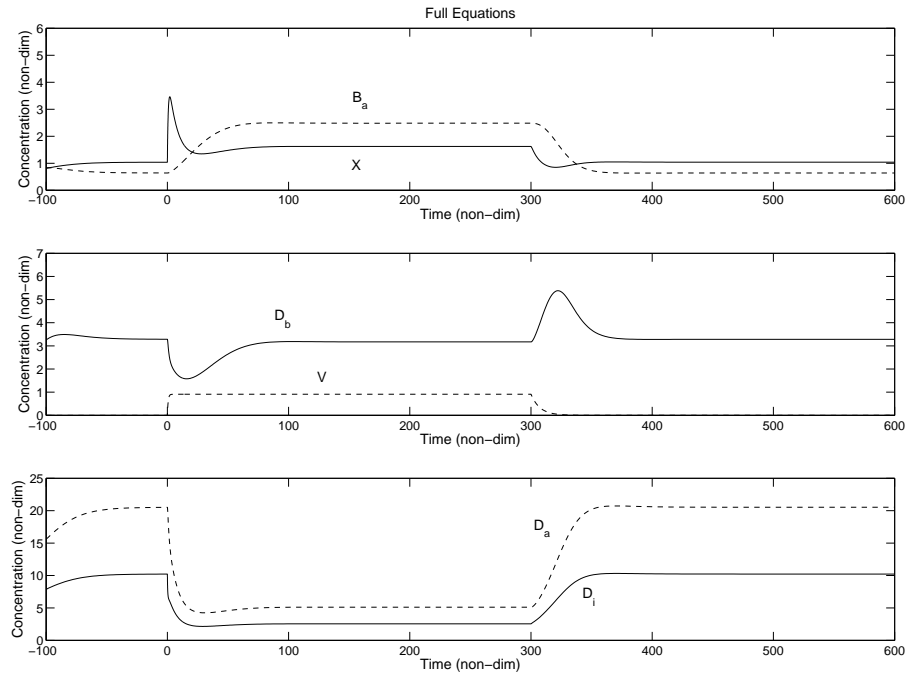
Figure 2.8: A simulation of the Wnt model with Axin feedback (equations (2.14), (2.15), (2.16), (2.18), (2.19) and equation (2.56)) for comparison with the original Wnt model (see Figure 2.2). The Wnt level, W, is increased from 0 to 1 at time $t = 0$ and removed at $t = 300$. Top: solid line X (Axin), dashed line B_a (β-catenin). Middle: solid line D_b (destruction complex bound to β-catenin), dashed line V (active Dishevelled). Bottom: solid line D_i (inactive destruction complex), dashed line D_a (active destruction complex). Parameter values can be found in Table 2.2 and the initial conditions are the steady states for the Lee model without feedback and $W = 0$, as shown in Table 2.3.

Using equation (2.56) in place of equation (2.17) and repeating the analysis of section 2.3.1, we obtain, in place of equation (2.25), the following ODE for Axin:

$$\frac{dX}{dt} = \frac{\left(\hat{k}_3 V + \hat{k}_{-6}\right) D_i - \left(\hat{k}_6 + \hat{k}_{15}\right) X + 1 + \hat{k}_{18} \left(1 + \frac{\widehat{TCF}^0}{1+B_a}\right) B_a}{1 + \hat{K}_7}. \tag{2.57}$$

2.4.3 Multiple Timescale Analysis

The behaviour of the system on a short timescale ($t = O(\varepsilon)$) does not change, since there are no terms which are $O(\varepsilon^{-1})$ in equation (2.57) and so the concentration of Axin does not change. We compare the predicted steady concentrations at a short-time with the numerical solutions of the full equations (2.14),(2.15), (2.16), (2.18), (2.19) and equation (2.56) in Figures 2.9 and 2.10. As before, we find an excellent fit until times increase to $t = O(1)$.

On an intermediate timescale ($t = O(1)$) we can repeat the analysis of section 2.3.2, the result being the replacement of equation (2.39) with

$$\frac{dX_0}{dt} = \left(\hat{k}_3 V_0 D_{i0} + \hat{k}_{-6} D_{i0} + 1 - \hat{k}_{15} X_0 - \hat{k}_6 X_0 + \hat{k}_{18}\left(1 + \frac{\widehat{TCF}^0}{1+B_{a0}}\right) B_{a0}\right) \bigg/ \left(1 + \hat{K}_7\right). \tag{2.58}$$

In equation (2.58) there is a $\hat{k}_{18}$ term providing feedback from β-catenin levels. However because β-catenin remains constant on the intermediate timescale the feedback loop has not yet activated, consequently the behaviour of Cho *et al.*'s feedback model is similar to that of the original Lee *et al.* model (comparing the dotted lines of Figures 2.4 & 2.5 with those of Figures 2.9 & 2.10).

On the long timescale ($t = O(\varepsilon^{-1})$) we have already seen that the behaviour of the system changes substantially (see Figure 2.8). The only change to the long time behaviour of equations (2.46)–(2.51) is the replacement of equation (2.46), $X_0(T) = 1/\hat{k}_{15}$, with

$$X_0(T) = \frac{1}{\hat{k}_{15}} \left(1 + \hat{k}_{18}\left(1 + \frac{\widehat{TCF}^0}{1+B_{a0}(T)}\right) B_{a0}(T)\right). \tag{2.59}$$

We can see that the value of the long-time approximation of X has increased, and is now dependent on B_{a0} and hence time, T, rather than being constant. While this change propagates through equations (2.48)–(2.51), the functional form of equation (2.51) remains unchanged with a single ODE for $B_{a0}(T)$:

$$\frac{d}{dT} B_{a0}(T) = \hat{v}_{12} - \left(\hat{k}_{14} D_{a0}(T) + 1\right) B_{a0}(T).$$

In Lee *et al.*'s model only D_b and B_a varied on the long timescale (Figure 2.3), whilst in Cho *et al.* (2006)'s model, all variables, apart from V, vary over this timescale (as they all depend on B_a).
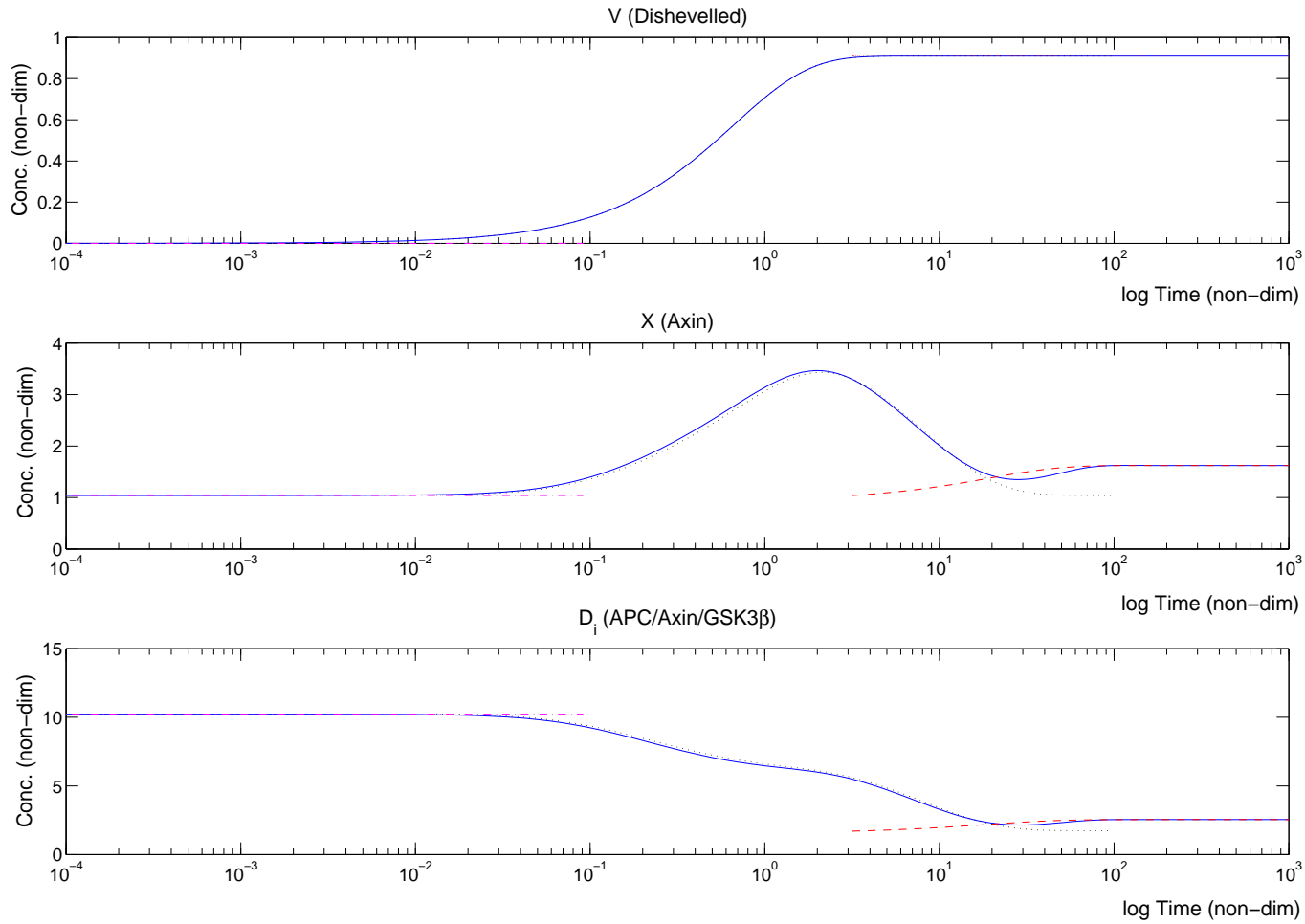
Figure 2.9: Cho model reaction to a sudden Wnt stimulus ($W = 1$) introduced into a system in equilibrium ($W = 0$) at $t = 0$. Numerical simulations of the full equations (2.14), (2.15), (2.16), (2.18), (2.19) and equation (2.56) are shown with a solid line. Short, medium and long time approximations are shown with dash-dotted, dotted and dashed lines respectively. There is good agreement between the approximations and numerical solutions at all timescales. Parameter values can be found in Table 2.2.
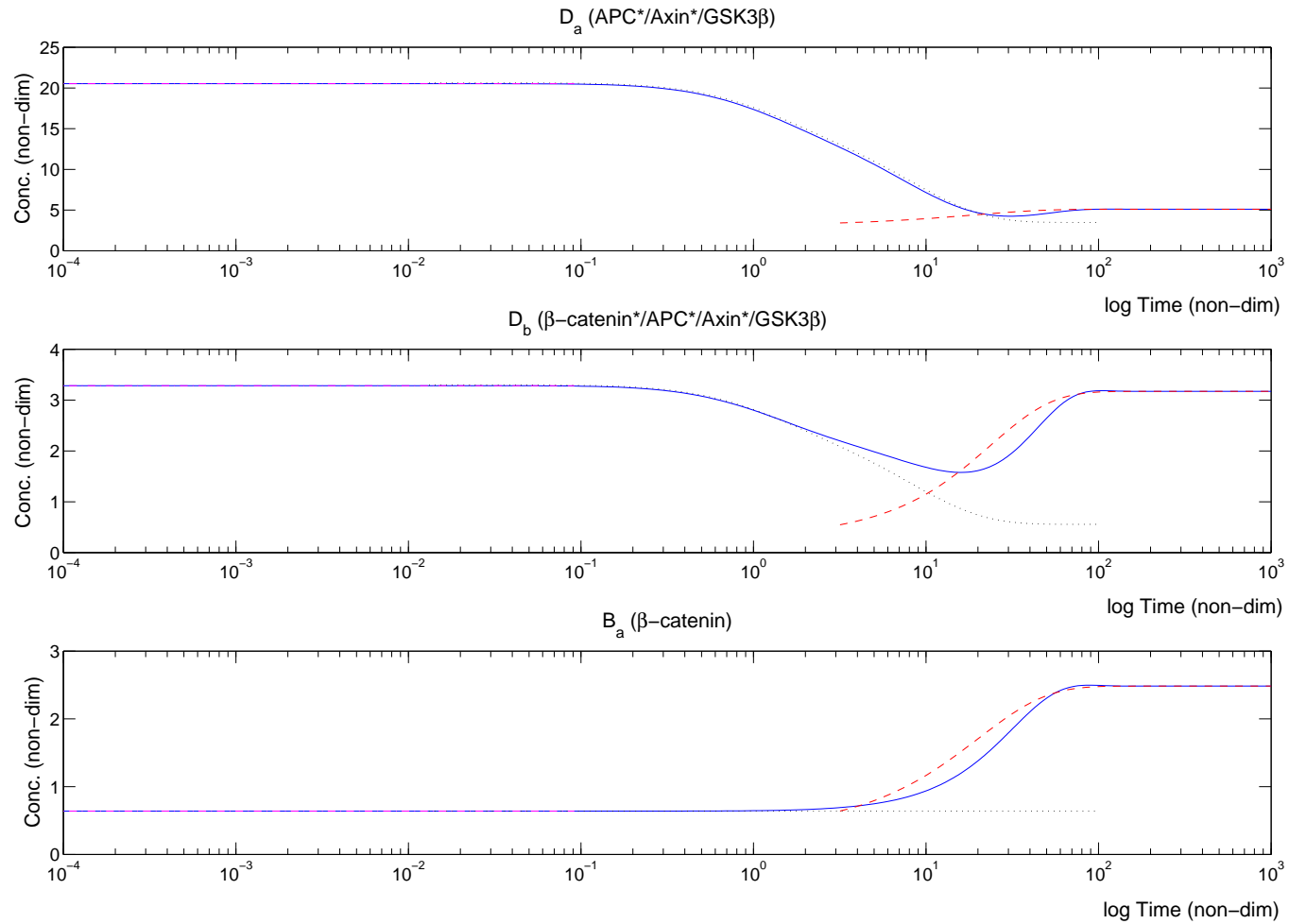
Figure 2.10: Cho model reaction to a sudden Wnt stimulus ($W = 1$) introduced into a system in equilibrium ($W = 0$) at $t = 0$. Numerical simulations of the full equations (2.14), (2.15), (2.16), (2.18), (2.19) and equation (2.56) are shown with a solid line. Short, medium and long time approximations are shown with dash-dotted, dotted and dashed lines respectively. There is good agreement between the approximations and numerical solutions at all timescales. Parameter values can be found in Table 2.2.

Biologically the increase in B_a (as a result of the processes discussed in section 2.3.2) leads to increased expression of Axin (X) over a long timescale. As Axin is the limiting factor in destruction complex formation this allows the levels of destruction complex, in all forms, to increase (as the levels of each separate pool of destruction complex equilibrate on an intermediate timescale). This increase in destruction complex levels leads in turn to more phosphorylation of β-catenin which reduces its level below that seen when the feedback loop is absent.

The feedback model's equivalent of equation (2.51) for the evolution of β-catenin on a long timescale reads

$$
\begin{aligned}
\frac{\mathrm{d}}{\mathrm{d}T}B_{a0}(T) \;=\; & \hat{v}_{12} - \Bigg(\frac{\hat{k}_{14}\hat{k}_4\hat{k}_6}{\hat{k}_{15}\big(\hat{k}_3 V_0(T) + \hat{k}_{-6}\big)\big(1 + K'_{16}B_{a0}(T)\big)} \times \\
& \left(1 + \hat{k}_{18}\Big(1 + \frac{\widehat{TCF}^0}{1 + B_{a0}(T)}\Big)B_{a0}(T) \right) + 1 \Bigg)B_{a0}(T),
\end{aligned}
\tag{2.60}
$$

with the dimensional form given by

$$
\frac{\mathrm{d}X_{11}}{\mathrm{d}t} = v_{12} - \left(a\big(W(t)\big)\frac{k_{18}K_{17}}{K_{17}+X_{11}(t)}\left(1 + \frac{TCF^0}{K_{16}+X_{11}(t)}\right)X_{11}(t) + k_{13} \right)X_{11}(t),
\tag{2.61}
$$

where $a\big(W(t)\big)$ is given by equation (2.53), as before.

Equation (2.61) represents a simpler model of Wnt signalling with Axin feedback than that presented by Cho *et al.* (2006) in that we have substantially reduced the number of equations in the system. Note that equation (2.61) is the equivalent of equation (2.52), but including Axin feedback. Equation (2.61) could be combined with equation (2.54) to produce a simple model for β-catenin/TCF transcription in response to Wnt signalling.

2.4.4 Variation of Feedback Model

We remark that a production term of the form $k_{18}(X_{11} + X_{14})$ (equation (2.55)) seems a strange choice, since there is no evidence that free β-catenin ($[\beta$-catenin$] = X_{11}$) stimulates production of Axin2 unless it is in complex with TCF ($[\beta$-catenin/TCF$] = X_{14}$). We would suggest a more conventional rate-limiting term of the form $k_{18}X_{14}/(K_{18} + X_{14})$, where Axin2 production is an increasing and saturating function of β-catenin/TCF.

Replacing Cho *et al.*'s term in equation (2.55) with the suggested term leads to

$$
\begin{aligned}
\frac{\mathrm{d}X_{12}}{\mathrm{d}t} = {} & \left(k_3 X_2 X_4 - \frac{k_6 GSK^0 APC^0 K_{17} X_{12}}{K_7 (K_{17} + X_{11})} + k_{-6} X_4 + v_{14} - k_{15} X_{12} + \right. \\
& \left. k_{18b} \frac{TCF^0 X_{11}}{K_{18} + (K_{18} + TCF^0) X_{11}} + \frac{\mathrm{d}X_{11}}{\mathrm{d}t} \left(\frac{APC^0 K_{17} X_{12}}{K_7 (K_{17} + X_{11})^2} \right) \right) \\
& \Bigg/ \left(1 + \frac{APC^0 K_{17}}{K_7 (K_{17} + X_{11})} \right).
\end{aligned}
\tag{2.62}
$$

Note that k_{18b} must take different units, and therefore a different value, in this equation; results are approximately the same when the original value of $k_{18} = 1 \times 10^{-6}$ min^{-1} is modified to read $k_{18b} = 1 \times 10^{-4}$ nM min^{-1} and $K_{18} = 1.0$ nM. We show the result of a typical run for this model in Figure 2.11, to be compared with the results presented in Figure 2.8. We see very similar results both qualitatively and quantitatively, with slightly higher levels of Axin (X) present.

The change is reflected in the nondimensional equation (2.56) as follows

$$
\begin{aligned}
\frac{\mathrm{d}X}{\mathrm{d}t} = {} & \left((\hat{k}_3 V + \hat{k}_{-6}) D_i - \left(\frac{\hat{k}_6}{(1 + \varepsilon \hat{K}_{16} B_a)} + \hat{k}_{15} \right) X + 1 + \hat{k}_{18b} \frac{\widehat{TCF}^0 B_{a0}(T)}{1 + \left(1 + \hat{K}_{18} \widehat{TCF}^0 \right) B_{a0}(T)} \right. \\
& \left. + \varepsilon \hat{K}_{16} \frac{\mathrm{d}B_a}{\mathrm{d}t} \frac{\hat{K}_7 X}{(1 + \varepsilon \hat{K}_{16} B_a)^2} \right) \Bigg/ \left(1 + \frac{\hat{K}_7}{(1 + \varepsilon \hat{K}_{16} B_a)} \right).
\end{aligned}
\tag{2.63}
$$

With

$$
\frac{\mathrm{d}X}{\mathrm{d}t} = \left(\left(\hat{k}_3 V + \hat{k}_{-6} \right) D_i - \left(\hat{k}_6 + \hat{k}_{15} \right) X + 1 + \hat{k}_{18b} \frac{\widehat{TCF}^0 B_a}{1 + \left(1 + \hat{K}_{18} \widehat{TCF}^0 \right) B_a} \right) \Bigg/ \left(1 + \hat{K}_7 \right),
\tag{2.64}
$$

following directly as a replacement for equation (2.57).

These changes continue through the equations of section 2.4.3 to give the following long-time approximation for Axin levels:

$$
X_0(T) = \frac{1}{\hat{k}_{15}} \left(1 + \hat{k}_{18b} \frac{\widehat{TCF}^0 B_{a0}(T)}{1 + \left(1 + \hat{K}_{18} \widehat{TCF}^0 \right) B_{a0}(T)} \right).
\tag{2.65}
$$

Again the functional form of the long-time approximation (equation (2.51)) remains unchanged. Substituting in equation (2.65) we are left with a dimensional equation which reads

$$
\frac{\mathrm{d}X_{11}}{\mathrm{d}t} = v_{12} - \left(a\big(W(t)\big) \frac{k_{18} K_{17}}{K_{17} + X_{11}(t)} \left(\frac{TCF^0 X_{11}(t)}{K_{18} + (K_{18} + TCF^0) X_{11}(t)} \right) + k_{13} \right) X_{11}(t).
\tag{2.66}
$$

where $a\left(W(t)\right)$ is unchanged and given by equation (2.53).
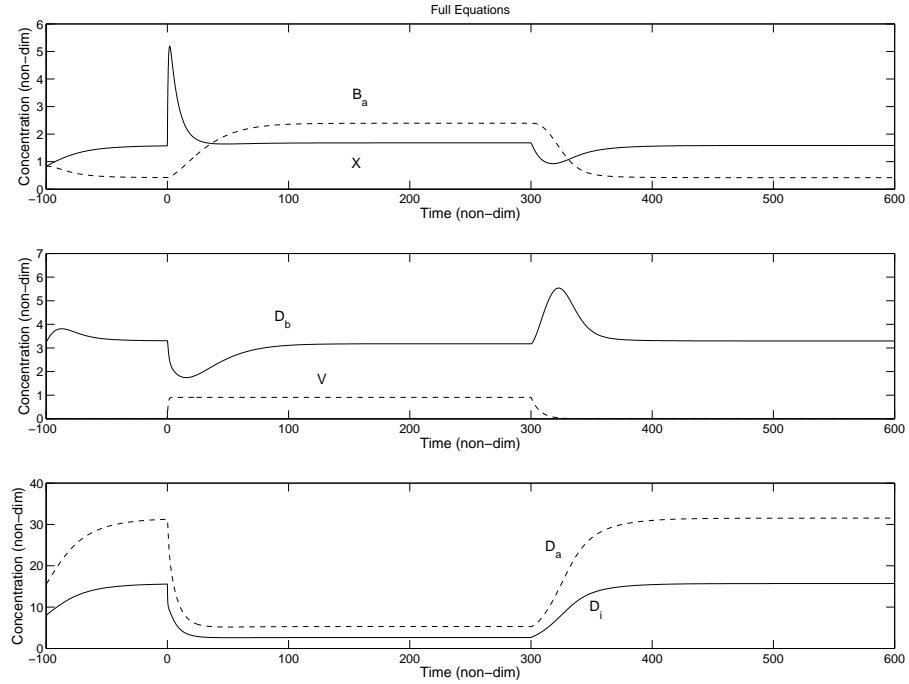
Figure 2.11: A simulation of the Wnt model with Axin feedback (equations (2.14), (2.15), (2.16), (2.18), (2.19) and equation (2.63)) for comparison with the Cho *et al.* (2006) model (see Figure 2.8). The Wnt level, W, is increased from 0 to 1 at time $t = 0$ and removed at $t = 300$. Top: solid line X (Axin), dashed line B_a (β-catenin). Middle: solid line D_b (destruction complex bound to β-catenin), dashed line V (active Dishevelled). Bottom: solid line D_i (inactive destruction complex), dashed line D_a (active destruction complex). Parameter values can be found in Table 2.2 and the initial conditions are the steady states for the Lee model without feedback and $W = 0$, as shown in Table 2.3.

This variation of the feedback model yields excellent asymptotic matches for the asymptotics, almost identical to those shown in Figures 2.9 and 2.10, and equation (2.66) forms another single-ODE model which encapsulates the response of β-catenin to Wnt signalling.

2.5 Discussion

The Lee *et al.* (2003) Wnt signalling model is an excellent example of how experiments carried out in partnership with modelling can enhance understanding of a biological system, with fresh insight into the role of Axin resulting. By nondimensionalising their model and performing a systematic asymptotic analysis we have been able to make some interesting observations about the action of the Wnt pathway.

The pathway operates on three distinct timescales. The fastest timescale is associated with the action of the destruction complex, which quickly both phosphorylates and releases β-catenin. Over an intermediate timescale the dominant reactions regulate levels of destruction complex by removing Axin under the influence of Wnt and Dishevelled. Changes in β-catenin levels happen over a slower timescale than either of these processes. Guided by comparison with the full models we conclude that our reduced models (equations (2.52) and (2.61)) retain the essential behaviour of the Lee *et al.* (2003) and Cho *et al.* (2006) models that is needed to study the effect of Wnt signalling on β-catenin accumulation.

Use of this simplified model could reduce the complexity of models such as Kim *et al.* (2007) considerably. The full Wnt pathway in Kim *et al.*'s model could be represented by equation (2.61), with only the slight modification of GSK^0 in equation (2.53) being replaced by $\left(GSK^0 - X_{28}(t)\right)$ to couple to the rest of their model, and equation (2.54) giving the output of the Wnt pathway. This would eliminate 14 ODEs from their system and, we believe, facilitate a much greater understanding of the underlying processes.

Many of the parameter values we have used derive from experiments performed in vitro on *Xenopus* egg extracts by Lee *et al.*; many others could not be measured directly. Ideally, the parameter values should be based on kinetic parameters, directly measured from human cells in vivo. However the Wnt/β-catenin pathway is thought to be highly conserved between species, so the operation of the human pathway is likely to be very similar to that of the *Xenopus* pathway.

Many of the Wnt pathway's components exist in separate 'compartments' inside the cell (such as the nucleus, membrane and cytoplasm) and spatial effects have been considered for β-catenin in

van Leeuwen *et al.* (2007); possible future work would be considering the localisation of other Wnt pathway components, which have been shown to localise to the cell membrane and cytoskeleton, and considering the role of nuclear import and export of various components.

Through our asymptotic analysis we have provided insight into the biological action of many of the components in the overall system. Given that it is the accumulation and degradation of β-catenin that is often of interest to biologists and modellers, we have shown how this may be determined from a highly simplified model which relates the evolution of β-catenin directly to the Wnt stimulus. As we will include models of Wnt signalling in a cell-based tissue model in chapters 5 and 6 we have greatly reduced the computation involved in running such simulations.

CHAPTER 3

The Impact of Wnt Signalling on the Cell Cycle in the Colorectal Crypt

3.1 Introduction

A
s mentioned in chapter 1, over 90% of colorectal cancer (CRC) tumours carry mutations which result in abnormal activation of the Wnt signalling pathway. A number of mathematical models of CRC have been proposed (see van Leeuwen *et al.*, 2006, for a review), but as yet none quantitatively link aberrant Wnt signalling to cancer initiation. In this chapter we develop a deterministic model to study a possible mechanism by which Wnt signalling affects cell proliferation in the colon.

β-catenin is a transcription factor for D-type cyclins (Tetsu & McCormick, 1999; Shtutman *et al.*, 1999; Sansom *et al.*, 2004). The level of β-catenin/TCF target-gene expression in a colorectal crypt is observed to be highest at the base of a crypt, where the proliferating cells are located, and to decrease towards the top (Gaspar & Fodde, 2004; Larsson, 2006). In this chapter we develop a model to investigate how Wnt signalling might influence the cell cycle. Hence we determine whether a Wnt gradient in a colorectal crypt may be responsible for the observed proliferative hierarchy along the crypt axis. We will also examine the impact of mutations in components of the Wnt pathway.

In section 1.3.3 we reviewed several mathematical models of the cell cycle that include Cyclin D (Obeyesekere *et al.*, 1997; Obeyesekere & Zimmerman, 1999; Aguda & Tang, 1999; Novak & Tyson, 2004). Below we introduce a model which reproduces two specific phenomena observed in the crypts: firstly, lack of Cyclin D can induce quiescence (Gemin *et al.*, 2005) and, secondly, reduction of Cyclin D levels can slow the onset of the G_1/S transition (Han *et al.*, 1999). In section 3.2 we develop a simple model for the Wnt signalling pathway, based upon our findings in chapter 2. In

section 3.3 we couple the models and use them to predict proliferation patterns in healthy and aberrant colorectal crypts.

3.1.1 The Swat *et al.* (2004) Cell-Cycle Model

The cell-cycle model on which we focus was developed by Swat *et al.* (2004) and is, we believe, a minimal one able to exhibit the behaviour we would like to describe. The model takes the form of a system of coupled ODEs; with each ODE describing the rate of change in the concentration of a single protein or complex. In the 'core model' the key variables are the concentrations of retinoblastoma protein, [pRb], and a transcription factor, [E2F1]. As discussed in section 1.3, these proteins govern the G_1/S transition. Following Swat *et al.*'s notation we denote by $[CycD_a]$ and $[CycD_i]$ the concentrations of active or inactive Cyclin D kinase complexes respectively, and by $[pRb_p]$ that of phosphorylated retinoblastoma protein.

The time evolution of the model variables is derived by referring to the bottom half of Figure 3.3 and using mass-action kinetics, with Michaelis-Menten kinetics for reaction rates that become saturated. Figures 3.1 and 3.2 show how the terms that appear in the governing equations can be derived and, in particular, how the rate of production of a protein is up- or down-regulated by a second protein.

Table 3.1: Dependent variables in the Swat *et al.* (2004) model.

Swat Model Variable	Protein/Complex Description
[pRb]	Retinoblastoma Protein
$[pRb_p]$	Retinoblastoma Protein (phosphorylated)
[E2F1]	Transcription Factor (for S phase proteins)
$[CycD_i]$	Cyclin D (inactive)
$[CycD_a]$	Cyclin D (active)
[AP-1]	Transcription Factor (for Cyclin D)

The dependent variables for the 'first extension' of the Swat model that we utilise here are shown in Table 3.1. The model is formulated using terms such as those shown in Figures 3.1 and 3.2 and the schematic shown in Figure 3.3. In general terms, for a non-phosphorylated protein (modifications
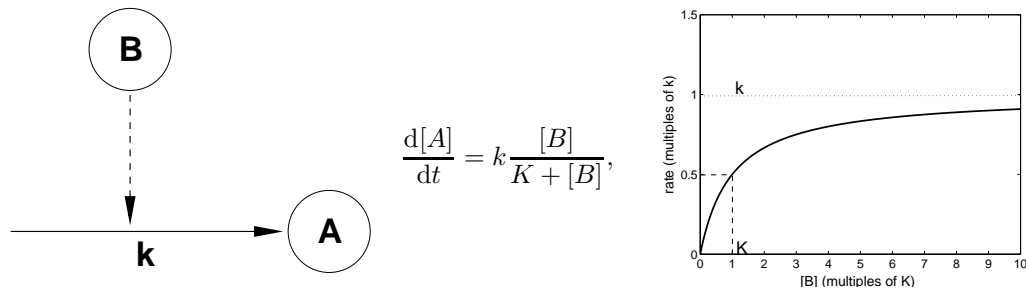
Figure 3.1: Production of protein A is upregulated by protein B (square brackets denote the concentration of a protein). The production rate of $[A]$ is zero when $[B] = 0$ and tends to k as $[B] \to \infty$.
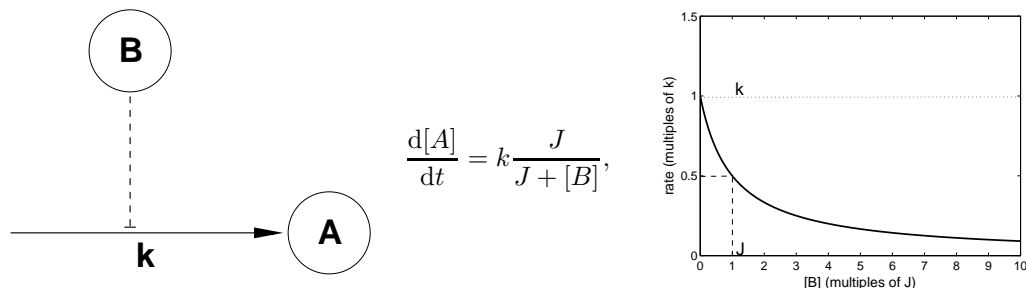
Figure 3.2: Production of protein A is downregulated by protein B (square brackets denote the concentration of a protein). The production rate of $[A]$ is k when $[B] = 0$, but tends to zero as $[B] \to \infty$.

needed for phosphorylated proteins are stated in parentheses) we have

$$
\text{rate of change of protein concentration} \quad = \quad + \text{ increase due to production}
$$

$$
+ \text{ increase due to dephosphorylation (phosphorylation)}
$$

$$
- \text{ loss due to (de)phosphorylation}
$$

$$
- \text{ loss due to degradation.}
$$
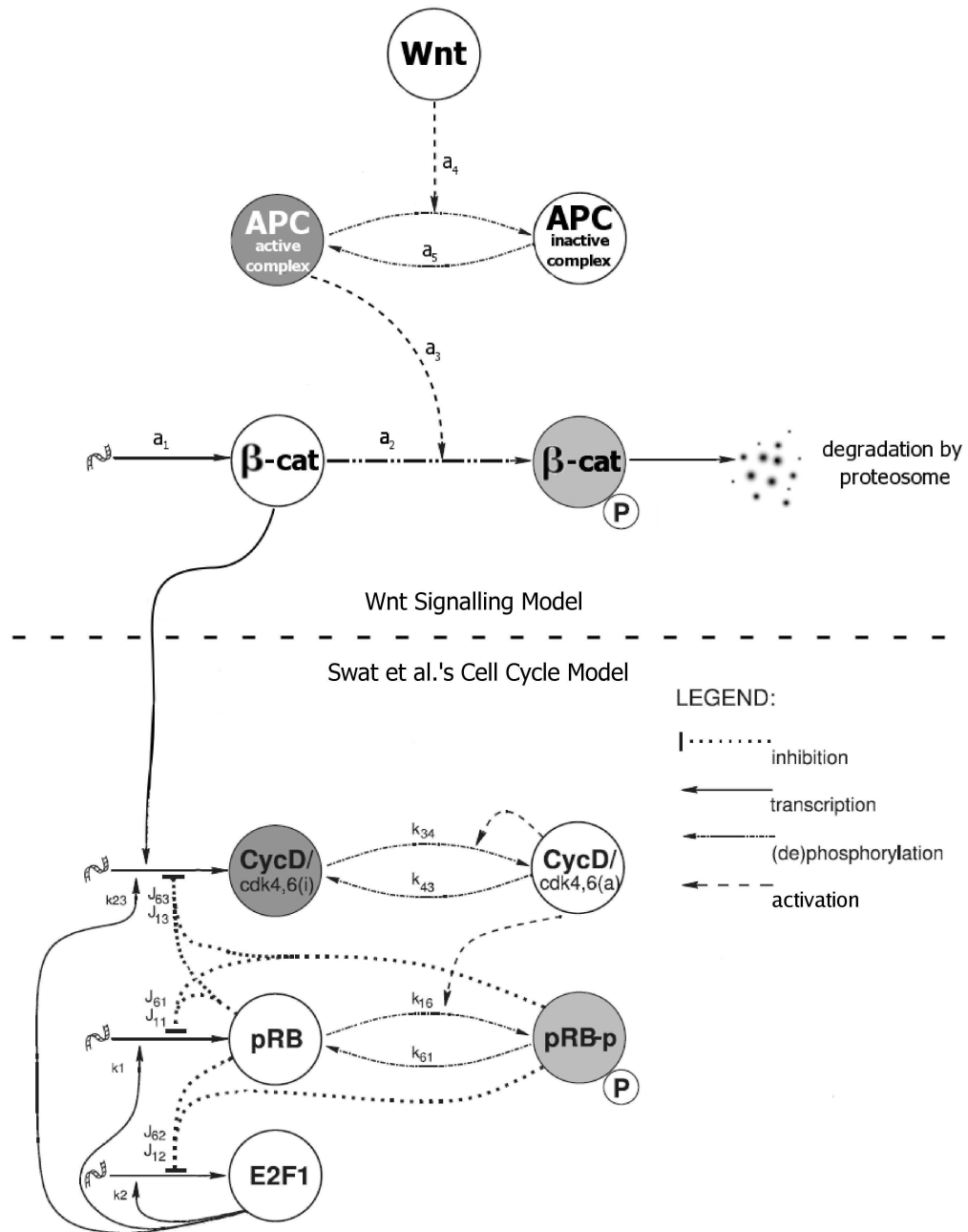
Figure 3.3: A schematic diagram of our model for the Wnt pathway and how it is linked to the Swat *et al.* (2004) model for the G_1/S transition of the cell cycle in mammalian cells. The lower half of the figure is adapted from Swat *et al.* (2004, Figure 1) by permission of Oxford University Press.

This leads to the following set of equations:

$$\frac{d[pRb]}{dt} = k_1 \frac{[E2F1]}{K_{m1} + [E2F1]} \frac{J_{11}}{J_{11} + [pRb]} \frac{J_{61}}{J_{61} + [pRb_p]}$$
$$-k_{16}[pRb][CycD_a] + k_{61}[pRb_p] - \phi_{pRb}[pRb], \tag{3.1}$$

$$\frac{d[E2F1]}{dt} = k_p + k_2 \frac{a^2 + [E2F1]^2}{K_{m2}^2 + [E2F1]^2} \frac{J_{12}}{J_{12} + [pRb]} \frac{J_{62}}{J_{62} + [pRb_p]} - \phi_{E2F1}[E2F1], \tag{3.2}$$

$$\frac{d[CycD_i]}{dt} = k_3[AP\text{-}1] + k_{23}[E2F1]\frac{J_{13}}{J_{13} + [pRb]} \frac{J_{63}}{J_{63} + [pRb_p]}$$
$$+k_{43}[CycD_a] - k_{34}[CycD_i]\frac{[CycD_a]}{K_{m4} + [CycD_a]} - \phi_{CycD_i}[CycD_i], \tag{3.3}$$

$$\frac{d[CycD_a]}{dt} = k_{34}[CycD_i]\frac{[CycD_a]}{K_{m4} + [CycD_a]} - k_{43}[CycD_a] - \phi_{CycD_a}[CycD_a], \tag{3.4}$$

$$\frac{d[AP\text{-}1]}{dt} = F_m + k_{25}[E2F1]\frac{J_{15}}{J_{15} + [pRb]} \frac{J_{65}}{J_{65} + [pRb_p]} - \phi_{AP\text{-}1}[AP\text{-}1], \tag{3.5}$$

$$\frac{d[pRb_p]}{dt} = k_{16}[pRb][CycD_a] - k_{61}[pRb_p] - \phi_{pRb_p}[pRb_p]. \tag{3.6}$$

In equations (3.1)–(3.6) the k's and ϕ's are non-negative rate constants, whilst the K's and J's are (Michaelis-Menten) dissociation constants and F_m represents the mitogenic stimulus applied to the system (for parameter values, see Table 3.2). The behaviour of the model depends crucially on the size of F_m, the mitogenic transcription factor.

In Swat *et al.*'s (2004) paper they established the steady state behaviour of the model as F_m varies, their results being shown in Figure 3.4: for low F_m there is a unique steady state characterised by low levels of E2F1 (G_0 phase); for high F_m the only steady state has high levels of E2F1 (S phase); and for intermediate F_m both steady states are present and the steady state that is attained depends on the initial levels of proteins present. If a cell is exposed to a constant low F_m then its E2F1 levels will remain low (and the cell will stay in G_0 phase). If, however, the stimulus F_m slowly increases then the cell's E2F1 levels will move along the lower branch (G_1 phase) of Figure 3.4 towards the phase transition. When the stimulus exceeds a threshold value the only steady state is on the upper branch and the level of E2F1 jumps (cell enters S phase). This is an irreversible transition — if the level of F_m now falls slightly then the cell will not return to G_1 phase, but will follow the upper steady state line (stay in S phase).

The three types of behaviour that the system can exhibit are presented in Figure 3.5. For low values of F_m (upper panel) the cells remain quiescent, whilst for high values (lower panel) the cells complete the G_1/S transition. For intermediate values of F_m (middle panel) the cells progress further through the cell cycle than for the top simulation, as in this case F_m exceeds the transcritical bifurcation value seen in Figure 3.4. The lower simulation, having the highest Wnt level, has a mitogenic stimulus

Table 3.2: Swat *et al.* (2004) parameters.

		Dimensional				Nondimensional		
k_1	=	1.0	$nMmin^{-1}$		F		=	6×10^{-3}
k_2	=	1.6	$nMmin^{-1}$	$\tilde{k}_2$	=	$k_2/(K_{m2}\phi_{E2F1})$	=	4.0
k_3	=	0.05	min^{-1}	$\tilde{k}_3$	=	$k_3 F a_1/(K_{m4}\phi_{E2F1}a_2)$	=	16.5
k_{16}	=	0.4	$nM^{-1}min^{-1}$	$\tilde{k}_{16}$	=	$k_{16}K_{m4}/\phi_{E2F1}$	=	1.2
k_{23}	=	0.3	min^{-1}	$\tilde{k}_{23}$	=	$k_{23}K_{m2}/(K_{m4}\phi_{E2F1})$	=	40
k_{25}	=	0.9	min^{-1}					
k_{34}	=	0.04	min^{-1}	$\tilde{k}_{34}$	=	k_{34}/ϕ_{E2F1}	=	0.4
k_{43}	=	0.01	min^{-1}	$\tilde{k}_{43}$	=	k_{43}/ϕ_{E2F1}	=	0.1
k_{61}	=	0.3	min^{-1}	$\tilde{k}_{61}$	=	k_{61}/ϕ_{E2F1}	=	3.0
a	=	0.04	nM	$\tilde{a}$	=	a/K_{m2}	=	0.01
J_{11}	=	0.5	nM	$\tilde{J}_{11}$	=	$J_{11}\phi_{E2F1}/k_1$	=	0.05
J_{12}	=	5.0	nM	$\tilde{J}_{12}$	=	$J_{12}\phi_{E2F1}/k_1$	=	0.5
J_{13}	=	2×10^{-3}	nM	$\tilde{J}_{13}$	=	$J_{13}\phi_{E2F1}/k_1$	=	2.0×10^{-4}
J_{15}	=	1×10^{-3}	nM					
J_{61}	=	5.0	nM	$\tilde{J}_{61}$	=	$J_{61}\phi_{E2F1}/k_1$	=	0.5
J_{62}	=	8.0	nM	$\tilde{J}_{62}$	=	$J_{62}\phi_{E2F1}/k_1$	=	0.8
J_{63}	=	2.0	nM	$\tilde{J}_{63}$	=	$J_{63}\phi_{E2F1}/k_1$	=	0.2
J_{65}	=	6.0	nM					
K_{m1}	=	0.5	nM	$\tilde{K}_{m1}$	=	K_{m1}/K_{m2}	=	0.125
K_{m2}	=	4.0	nM					
K_{m4}	=	0.3	nM					
k_p	=	0.05	$nMmin^{-1}$	$\tilde{k}_p$	=	$k_p/(K_{m2}\phi_{E2F1})$	=	0.125
ϕ_{pRb}	=	5×10^{-3}	min^{-1}	ϕ_r	=	ϕ_{pRB}/ϕ_{E2F1}	=	0.05
ϕ_{E2F1}	=	0.1	min^{-1}					
ϕ_{CycD_i}	=	0.023	min^{-1}	ϕ_i	=	$\phi_{CycD_i}/\phi_{E2F1}$	=	0.23
ϕ_{CycD_a}	=	0.03	min^{-1}	ϕ_c	=	$\phi_{CycD_a}/\phi_{E2F1}$	=	0.3
$\phi_{AP\text{-}1}$	=	0.01	min^{-1}					
ϕ_{pRb_p}	=	0.06	min^{-1}	ϕ_p	=	ϕ_{pRB_p}/ϕ_{E2F1}	=	0.6
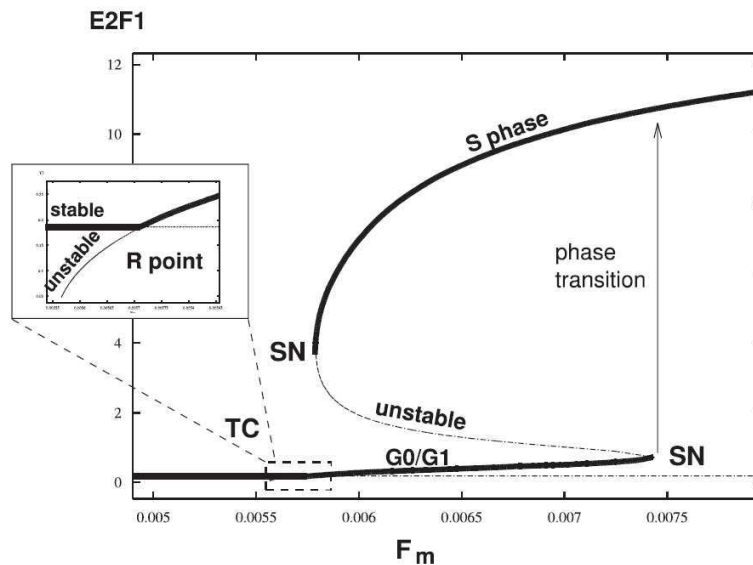
SN – saddle node bifurcation   **TC** – transcritical bifurcation

Figure 3.4: Steady E2F1 levels for different mitogenic stimuli, F_m. The solid lines are stable steady states and the dashed lines are unstable steady states. Reproduced from Swat *et al.* (2004, Figure 3) by permission of Oxford University Press.

above both the transcritical and saddle node bifurcations and quickly enters S phase. As discussed in section 1.3, β-catenin acts as a transcription factor for Cyclin D. In section 3.2 we formulate a Wnt signalling model for the accumulation of β-catenin in cells exposed to an external Wnt stimulus. In section 3.3 we link this model to that of Swat *et al.* in order to examine the effect of Wnt signalling on the cell cycle, and use the coupled model to determine whether a Wnt gradient in a colorectal crypt may be responsible for the pattern of proliferation that characterises normal crypts. We also use the model to examine the impact of mutations in components of the Wnt pathway, discussing

Table 3.3: Initial conditions for the first extension of Swat *et al.*'s cell-cycle model

Dimensional variable		Dimensional value	Units	Dimensionless variable		Dimensionless value
[pRb]	=	7.357	nM	r	=	0.735
[CycD$_i$]	=	0.0207	nM	i	=	0.069
[E2F1]	=	0.6852	nM	e	=	0.171
[CycD$_a$]	=	0.001	nM	j	=	0.003
[pRb$_p$]	=	0.001	nM	p	=	0.0001

73
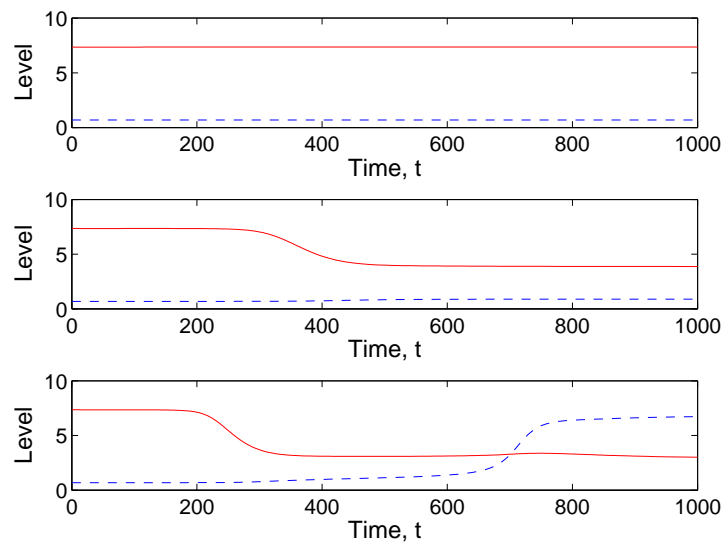
Figure 3.5: A series of simulations showing how the evolution of [pRb] (solid lines) and [E2F1] (dashed lines) change as the strength of the mitogenic stimulus (F_m) varies. In the top simulation, the mitogenic stimulation is very small ($F_m = 0.001$) and the cell stays in G_0 phase; in the middle simulation ($F_m = 0.003$) the cell makes some progress through G_1 phase, but does not produce enough Cyclin D to progress into S phase and so becomes quiescent (albeit at a later stage of G_1); and in the bottom simulation ($F_m = 0.0045$) the cell passes through the G_1 phase and its E2F1 levels rise, marking the progression into S phase. The parameter values and initial conditions used to obtain the above simulations are presented in Tables 3.2 and 3.3 respectively.

our findings in section 3.4.

3.2 Wnt Signalling Model

In this section we derive a Wnt signalling model for the amount of β-catenin available to act as a transcription factor for Cyclin D. We focus on the transcriptional side of the Wnt pathway, and for simplicity ignore β-catenin's other roles in functions such as cell-cell adhesion.

3.2.1 Formulating the Model

Since we want a system that permits a full analysis of its behaviour, our model formulation is much simpler than that of Lee *et al.* (2003), and is based upon our reduced version of Lee *et al.* (2003) (equation (2.52) in chapter 2) which was shown to reproduce all of the necessary behaviour. In particular, the main component of our model is the concentration of β-catenin, [β-cat]. We have added another variable: active APC/Axin/GSK3β destruction complex, [C_{active}] in order to study the effect of mutations in APC on the Wnt pathway. The concentration of extracellular Wnt, [Wnt], is an input parameter.

We assume that β-catenin is produced at a constant rate (a_1) inside cells, and is degraded at a rate proportional to its concentration (with rate constant a_2). As shown in Figure 3.3, C_{active} phosphorylates β-catenin (with rate constant a_3) which marks it for subsequent degradation (see section 1.4.3). Using a mass-action formulation this leads to the equation

$$\frac{\mathrm{d}[\beta\text{-cat}]}{\mathrm{d}t} = a_1 - (a_2 + a_3[C_{active}])\,[\beta\text{-cat}]. \tag{3.7}$$

We remark that this ODE is very similar in structure to that of equation (2.52) and our model predicts that [β-cat] will be maintained at a constant level (a_1/a_2) in the absence of C_{active}. Some Wnt signalling pathway feedback targets have been identified[1]. For example, Axin2 is upregulated by β-catenin (Jho *et al.*, 2002), but β-catenin-induced feedback is omitted in Lee *et al.*'s detailed model which appears to simulate the pathway accurately. We therefore neglect feedback and assume that the total amount of destruction complex in the cell remains constant over time, i.e. [C_{Total}] = [C_{active}] + [$C_{inactive}$] = constant. In reality the 'inactive destruction complex' may not constitute a destruction complex, the components remaining dissociated within the cell. However, this remains a useful way to describe the level of destruction complex contained within the cell. It appears that the limiting protein in the formation of the destruction complex is Axin, since it is present in the

---

[1] http://www.stanford.edu/~rnusse/pathways/targetcomp.html

Table 3.4: Parameter values for the Wnt pathway model

		Dimensional				Nondimensional		
a_1	=	0.423	$nMmin^{-1}$					
a_2	=	$2.57{\times}10^{-4}$	min^{-1}	$\tilde{a}_2$	=	a_2/ϕ_{E2F1}	=	$2.57{\times}10^{-3}$
a_3	=	1.72	$nM^{-1}min^{-1}$	$\tilde{a}_3$	=	$a_3[\mathrm{C}_{Total}]/\phi_{E2F1}$	=	0.344
a_4	=	10.0	$nM^{-1}min^{-1}$	$\tilde{a}_4$	=	$a_4[\mathrm{Wnt}]_{max}/\phi_{E2F1}$	=	1000
a_5	=	0.5	min^{-1}	$\tilde{a}_5$	=	a_5/ϕ_{E2F1}	=	5.00
$[\mathrm{C}_{Total}]$	=	0.02	nM	$[\mathrm{Wnt}]_{max}$	=	10.0 nM		

cell in by far the lowest concentration (see Lee *et al.* (2003) and section 2.2.2) and so we base our estimate of $[\mathrm{C}_{Total}]$ on the concentration of Axin.

The ratio of active to inactive complex is influenced by the Wnt signal. In reality this process is initiated by extracellular Wnt binding to a Frizzled receptor, which initiates a cascade of events including the disabling by Dishevelled and LRP6 of the active destruction complex. We model this as a single interaction — more Wnt leads to more inactivation of the destruction complex. We use a mass-action formulation, based on the interactions depicted in Figure 3.3, leading to the following equation

$$
\begin{aligned}
\frac{\mathrm{d}[\mathrm{C}_{active}]}{\mathrm{d}t} &= -a_4[\mathrm{Wnt}][\mathrm{C}_{active}] + a_5[\mathrm{C}_{inactive}], \\
&= a_5[\mathrm{C}_{Total}] - (a_4[\mathrm{Wnt}] + a_5)[\mathrm{C}_{active}].
\end{aligned} \tag{3.8}
$$

In equation (3.8) a_4 represents the rate at which C_{active} is inactivated by Wnt and a_5 that at which $\mathrm{C}_{inactive}$ is activated. Equations (3.7) and (3.8) constitute our model of the Wnt signalling pathway. In chapter 2 we estimated values for a_1 to a_5 (Table 3.4) by reducing the Lee *et al.* (2003) model, for which the parameter values were inferred from experimental results.

3.2.2   Rescaling the Model

It is again helpful to rescale the protein concentrations in terms of dimensionless values as this simplifies the governing equations. We denote our measure of the destruction complex by 'c' and set

$$
c = \frac{[\mathrm{C}_{active}]}{[\mathrm{C}_{Total}]},
$$

so that $0 \leqslant c \leqslant 1$. Similarly we scale β-catenin levels with the highest steady state value, a_1/a_2 (this is the steady state concentration of equation (3.7) when no destruction complex is present).

Then a measure of β-catenin levels becomes 'b' where

$$b = \frac{[\beta\text{-cat}]}{[a_1/a_2]},$$

so that the steady state of b will satisfy $0 \leqslant b \leqslant 1$. We also scale our Wnt stimulus so that

$$W = \frac{[\text{Wnt}]}{[\text{Wnt}]_{max}},$$

where $[\text{Wnt}_{max}]$ is the maximum concentration of Wnt observed in the crypt and therefore $0 \leqslant W \leqslant 1$. We have chosen this value (see Table 3.4) to be that value beyond which only small changes to behaviour are observed. Finally, we scale time, t, on a characteristic degradation time (1/degradation rate) for E2F1, denoted by ϕ_{E2F1} in the full equations (3.1)–(3.6), so that

$$t^* = \phi_{E2F1} t.$$

Swat *et al.* (2004) estimate $\phi_{E2F1} = 0.1 \text{ min}^{-1}$. In terms of the new rescaled variables our two model equations become

$$\frac{\mathrm{d}c}{\mathrm{d}t^*} = \tilde{a}_5(1 - c) - \tilde{a}_4 W c, \tag{3.9}$$

$$\frac{\mathrm{d}b}{\mathrm{d}t^*} = \tilde{a}_2(1 - b) - \tilde{a}_3 b c. \tag{3.10}$$

Rescaled parameter values are shown in Table 3.4. The steady states of our wild-type (wt) model, c_{steady} and b_{steady}, can be easily determined by setting $\mathrm{d}/\mathrm{d}t = 0$ in equations (3.9) and (3.10) to give

$$c_{steady}^{wt} = \frac{\tilde{a}_5}{\tilde{a}_4 W + \tilde{a}_5} = \left(1 + \frac{\tilde{a}_4}{\tilde{a}_5} W\right)^{-1}, \tag{3.11}$$

and

$$b_{steady}^{wt} = \frac{\tilde{a}_2}{\tilde{a}_2 + \tilde{a}_3 c_{steady}} = \left(1 + \frac{\tilde{a}_3}{\tilde{a}_2} c_{steady}\right)^{-1}. \tag{3.12}$$

Note that equations (3.11) and (3.12) have only two nondimensional parameter groupings, which is advantageous when examining the effects of parameter changes on the steady states. In Figure 3.6 b_{steady} is plotted for various levels of Wnt stimulation, W. For comparison, the associated steady levels of β-catenin for the most commonly detected CRC mutations are also shown, being obtained using the approach outlined below.

3.2.3 Modelling Mutations

APC mutations can occur at many different sites on the gene, leading to proteins with many different structures. The majority of mutations are harmless, but of those *APC* mutations observed
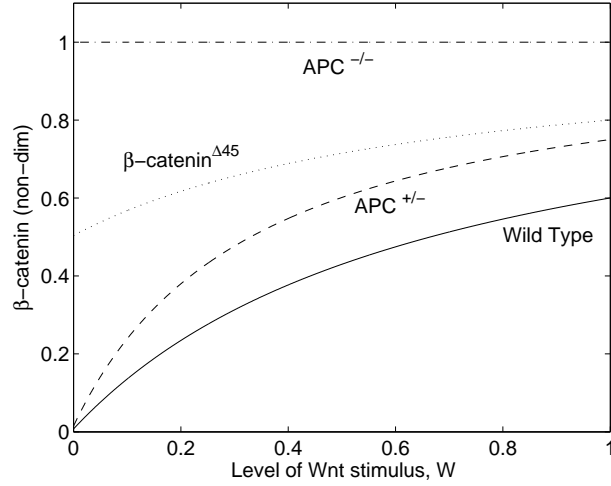
Figure 3.6: The steady level of β-catenin under different Wnt stimuli for wild type cells and cells with the common mutations, given by equations (3.12)–(3.15) using the parameter values in Table 2.2. Dimensionless values are plotted.

in tumours there are two different categories of mutation which have different effects if only one APC allele is mutated (a 'single hit'). Some mutations lead to APC forming a destruction complex that cannot function properly, the destruction complexes will be permanently inactive and incapable of degrading β-catenin; other mutations render APC unable to bind to Axin and hence to the other destruction complex components, but these components are still able to bind to normal APC encoded by the other allele and thus to create additional active destruction complexes, that can still degrade β-catenin. If both APC alleles are mutated (a 'double hit') then either scenario leads to complete absence of active destruction complex.

We model a single hit as one which causes APC to form inert destruction complexes (the worst-case scenario for the cell), we assume that half of the destruction complexes become active and degrade β-catenin, b. If both copies of the APC gene are mutated then there are no active destruction complexes present. We can therefore represent the one and two hit cases by varying the parameter $\tilde{a}_3$ term that appears in equation (3.10), to half its wild-type value for a single-hit ($APC^{+/-}$) and to zero for a double-hit ($APC^{-/-}$). The steady state of β-catenin then becomes

$$b_{steady}^{apc^{+/-}} = \frac{\tilde{a}_2}{\tilde{a}_2 + \frac{\tilde{a}_3}{2} c_{steady}}, \tag{3.13}$$

for $APC^{+/-}$, where c_{steady} is given by equation (3.11), and

$$b_{steady}^{apc^{-/-}} = 1, \tag{3.14}$$

for $APC^{-/-}$. To model a mutation in a single β-catenin allele we decompose b into two subtypes,

with the wild-type produced with proportion $0 < \theta < 1$ and the mutant produced with proportion $0 < (1 - \theta) < 1$; we assume that subtype b_1 is wild-type and can be degraded by the destruction complex and b_2 is mutant and cannot:

$$
\begin{aligned}
b &= \theta b_1 + (1 - \theta) b_2, \\
\frac{\mathrm{d}b_1}{\mathrm{d}t^*} &= \tilde{a}_2 (\theta - b_1) - \tilde{a}_3 b_1 c, \\
\frac{\mathrm{d}b_2}{\mathrm{d}t^*} &= \tilde{a}_2 ((1 - \theta) - b_2).
\end{aligned}
$$

In these equations b_1 is the wild-type protein (without mutations), whilst b_2 represents the mutated protein. We stress that this model accounts only for those mutations observed in tumours, which allow β-catenin to function whilst being immune to the destruction complex. The steady state level of b for a single mutant β-*catenin* (β-*catenin*^{mut}) is given by

$$
b_{steady}^{mut} = b_{1\ steady} + b_{2\ steady} = \left((1 - \theta) + \frac{\theta \tilde{a}_2}{\tilde{a}_3 c_{steady} + \tilde{a}_2} \right). \tag{3.15}
$$

As can be seen by comparing equations (3.12)–(3.15) it is always true that

$$
b_{steady}^{wt} < b_{steady}^{apc^{+/-}} < b_{steady}^{apc^{-/-}},
$$

and

$$
b_{steady}^{wt} < b_{steady}^{mut} < b_{steady}^{apc^{-/-}}.
$$

The inequality for b_{steady}^{mut} and $b_{steady}^{apc^{+/-}}$ cannot be determined until θ is chosen. We choose $\theta = \frac{1}{2}$ (equal expression of wild type and mutant β-catenin) to establish that $b_{steady}^{apc^{+/-}} < b_{steady}^{mut}$. The steady levels of β-catenin resulting from the three mutations mentioned above are shown alongside a healthy (wild-type) cell's response to Wnt signals in Figure 3.6. The qualitative behaviour of the results presented in Figure 3.6 are robust to variations in parameter values. The model suggests that in wild type cells, with a zero Wnt stimulus, the destruction complex is highly active and so the level of β-catenin will be kept low. As the Wnt signal increases, the destruction complex becomes inactivated and the equilibrium concentration of β-catenin rises before plateauing as Wnt reaches its maximum value ($W = 1$). Taken together these results suggest that the observed variation in β-catenin seen along the crypt axis (Gaspar & Fodde, 2004) may be due to variation in the Wnt concentration, the action of the Wnt pathway being mediated by the destruction complex.

$APC^{+/-}$ cells present a slightly higher level of β-catenin than wild type cells. Moreover, β-*catenin*$^{\Delta 45}$ cells have much higher β-catenin levels under a low Wnt stimulus, with a larger β-catenin concentration than the $APC^{+/-}$ for all levels of Wnt. In $APC^{-/-}$ cells the destruction complex cannot phosphorylate β-catenin and the latter reaches its highest level, independent of the

Wnt stimulus. In these three types of mutations Wnt has successively less control over levels of β-catenin; in $APC^{-/-}$ mutants Wnt's control is completely lost.

3.3 Coupling Wnt Signalling and Cell Proliferation

To form the full coupled model we simplify equations (3.1)–(3.6) by nondimensionalising using the rescalings

$$
\begin{array}{lclclcl}
[\text{pRb}] & = & \frac{k_1}{\phi_{E2F1}}r, & [\text{E2F1}] & = & K_{m2}e, & [\text{CycD}_i] & = & K_{m4}i, \\
[\text{CycD}_a] & = & K_{m4}j, & [\text{AP-1}] & = & \frac{F_m a_1}{\phi_{E2F1}a_2}x, & [\text{pRb}_p] & = & \frac{k_1}{\phi_{E2F1}}p, \\
t & = & t^*/\phi_{E2F1}, & & & & [\text{Wnt}] & = & [\text{Wnt}]_{max}W.
\end{array}
$$

As discussed above, we also rescale the Wnt pathway components, according to

$$
c = \frac{[\text{C}_{active}]}{[\text{C}_{total}]}, \quad b = \frac{[\beta\text{-cat}]}{[a_1/a_2]}.
$$

β-catenin is a direct transcription factor for Cyclin D, so we can ignore equation (3.5) and use β-catenin instead of AP-1 in the transcription-factor-dependent production term in equation (3.3). A scaling factor F premultiplies the rate constant k_3 to account for the fact that β-catenin and AP-1 are present at different concentrations: in Swat *et al.* (2004) $8\times10^{-3} < [\text{AP-1}] < 1.24$ whereas in Lee *et al.* $25 < [\beta\text{-cat}] < 155$. We fix $F = 6\times10^{-3}$ to compensate for the difference in concentrations. Since we are interested in the cell-cycle times for a cell under a constant Wnt stimulus, we take the steady-state level of β-catenin as an input, rather than solving two more ODEs; as a result b_{steady} is the input into the cell-cycle model. Under the above transformations, equations (3.1) – (3.6) become

$$
\frac{\mathrm{d}r}{\mathrm{d}t^*} = \frac{e}{\tilde{K}_{m1} + e}\frac{\tilde{J}_{11}}{\tilde{J}_{11} + r}\frac{\tilde{J}_{61}}{\tilde{J}_{61} + p} - \tilde{k}_{16}rj + \tilde{k}_{61}p - \phi_r r, \tag{3.16}
$$

$$
\frac{\mathrm{d}e}{\mathrm{d}t^*} = \tilde{k}_p + \tilde{k}_2\frac{\tilde{a}^2 + e^2}{1 + e^2}\frac{\tilde{J}_{12}}{\tilde{J}_{12} + r}\frac{\tilde{J}_{62}}{\tilde{J}_{62} + p} - e, \tag{3.17}
$$

$$
\frac{\mathrm{d}i}{\mathrm{d}t^*} = \tilde{k}_3 b_{steady} + \tilde{k}_{23}e\frac{\tilde{J}_{13}}{\tilde{J}_{13} + r}\frac{\tilde{J}_{63}}{\tilde{J}_{63} + p} + \tilde{k}_{43}j - \tilde{k}_{34}i\frac{j}{1 + j} - \phi_i i. \tag{3.18}
$$

$$
\frac{\mathrm{d}j}{\mathrm{d}t^*} = \tilde{k}_{34}i\frac{j}{1 + j} - (\tilde{k}_{43} + \phi_j)j, \tag{3.19}
$$

$$
\frac{\mathrm{d}p}{\mathrm{d}t^*} = \tilde{k}_{16}rj - \tilde{k}_{61}p - \phi_p p. \tag{3.20}
$$

with the rescaled parameters shown in Table 3.2.

The dimensionless system was solved numerically using routine `ode15s` (a stiff ODE system solver) in MatLab. The initial conditions (namely the protein concentrations at the beginning of G_1 phase) were taken as the steady states of the original model with $F_m = 0$ and are listed in Table 3.3; note

that these steady states are identical to the steady states of equations (3.16)–(3.20) with $b_{steady} = 0$. We simulated the G_1 phase under a steady Wnt stimulus where b_{steady} is given by one of equations (3.12)–(3.15) depending on the mutation state.

The cell is deemed to enter S phase when the E2F1 level crosses a suitable threshold (on the phase transition arrow of Figure 3.4, for example, [E2F1] = 5) and the time this occurs is recorded as the duration of the G_1 phase. Since the level of E2F1 rises very quickly after a slow progression, the result is not sensitive to the exact choice of threshold value. If the cell never reaches this threshold because the level of β-catenin, and hence Cyclin D, remains too low (the mitogenic stimulus is to the left of the right-hand SN bifurcation in Figure 3.4) then the cell is said to be quiescent. The results of our simulations, for healthy and mutant cells, are shown in Figure 3.7.
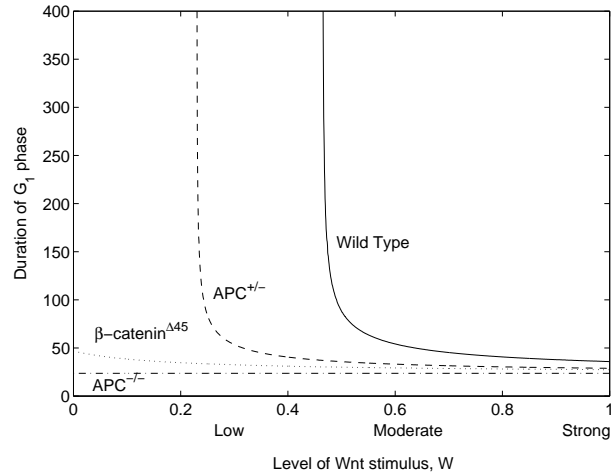
Figure 3.7: The variation in G_1 phase duration of our combined model under different Wnt stimuli, W, for wild type cells and cells with the common mutations, using the parameter values in Table 3.2 and Table 3.4 with the initial conditions in Table 3.3. To the left of the vertical sections the cells are quiescent (in G_0 phase) and will not proliferate. Rescaled (dimensionless) values are plotted.

Figure 3.7 shows the general trend for a shorter G_1 phase when the cell is exposed to a stronger Wnt stimulus. We observe that wild-type cells proliferate quickly under a strong Wnt stimulus (e.g. at the base of a crypt), proliferate less rapidly as the stimulus reduces and become quiescent at low Wnt stimuli (e.g. at the top of a crypt). This mechanism could explain the observed proliferation patterns in a healthy crypt. The model predicts a variation in the duration of G_1 phase, from typically around 6 hours (in a strong Wnt signal, $W \approx 1$) to 25 hours (under a moderate Wnt signal, $W \approx 0.6$), with quiescent cells under lower Wnt stimuli.

Cells with a single *APC* mutation exhibit the same qualitative behaviour as their wild-type counterparts, becoming quiescent under low Wnt stimuli and proliferating more rapidly as Wnt levels increase. The G_1 phase duration in an $APC^{+/-}$ cell is shorter than wild-type cells for a given Wnt stimulus, and the Wnt threshold for quiescence is lower.

Cells with a $\beta\text{-}catenin^{\Delta 45}$ or $APC^{-/-}$ mutation fail to keep levels of β-catenin low enough to remain (or become) quiescent for any Wnt signal strength. Consequently, they proliferate rapidly (with G_1 phase durations always under approximately 8 hours) and uncontrollably, which suggests a route to adenoma formation and colorectal cancer initiation. $\beta\text{-}catenin^{\Delta 45}$ cells retain some sensitivity to Wnt stimulation (the duration of their cell cycle varying between 4.5 and 8 hours) but the $APC^{-/-}$ cells proliferate independently of the Wnt signal (with the fastest duration of any mutation case — approximately 4 hours). In reality cells with a double *APC* hit will probably be regulated by other factors and may never replicate this quickly. Our model presents the expected increase in proliferation when the Wnt pathway becomes disregulated and Cyclin D levels are no longer controlled.

Our model predicts that a $\beta\text{-}catenin$ double-hit would have the same effect on β-catenin concentrations as the APC double-hit (in both cases there would be no phosphorylation by the destruction complex). The reason that $\beta\text{-}catenin^{-/-}$ cells are not observed in colorectal cancer tumours is that a $\beta\text{-}catenin^{\Delta 45}$ mutation removes Wnt's control of the cell sufficiently to allow colorectal cancer to develop (Figure 3.7); the cell does not need to acquire another mutation to lose control of proliferation. In contrast in $APC^{+/-}$ mutants the cell's activity is still Wnt dependent and there remains some control of the mutant cell until further genetic alterations are acquired and the cell becomes Wnt independent.

3.4 Discussion

In this chapter we have coupled a simple model for the intracellular accumulation of β-catenin in response to Wnt signalling to a simplified model of the G_1/S transition of the cell cycle, in order to gain insight into how extracellular Wnt signalling might affect cell proliferation.

We produced a quantitative model predicting cell proliferation rates in the presence of a Wnt stimulus. The proposed Wnt gradient, through the action of β-catenin and Cyclin D, can explain the observed proliferation in a colorectal crypt. Some experiments suggest that stem cells (at the very base of the crypt) proliferate less rapidly than the cells above (Potten *et al.*, 1997); however our model does not distinguish between stem cells and transit cells, and so does not reproduce this

effect. There may be other biological processes that have been neglected which limit stem cell proliferation.

As our model includes those components of the Wnt pathway that become mutated in colorectal cancer, we have been able to investigate the effects of three common mutations. We predict that a single *APC* hit increases the rate of cell proliferation but is unable to disregulate growth completely, and indeed this mutation is not observed in CRC tumour samples. A single *β-catenin* mutation is sufficient to cause disregulated proliferation throughout the crypt, although there is still some response to Wnt stimulation, whilst a double *APC* hit removes Wnt control completely, and indeed these mutations are those most commonly observed in CRC adenomas.

We assumed that all proteins in a cell are freely available to interact with each other; in reality the localisation of proteins to different parts of the cell may be important. For example, $β$-catenin is found in the cytoplasm, at the cell membrane where it acts in cell-cell adhesion and it also moves to and from the nucleus, where it promotes transcription. Such spatial effects, for $β$-catenin and the other proteins in the Wnt pathway, could play an important role. As discussed in section 1.4, it is probable that, in addition to *Cyclin D*, other Wnt target genes have some impact on the cell cycle and could affect our predictions. Furthermore, our model assumes that, of the proteins involved in the regulation of the Wnt pathway, only $β$-catenin influences the cell cycle; however GSK3$β$ has been shown to interact with Cyclin D (Diehl *et al.*, 1998). During the different phases of the cell cycle, components which influence the Wnt signalling pathway may be temporarily expressed, leading to feedback loops which are not currently included in this model. Other possible extensions involve the investigation of the reduced Wnt-signalling-feedback model (derived in the previous chapter, see equation (2.61)) and the cell cycle.

Many of the interactions that we have modelled are still keenly disputed. Experimental estimates of parameter values for both the cell cycle and Wnt signalling models in human colorectal tissue are currently lacking; these would greatly help to validate and improve our model.

At first glance our Wnt pathway model may appear overly simplistic, but it retains the crucial components for studying colorectal cancer initiation. We believe this is the first quantitative model linking Wnt signalling to cell proliferation and, therefore, the first to explain how the most common mutations of the Wnt pathway may be implicated in the initiation of colorectal cancer.

CHAPTER 4

The Influence of Wnt Signalling
on c-Myc and the Cell Cycle

4.1 Introduction

THE model constructed in chapter 3 predicts the healthy response of a cell cycle to a Wnt stimulation, and hyperproliferation following APC or β-*catenin* mutations. That model focuses on the link between β-catenin and Cyclin D levels to represent the influence of Wnt signalling on the cell cycle. Recently Sansom *et al.* (2007) performed experiments which suggest that increased levels of c-Myc (or Myc[1]), rather than Cyclin D, are responsible for the increased proliferation observed after an APC knockout. The model of chapter 3 cannot replicate these results because it does not account for the role of Myc. In this chapter we formulate a model which relates β-catenin, Myc, Cyclin D and CDK4 levels in an attempt to replicate Sansom *et al.*'s results, which we discuss in more detail below.

4.1.1 Experimental Results

Sansom *et al.* (2007) have performed targeted gene-knockout experiments on adult mice. Mice are engineered with extra markers (loxP) either side of a target gene. This is known as "floxing" a gene. A compound is injected which activates Cre (Cyclization recombinase enzymes), Cre recognises the two loxP sites and splices them together, 'chopping-out' the floxed target DNA, as shown in Figure 4.1.

Transcription of the target gene is silenced as there is no longer a 'start' site associated with it.

---

[1] Whilst other Myc proteins exist, "Myc" generally represents c-Myc and others, such as N-Myc, retain their prefixes.

Cre inactive – target and reporter genes expressed

Cre active – target gene removed, reporter gene expressed
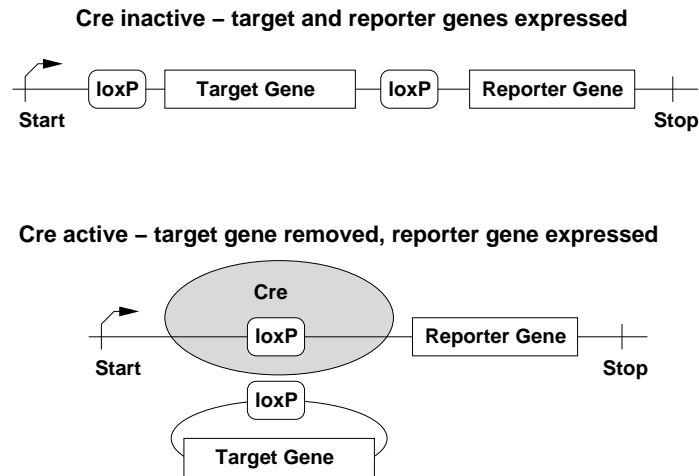
Figure 4.1: The action of Cre. Top: Mice are engineered to have two 'loxP' sites either side of a target gene, and to express a reporter gene, such as *GFP*. The mice will express both the target gene and the reporter gene in the absence of Cre. Bottom: Cre is induced and the target gene is removed from the DNA, leaving only the reporter gene being expressed.

Translation from existing target mRNAs will continue for some time, and the existing target proteins will not be degraded immediately. Using this inducible-knockout technique means that an organism develops into its fully grown, wild-type state. The gene knockout can then be performed on healthy tissue, rather than observing the tissues of an organism that developed with a missing gene.

When Sansom *et al.* induced APC loss they found highly proliferating crypts, with increased adhesion and decreased migration, as expected and observed previously. Myc knockouts appeared to have little effect on the homeostasis of the healthy crypt. Surprisingly, a double knockout of APC and Myc resulted in near-healthy crypts, the Myc knockout reversing the effects of the APC knockout. We aim to recreate these findings by performing virtual knockout experiments on a mathematical model. In contrast to the model in chapter 3, we now take into account the action of Myc and CDK4 as well as Cyclin D.

The remainder of the chapter is structured as follows. We develop our model in section 4.2, present our results in section 4.3, propose possible drug targets in section 4.4 and discuss our conclusions in section 4.5.
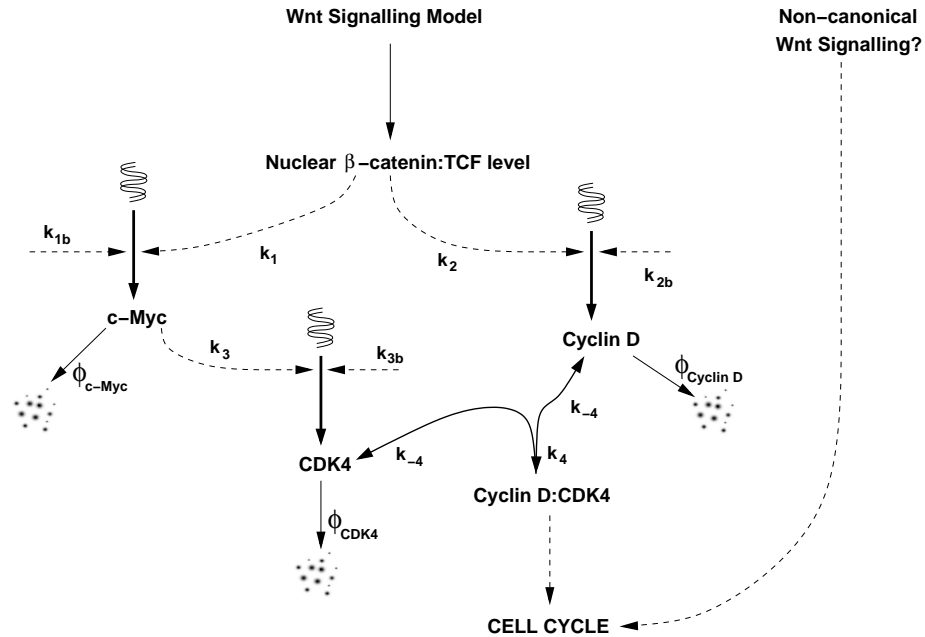
Figure 4.2: Schematic of the model. Dashed lines indicate promotion of their target, solid lines denote production of their target and, in the case of a protein, reduction of their source.

4.2 Model Derivation

We explained in chapter 2 how most Wnt-signalling models predict how a Wnt stimulus might affect the levels of β-catenin, many using the level of nuclear β-catenin:TCF as their output, so we may adapt this as the input into our new model.

Figure 4.2 shows how Myc and Cyclin D are upregulated by β-catenin. Myc independently upregulates CDK4. Cyclin D and CDK4 then associate to form a complex Cyclin D:CDK4. A high level of Cyclin D:CDK4 complex is required to 'kick-start' the cell cycle and pass the G_1/S checkpoint.

In what follows we use the term "Cyclin D" to represent all D-type cyclins within the crypt, as various reports indicate that Cyclin D1, Cyclin D2 or both are major targets of β-catenin (Shtutman *et al.*, 1999; Tetsu & McCormick, 1999; Wang *et al.*, 2002a; Sansom *et al.*, 2005, 2007). Similarly CDK4 and CDK6 appear to be equally important binding partners for Cyclin D. However, since only CDK4 is upregulated by Myc we concentrate on CDK4, neglecting CDK6.

4.2.1 Governing Equations

The dependent variables of our model are the levels of Myc, Cyclin D, CDK4 and Cyclin D:CDK4 complex, with the concentration of β-catenin:TCF as a prescribed input into the system; the concentrations are denoted with square brackets as [Myc], [CycD], [CDK4], [CycD:CDK4] and [β-cat] respectively, as shown in Table 4.1.

Table 4.1: Summary of independent and dependent model variables and the scalings used to nondimensionalise the system.

Variable		Scaling	Nondimensional variable	Protein/complex description
t	$=$	$1/\phi_{\mathrm{Myc}}$ $(= \tau)$	T	time
[β-cat]	$=$	K_1	β	β-catenin:TCF (transcriptionally active)
[Myc]	$=$	$k_{1b}\tau$	M	c-Myc (transcriptionally active)
[CycD]	$=$	$k_{2b}\tau$	Y	Cyclin D (free)
[CDK4]	$=$	$k_{3b}\tau$	K	CDK4 (free)
[CycD:CDK4]	$=$	$\dfrac{k_4}{k_{-4}}k_{2b}k_{3b}\tau^2$	C	Cyclin D:CDK4 (active complex)

We assume that Myc is produced at a background rate k_{1b} and also, at a rate k_1, in response to β-catenin:TCF4 binding to the promoter region of *c-Myc* (He *et al.*, 1998). This reaction can be represented by a Michaelis-Menten term (see section 3.1.1 and Figure 3.1). In addition we assume that Myc degrades at a constant rate ϕ_{Myc}. Combining these effects we deduce that the evolution of [Myc] is governed by the following ODE:

$$\frac{\mathrm{d[Myc]}}{\mathrm{d}t} = k_{1b} + k_1 \frac{[\beta\text{-cat}]}{K_1 + [\beta\text{-cat}]} - \phi_{\mathrm{Myc}}[\text{Myc}], \tag{4.1}$$

where K_1 is a Michaelis-Menten constant. Myc is also promoted by E2F1 (Bracken *et al.*, 2004), which is an indicator of the S phase of the cell cycle, and c-Myc levels have been observed to vary throughout the cell cycle in rat liver development (Sanders & Gruppuso, 2006), but this has not yet been observed in colorectal tissue and therefore we omit it for simplicity.

We use a similar approach to derive an ODE for [CycD], assuming that Cyclin D is produced at

a constant background rate k_{2b}, and at a rate k_2 which is an increasing, saturating function of β-catenin:TCF. Cyclin D complexes with CDK4 at a rate k_4 which is dependent on the concentrations of the constituent parts, the complex dissociates at a rate k_{-4} which is dependent on the concentration of the complex. Cyclin D is assumed to degrade from its free state only at a rate ϕ_{CycD}. Combining these features we arrive at the following ODE for [Cyclin D]:

$$\frac{\mathrm{d}[\text{CycD}]}{\mathrm{d}t} = k_{2b} + k_2\frac{[\beta\text{-cat}]}{K_2 + [\beta\text{-cat}]} - k_4[\text{CycD}][\text{CDK4}] + k_{-4}[\text{CycD:CDK4}] - \phi_{\text{CycD}}[\text{CycD}]. \quad (4.2)$$

An equation for the concentration of CDK4 can be formed similarly, where k_{3b} is the background production rate, and k_3 represents the additional promotion by c-Myc, K_3 is the dissociation constant and ϕ_{CDK4} is the degradation rate of CDK4. Again CDK4 is incorporated into a complex with Cyclin D at a rate k_4 and dissociates from Cyclin D:CDK4 at a rate k_{-4}, giving the equation:

$$\frac{\mathrm{d}[\text{CDK4}]}{\mathrm{d}t} = k_{3b} + k_3\frac{[\text{Myc}]}{K_3 + [\text{Myc}]} - k_4[\text{CycD}][\text{CDK4}] + k_{-4}[\text{CycD:CDK4}] - \phi_{\text{CDK4}}[\text{CDK4}]. \quad (4.3)$$

We also include the formation of the Cyclin D:CDK4 complex, which is the output of this model, influencing the cell cycle. We assume that this complex forms at a rate k_4 and dissociates at a rate k_{-4}, there being no explicit degradation from the complex; i.e. the proteins dissociate before they decay. The evolution of [CycD:CDK4] is then given by

$$\frac{\mathrm{d}[\text{CycD:CDK4}]}{\mathrm{d}t} = k_4[\text{CycD}][\text{CDK4}] - k_{-4}[\text{CycD:CDK4}]. \quad (4.4)$$

We use the scalings shown in Table 4.1 to leave the final system

$$\frac{\mathrm{d}M}{\mathrm{d}T} = 1 + k_1'\frac{\beta}{1 + \beta} - M, \quad (4.5)$$

$$\frac{\mathrm{d}Y}{\mathrm{d}T} = 1 + k_2'\frac{\beta}{K_2' + \beta} - k_{43}'(YK - C) - \phi_Y Y, \quad (4.6)$$

$$\frac{\mathrm{d}K}{\mathrm{d}T} = 1 + k_3'\frac{M}{K_3' + M} - k_{42}'(YK - C) - \phi_K K, \quad (4.7)$$

$$\frac{\mathrm{d}C}{\mathrm{d}T} = k_{-4}'(YK - C). \quad (4.8)$$

Time is scaled so that $\tau = 1/\phi_{\text{Myc}}$, parameters have been rescaled as shown in Table 4.2. It would be more conventional to rescale so that the coefficients of $(YK - C)$ in equations (4.6), (4.7) and (4.8) are identical; this is equivalent to scaling Y, K and C by the same factor. However to eliminate further parameters and therefore simplify the system to the largest extent possible we scale the variables differently. When the steady-state values are considered the $(YK - C)$ term is eliminated (see equation (4.8)).

Table 4.2: Summary of model parameters and their dimensionless counterparts.

Dimensional Parameter	Estimate	Units	Non-dimensional Parameter	Estimate
K_1	1.0	nM	—	—
K_2	1.0	nM	$K_2' = K_2/K_1$	1.0
K_3	1.08	nM	$K_3' = K_3/(\tau k_{1b})$	1.08
k_{1b}	1.0	nM min^{-1}	—	—
k_1	9.0	nM min^{-1}	$k_1' = k_1/k_{1b}$	9.0
k_{2b}	1.0	nM min^{-1}	—	—
k_2	3.74	nM min^{-1}	$k_2' = k_2/k_{2b}$	3.74
k_{3b}	1.0	nM min^{-1}	—	—
k_3	4.21	nM min^{-1}	$k_3' = k_3/k_{3b}$	4.21
k_4	1.0	nM^{-1} min^{-1}	$k_{42}' = k_4 k_{2b}\tau^2$	1.0
—	—	—	$k_{43}' = k_4 k_{3b}\tau^2$	1.0
k_{-4}	1.0	min^{-1}	$k_{-4}' = k_{-4}\tau$	1.0
ϕ_{Myc}	1.0	min^{-1}	—	—
ϕ_{CycD}	1.0	min^{-1}	$\phi_Y = \phi_{\mathrm{CycD}}\tau$	1.0
ϕ_{CDK4}	1.0	min^{-1}	$\phi_K = \phi_{\mathrm{CDK4}}\tau$	1.0

4.2.2 Modelling Gene Knockouts

In Sansom *et al.*'s gene-knockout experiments both copies of a gene were removed from DNA by Cre recombinase. As discussed in section 4.1.1 the technique Sansom *et al.* used has the effect of immediately stopping mRNA transcription, although existing proteins survive (and translation of proteins from existing mRNAs may continue) for a short time until the natural turnover eliminates the protein from the cell. Here we address the modifications needed to equations (4.5)–(4.8) in order to model the process of Sansom *et al.*'s knockout experiments.

To model this experimental process of an APC knockout we assume that β-catenin will attain its maximum value, as discussed in section 3.2.3. We further assume that a large value of β in effect saturates the Michaelis-Menten terms in equations (4.5) and (4.6) such that equation (4.5) is modified to read

$$\frac{\mathrm{d}M}{\mathrm{d}T} = 1 + k_1' - M, \tag{4.9}$$

and equation (4.6) becomes

$$\frac{\mathrm{d}Y}{\mathrm{d}T} = 1 + k_2' - k_{43}'(YK - C) - \phi_Y Y. \tag{4.10}$$

To model a Myc knockout we assume that there is no longer any production of M, such that equation (4.5) transforms to simply

$$\frac{\mathrm{d}M}{\mathrm{d}T} = -M, \tag{4.11}$$

the natural protein turnover eliminates Myc from the cell.

To model a double knockout of APC and Myc we use equations (4.11) and (4.10) in place of (4.5) and (4.6) respectively.

4.3 Results

4.3.1 Time-dependent behaviour

Note that equation (4.5) decouples from the rest of the system. If β is time-independent, then equation (4.5) can be solved to give

$$M(T) = \tilde{M} + \left(M(0) - \tilde{M} \right) e^{-T}, \tag{4.12}$$

where $M(0)$ is the initial condition and $\tilde{M}$ represents the steady-state value for $M(T \to \infty)$, given by

$$\tilde{M}_{WT} = 1 + k_1' \frac{\beta}{1 + \beta}, \quad \tilde{M}_A = 1 + k_1', \quad \text{and} \quad \tilde{M}_M = \tilde{M}_{AM} = 0$$

for the wild-type, APC knockout, Myc and double knockouts respectively.

To examine the behaviour of the model as the protein knockouts take effect we have plotted equation (4.12) and solved equations (4.6)–(4.8), or their equivalents for the knockout experiments, numerically with the ODE solver routine `ode45` in MatLab. The solutions can be seen in Figure 4.3.

The effect of an APC knockout is presented in Figure 4.3(a). After the knockout the production of both Cyclin D and c-Myc is upregulated, leading to a higher rate of production of CDK4. However the level of free CDK4 in the cell drops, as it is quickly incorporated into Cyclin D:CDK4 (due to the high levels of Cyclin D). The increased production of CDK4 via Myc compensates for this over time and leads eventually to higher levels of CDK4 and Cyclin D:CDK4. We propose that this mechanism could be responsible for the hyperproliferation of the colonic epithelial cells when an APC mutation occurs (Sellin *et al.*, 2001).

The results of the Myc knockout are presented in Figure 4.3(b); the production of Myc is switched off, leading to an exponential decay in the Myc level towards zero. Myc's promotion of CDK4 falls as a result, and CDK4 levels are reduced by the natural turnover rate of the protein. Cyclin D:CDK4 levels fall to a new steady-state value, releasing Cyclin D, which causes a small transient peak before the Cyclin D level returns to its original steady-state value. The result of the Myc knockout is a reduction in the concentration of Cyclin D:CDK4.

The effect of a double (APC and Myc) knockout is shown in Figure 4.3(c). The level of Myc falls exponentially, as it did in the simulation shown in Figure 4.3(b) and as does the profile for CDK4, which eventually reaches the same equilibrium levels as for the Myc knockout. However the level of Cyclin D increases dramatically, as it did under the single APC knockout. This initially leads to a peak in Cyclin D:CDK4 levels, as (for our particular choice of parameter values) Cyclin D levels increase more rapidly than free CDK4 is degraded. After some time the levels of CDK4 become sufficiently low to balance the increase in Cyclin D levels, such that their product (YK, the rate of production of Cyclin D:CDK4) is similar to that of the wild-type case. This makes the level of C, [Cyclin D:CDK4], our input into the cell cycle, similar to that of the wild-type case; i.e. we have qualitative agreement with Sansom *et al.*'s results.

4.3.2 Steady States

To analyse the behaviour of the system without resorting to simulation we examine the steady states of the equations, which can all be found analytically. Equations (4.5)-(4.8) admit a unique

(a)

(b)

(c)
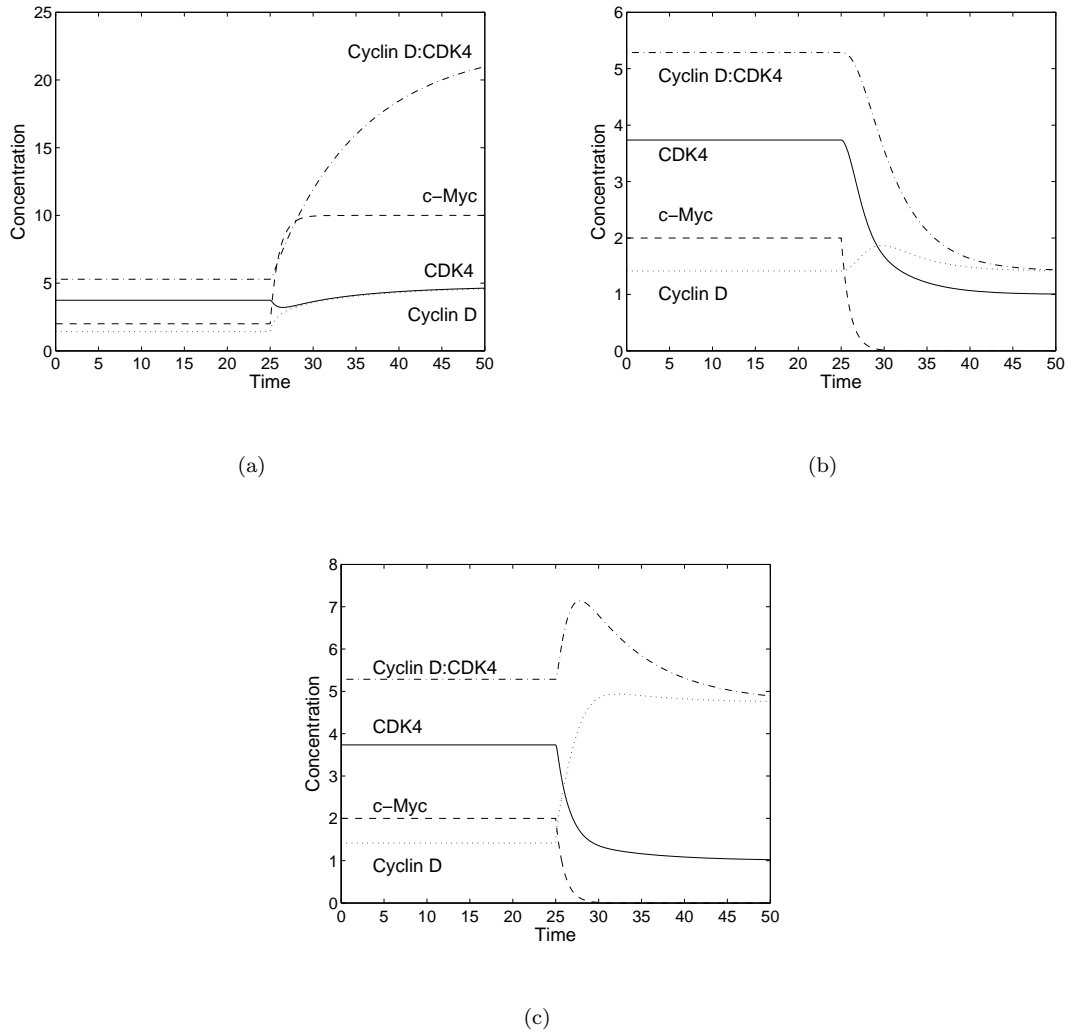
Figure 4.3: Time-dependent simulations of the three knockout experiments. (a) APC knockout, (b) Myc knockout and (c) APC, Myc double-knockout. The knockout experiments are performed as discussed in section 4.2.2 on the nondimensional equations (4.5)–(4.8) at $T = 25$, with the initial conditions being the steady state of the wild-type equations. Simulations performed with $\beta = \frac{1}{8}$ and the other parameter values shown in Table 4.2.

steady state, which can be found by setting the time derivative to zero in each equation. Denoting steady-state values with tildes, it is straightforward to derive analytic expressions for the steady-state solutions for the various cases or interest.

Wild-Type Steady States

At the wild-type steady state of equations (4.5)–(4.8), denoted by a subscript 'WT', we have:

$$\tilde{M}_{\mathrm{WT}} \;=\; 1 + k_1' \frac{\beta}{1+\beta}, \tag{4.13}$$

$$\tilde{Y}_{\mathrm{WT}} \;=\; \frac{1}{\phi_Y} \left(1 + k_2' \frac{\beta}{K_2' + \beta} \right), \tag{4.14}$$

$$\tilde{K}_{\mathrm{WT}} \;=\; \frac{1}{\phi_K} \left(1 + k_3' \frac{\tilde{M}_{\mathrm{WT}}}{K_3' + \tilde{M}_{\mathrm{WT}}} \right), \tag{4.15}$$

$$\tilde{C}_{\mathrm{WT}} \;=\; \frac{1}{\phi_K \phi_Y} \left(1 + k_2' \frac{\beta}{K_2' + \beta} \right) \left(1 + k_3' \frac{\tilde{M}_{\mathrm{WT}}}{K_3' + \tilde{M}_{\mathrm{WT}}} \right). \tag{4.16}$$

APC Knockout Steady States

If we denote the APC knockout steady states with a subscript 'A', then our steady state for equations (4.9), (4.10), (4.7) and (4.8) becomes:

$$\tilde{M}_{\mathrm{A}} \;=\; 1 + k_1', \tag{4.17}$$

$$\tilde{Y}_{\mathrm{A}} \;=\; \frac{1}{\phi_Y} \left(1 + k_2' \right), \tag{4.18}$$

$$\tilde{K}_{\mathrm{A}} \;=\; \frac{1}{\phi_K} \left(1 + k_3' \frac{\tilde{M}_{\mathrm{A}}}{K_3' + \tilde{M}_{\mathrm{A}}} \right), \tag{4.19}$$

$$\tilde{C}_{\mathrm{A}} \;=\; \frac{1}{\phi_K \phi_Y} \left(1 + k_2' \right) \left(1 + k_3' \frac{\tilde{M}_{\mathrm{A}}}{K_3' + \tilde{M}_{\mathrm{A}}} \right). \tag{4.20}$$

Comparing (4.13)–(4.16) with (4.17)–(4.20), we deduce that

$$\tilde{M}_{\mathrm{A}} \;>\; \tilde{M}_{\mathrm{WT}},$$
$$\tilde{Y}_{\mathrm{A}} \;>\; \tilde{Y}_{\mathrm{WT}},$$
$$\tilde{K}_{\mathrm{A}} \;>\; \tilde{K}_{\mathrm{WT}},$$
$$\tilde{C}_{\mathrm{A}} \;>\; \tilde{C}_{\mathrm{WT}}.$$

Thus, as expected, following an APC knockout the levels of all model variables are elevated relative to the wild-type.

Myc Knockout Steady States

We determine this steady state by fixing $\tilde{M} = 0$ in equations (4.13)–(4.16). if we denote it by a subscript 'M', then our Myc knockout steady state has

$$\tilde{M}_{\mathrm{M}} = 0, \tag{4.21}$$

$$\tilde{Y}_{\mathrm{M}} = \frac{1}{\phi_Y}\left(1 + k_2' \frac{\beta}{K_2' + \beta}\right), \tag{4.22}$$

$$\tilde{K}_{\mathrm{M}} = \frac{1}{\phi_K}, \tag{4.23}$$

$$\tilde{C}_{\mathrm{M}} = \frac{1}{\phi_K \phi_Y}\left(1 + k_2' \frac{\beta}{K_2' + \beta}\right). \tag{4.24}$$

Comparing (4.13)–(4.16) and (4.21)–(4.24) we note that

$$\tilde{M}_{\mathrm{M}} < \tilde{M}_{\mathrm{WT}},$$

$$\tilde{Y}_{\mathrm{M}} \equiv \tilde{Y}_{\mathrm{WT}},$$

$$\tilde{K}_{\mathrm{M}} < \tilde{K}_{\mathrm{WT}},$$

$$\tilde{C}_{\mathrm{M}} < \tilde{C}_{\mathrm{WT}}.$$

Therefore the levels of all variables are diminished following a Myc knockout, except for free Cyclin D (Y) whose levels remain unchanged as Myc is not a transcription factor for Cyclin D.

Double APC and Myc Knockout Steady States

A double (APC and Myc) knockout is denoted by a subscript 'AM'. The steady states of equations (4.11), (4.10), (4.7) and (4.8) are

$$\tilde{M}_{\mathrm{AM}} = 0, \tag{4.25}$$

$$\tilde{Y}_{\mathrm{AM}} = \frac{1}{\phi_Y}\left(1 + k_2'\right), \tag{4.26}$$

$$\tilde{K}_{\mathrm{AM}} = \frac{1}{\phi_K}, \tag{4.27}$$

$$\tilde{C}_{\mathrm{AM}} = \frac{1}{\phi_K \phi_Y}\left(1 + k_2'\right), \tag{4.28}$$

respectively. In this case, comparison of (4.13)–(4.16) and (4.25)–(4.28) reveals that

$$\tilde{M}_{\mathrm{AM}} < \tilde{M}_{\mathrm{WT}},$$

$$\tilde{Y}_{\mathrm{AM}} > \tilde{Y}_{\mathrm{WT}},$$

$$\tilde{K}_{\mathrm{AM}} < \tilde{K}_{\mathrm{WT}}.$$

Table 4.3: Experimental results from Sansom *et al.* (2007, supplementary material).

Protein	APC knockout vs. Wild-Type
Myc	4.99
Cyclin D2	4.09
CDK4	2.39

Protein	APC Myc knockout vs. Wild-Type
CDK4	0.51

The Myc knockout causes a downregulation in CDK4 levels (K), yet the APC mutation causes an increase in Cyclin D (Y) levels. It is not possible to derive an inequality for the concentration of Cyclin D:CDK4 (C) as it is proportional to the product of $\tilde{Y}_{AM}$ and $\tilde{K}_{AM}$. The size of $\tilde{C}_{AM}$ relative to $\tilde{C}_{WT}$ depends crucially upon parameter values. It is possible that under certain parameter regimes $\tilde{C}_{AM} \approx \tilde{C}_{WT}$, which would be consistent with Sansom *et al.*'s experimental observation of approximately equal levels of proliferation. Below we will use the experimental observations of Sansom *et al.* (2007) to fix some of our parameter values.

4.3.3 Parameter estimates

In this section we match the steady-states of our model with steady-state values recorded in Sansom *et al.* (2007), in order to estimate parameter values. In their supplementary material Sansom *et al.* (2007) record the overall protein concentrations relative to the wild-type case. These figures provide a measure of the total amount of protein present, including protein that is complexed with other proteins, and are shown in Table 4.3.

The values in Table 4.3 represent averages over many epithelial cells. In the wild-type case these cells would have been exposed to a range of Wnt stimuli, and hence have different β-catenin levels. To compare the experimental results with results from our model we first reinterpret β as representing the fixed, 'mean' level of β-catenin that these cells contained, labelling this $\hat{\beta}$. We explain below how the data contained in Table 4.3 may be combined with our expressions for the steady-state solutions to deduce four independent relationships between the system parameters.

From Table 4.3 we infer that:

1. Myc is 5 times higher for APC knockouts than for the wild type,

2. Cyclin D2 is 4.1 times higher for APC knockouts than for the wild type,

3. CDK4 is 2.4 times higher for APC knockouts than for the wild type,

4. CDK4 is 0.5 times the wild-type level in double knockouts.

Remembering that the relationships above refer to the total levels of proteins present, using the steady-states established in section 4.3.2, experimental observations (1)–(4) become

$$5\tilde{M}_{WT} = \tilde{M}_A, \tag{4.29}$$

$$4.1(\tilde{Y}_{WT} + \tilde{C}_{WT}) = \tilde{Y}_A + \tilde{C}_A, \tag{4.30}$$

$$2.4(\tilde{K}_{WT} + \tilde{C}_{WT}) = \tilde{K}_A + \tilde{C}_A, \tag{4.31}$$

$$0.5(\tilde{K}_{WT} + \tilde{C}_{WT}) = \tilde{K}_{AM} + \tilde{C}_{AM}. \tag{4.32}$$

These knockout experiment results could reflect influences from many other upstream and downstream targets of this, and other pathways and are not necessarily all due to the mechanism we have proposed; however, we will show that the model outlined in Figure 4.2 is consistent with these results when parameters are within certain ranges.

The dissociation rate of β-catenin:TCF with a Cyclin D promoter is likely to be the same as that with a Myc promoter, so we assume that $K_2 = K_1$, which implies that $K_2' = 1$. We also assume that the decay rate $\phi_K = \phi_Y = 1.0$ i.e. that Cyclin D and CDK4 have the same decay rate as Myc. The rates for k_4 and k_{-4} do not affect the steady states and are assumed to be equal to one. Here we use the relationships (4.29)–(4.32) to provide estimates for k_1', k_2', k_3' (parameters indicating the size of targeted production relative to background production rates) and K_3' (the Michaelis-Menten dissociation constant for Myc on the CDK4 promoter).

Substituting from equations (4.13) and (4.17) into equation (4.29) and rearranging leads to the following expression for k_1':

$$k_1' = \frac{4\left(1 + \hat{\beta}\right)}{1 - 4\hat{\beta}}. \tag{4.33}$$

Equation (4.33) defines the fixed value of k_1' in terms of the input $\hat{\beta}$; for instance, taking $\hat{\beta} = 0.1$ we obtain $k_1' = 7.33$. However β is an input into our model, and may vary; here we treat $\hat{\beta}$ as fixed, namely the mean value experienced by the cells in the experiments. From (4.33) we deduce that β should lie in the range $0 \leqslant \hat{\beta} < \frac{1}{4}$, for consistent solutions. This means that β-catenin is not close to saturation levels for promoting genes in healthy cells. We remark further that if $\hat{\beta} > \frac{1}{4}$ then it would

not be possible for Myc levels in APC knockouts to be five times greater than those in wild-type cells, i.e. the experimental results cannot be matched.

Substituting (4.14), (4.16), (4.18) and (4.20) into equation (4.30) provides us with a rather more complicated expression for k_2', given by

$$k_2' = \frac{4.1\left(\phi_K + 1 + k_3'\frac{\tilde{M}_{WT}}{K_3' + \tilde{M}_{WT}}\right) - \left(\phi_K + 1 + k_3'\frac{\tilde{M}_A}{K_3' + \tilde{M}_A}\right)}{\left(\phi_K + 1 + k_3'\frac{\tilde{M}_A}{K_3' + \tilde{M}_A}\right) - 4.1\frac{\beta}{K_2' + \beta}\left(\phi_K + 1 + k_3'\frac{\tilde{M}_{WT}}{K_3' + \tilde{M}_{WT}}\right)}. \tag{4.34}$$

Taken together, observations (4.31) and (4.32) imply that

$$\tilde{K}_A + \tilde{C}_A = 4.8\left(\tilde{K}_{AM} + \tilde{C}_{AM}\right),$$

which gives us a value for k_3', namely

$$k_3' = 3.8\frac{K_3' + 1 + k_1'}{1 + k_1'}. \tag{4.35}$$

Finally equation (4.32) can be written

$$K_3' = \frac{\left(k_3'(1 + \phi_Y) + k_2'\frac{\beta}{K_2' + \beta} - \phi_Y + 1 + k_2'\frac{\beta}{K_2' + \beta} - 2(1 + k_2')\right)\tilde{M}_{WT}}{\phi_Y - 1 - k_2'\frac{\beta}{K_2' + \beta} + 2(1 + k_2')}. \tag{4.36}$$

We now have k_1', k_2', k_3' and K_3' defined in terms of the other parameters by equations (4.33)–(4.36), to satisfy the requirements of (1)–(4) above. In Figure 4.4 we show how these parameters vary for $0 < \hat{\beta} < \frac{1}{4}$. In Figure 4.4 we observe that k_1' and K_3' are highly sensitive to variations in $\hat{\beta}$, varying by several orders of magnitude as equations (4.33) and (4.36) both have asymptotes at $\hat{\beta} = \frac{1}{4}$. The parameters k_2' and k_3' increase with increasing β, but remain $O(1)$ as $0 < \hat{\beta} < \frac{1}{4}$. k_1' controls the level of production of Myc via β-catenin promotion, whilst K_3' affects the level of Myc's promotion of CDK4, which suggests that the model is sensitive to these interactions. The fact that we can establish a range of parameter values in Figure 4.4 which recreate the steady state behaviours observed, suggests that this model is a plausible mechanism by which the Wnt/β-catenin signalling pathway influences Cyclin D and CDK4 levels.

We fix $\hat{\beta} = \frac{1}{8}$ as our 'mean' stimulus for the pathway, as it falls in the centre of the range of stimuli which reproduce the observed experimental results. With $\hat{\beta} = \frac{1}{8}$ in (4.33)–(4.36) we calculate the nondimensional parameters shown in Table 4.2, suggesting combinations of dimensional parameters which would lead to these dimensionless parameters where appropriate. Notice that all of the 'k' parameters are greater than one, suggesting the promotion rates are capable of being higher than background expression rates.
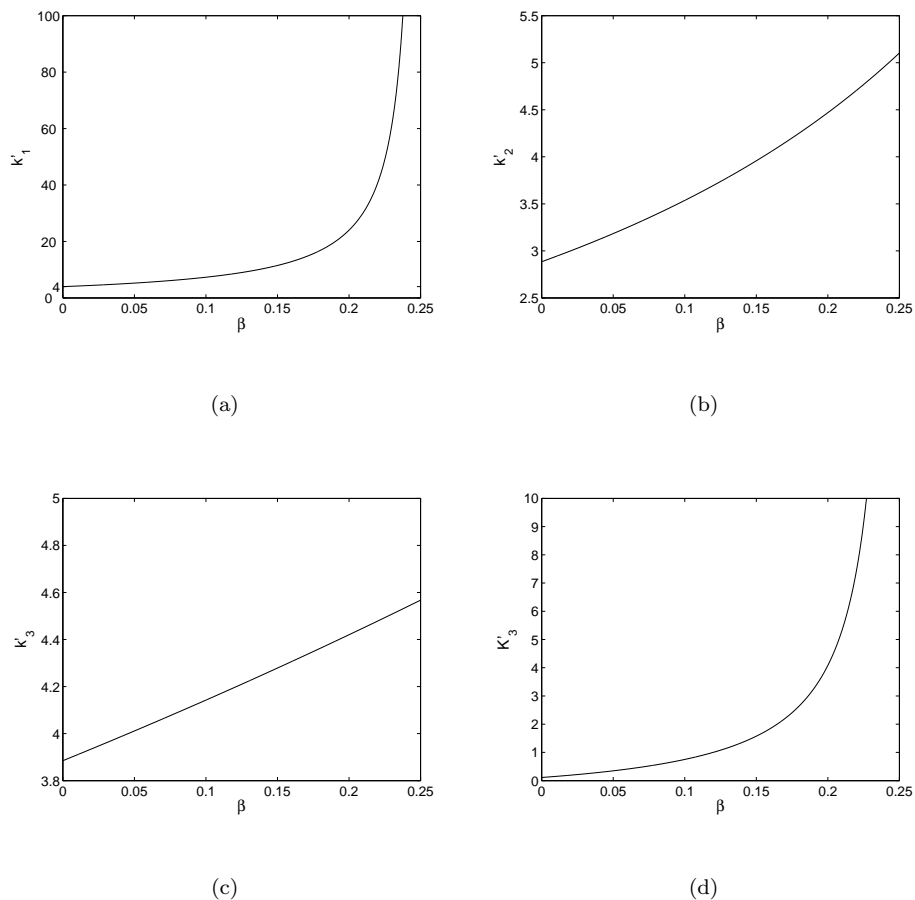
Figure 4.4: Dependence of nondimensional parameters (a) k_1', (b) k_2', (c) k_3' and (d) K_3' on β; for $0 < \beta < \frac{1}{4}$. All other parameters are set to one.

4.3.4 Steady-state variation throughout the crypt

In Figure 4.5 we present the steady states for different knockout experiments under the fixed parameters, defined by substituting $\beta = \hat{\beta} = \frac{1}{8}$ into the expressions of section 4.3.2. The protein/complex concentrations are scaled to one in the wild-type (WT) case. Note that the levels of Cyclin D:CDK4 are our model 'output' as this is the complex involved in stimulating the cell cycle.

Figure 4.5 shows that the APC knockout leads to high levels of β-catenin, causing an increase in Myc and Cyclin D levels. The elevated Myc levels cause a knock-on increase in CDK4. This leads to elevated levels of Cyclin D:CDK4, which are responsible for the increased proliferation of APC knockout cells.

The Myc knockout removes any Myc from the system, leading to reduced levels of CDK4. Free
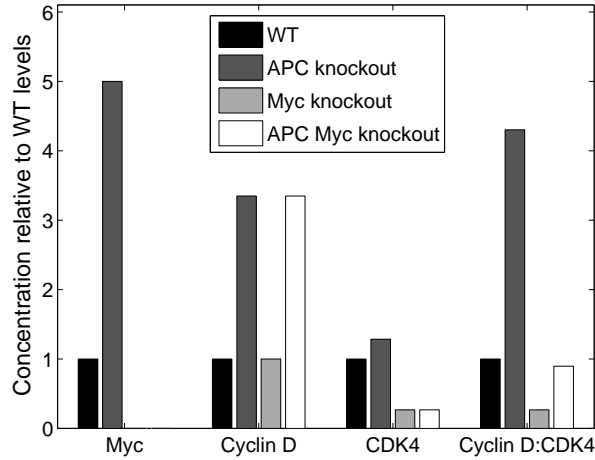
Figure 4.5: Steady-states of equations (4.5)–(4.8), defined by equations (4.13)–(4.28), using the parameter values in Table 4.2 and the mean stimulation of $\beta = \frac{1}{8}$.

Cyclin D levels remain constant and the level of Cyclin D:CDK4 is reduced as there is less CDK4 available. We would expect Myc deficient cells to display less proliferation than wild-type cells.

The APC-Myc double knockout leads to lower levels of CDK4 (as there is no Myc promotion), but high levels of Cyclin D (as there are high levels of β-catenin). The high availability of Cyclin D and low availability of CDK4 balance out in the formation term for Cyclin D:CDK4 (equation (4.4)); these steady state levels are close to those of WT cells, compensating for the effects of an APC knockout. We remark that this observation was not used when we estimated our parameters: it emerged naturally from the model as a result of the parameters fixed by the experimental observations in Table 4.3.

In Figure 4.6 we plot the variation of the steady states (equations (4.13)–(4.28)), since β-catenin levels have been observed to vary along the axis of a colorectal crypt. Since the mean level, $\hat{\beta}$ that is experienced in all cells is here within the range $0 < \hat{\beta} < \frac{1}{4}$ it is possible that the actual range of β which individual cells experience varies more widely. Here we have chosen the base of the crypt to take a value of $\beta = \frac{1}{2}$, and the top of the crypt to take a value of $\beta = 0$.

In the wild-type case shown in Figure 4.6(a) we can see that the low values of β (representing the top of the crypt) cause low values of all proteins. Crucially, a low value of C (Cyclin D:CDK4) allows the cell to cease cycling, though the cell cycle can still be initiated by Cyclin D:CDK complexes involving other Cyclin Ds or CDK6, which are not included in the model. As β increases the levels of all proteins, including C, increase monotonically, suggesting that this increase in the level of C
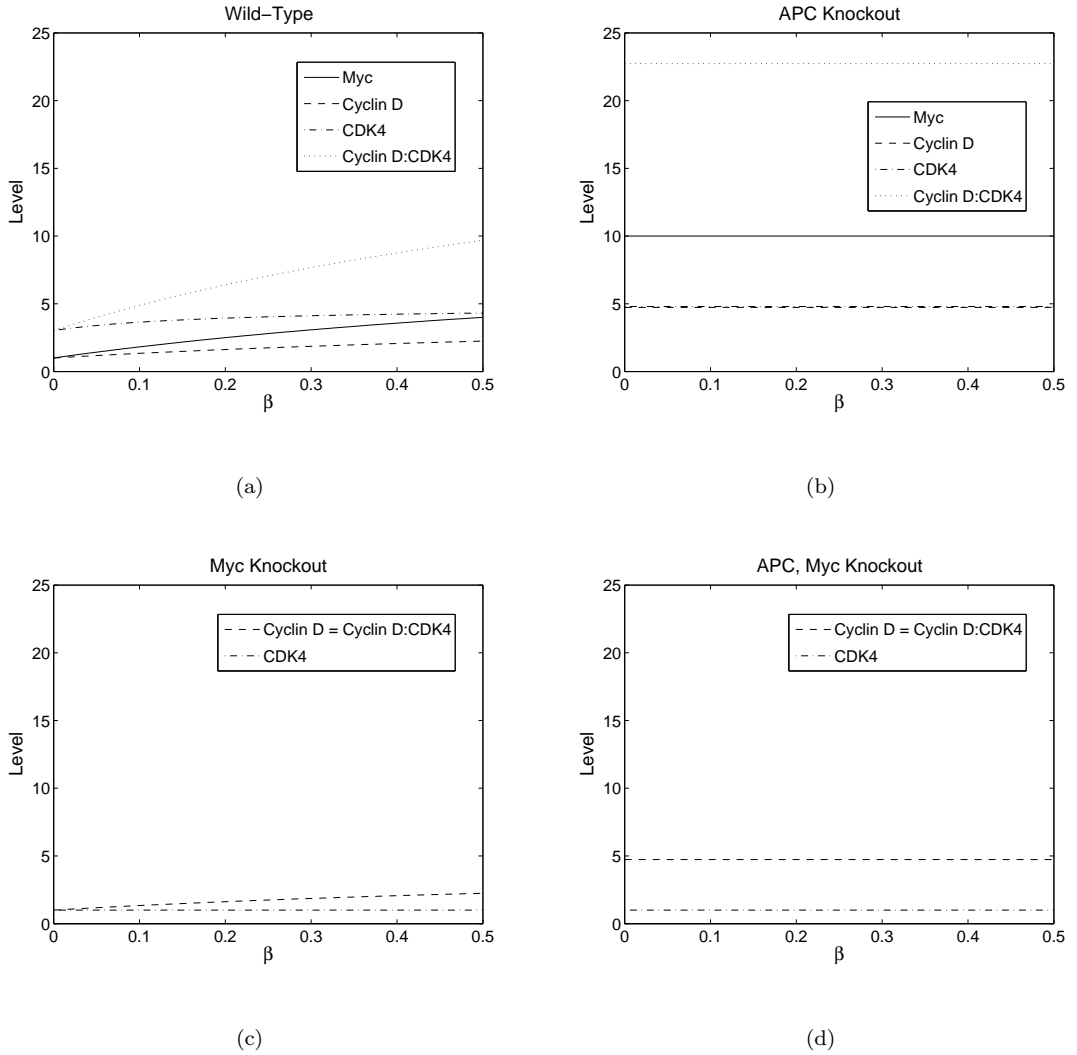
Figure 4.6: Variation of the steady states of the model with β for (a) wild-type; (b) APC knock-
outs; (c) Myc knockouts and (d) APC Myc double-knockouts. In (c) and (d) the
Cyclin D:CDK4 (C) and Cyclin D (Y) lines are coincident, since $\tilde{C} = \tilde{Y}\tilde{K}$ and
$\tilde{K}_M = \tilde{K}_{AM} = 1$ in this parameter regime. Generated using equations (4.13)–(4.28)
and the parameter values in Table 4.2.

forces cells to undergo proliferation at the base of the crypt.

Figure 4.6(b) shows the protein levels under an APC mutation. The values of the variables are
independent of β. The level of C is highly upregulated throughout the crypt, leading to uncontrolled
cell-cycling, as observed in experiment (Nagase & Nakamura, 1993).

In Figure 4.6(c) we see the effect of a Myc knockout. Cyclin D behaves in the same way as the

wild-type case, but levels of CDK4 remain constant as there is no β-dependence via Myc levels. For this reason the level of C is reduced, which we would expect to reduce the crypt's proliferation rate.

Figure 4.6(d) shows the results for the double APC-Myc knockout. Here the level of Cyclin D follows the APC knockout (increased relative to wild-type), and the level of CDK4 follows the Myc knockout (reduced relative to wild-type). The product of Cyclin D (Y) and CDK4 (K) informs the level of Cyclin D:CDK4 (C), which can therefore attain values which are similar to that of wild-type crypts. This is a potential mechanism for reversing the effects of the APC knockout. However, we note that there is no control over C levels throughout the crypt. Since crypts with the double-knockout appear to maintain a healthy architecture of proliferation at the base and differentiation towards the top we postulate that another mechanism must be responsible for this control, possibly a non-canonical Wnt signalling pathway (as postulated in Figure 4.2).

4.4 Therapeutic Implications

The loss of APC in the knockout experiments has the same effect upon β-catenin levels as one of the truncating mutations which often occur in early colorectal cancer (Näthke, 2006). Since an additional Myc knockout reverses the effects of the APC knockout, it is possible that a novel therapy involving down-regulation of Myc or one of its downstream targets could be used to treat patients carrying a truncating APC mutation. In this section we will use our model to predict which of our parameters are most important in regulating Cyclin D:CDK4 levels and hence suggest the most likely candidates for drug targets.

The steady-states of Cyclin D:CDK4 levels were given by equations (4.16), (4.20), (4.24) and (4.28) for the wild-type, APC knockout, Myc knockout and double knockout cells respectively.

An ideal drug target for this pathway would be β-catenin. As the upstream input, β upregulates all proteins in the pathway. However, this has long been known and investigated as a possible therapeutic target. β-catenin seems to be crucial for healthy operation of cells (see Luu *et al.*, 2004; Galmozzi *et al.*, 2006, for reviews); here we use our model to suggest new possibilities.

4.4.1 Myc

Downregulation of Myc, mimicking the effect of the double-knockout, is an obvious new therapy suggested by Sansom *et al.*'s experiments. In the case of an APC knockout the level of Cyclin D:CDK4 is elevated to four times that seen in wild-type cells (see Figure 4.5). However we cannot completely

block transcription of a gene to mimic the experimental results, without deleting it from the DNA which could be disastrous if Myc is required in other tissues. Alternatively the introduction of specially engineered small interfering RNA (siRNA) can degrade a specific mRNA and block translation of a protein, however this is not yet a standard medical treatment either. A feasible drug target would be one which blocks the promoter region of a gene (or the transcription factor itself), by binding to it and repressing transcription. In Figure 4.7(a) we see how varying the size of k_1' by up to a factor of two affects the final level of $\tilde{C}_A$ (Cyclin D:CDK4 in a mutant cell) relative to the level in a wild-type cell.

Figure 4.7(a) suggests that on reducing k_1' to zero, the mutant cell will still have Cyclin D:CDK4 levels which are 2.5 times higher than in wild-type cells. This suggests that even reducing k_1' to zero — blocking all β-catenin-dependent transcription of Myc, would not reverse the effects of an APC mutation, as the background level of Myc promotion (k_{1b}) would provide enough Myc to maintain an aberrant phenotype. Alternatively the degradation rate of c-Myc could be increased, although this would seem to be more difficult to target in practice.

4.4.2   Cyclin D

Levels of Cyclin D do not change between the APC knockout and double-knockout (Figure 4.5), although it is proposed that their upregulation is the main cause of the disregulation observed in the APC knockout. For this reason downregulation of Cyclin D is worth investigating as a potential therapeutic target.

The parameters which control Cyclin D levels can be seen by comparing equation (4.18) for the steady-state level of Cyclin D in an APC knockout with equation (4.14) for the wild-type cells.

Figure 4.7(b) shows the extent to which k_2' would have to be reduced to achieve wild-type levels of Cyclin D:CDK4. This could be achieved with a molecule which has a high affinity for the β-catenin:TCF promoter region of Cyclin D2. Upregulation of ϕ_Y would also be a valid approach, but is again difficult to target uniquely.

In all cases it is difficult to find drugs which target only the promoter region of a single gene. As we saw in section 1.4.2 β-catenin:TCF binds to the promoter region of around 100 genes. It may, however, be possible to find a molecule which binds to a unique DNA sequence that includes the β-catenin:TCF promoter region.

(a)

(b)

(c)
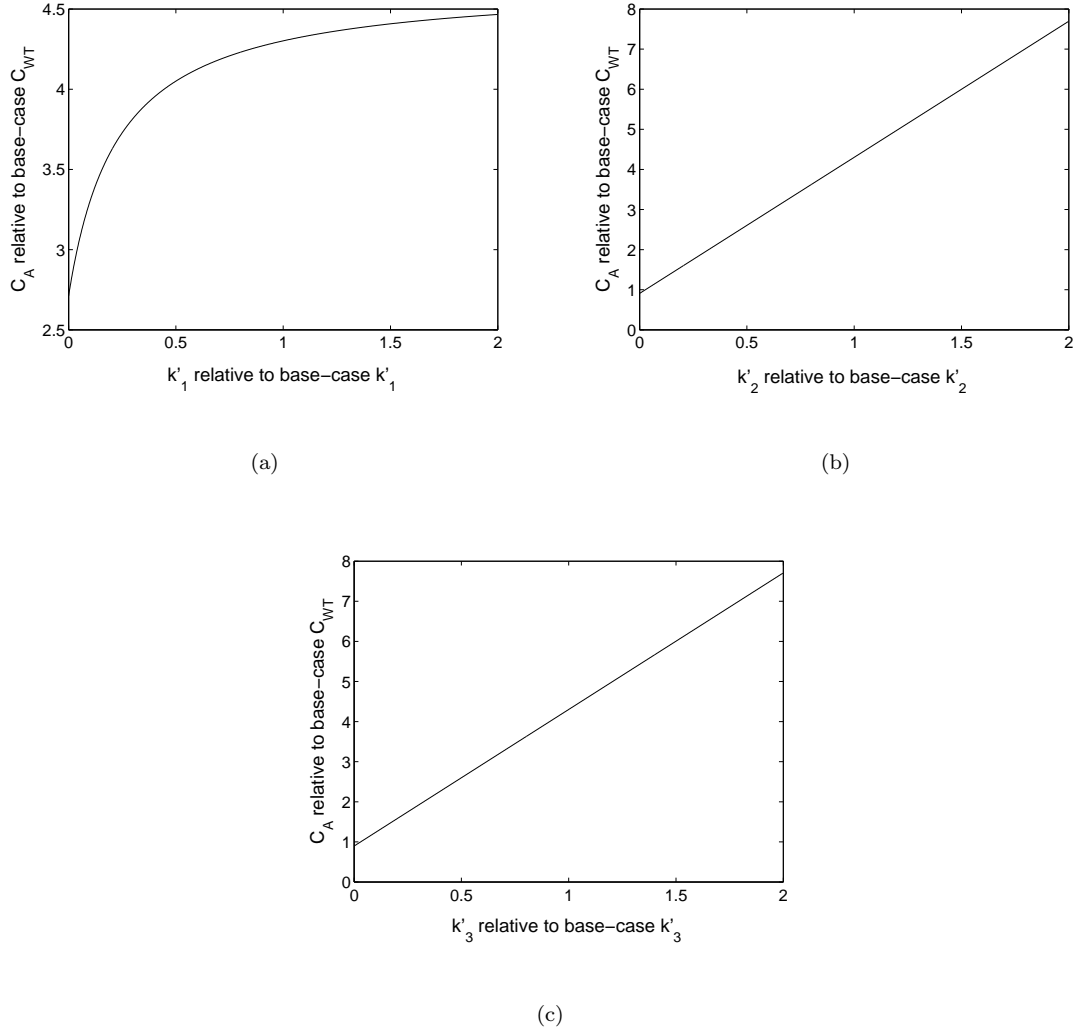
Figure 4.7: Parameter sensitivity: The effect of varying a parameter on the steady-state level of Cyclin D:CDK4 ($\tilde{C}_A$) in a cell with an APC knockout given by equation (4.20). The level of $\tilde{C}_A$ is given relative to that of a wild-type cell for our base-case of $\beta = \frac{1}{8}$. We vary only the following parameters in subfigure (a) k_1', (b) k_2', and (c) k_3' all other parameters are as shown in Table 4.2.

4.4.3 CDK4

Another possible drug target is CDK4, the only difference between the level of Cyclin D:CDK4 in the APC knockout (equation (4.20)) and the double knockout (equation (4.28)) being the size of $\tilde{K}$ — the steady state level of CDK4. The aim would be to reduce the level of $\tilde{K}_A$ given by equation (4.19) to be the same numerical value as $\tilde{K}_{AM}$ given by equation (4.27).

To do this we could increase the degradation rate ϕ_K, or reduce the rate k_3'. If k_3' could be reduced to zero then the level of $\tilde{K}_A$ and $\tilde{C}_A$ would fall to their healthy or double-knockout levels, as shown in Figure 4.7(c); we therefore propose that a healthy proliferation rate could be achieved by this route. To reduce k_3' we would have to block Myc's upregulation of CDK4. One way to do this would be to find a molecule which has a higher affinity than Myc for the DNA sequence of the Myc promotion region of the CDK4 gene. It is possible that CDK6 would fulfil the role of CDK4 in most tissues, and so targetting CDK4 could be the least damaging approach for a viable therapy.

4.5 Discussion

In this chapter we formulated a model to explore the regulation of the cell cycle by β-catenin. We have examined the role of c-Myc, Cyclin D and CDK4 and our results suggest that all three proteins interact to determine the cellular level of Cyclin D:CDK4, an input into the cell cycle. The model reproduces the results of a recent set of knockout experiments suggesting it represents a feasible mechanism by which Wnt signalling regulates the cell cycle.

Given the overwhelming complexity of pathways involved in regulating the cell cycle, many assumptions have to be made to make any progress analysing a model. In our initial collaborations with Dr Owen Sansom at the Beatson Institute it was suggested that p21 would be an important downstream repression target of c-Myc (Wanzel *et al.*, 2003; Liu *et al.*, 2006b). As we explained in section 1.3.2, p21 plays an important role in promoting the cell cycle. Interestingly p21 is required to activate the Cyclin D:CDK4 complex (Sherr & Roberts, 1999; Gartel & Radhakrishnan, 2005) and yet it disables Cyclin E:CDK2 complexes. Additionally p21 can form inactive complexes with c-Myc (p21:Myc) and E2F1 (p21:E2F1).

We incorporated these interactions into a framework based upon Figure 3.3, formulating an intricate model, but suffered from a lack of any experimental data on which to base parameter values. Varying the levels of p21 did not seem to affect the output of the model significantly. Recently Dr Sansom's group performed a treble knockout of c-Myc, APC and p21 and found this to have much the same phenotype as the c-Myc APC double-knockout (O. Sansom, personal communication, December 2007) so this model may be worth revisiting in the future.

Wnt signalling models such as Lee *et al.* (2003) and Cho *et al.* (2006) cannot explain the knockout experiments, as they focus on the Wnt/β-catenin pathway (upstream of Myc). We believe that the model of chapter 3 was the first to link Wnt signalling quantitatively to the cell cycle, yet this model did not feature c-Myc and so could not explain Sansom *et al.*'s (2007) results. For these reasons the

model presented in this chapter would seem to be as simple as possible whilst retaining the desired behaviour under the various knockout experiments.

However, we note that we cannot represent a fully healthy crypt for a double-knockout using this model: our results in Figure 4.6(d) have lost any Wnt-dependence. Since we use the Wnt dependence to represent a spatial location this suggests that the cells' behaviour would be the same in all areas of the crypt. This is not entirely consistent with the results of Sansom *et al.* (2007), which showed a normal crypt phenotype for the double knockout. This leads us to postulate a separate pathway, shown in Figure 4.2, which retains some control over the cell cycle. Such a pathway could possibly be due to non-canonical Wnt signalling or a related signalling pathway such as Notch or Hedgehog. Consideration of this pathway and its influence over the cell cycle is a line of future research.

Yet further experiments have shown that "over the longer term both Myc and APC Myc deficient cells are lost from the intestinal epithelium" (O. Sansom, personal communication, September 2007). This could be due to a reduction in cell-cycle stimulus, such that a long-term homeostasis is not possible, which would be consistent with our model for the reduced levels of cell-cycle proteins under the Myc knockout. Alternatively another Myc target gene could be necessary to maintain longer-term homeostasis for a healthy crypt.

The finding that our model can replicate the levels of proteins observed in Sansom *et al.* (2007) for a number of different parameter regimes (Figure 4.4) suggests that it represents a possible mechanism by which mutations in the Wnt pathway cause hyperproliferation, which an additional Myc knockout can reverse. We have suggested some targets for reversing the effects of an APC mutation, with the promoter regions of CDK4 and Cyclin D being promising subjects for further investigation.

CHAPTER 5

CHASTE Scientific Computing Environment

5.1 Introduction

THE Integrative Biology[1] project is a large collaboration between mathematical modellers, biologists and computer scientists aiming to create multiscale computational models, which exploit High Performance Computing (HPC) resources, to better understand how cancer and heart disease occur. Over the past three years the Integrative Biology project has been developing a scientific computing environment, featuring common code which can be implemented to solve a range of biological problems. The computing environment is known as CHASTE — **C**ancer, **H**eart **A**nd **S**oft **T**issue **E**nvironment.

The Integrative Biology cancer PhD students have been the core developers for the cancer side of the project, focussing initially on creating a software package to run simulations of a basic model of crypt dynamics developed by Meineke *et al.* (2001) together with various extensions. The main development work has been done by a team of six PhD students involved with cancer modelling (myself, Alex Fletcher, Philip Murray, Pras Pathmanathan, James Osbourne and Alex Walter) along with support from three computer scientists (Jonathan Cooper, Lee Momtahan and Joe Pitt-Francis). Individually, I have spent approximately half of my time over 18 months in the development of both the cell-cycle models, cylindrical mesh and experiment-mimicking simulation areas of the code, although, as we will see in this chapter, no one person is solely responsible for any part of the code.

In section 5.2 we introduce the Meineke *et al.* (2001) model, looking at the different componenets and how they interact. In section 5.3 we explore some of the software engineering principles that we have adopted for the CHASTE project. In section 5.4 we explain how these principles have

---

[1]www.integrativebiology.ox.ac.uk

influenced the design of our model for the colorectal crypts and demonstrate how it may now be used to simulate other cell-based models. In section 5.5 we discuss some of the advantages and disadvantages of the approach we have taken. Firstly we motivate our decision to embark upon the CHASTE project, highlighting the need for such a code.

5.1.1 Lessons from cardiac modelling

Cardiac modelling groups are well-established, having used numerical methods for over 40 years. They began by simulating an action potential within a single cell (Noble, 1960), and now have whole-organ heart models which can accurately predict the onset of arrhythmia under different intra-cellular conditions (Noble, 2007). These groups have come to understand the need for shared code, to avoid single researchers 'reinventing the wheel' when, for example, solving PDEs using finite element methods.

Problems often occur when a research contract expires or a PhD student moves on, leaving a code which only one person understands; usually this code has to be discarded, or is, at best, used as a 'black-box' with no understanding of how it performs its function. Large codes rapidly become untidy, containing many 'black-boxes' and, as one part of the code is expanded or improved, no-one knows how this will affect the performance of the rest of the code. As a result, some heart modelling codes can no longer even replicate some of their own past results.

The Integrative Biology project has developed a new cardiac modelling environment from scratch, using a software engineering approach designed to avoid the pitfalls discussed above. In parallel with this activity, we have developed a cancer modelling environment, sharing, amongst other things, the mesh structure and ODE/PDE solvers with the cardiac modellers.

5.1.2 Common themes in cancer

If our sole aim were to run simulations of a single model, then it would not be appropriate to use an approach where components are shared and made as flexible as possible. However we have developed a code which we hope is easy to adapt to run simulations of many different models, utilising common code for common modelling components.

As we saw in section 1.5.2, many models of colorectal cancer operate at the cell scale, and share common features, such as subcellular models of the cell cycle and the need to pass information to a daughter cell upon division. It is desireable that such sub-models for the cell cycle should share

a common format, so that the same cell-cycle model may be incorporated into different cell-based models. Similarly, models for other cell behaviours such as cell-cell or cell-substrate adhesion and cell death may be applicable to many different systems.

Many cancer models include PDEs to describe the production, diffusion and uptake of vital chemicals: nutrients such as oxygen, growth factors, and drugs (Byrne & Chaplain, 1995; Jackson & Byrne, 2000; Mallet & De Pillis, 2006; Gerisch & Chaplain, 2008). Codes for solving such a PDE using a finite element method on a mesh would be applicable to many cancer (and other) models. Before the CHASTE project no flexible framework for incorporating such elements into different cancer models existed. By including codes for solving these sub-problems into a software environment, we have made it easier to develop new models that include combinations of these features. Our initial aim was to create a software package to run simulations of the Meineke *et al.* (2001) crypt model, which we introduce in section 5.2 below.

5.2 The Meineke *et al.* (2001) Crypt Model

Meineke *et al.*'s (2001) model is a distinct improvement on earlier lattice-based models for the cellular dynamics of crypts (Loeffler *et al.*, 1986, 1988). As discussed in section 1.5.2, its main advantage lies in preventing long-distance effects from distorting local activities such as cell birth, by moving to an off-lattice framework. It consists of a cylindrical 2D mesh, constructed using a Delaunay triangulation (or, equivalently, a Voronoi tessellation). Each node of the mesh represents the centre of a cell. Cells are connected by springs, defined by the Delaunay triangulation, and move in a heavily-damped manner according to the forces exerted on them by their springs. At the base of the cylinder are a number of fixed Paneth and 'stem' cells. Stem cells (generation = 0) produce daughter 'transit' cells (generation = 1) at a constant rate. Transit cells divide a fixed number of times, and then become 'differentiated'. In this way the introduction of daughter cells drives migration throughout the crypt and cells are removed once they reach the top of the crypt.

5.2.1 Cells represented by nodes

Meineke *et al.* note that cells in an *in vivo* crypt pack polygonally, and the inability to reproduce this is a weakness of previous lattice-based models. A set of nodes, meshed using a Delaunay triangulation, is used to describe the positions of cell centres. The Delaunay triangulation is equivalent to a Voronoi tessellation, which here describes the area of the cell belonging to each node. A Voronoi tessellation allocates every point in space to the node nearest it, with cell boundaries demarcating

lines of equal distance between two nodes.

A Delaunay triangulation and its corresponding Voronoi tessellation are presented in Figure 5.1. When a 2D spring system is allowed to relax fully it forms a regular mesh of equilateral triangles, whose accompanying Voronoi tessellation is a 'honeycomb' pattern of regular hexagons; the nodes towards the top of the crypt depicted in Figure 5.1 behave in this way; the Voronoi representation appears to emulate naturally the shape of epithelial cells (cf. Meineke *et al.*, 2001, Figure 1).

The mesh presented in Figure 5.1 is in fact surrounded by some invisible nodes, which we term 'ghost nodes'. The nodes are meshed into a 'convex hull' which leaves very long connections (springs in this case) on the edges of the mesh; by creating ghost nodes the long springs and large forces do not affect the real cells. Additionally this avoids the Voronoi tessellation for cells on the edge of the mesh becoming semi-infinite and making visualisation difficult. This effect is a direct consequence of the definition of a Voronoi tessellation: any point in space outside our mesh is closest to one of the nodes on the edge of the mesh, and so the Voronoi tessellation extends infinitely in all directions. By including a layer of 'ghost nodes' around the cells on the edge of the mesh we introduce finite limits to the Voronoi tessellation for all of our cells, leaving some of the ghost nodes with infinite tessellations.
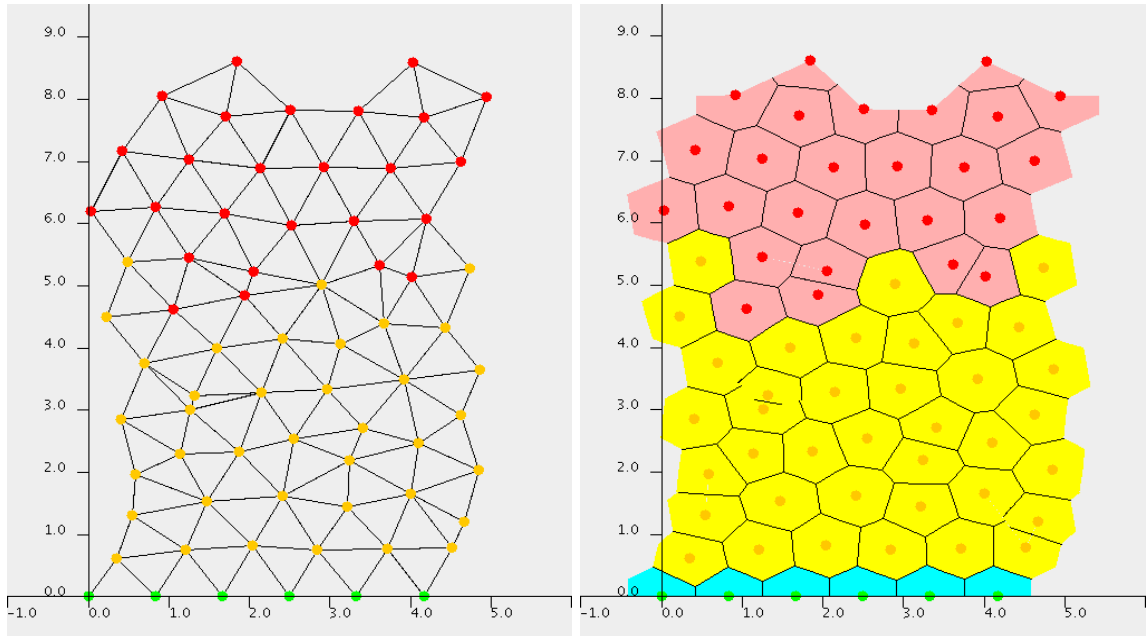

Figure 5.1: A Delaunay triangulation of a set of nodes (left) and the corresponding Voronoi tessellation (right). The number of Delaunay triangles (mesh elements) that a node is involved in is equivalent to the number of sides that the cell has, as defined by the Voronoi tessellation.

Since nodes move at every timestep (discussed in the next section), are added because of cell birth and are removed because of cell death, a remeshing must be performed at each timestep; the remeshing is performed as discussed in section 5.4.1.

5.2.2 Cell Mechanics

The black lines connecting the nodes in Figure 5.1 are the edges of elements in the mesh. The Meineke *et al.* (2001) model places springs along each of these edges, thereby connecting each node (or cell) to its nearest neighbours. The total force, $\mathbf{F}_i$, acting on a cell, i, due to cell-cell interactions is obtained by summing the forces associated with the deformation of the springs that connect it to all other cells in its neighbourhood. Using the suffix j to denote cells that are adjacent to cell i we have

$$\mathbf{F}_i(t) = \mu \sum_{\forall j(t)} \hat{\mathbf{r}}_{ij}(t) \left(s_{ij}(t) - |\mathbf{r}_{ij}(t)| \right), \tag{5.1}$$

where $\mathbf{r}_{ij}$ is the vector from cell i to cell j, $\hat{\mathbf{r}}_{ij}$ is the corresponding unit vector, s_{ij} is the resting length of the spring connecting cells i and j, and μ is the spring stiffness constant, which models the strength of cell-cell adhesion. By giving individual pairs of cells different values of μ_{ij} we could model differential adhesion characteristics.

For an overdamped ('high Reynold's number') system, where inertial terms are considered small compared to dissipative terms, the velocity of node i is then given by

$$\eta \frac{\mathrm{d}\mathbf{r}_i}{\mathrm{d}t} = \mathbf{F}_i(t), \tag{5.2}$$

where $\mathbf{r}_i$ is the position of node i, and η is the damping constant representing the strength of cell-substrate adhesion.

The displacement of node i, in a given time interval Δt, is then given by the following equation derived from equation (5.2) and formed using a Forward Euler discretisation

$$\mathbf{r}_i(t + \Delta t) = \mathbf{r}_i(t) + \frac{1}{\eta} \mathbf{F}_i(t) \Delta t. \tag{5.3}$$

Unless otherwise stated we fix $\Delta t = 30$ s, $\mu = 30$ kg s^{-2} and $\eta = 1$ kg s^{-1} in the simulations that follow. We find that the ratio of μ/η leads to different behaviours: if this ratio is too large then oscillations in cell movements can occur, as there is insufficient damping; if the value is too low then cell birth causes a build up of cell density in the crypt, cells do not leave the crypt as their movement is too heavily damped and the crypt does not reach a steady population. Using the above parameters no oscillations are observed and the crypt reaches a quasi-steady population.

5.2.3 Cell Birth

Addition of new nodes

A cell is added by picking an angle θ at random, moving the parent node a small distance in the θ direction and adding a daughter cell a small distance in the $\pi + \theta$ direction. After a remesh the nodes are inevitably joined by a new spring (as they are very close toegether). The spring's rest length evolves as follows

$$s_{ij} = \begin{cases} s & \text{for } a_{ij} \geqslant t_M, \\ a_{ij}s/t_M & \text{for } a_{ij} < t_M, \end{cases} \tag{5.4}$$

where a_{ij} is the age of spring s_{ij}, t_M is the length of the M phase of the cell cycle, and s is the mature resting spring length. We have nondimensionalised space in our simulations such that $s = 1$ and space is measured in 'mature spring lengths' or equivalently 'mature cell widths'.

Cell cycle model

In Meineke *et al.* (2001) the cell cycle is controlled by the generation number of a particular cell. A stem cell is always of generation 0. After a fixed length of time it divides asymmetrically, and produces a daughter cell of generation 1. Cells of generation 1 are called 'transit' cells and, after a fixed amount of time, divide symmetrically to produce two transit cells of generation 2. When cells reach a certain generation number (a parameter, usually set to 3 or 4) they 'differentiate' and no longer progress through the cell cycle.

The duration of a cell cycle is determined at birth, by selecting the length of the G_1 phase, t_{G1}, from a uniform distribution of $U(t_{G1}; 10, 15)$ hours. The duration of the other cell-cycle phases is fixed throughout the simulation. Cells can report which phase of the cell cycle they are currently undergoing. To use this type of cell-cycle model the stem cells must remain in the crypt indefinitely, otherwise the loss of one or more stem cells would dramatically change the homeostasis of the crypt. As a result stem cells must be held pinned at the base of the crypt.

5.3 The CHASTE Approach

Often MatLab or Mathematica are used to run simulations of small to medium sized models, being easy to use and well-supported. However these are interpreted languages, which read and run the code one line at a time. CHASTE is written in C++. As it is a compiled language, the entire

code is read and built into an executable file of machine-code, optimised for speed on the individual processor(s) that will run the program. Compiled languages are up to 1000 times faster than interpreted languages when performing numerical tasks (DeRose & Padua, 1999), and hence better suited for large problems where the run-time is a limiting factor.

The CHASTE project was initiated during a month long programming session in 2005, when we set up the common parts of the code. This has been followed by sixteen cancer group programming sessions, based in the Oxford ComLab and typically of three to five days duration. We have also worked individually to develop the code in-between these group sessions.

In this section we will outline and discuss the merits of the main software engineering principles that we have adopted for the CHASTE project.

5.3.1 Test-driven development

The fundamental principle we have used to develop CHASTE is known as *test-driven development*. At a basic level 'testing' means that every line of code is tested to ensure it does what it was written to do. This could take the form of a single high-level test; testing, for example, that a crypt simulation progresses as it should. But such high-level tests do not tell you anything about precisely what has changed when something goes wrong.
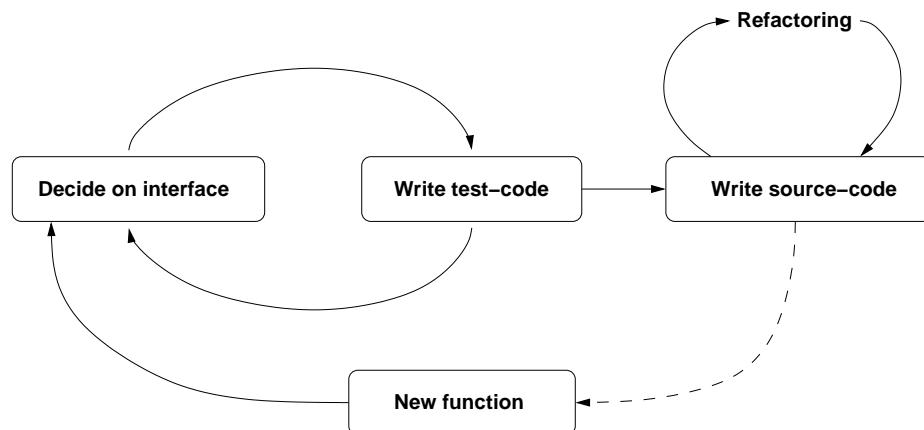
Figure 5.2: The process of test-driven development.

Instead, *test-driven development* is a way of writing code. Before any source-code is written a test-code must be made to test its function. This process is illustrated in Figure 5.2. The first task when a new function is required is to work out the interface that the new code will use, this being performed by writing a test code. This process often leads to changes in the interface, as the simplest

form becomes more evident upon implementation. Once a test-code is written the source-code can be developed until the test passes. Only once this has been achieved can more functions be added. The process of 'refactoring' is also shown in Figure 5.2. This is a name for the constant revisiting of the source-code, attempting to make the whole code base as tidy and user-friendly as possible, avoiding repetition of code and optimising performance. Because the whole code is thoroughly tested, refactoring is done without changing tests to ensure that the code still performs its original function properly.

A test-code is presented in Figure 5.3. In this example we have decided that a `FixedCellCycleModel` will need to return the time until the next division, and that this will vary depending on the cell type. Once this test is in place the minimum amount of source-code necessary should be written to make the test pass. In Figure 5.4 we see the source-code that was written to perform the functions tested by the code in Figure 5.3. If we decide the source-code needs to do more, then the test-code must first be extended to cover the extra functionality.

```
1   #ifndef TESTCELLCYCLEMODELS_HPP_
2   #define TESTCELLCYCLEMODELS_HPP_
3
4   #include <cxxtest/TestSuite.h>
5   #include "FixedCellCycleModel.hpp"
6
7   class TestCellCycleModels : public CxxTest::TestSuite
8   {
9   public:
10      void TestFixedCellCycleModel(void) throw(Exception)
11      {
12          FixedCellCycleModel our_fixed_cell;
13
14          our_fixed_cell.SetCellType(TRANSIT);
15          TS_ASSERT_DELTA(our_fixed_cell.GetInterDivisionTime(),12,1e-6);
16
17          our_fixed_cell.SetCellType(STEM);
18          TS_ASSERT_DELTA(our_fixed_cell.GetInterDivisionTime(),18,1e-6);
19
20          our_fixed_cell.SetCellType(DIFFERENTIATED);
21          TS_ASSERT_DELTA(our_fixed_cell.GetInterDivisionTime(),1e99,1e-6);
22      }
23  };
24  #endif /*TESTCELLCYCLEMODELS_HPP_*/
```

Figure 5.3: The test code for a `FixedCellCycleModel`, an example of one of the simpler CHASTE cell-cycle models.

This style of development may appear overly complex, taking much longer than writing a piece of source-code. However there are many advantages. Once a piece of source-code has been 'protected'

```
1   #ifndef FIXEDCELLCYCLEMODEL_HPP_
2   #define FIXEDCELLCYCLEMODEL_HPP_
3
4   #include "AbstractCellCycleModel.hpp"
5
6   class FixedCellCycleModel : public AbstractCellCycleModel
7   {
8     public:
9       double GetInterDivisionTime()
10      {
11          double inter_division_time;
12          switch(this->mCellType)
13          {
14              case STEM:
15                  inter_division_time = 12;
16                  break;
17              case TRANSIT:
18                  inter_division_time = 18;
19                  break;
20              default:
21                  inter_division_time = 1e99;
22                  break;
23          }
24          return inter_division_time;
25      }
26  };
27  #endif /*FIXEDCELLCYCLEMODEL_HPP_*/
```

Figure 5.4: The source code for a `FixedCellCycleModel`, an example of one of the simpler CHASTE cell-cycle models.

by a test, nobody can accidentally change the code's function without the test failing, and highlighting the problem. If another developer changed the way `SetCellType()` functioned (used on lines 14, 17 and 20 of Figure 5.3), such that `mCellType` was not properly updated, then the test (which uses `mCellType` on line 12 of the source-code in Figure 5.4) would fail and highlight a problem.

Sometimes changes are far more subtle: a change to a low-level piece of source code (e.g. the nodes of a mesh) could adversely affect some higher-level source code (e.g. a simulation involving cells associated with particular nodes). However the low-level source code is automatically called by the test codes of all the relevant higher-level functions; this ensures that one developer can never break a part of the code that they did not intend to change.

Thoroughly tested code is almost guaranteed to be bug-free, whereas in a 'traditional' coding setting most effort is not expended in coding, but in hunting for bugs in the code, especially in the case of large codes.

5.3.2   Central code-repository

All CHASTE code is stored on a central server known as the 'repository'. To work on a piece of code the whole code must be 'checked-out' of the repository, with its relevant version number. To upload any changes to the repository all tests must be run to ensure nothing has been broken. Any changes are then 'committed' to the repository and are given a revision number.

Central Testing

As soon as a 'commit' has occurred, the server 'checks-out' the code and runs all of the tests. This ensures that any discrepancies in software or hardware are quickly eliminated, ensuring that CHASTE runs on any machine. These central test results are displayed on the project website at https://chaste.ediamond.ox.ac.uk/tests.py.

Version Control

https://chaste.ediamond.ox.ac.uk gives access to a complete history of the project, all revisions of the code being permanently recorded. The different versions are managed by SVN[2] version management which can merge together two files if more than one team has been working on the same piece of code. This guarantees that all results can be replicated, as an older revision can be 'checked-out' and re-run if necessary.

Wiki pages

The website also hosts wiki-style project management software. There is a timeline showing the history of 'commit's to the repository. 'Tickets' can be raised for: new pieces of work, defects which have been found or 'refactoring'. These tickets contain a description of the work to be done, an estimate of how long it will take to complete, and effort expended to date. There are also links to the test results webpage and the project documentation discussed below.

5.3.3   Pair-programming

One of the software engineering principles we have used is pair-programming, where two people share a computer and keyboard. Again, this may sound an extravagant use of resources, but it

---

[2]http://subversion.tigris.org/

has proved to be a valuable practice. Typically one person types for half an hour, whilst the other checks for typos and thinks about how the code could be structured better; the pair then swap roles. Individuals rotate between pairs on average twice a day with one programmer moving on to a different task. As a result everybody in the team develops a working knowledge of the whole code. Additionally, best practice is transferred from experienced programmers to newer ones.

The requirement for pair-programming has been relaxed to allow for single programmers to work in-between group sessions, but all code that enters the repository is checked by a second programmer, to maintain a high standard and reduce the risks of mistakes entering the code.

5.3.4   Agile approach

We have used an 'agile' software engineering approach: the cancer coding has been decomposed into fifteen 'iterations' each lasting approximately a month. At the start of an iteration a list of tickets which should be achievable by the end of the iteration is established, defining the 'scope' of the iteration. Programming then begins, but can only be on tickets which are 'in-scope', the idea being to expand gradually the functionality of CHASTE, rather than plan for large changes or additions. This approach inevitably leads to code being constantly revisited to change its interface or functionality. This is only possible when it is protected by tests to ensure that function has not changed, or changes in a controlled manner.

As an example of this process consider the following changes to the `FixedCellCycleModel` introduced in Figures 5.3 and 5.4. We now wish to have cell-cycle models report whether they are ready to divide or not (based upon external influences, they can no longer predict when this will be in advance). Now our cell-cycle models cannot return a `cell.GetInterDivisionTime()`, but must instead simply report whether `cell.ReadyToDivide()`. Our `FixedCellCycleModel` must be updated to this new function using the changes shown in Figures 5.5 and 5.6.

Collective code ownership

Another aspect of agile programming is the concept of 'collective code ownership'. This ensures that no one person 'owns' or takes responsibility for any part of the core code. Everybody is allowed, and encouraged, to review the code and improve it where possible. As a test will be in place for any desirable behaviour, this does not allow anyone to break functionality that has been added to the code.

This agile programming requirement has been adapted to allow for 'user projects', branches of the

```
1   void TestFixedCellCycleModel(void) throw(Exception)
2   {
3       FixedCellCycleModel our_fixed_cell;
4
5       our_fixed_cell.SetCellType(TRANSIT);
6       TS_ASSERT(!our_fixed_cell.ReadyToDivide(11.99));
7       TS_ASSERT(our_fixed_cell.ReadyToDivide(12.0));
8       TS_ASSERT(our_fixed_cell.ReadyToDivide(12.01));
9
10      our_fixed_cell.SetCellType(STEM);
11      TS_ASSERT(!our_fixed_cell.ReadyToDivide(23.99));
12      TS_ASSERT(our_fixed_cell.ReadyToDivide(24.0));
13      TS_ASSERT(our_fixed_cell.ReadyToDivide(24.01));
14
15      our_fixed_cell.SetCellType(DIFFERENTIATED);
16      TS_ASSERT(!our_fixed_cell.ReadyToDivide(1.0));
17      TS_ASSERT(!our_fixed_cell.ReadyToDivide(1e10));
18      TS_ASSERT(!our_fixed_cell.ReadyToDivide(1e100));
19  }
```

Figure 5.5: The new test function for a `FixedCellCycleModel`, compare with Figure 5.3.

```
1   bool FixedCellCycleModel::ReadyToDivide(double time)
2   {
3       bool ready;
4       switch(mCellType)
5       {
6           case STEM:
7               ready = (time - mBirthTime >= mStemCellCycleTime);
8               break;
9           case TRANSIT:
10              ready = (time - mBirthTime >= mTransitCellCycleTime);
11              break;
12          default:
13              ready = false;
14              break;
15      }
16      return ready;
17  }
```

Figure 5.6: A refactored `ReadyToDivide()` method for `FixedCellCycleModel`, compare with `GetInterDivisionTime()` on line 9 of Figure 5.4.

repository owned by a single programmer. These projects can call upon any code in the main ('core') repository and allow users to do their own work. Often code from user projects is reviewed and committed into the core if it is thought to be more widely useful.

5.3.5 Doxygen

All good code should include comments documenting its function, and giving any relevant information about how the code should be utilised. Doxygen[3] ensures that the CHASTE code is fully documented. This is a utility which scans through the source code, reading relevent comments left in the code about classes and functions. It assembles a website (https://chaste.ediamond.ox.ac.uk/docs/) which contains all the information about the interactions between different pieces of code, along with any other comments about the operation of pieces of code and even individual functions. This website is automatically updated to keep in step with the latest revision. An example of some Doxygen output can be seen in Figure 5.8.

5.3.6 Further testing

In addition to the continuous testing referred to above, other tests are run nightly. Memory testing ensures that none of the tests uses up memory without freeing it; this should ensure that our code can run indefinitely. Coverage tests ensure that all code is covered by the continuous tests. The entire code is run on a parallel machine and under different compilers to ensure that it will work on High Performance Computing (HPC) systems, which we utilise for running our simulations.

5.4 Cancer Models in CHASTE

In this section we outline the structure of CHASTE's cancer code. The primary aim is to create an environment to run simulations of the Meineke *et al.* (2001) model, so many of the code structures were designed with this in mind. We describe the structure of this code in section 5.4.1. By using the techniques described above we have generalised some sections of the code to other cancer models, and we describe how these models use CHASTE in section 5.4.2.

---

[3]http://www.doxygen.org

5.4.1   Implementing the Meineke *et al.* (2001) model

Where possible we have tried to use a code structure which is as faithful to the biology as possible, dividing our code into separate *classes* to represent different biological components. A schematic of the main classes we have created is shown in Figure 5.7. We will use the example of cell-cycle

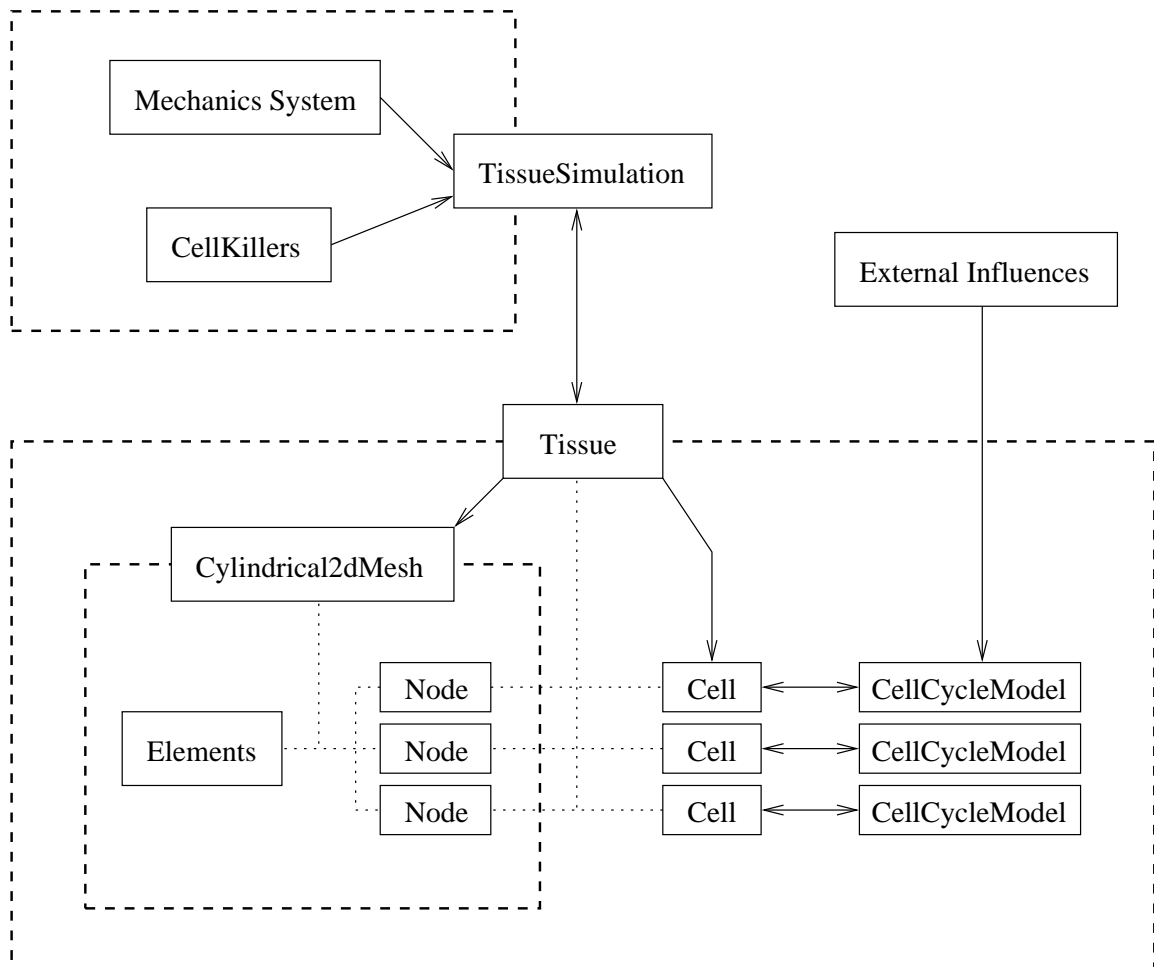**Figure 5.7:** A schematic of the interactions between different classes of the CHASTE cancer code. Solid lines with arrows denote interactions, and the direction of the influence. A dashed line encloses objects which are members of another class, whilst dotted lines denote a class managing the correspondence between objects.

models to illustrate how different classes inherit from one another.

Cell-Cycle Models

In the Meineke *et al.* (2001) model a new node is created, in anticipation of a daughter cell, at the beginning of M phase, and the rest length of the spring joining the two nodes increases to its natural rest length during M phase. So, somewhat unusually, our cell-cycle models are defined to start in M phase rather than G_1.

As we saw in section 1.3.3, many different approaches can be used to model the cell cycle. We have constructed a framework in which simulations can use the simple `FixedCellCycleModel` mentioned above, or a more complicated ODE-based model in order to decide when to progress to a new phase. Different cell-cycle models take the form of different classes. Classes can inherit methods and variables from other classes. For example, all cell-cycle models are responsible for reporting the `CurrentCellCyclePhase()`, whether or not a cell is `ReadyToDivide()`, performing a `Reset()` upon division, and providing a `CreateDaughterCellCycleModel()`. These functions are all implemented in an `AbstractCellCycleModel` from which the individual cell-cycle models inherit. A schematic showing the inheritance of the different models is presented in Figure 5.8.
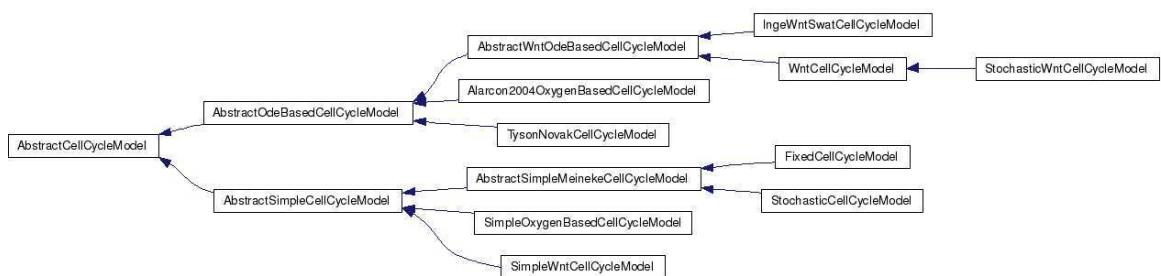
Figure 5.8: A schematic of the inheritance between different classes of the CHASTE cell-cycle models, automatically generated as part of our Doxygen documentation (https://chaste.ediamond.ox.ac.uk/docs/inherits.html).

The inheritance shown in Figure 5.8 follows an "is a" relationship, to avoid repeating code between similar cell-cycle models. So that an `AbstractOdeBasedCellCycleModel` *is an* `AbstractCellCycleModel`, and `WntCellCycleModel` *is an* `AbstractWntOdeBasedCellCycleModel`. Some of the resulting classes are very simple, for example `StochasticWntCellCycleModel` only re-implements one method, `SetG2PhaseDuration()`, changing the length of the cell cycle's G_2 duration to introduce a stochastic element into the simulations to avoid cells cycling completely synchronously.

Cells

A `TissueCell` has a `CellCycleModel`, and knows: whether it is ready to divide, the cell-type (stem, transit or differentiated), its mutation state, whether it is currently undergoing apoptosis and other cell-level properties. The `TissueCell` class can be asked if it is `ReadyToDivide()`, for this the cell calls `ReadyToDivide()` on its `CellCycleModel`. The cell can be told to `Divide()` and will return a daughter cell. The `Divide()` method consists of resetting its own cell-cycle model before setting up a new cell with a cell-cycle model in the correct state, and passing on relevant information (such as the parent's mutation state).

Tissue

To associate our cells with a point in space, we have a `Tissue` class, as shown in Figure 5.7. This class stores a list of `TissueCells`, and a `Cylindrical2dMesh`, keeping track of which cell is associated with which `Node` in the mesh. `Tissue` handles all requests for cell locations, and the logic for adding/removing cells and nodes to/from the simulation.

Cylindrical 2D Mesh

To implement periodic boundaries we created a `Cylindrical2dMesh` class which inherits all the functions of a general `Mesh<DIMENSION=2>` class. The `Cylindrical2dMesh` class is given a crypt width, C, and overrides some of the planar geometry methods to map the results onto a cylinder.

Nodes are moved at every time step using equation (5.3), are added when cells are born, and removed when cells die; so we recalculate the Voronoi tessellation at every time step. It is possible to construct a cylindrical Delaunay triangulation (see Okabe *et al.*, 2000, p209–211). However to save time we have been using the Triangle software package; a robust, efficient and optimised Delaunay triangulator (Shewchuk, 1996). Because Triangle works only in a 2D planar geometry, it was necessary to add more functions to `Cylindrical2dMesh` to utilise Triangle.

Before calling Triangle's re-meshing algorithm `Cylindrical2dMesh::ReMesh()` creates a horizontal row of 'ghost' nodes above and below the crypt to maintain the convex-hull property of the triangulation, see Figure 5.9(b). `Cylindrical2dMesh` then creates 'images' of all the nodes in $0 \leqslant x < C/2$ and places them in $C \leqslant x < 3C/2$ and also takes the nodes in $C/2 \leqslant x < C$ and places images of them in $-C/2 \leqslant x < 0$; this creates double the number of nodes, covering twice the area (Figure 5.9(c)). We keep a list of which 'real' node is associated with which 'image'. Triangle is then

called on this extended set of nodes and creates their Delaunay triangulation. Note that elements which cross $x = 0$ or $x = C$ are repeated on each side of the tessellation — in one case with one real and two image nodes, and in the corresponding element with two real nodes and one image node (Figure 5.9(d)).

(a) (b) (c)

(d) (e) (f)
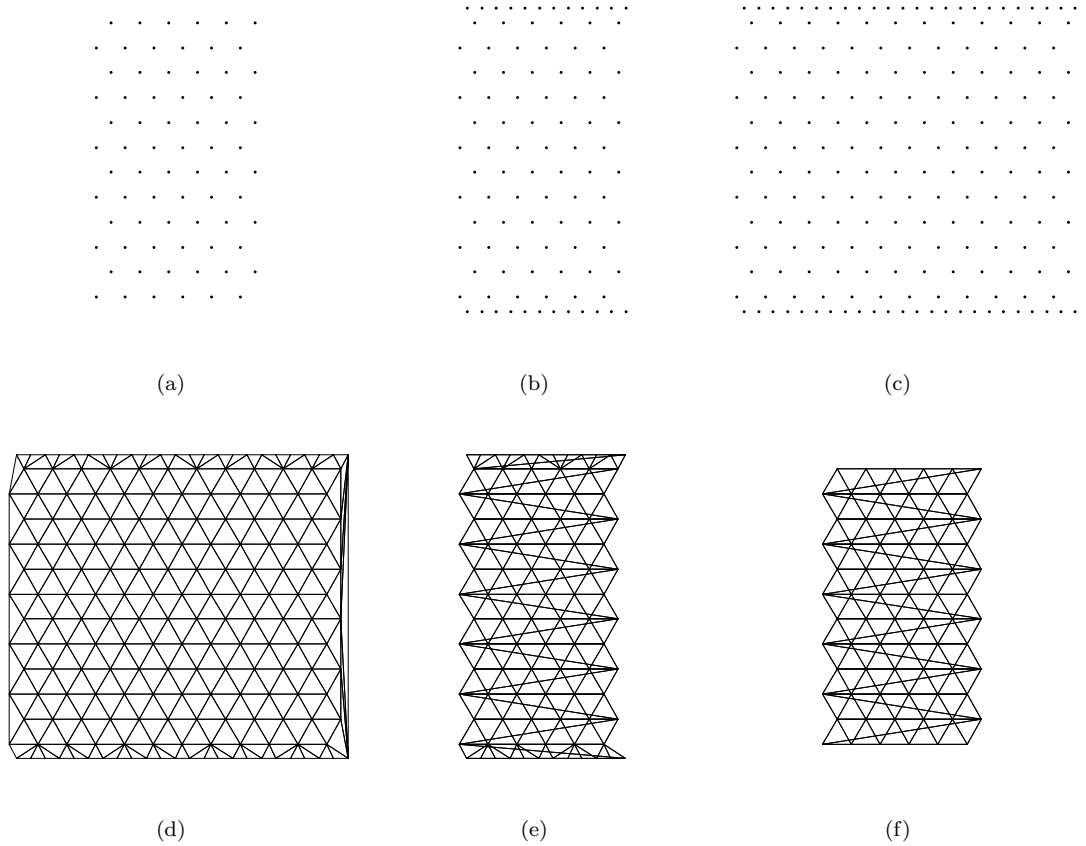
Figure 5.9: The cylindrical remeshing process. (a) original set of nodes, (b) 'ghost nodes' added, (c) 'image' nodes added, (d) Triangle meshing performed, (e) cylindrical mesh reconstructed, (f) 'ghost' nodes and elements removed.

We then reconstruct the cylindrical mesh by selecting each element containing one image node, and replacing the image node with its real counterpart in the element definition. We then delete all elements containing two or three image-nodes, and all of the image nodes (Figure 5.9(e)). Finally we remove the ghost nodes (and associated elements) from the top and bottom of the crypt, leaving us with a mesh which is a Voronoi tessellation in a cylindrical geometry (Figure 5.9(f)).

Mechanics System

The Meineke *et al.* (2001) spring force calculation (equation (5.1)) and node-speed calculation (equation (5.2)) are performed in a separate class `Meineke2001SpringSystem` which returns the speed of each node to the simulation class. The mechanics system can be subclassed to give individual cells different spring or damping constants, or to change the mechanics laws for the cells altogether.

Simulation Class

The simulations are run from a `TissueSimulation` class, whose main role is to coordinate all the activities of the other classes. `TissueSimulation` does most of its work in a `Solve()` method, shown in Figure 5.10.

```
1    while (SimulationTime::Instance()->GetTimeStepsElapsed() < num_time_steps)
2    {
3        mNumDeaths += DoCellRemoval();
4
5        mNumBirths += DoCellBirth();
6
7        mpTissue->ReMesh();
8
9        drdt = mpMechanicsSystem->rCalculateVelocitiesOfEachNode();
10
11       UpdateNodePositions(drdt);
12
13       SimulationTime::Instance()->IncrementTimeOneStep();
14
15       mrTissue.WriteResultsToFiles();
16   }
```

Figure 5.10: An outline of the `TissueSimulation` main `Solve()` method.

The `TissueSimulation::Solve()` method shown in Figure 5.10 contained much more of the Meineke-specific spring calculations and cell birth and death in earlier revisions. As new projects have come into scope our agile approach has factored out common code into the `MechanicsSystems`, and different rules for removing cells into `CellKillers`, leaving a simple and easily extendible base for all of our tissue simulations. The different class interactions are shown in Figure 5.7.

Modifications

Using our agile approach has allowed us easily to introduce new features that extend the basic Meineke *et al.* (2001) model. We have introduced an external `WntConcentration`, which influences

the `CellCycleModels`, as shown in Figure 5.7. We have also used a new `WntCellCycleModel` to remove the need for pinned stem cells, with a cell's behaviour now defined by the `WntConcentration` it experiences, rather than its generation number. This allows different populations to establish in the crypt rather than all cells being descended from a fixed number of stem cells. We have modified the spring stiffness to depend upon the length of the cell-cell contacts, defined by the Voronoi tessellation. Additionally we have added a new model for cell-cell adhesion, dependent on levels of membrane-bound β-catenin, influenced by a subcellular Wnt-signalling model. We will explore the results of these modifications in Chapter 6.

5.4.2 Extending CHASTE for other models

We have extended the CHASTE cancer code to simulate other models, using the same framework as that shown in Figure 5.7. Here we briefly explain how this has been done for two alternative models.

Tumour spheroid simulations

The crypt modelling framework which we have been using, shown in Figure 5.7, can model tumour monolayers or spheroids by simply replacing the `Cylindrical2dMesh` with a `Mesh<2D>` or `Mesh<3D>` respectively. The group has been exploring the solving of PDEs alongside the simulation, for example a PDE for oxygen concentration, with source and sink terms controlled by the individual cells. This introduces feedback into the 'External Influences' of Figure 5.7, and allows for cell-based simulations to be compared to classical continuum approaches for tumour spheroid growth, with the added possibility of studying asymmetric tumour growth.

Crypt Projection model

The group has also produced a 'crypt projection' model by using a standard 2D monolayer simulation, and adding a new `CryptProjectionMechanicsSystem` which projects the 2D mesh onto a 3D parabola before performing the spring calculations. A new `RadialCellKiller` is used to remove cells based on their radial position instead of height. These new classes have slotted into the existing framework and have quickly allowed this new model to be simulated.

5.5   Discussion

By using software-engineering design and coding principles we have developed a new C++ library for simulating cell-based models of healthy and cancerous tissues. There are many benefits to this style of development, discussed in the paragraphs below.

A huge benefit of test-driven development is the users' confidence that the code is doing the task that it was created to do, and will continue to perform this task as new functionality is added. Knowing that a change cannot break existing code gives the team freedom to experiment with new components, and refine existing components. As extra capabilities have been added the code has been through some large changes, completely altering the interfaces and interactions of many components, with complete confidence that it still performs the same tasks it was originally programmed to perform. Without constant testing it would be impossible to change the existing code to accommodate new components and the project would have to adhere to well-defined limits defined during an initial design phase; instead we have a code which can adapt to new demands as necessary.

The use of classes and inheritance allows us to change a simulation very easily; for example using a different cell-cycle model inside every cell of a tissue simulation becomes a trivial exercise of changing one word in a test script. This is excellent for modelling processes on different scales as we can change a single component on a single scale and observe the effect on a different scale of behaviour. The class based structure also makes it very easy to incorporate new components, as repeated code can be inherited from a base class, leaving only the new function to test and code.

The central code repository automatically tracks the revisions that the team makes to the code and displays them in a timeline. This allows the whole team to keep up to date with changes and allows them to make improvements to any part of the code. Such transparency ensures that the code is written to a high standard. The different revisions of the code can be retrieved at any time allowing us to replicate past results easily. If it is important for the code to be able to produce the results at any time then a test can be written. Because the code is compiled and tested on parallel systems, and different companies' processors, we have been able to utilise HPC clusters to run our simulations.

There are some disadvantages to the agile methods we have been using. Despite knowing that we were setting out to construct a code that could simulate a Meineke-style model, the use of small iterations (of limited 'scope') meant that we could not think ahead to make code easily useable in the future. There have been instances where assumptions which had been built into the code were hard to remove later, but would have been relatively easy to make flexible initially. This has led to

many hours of work to refactor the code into a more extendable form, without the end requirement changing. However the agile approach has allowed these changes to be made, whilst knowing that the underlying code retains its function. Over the course of the project we have changed the amount of planning that is done accordingly, to fit the requirements of scientific computing better, rather than keeping it to a minimum as agile methods would suggest.

In chapter 6 we show how we have used the CHASTE code to simulate Meineke *et al.*'s (2001) model and various extensions, discussing the results and their relevance to important scientific questions about the mechanisms controlling cell dynamics in colorectal crypts.

CHAPTER 6

Wnt Signalling in Colorectal-Crypt Models

6.1 Introduction

A s we saw in section 1.5.2, there are a number of different cell-based models for colon crypts and the initiation of colorectal cancer. In this chapter we extend the model proposed by Meineke *et al.* (2001), to study the impact of Wnt signalling on the behaviour of a colorectal crypt.

All of the experiments and simulations refer to murine crypts since they are smaller than their human counterparts and hence easier to simulate. Murine crypts are believed to operate in the same way as human ones (Stappenbeck *et al.*, 1998) and there is more data available on the murine crypt (Potten & Loeffler, 1987).

We would like to study the impact of different cell-cycle models on the dynamics of an entire crypt: for example, does a model in which a cell divides a certain number of times or a model in which a cell divides under a certain Wnt signal best describe the observed dynamics? We aim to reveal what level of modelling detail is needed to simulate the observed behaviour realistically.

Crypts have been observed to become monoclonal; all cells are descended from one original cell (Taylor *et al.*, 2003). By following the lineage of individual cells in our simulations we hope to provide insight into this process. We also simulate a common cell-labelling and crypt-section experiment to determine how accurately the results represent the true crypt dynamics.

As we discussed in chapter 5, the CHASTE software library was developed to simulate all the models we examine in this chapter. The chapter is structured as follows: firstly we describe our extensions to Meineke *et al.*'s (2001) crypt model, then we introduce some of the experimental results, before presenting our simulation results.

6.2   Modifications to the basic Meineke *et al.* (2001) model

As we saw in section 5.2, Meineke *et al.* (2001) developed a cell-based, lattice-free model for the cellular dynamics in a small-intestinal crypt. It consists of a cylindrical 2D mesh, constructed using a Delaunay triangulation (or, equivalently, a Voronoi tessellation). Each node of the mesh represents the centre of a cell. Cells are connected by springs, defined by the Delaunay triangulation, and move in a heavily-damped manner according to the forces exerted on them by their springs. At the base of the cylinder are a number of fixed Paneth cells (which secrete antimicrobial enzymes) and 'stem' cells. Stem cells (generation = 0) produce daughter 'transit' cells (generation = 1). Transit cells divide a fixed number of times, and then become 'differentiated'. In this way the introduction of daughter cells drives migration throughout the crypt and cells are removed once they reach the top of the crypt.

It should be noted that the Meineke *et al.* (2001) model described above was designed to emulate cell dynamics in the small-intestinal crypts, rather than the colorectal crypts. We have adapted Meineke *et al.*'s model by using different dimensions, based upon measurements by Sunter *et al.* (1979), and by removing the Paneth cells which are not present in the colorectal crypts (see section 1.2.1). We present a simulation of the standard Meineke *et al.* model in Figure 6.1: we label one of the stem cells at $t = 0$ and track its progeny through further simulations, the cells produced at the base of the crypt are swept to the top, and eventually leave the crypt.

In the rest of this section we will discuss the other extensions that we have made to Meineke *et al.*'s (2001) basic model.

6.2.1   Wnt Concentration

We have imposed a fixed, spatially-varying `WntConcentration`, decreasing linearly from 1 at the base to 0 at the top of the crypt. This distribution is based on the assumption that Wnt is produced by myofibroblasts at the base of the crypt and then diffuses upward along the crypt axis. The Wnt concentration at a particular point in space can then be used as an input into, for example, the cells' ODE-based Wnt signalling models.

6.2.2   Cell Cycle Models

We have simulated many different cell-cycle models, the full range of models currently incorporated into CHASTE is shown in Figure 5.8. In this section we will introduce some of the models which
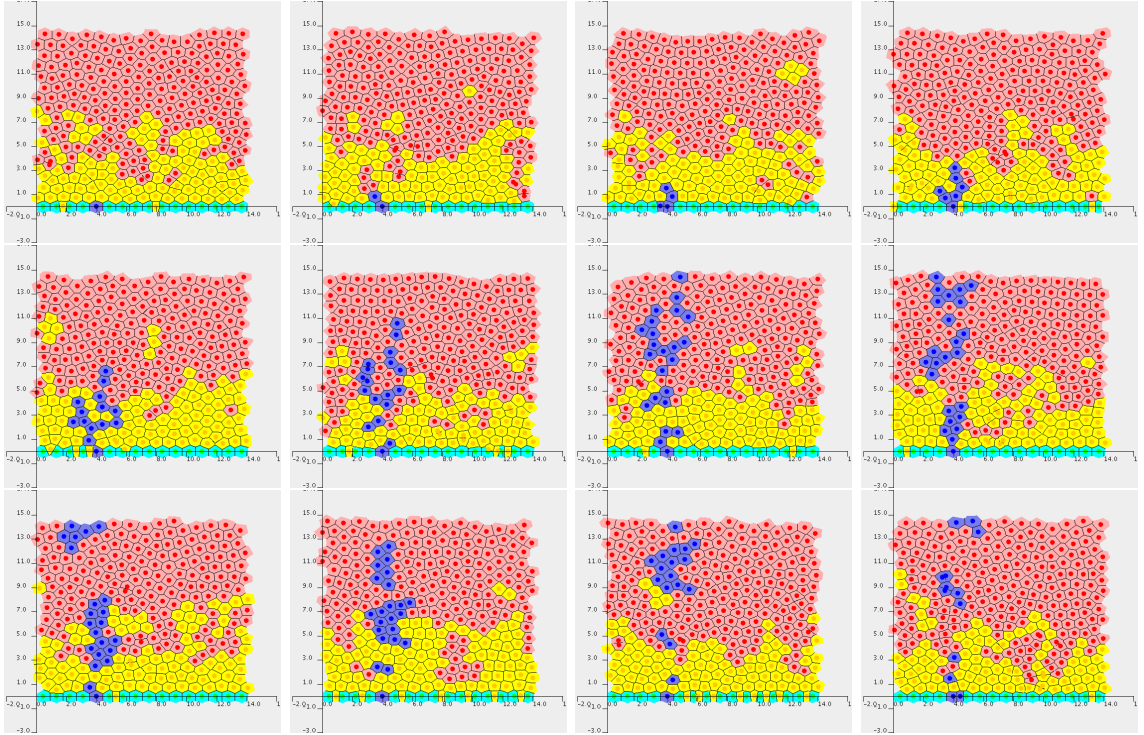
Figure 6.1: A simulation of the standard Meineke *et al.* model in the CHASTE environment. Light blue cells are stem cells, yellow cells are transit cells, and red cells are differentiated cells. Blue cells are a labelled population descended from the stem cell labelled at $t = 0$. Top row: $t = 0$, $t = 10$, $t = 20$, $t = 30$; middle row: $t = 40$, $t = 50$, $t = 60$, $t = 70$; bottom row: $t = 80$, $t = 90$, $t = 100$, $t = 110$. Time, t, is in hours. For parameter values see Appendix A.

have been implemented in our extensions to Meineke *et al.*'s model.

Simple Wnt Cell Cycle Model

The simplest new model we have included is a `SimpleWntCellCycleModel`, which uses the `WntConcentration` as an input. The duration of G_1 phase for a particular cell is determined upon birth or after division, and selected from a normal distribution of mean t_{G1}, with a standard deviation of 1 hour. The cell will progress through the cell cycle into a new phase if the `WntConcentration` at its node's location exceeds a threshold value. We have set the threshold value to 0.65 (dimensionless) to match the overall rates of cell production with those of the Meineke cell-cycle model.

Van Leeuwen Wnt Signalling and Swat Cell Cycle Model

Van Leeuwen *et al.* (2007) developed a model to investigate the interaction between β-catenin's role in adhesion and transcription. There are two main hypotheses: under hypothesis one, β-catenin's fate is determined by competition for binding partners; under hypothesis two, β-catenin undergoes a conformational change which favours transcription. The authors formulate an ODE model distinguishing between all these different pools of β-catenin. A schematic and the governing equations of the van Leeuwen *et al.* (2007) Wnt signalling model can be seen in Appendix B.
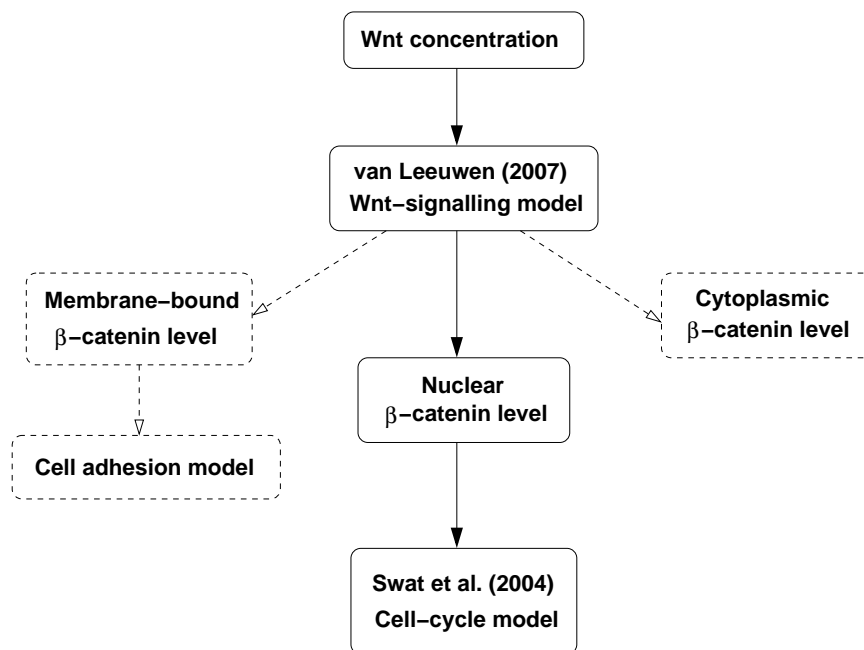
Figure 6.2: Inputs and outputs of the van Leeuwen *et al.* (2007) Wnt-signalling model inside a single cell. Solid lines indicate those components that are used in the simulations presented in this chapter; dashed lines indicate other components which have been included in CHASTE, which are not utilised in the simulations of this chapter.

The implementation of the model for a single cell is presented in schematic form in Figure 6.2. The `WntConcentration` is an input to the model, and the level of nuclear β-catenin is one of the three outputs. Nuclear levels of β-catenin are used as an input into the Swat *et al.* (2004) model of the G_1/S transition of the cell cycle, as β-catenin is a transcription factor for cell-cycle proteins as we have previously studied in chapters 3 and 4. The implementation of this link between the models is performed as discussed in section 3.3 for a simpler Wnt-signalling model. Membrane-bound β-catenin levels could be used as an input into a cell-cell adhesion model, this is implemented by other developers of CHASTE. Each cell carries its own copy of these Wnt-signalling and cell-cycle models,

as the `WntConcentration` varies throughout the crypt.

Interestingly the `WntConcentration` object has to be changed to create a quasi-steady crypt with the same levels of proliferation as those observed using the Meineke and `SimpleWntCellCycleModel`. The van Leeuwen *et al.* (2007) model includes time-dependent ODEs for the response of β-catenin levels to the extra-cellular Wnt concentration; the time-dependence means it takes the cells a certain amount of time to respond to changes in the Wnt concentration. Subsequently, a cell near the base of the crypt under a strong Wnt stimulus will retain high β-catenin levels for some time after moving up the crypt into a region of lower Wnt stimulus. The importance of this effect depends upon the difference in rates of cell migration and β-catenin response.

To match proliferation rates with those of the other two models, under our parameter regime, the `WntConcentration` has to be set to zero at 44% of the crypt height for Hypothesis One, and 61% of the crypt height for Hypothesis Two. There is some evidence that many Wnt factors are only found near the base of the crypt, and not at the top (Gregorieff *et al.*, 2005). Notably, different Wnts are expressed in different regions of the crypt, but as yet all mathematical models feature a single, general Wnt factor since the differences in function are poorly understood. Our findings suggest that a gradient in intracellular levels of β-catenin along the crypt axis could be established by Wnt factors being expressed only around the base of the crypt.

6.2.3   Unpinned stem cells

In Meineke *et al.* (2001) stem cells are pinned at the crypt base. This means that the crypt is always filled with cells descended from n ancestors, where n is the number of fixed stem cells.

After introducing new cell-cycle models, which are not reliant on asymmetric division and cells dividing a fixed number of times, we can 'unpin' the stem cells at the base of the crypt. Stem cells can then be treated simply as 'transit' cells, which happen to be under a strong Wnt stimulus. The crypt is no longer restricted to having n separate clonal populations, and we have added a variable that enables us to relate each cell to its oldest ancestor. This allows us to study which populations of cells are washed out of the crypt and which populations persist.

6.3   Experimental Results

In this section we present some experimental results for healthy murine crypts, using the CHASTE programming environment to replicate and explain them in section 6.4

6.3.1 Labelling Experiments

Cell labelling is well established in experimental labs, markers such as tritiated thymidine (^{3}HTdR) or bromodeoxyuridine (BrdU) can be introduced into cells and incorporate themselves into the cell's DNA as it is synthesised (during the S phase of the cell cycle). Such markers are then passed on to the cells' progeny and, in a colorectal crypt, degrade on a slower timescale than the cell cycle. In this way it is possible to identify which cells in a population are in the S phase and to track their movement and proliferation.

We now present murine data due to Sunter *et al.* (1979) in Figure 6.3. Samples were taken an hour after a ^{3}HTdR radioactive marker was introduced. Mice are killed, crypts are dissected out and sliced into sections along the crypt axis, allowing either one or two sections to be taken from each crypt. The number of cells in these sections and positions of labelled cells were then recorded. Sunter *et al.* (1979) performed these experiments at a range of different sites, finding considerable variation along the length of the colon (see Figure 6.3). The data presented suggest that most
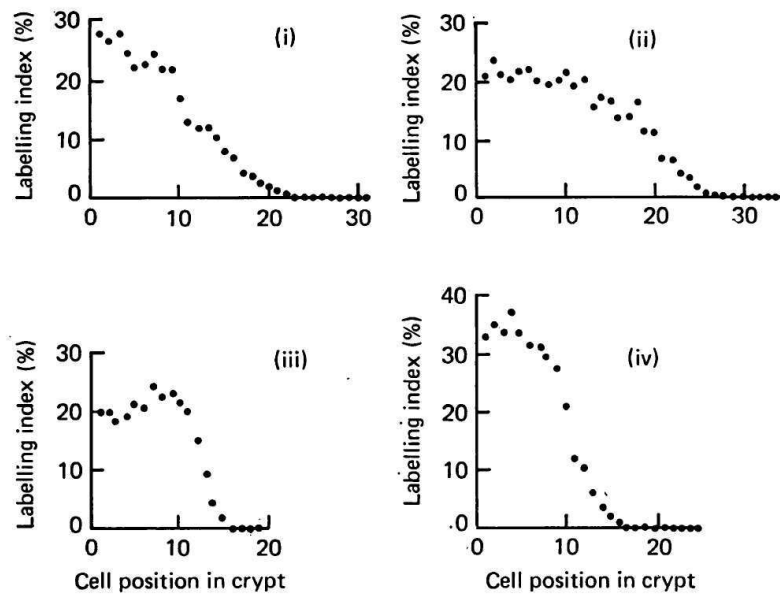
Figure 6.3: Results of Sunter *et al.* (1979) labelling experiments 1 hour after injection. (i), (ii), (iii) and (iv) correspond to different sites along the mouse colon. Reproduced from Sunter *et al.* (1979).

proliferation occurs at the base of the colon: with up to 40% of the cells in S phase at any one time, the data suggest that all of the cells at the base of the crypt are actively cycling. Towards the top of the crypt the labelling index reduces to zero, suggesting that all of the cells towards the top of

the crypt are differentiated.

In section 6.4.1 we demonstrate how to recreate the results of Figure 6.3 by simulating these labelling experiments, using the CHASTE environment.

6.3.2   Mitochondrial DNA Experiments

There are many hundreds of mitochondria in every cell, each with many copies of their own small 16.5kb genome (Taylor *et al.*, 2003). Mitochondrial DNA (mtDNA) is prone to sporadic mutations, some of which leave the cell cytochrome c oxidase-deficient. These mutations are thought to occur randomly and relatively commonly upon replication of mtDNA. As the cells in the colon are dividing continually from the organism's birth onwards, this makes mutations in the mtDNA reasonably probable, with the likelihood of (at least) one mutation occurring increasing with age (McDonald *et al.*, 2006). Cells can be labelled for cytochrome c oxidase-deficiency (see Figure 6.4). In experiments the cells carrying the cytochrome c oxidase-deficiency are labelled blue.

Cytochrome c oxidase is involved in respiration within the cell, but the cell-cycle time, migration and behaviour of the cell within the crypt are thought to be unaffected by this mutation. The cells behave as normal crypt cells, and this mutation is not associated with colorectal cancer or aberrant behaviour. Patches of clonally-identical crypts are shown in Figure 6.4 (c) and (d), and were confirmed to carry precisely the same mutations (Taylor *et al.*, 2003), suggesting a common cell gave rise to the labelled population. Neighbouring crypts are thought to become part of the same monoclonal population due to crypt fission (Greaves *et al.*, 2006). Given that there is thought to be more than one stem cell in a crypt, it was suprising to find that a single crypt is usually monoclonal (Figure 6.4 (a) and (b)).

To explain this finding the concept of 'stem-cell niche succession' has been proposed. This hypothesis states that the crypt has a pool of stem cells (the 'niche'). Since the crypts become monoclonal, stem cells must move in and out of the 'stem-cell niche', leading to a succession of stem cells from which the entire population arises.

However some crypts are found which are not monoclonal: a clonal population may form a 'ribbon' which extends from the bottom to the top of the crypt (see Figure 6.5). The labelled ribbons of cells from the stem-cell niche to the top of the crypt form 'wavy columns'. The band of cells does not maintain a constant width as one might first expect (see Figure 6.5). Other results, similar to those in Figure 6.5, show these uneven columns beginning at a higher position in the crypt, rather than at the base of the crypt. Professor Nicholas Wright (Queen Mary's School of Medicine and Dentistry,
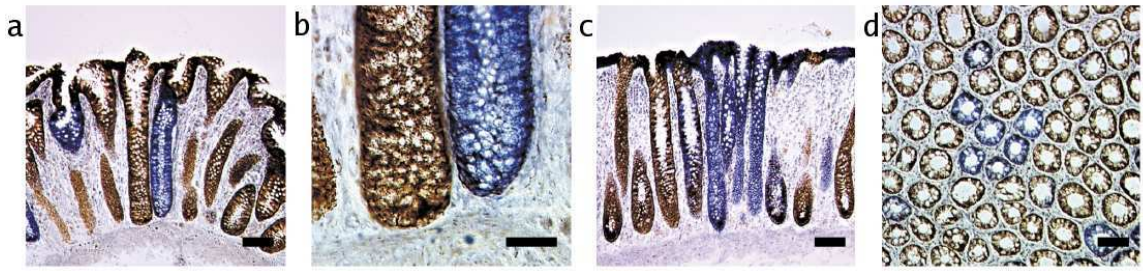
Figure 6.4: Results of mtDNA labelling experiments from Taylor *et al.* (2003). Mutations occur in a single cell, taking over a single crypt (a) and (b), then spreading to produce a patch of clonally identical crypts (c) and (d). Reproduced from Taylor *et al.* (2003).

London) has postulated that these populations could be descended from a new pool of stem cells, found higher in the crypt than previously thought (Wnt Meeting, QMC Nottingham, 29th October 2007). We investigate other possible explanations for these observations in section 6.4.2.

6.4   Simulation Results

We ran all of our simulations using the CHASTE framework described in Chapter 5, using the parameter values shown in Appendix A. Firstly we examine how well our labelling experiments match those in section 6.3.1, secondly we provide some insight into the mtDNA labelling results of section 6.3.2 and finally we suggest how the multiscale nature of our model might provide new predictions.

6.4.1   Comparison with labelling data

We saw in section 6.3.1 how experimentalists have produced crypt sections and labelling data for over 30 years. Here we describe how we may simulate this process.

To take a virtual crypt-section we simply choose a point at the base of the crypt cylinder at random, choose another random point along the top of the cylinder and draw a line along the 2D cylinder-surface connecting the two. Note that this section could pass across the periodic boundary if this is the most direct line. We then produce a list of the cells whose nodes fall within 0.5 (relaxed spring lengths) of this line, ordered from the base to the top of the crypt. We interrogate these cells to establish whether they are labelled or not and produce a binary vector (of the same length as the cell section) containing this information.
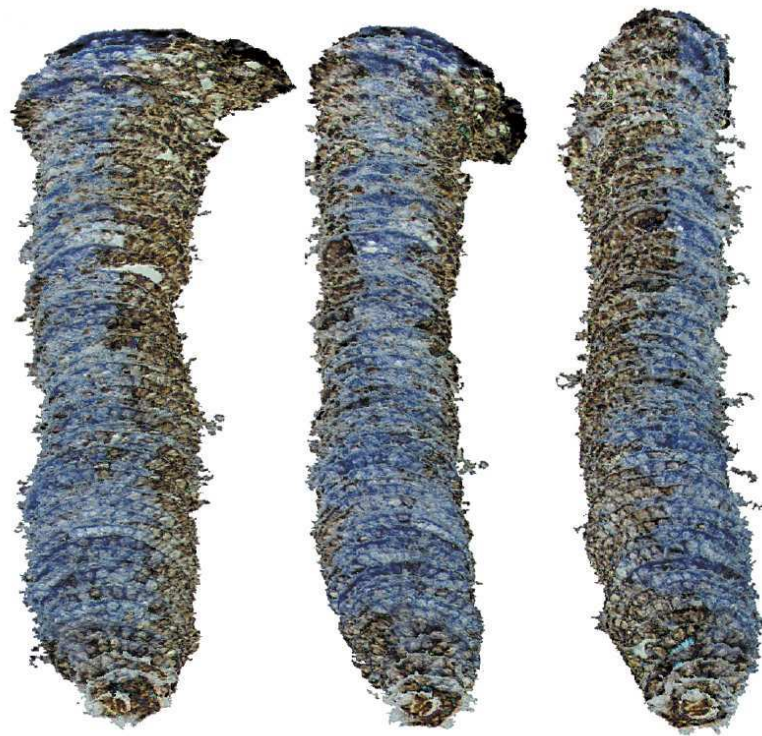
Figure 6.5: Results of mtDNA labelling experiments from Taylor *et al.* (2003) showing a labelled clonal population spreading through a crypt. This is a reconstructed image of a single crypt built up from 59 2D slices. The crypt is rotated by 45° about its main axis between each of the three views above. Reproduced from Taylor *et al.* (2003).

We can then simulate the labelling experiments as follows (with bracketed steps where appropriate);

- A healthy crypt simulation is run until it settles into a quasi-steady state (cell production rates are steady), time is set to $t = 0$.

- At $t = 0$ hours all cells in S phase are labelled.

- Simulation is run to the first time-point.

- Two crypt sections are taken.

- (Simulation is run to the second time-point.)

- (Two further crypt sections are taken.)

- All cells are un-labelled.

- Results are recorded.

- Process is repeated for the same number of runs as mouse-experiments, using the end position as a new quasi-steady starting point.

In the following graphs we display the results of 250 'virtual dissection' experiments for a number of different cell-cycle models. We display the results of taking crypt sections in scatter plots, compared with the averaged results for all the cells in bar charts. We have used the geometry denoted (i) in the Sunter *et al.* (1979) paper: a crypt width of 20 and a height of 30 (units are cells or relaxed spring lengths); see Figure 6.3 for the experimentally observed patterns. Three different cell-cycle models have been used to review the impact of different cell-cycle models on labelling experiment results. In all cases the quasi-steady starting point has the same crypt cell-production rate, as described in section 6.2.2.

Computations were performed using CHASTE executables run on the University of Nottingham's HPC resource 'Jupiter'. The code runs on a single processor at approximately 300 'simulation hours' per hour of computation for cell-cycle models with no ODEs, slowing down to around 100 'simulation hours' per hour of computation using cell-cycle models with over 20 ODEs.

Meineke cell-cycle model

Figure 6.6 displays the result of a set of 'virtual dissection' labelling experiments, and the averaged results, in a crypt with Meineke cell-cycle models. As we might expect, the graphs show that more of the cells towards the base of the crypt are labelled as being in S phase than the cells towards the top. Nine hours later the label has spread some distance up the crypt, which again is consistent
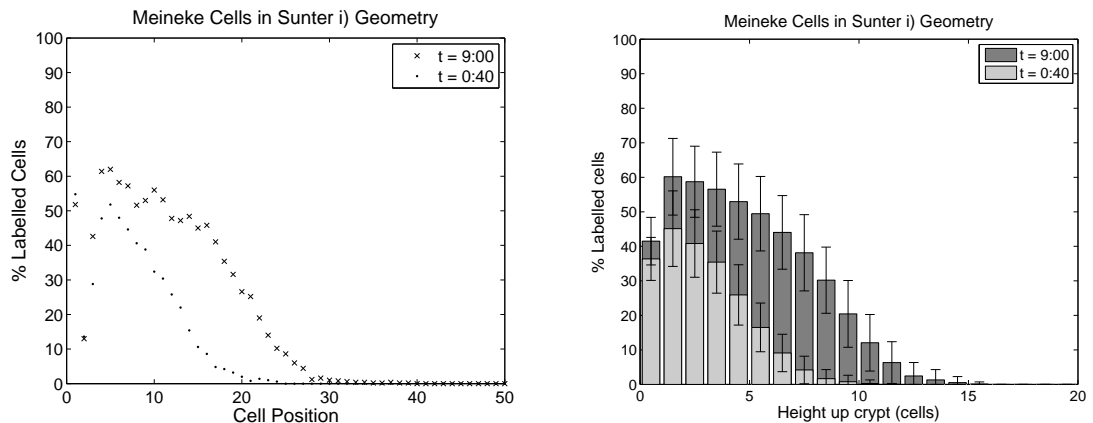
Figure 6.6: Left: Virtual dissection and Right: Averaged labelled cells by height for
Meineke *et al.* (2001) cells in Sunter i) Geometry.   Results shown for 250 simula-
tions. For parameter values see Appendix A.

with experimental results. The labelled fraction has increased as labelled cells which were in S
phase have now divided and a greater percentage of the crypt now carries the label. Despite both
plots exhibiting these characteristics, there are differences between the scatter graph on the left of
Figure 6.6 and the bar-chart on the right: the 'virtual dissection' skews the results suggesting that
labelled cells reach much further up the crypt than the averaged results show.

Simple Wnt cell-cycle model

Figure 6.7 shows the same set of results, in this case for a crypt which has cells running the simple
Wnt cell-cycle model. The simple model generates a square wave in the averaged results, as the
division rule becomes effectively "divide only below a certain height". It is interesting to observe how
this simple set of results becomes skewed by the 'virtual dissection' process to leave a complicated
labelling graph which is not easily distinguishable from Figure 6.6, or indeed the experimental results
presented in Figure 6.3.

Wnt ODE-based cell-cycle model

Figure 6.8 shows the labelling experiment results, in this case for a crypt which has cells running
the Wnt ODE-based cell-cycle model of chapter 3. To add stochasticity the G_2 phase is allocated
from a normal distribution with the mean G_2 phase given in Table A.2, and a standard deviation
of 0.9 hours. In the unlikely event that the allocated time is negative, it is rejected and resampled.

In Figure 6.8 we see a pattern which, as we might expect, falls between those seen in Figure 6.6 and

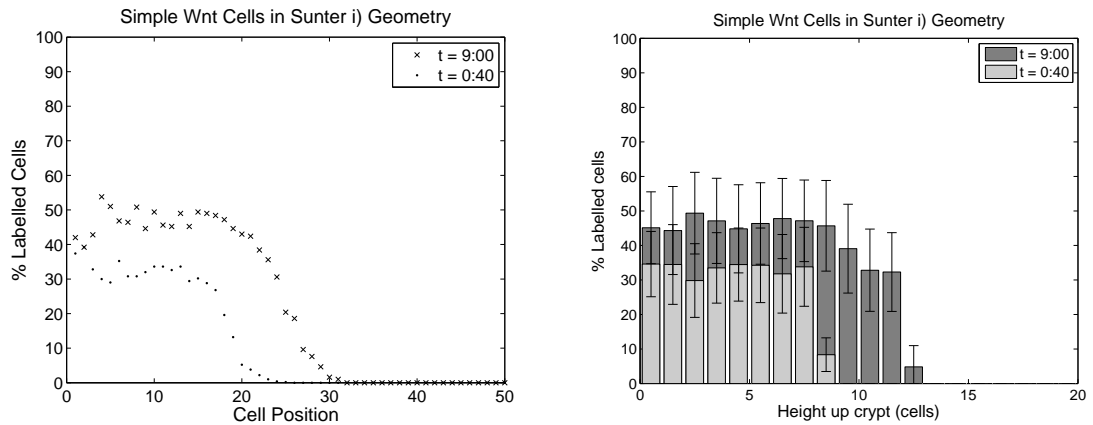**Figure 6.7:** Left: Virtual dissection and Right: Averaged labelled cells by height for SimpleWnt
cells in Sunter i) Geometry. Results shown for 250 simulations. For parameter values
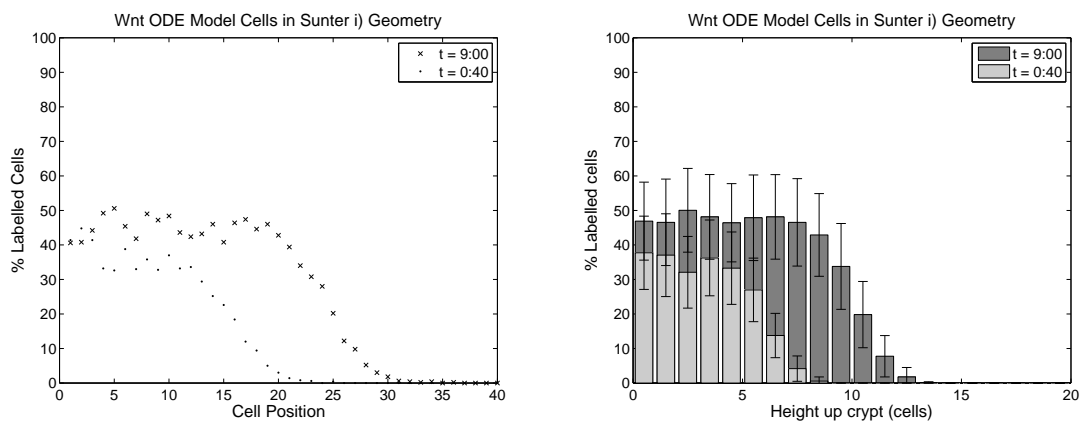see Appendix A.

Figure 6.8: Left: Virtual dissection and Right: Averaged labelled cells by height for Wnt ODE-
based cells in Sunter i) Geometry. Results shown for 250 simulations. For parameter
values see Appendix A.

Figure 6.9: Left: Virtual dissection and Right: Averaged labelled cells by height for van Leeuwen *et al.* (2007) Hypothesis One cells in Sunter i) Geometry. Results shown for 250 simulations. For parameter values see Appendix A.

6.7. Again we have a good agreement with the experimental data presented in Figure 6.3.

Van Leeuwen-Swat cell-cycle model

The van Leeuwen Wnt signalling/Swat cell-cycle model has also been used in these labelling experiment simulations, producing Figure 6.9, when using the van Leeuwen model in its first hypothesis, and Figure 6.10 when using the second hypothesis. Figures 6.9 and 6.10 are almost indistinguishable, so it seems unlikely that one could distinguish between the two hypotheses on the basis of labelling experiments. We will see what differences are predicted by simulations including these two hypotheses later.

We predict that the large error bars are due to a lack of stochasticity in this model, which leads to cells cycling largely in synchrony. This in turn leads to either a large labelled population in a part of the crypt or a lack of a labelled population, increasing the error from that seen in Figure 6.8 which is performing a very similar task with a stochastic element.

The overestimates of the height of the labelled cells are due to an artefact of the dissection process: cell packing means there are more 'cell positions' than the actual crypt height measured in cells. Because crypt sections do not always cut directly down the crypt axis, but are usually slightly off centre this also pushes the labelling results to higher cell positions. These effects skew the results to give the impression that the label has reached further up the crypt than it has in reality. Taking crypt sections also smooths any steep gradients in the underlying proliferation patterns as we saw in Figure 6.7.
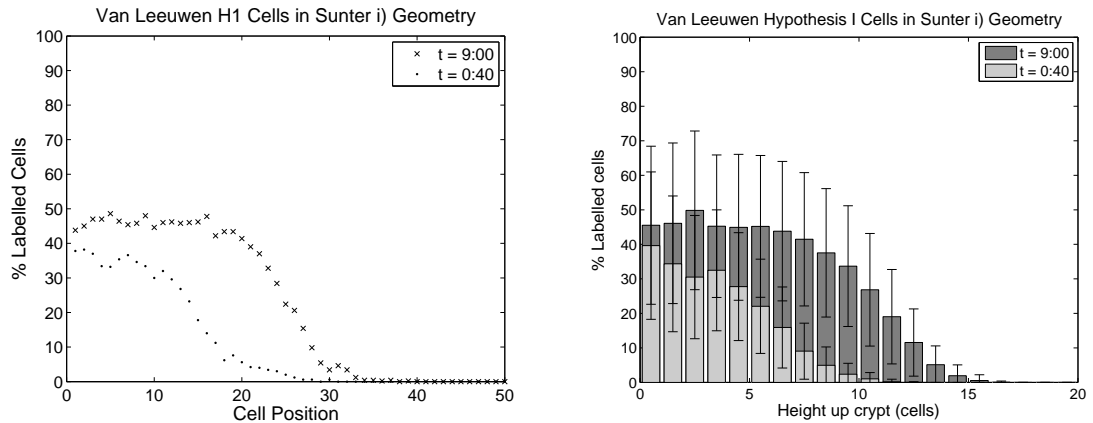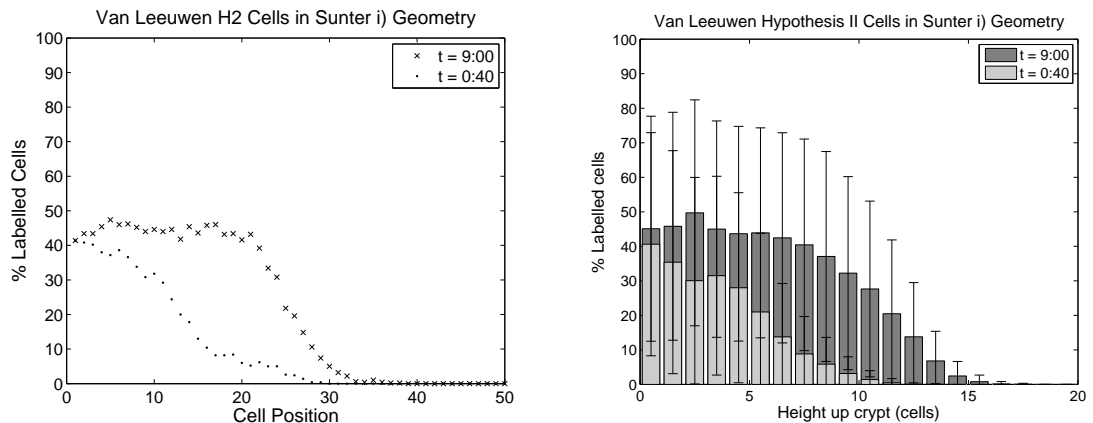
Figure 6.10: Left: Virtual dissection and Right: Averaged labelled cells by height for van Leeuwen *et al.* (2007) Hypothesis Two cells in Sunter i) Geometry. Results shown for 250 simulations. For parameter values see Appendix A.

An interesting direction for future work would be to create PDE continuum models for the fraction of cells in S phase at a certain height up the crypt. Studying where the progeny of these cells migrate to over time would allow comparisons with both the data we have generated and experimental results. We would also like to vary some of the parameters within the model, such as spring stiffness, viscosities and cell-cycle parameters to see their effect on the labelling experiment results.

Although the 'virtual dissection' and averaged simulation results show some differences the main trends are preserved between the two, and taking crypt sections remains a good method for studying the proliferation and migration within the crypt. The artefacts that we have observed when taking crypt sections should be noted when drawing conclusions from such experiments.

6.4.2 mtDNA Experiments

We can easily simulate mtDNA experiments by simply labelling a cell with a harmless mutation, the label spreading to all of its progeny. Figure 6.11 shows how clonal populations develop for Meineke simulations (first and second columns), and for a `SimpleWntCellCycleModel` based simulation (third and fourth columns); in columns one and three we represent the ancestor of each cell with a colour, in columns two and four we follow a single labelled population (to represent a mtDNA experiment). It is clear that the Meineke simulation produces clonal populations which extends to the top of the crypt, and each of the stem cells maintains a quasi-steady sub-population. This is because all stem cells are pinned and so contribute equally to the crypt.

In the `SimpleWntCellCycleModel` simulation we label a single cell located near the base of the crypt
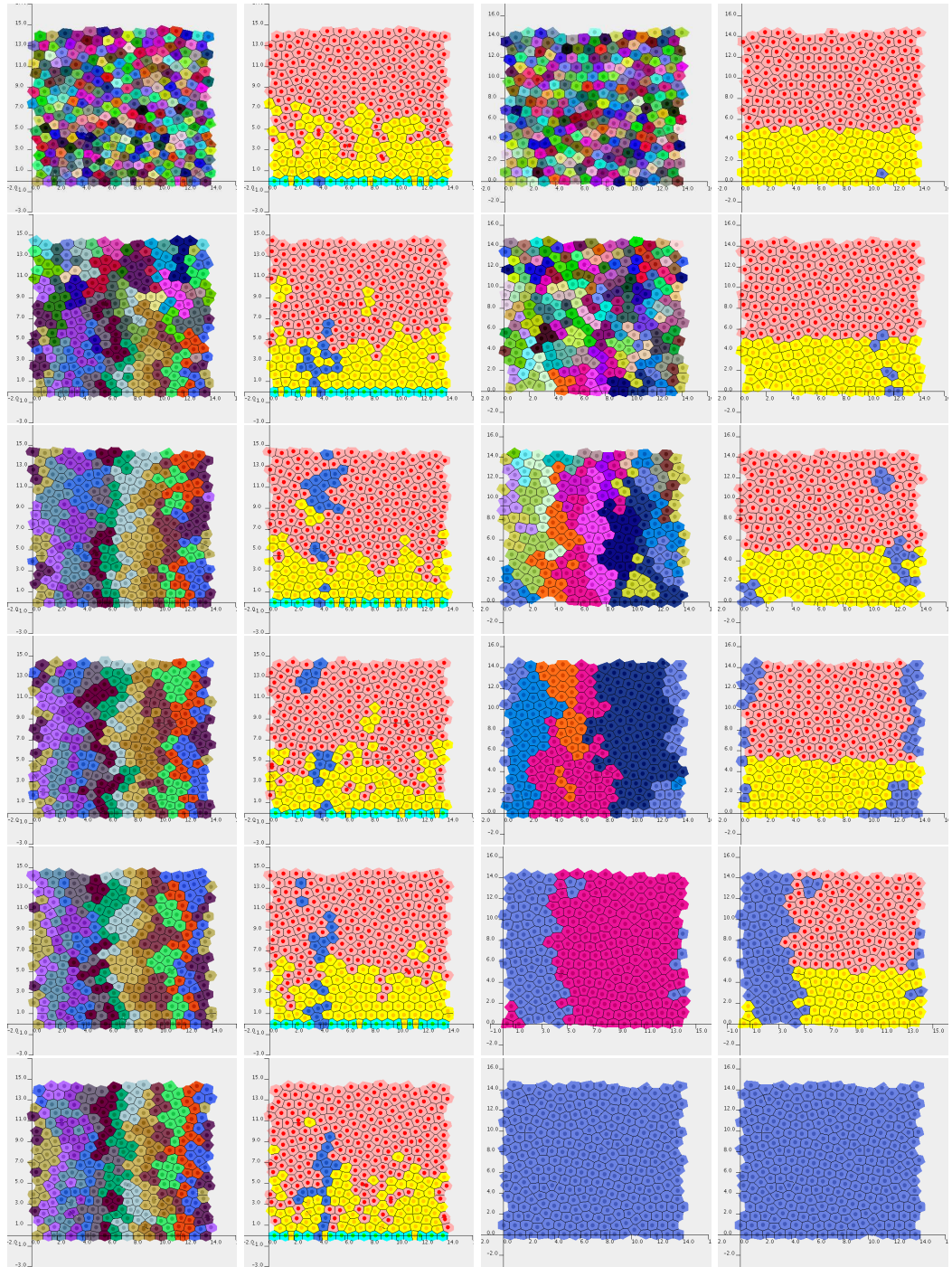
Figure 6.11: Clonal expansion in the crypt, in columns 1 and three each colour represents a different clonal population. Column 1: A Meineke-style simulation with pinned stem cells. Column 2: A single clone of column 1. Column 3: A Simple-Wnt simulation with unpinned stem cells. Column 4: A single clone of column 3. Row 1: $t = 0$hrs, row 2: $t = 40$hrs, row 3: $t = 100$hrs, row 4: $t = 300$hrs, row 5: $t = 800$hrs, row 6: $t = 1340$hrs. For parameter values see Appendix A.

in column four of Figure 6.11 and follow its lineage over time. We observe that this single cell is the ancestor of the whole crypt at the end of the simulation. All of our unpinned-stem-cell simulations have been observed to reach a monoclonal state, through random movement of cells around the base of the crypt. The model simulations support the evidence for, and can replicate, the monoclonal nature of the crypt.

Figure 6.12 shows how the number of distinct populations present in the simulation of columns three and four of Figure 6.11 changes over time. Note that all the cells in the crypt are initially labelled as distinct populations, so the number of different clones in the population reduces approximately exponentially to around 7. This phase continues until the crypt is populated by cells descending only from the viable long-term positions at the base of the crypt. The next losses of clonal populations follow a slower decay, with monoclonality occurring after 1350 hours (roughly 8 weeks).
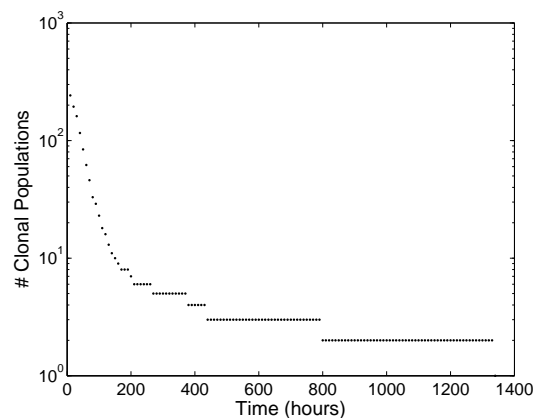
Figure 6.12: The number of clonal populations present in the simulation shown in the third and fourth columns of Figure 6.11. At time $t = 0$ all cells are labelled as separate populations, giving 242 clonal populations. At $t = 1350$ hours only one population remains and the crypt has become monoclonal.

We have performed the above experiment 500 times, recording the amount of time taken for the crypt to become monoclonal, the results are presented in Figure 6.13. We see how the time it takes for a crypt to become monoclonal is distributed in Figure 6.13 (a) with a median of around 40 days, or 960 hours. The cumulative distribution is shown in Figure 6.13 (b), with a smooth transition and all crypts becoming monoclonal after around 160 days (or 4000 hours).

To further examine the concept of 'stem cells' we follow the the cell which gives rise to the entire population in simulations such as those displayed in Figure 6.13. In every simulation the original 'ancestor' cell drifed out of the crypt, we examine how many times each of these cells divided before leaving the crypt in Figure 6.14. We see that the model does not support the theory that any
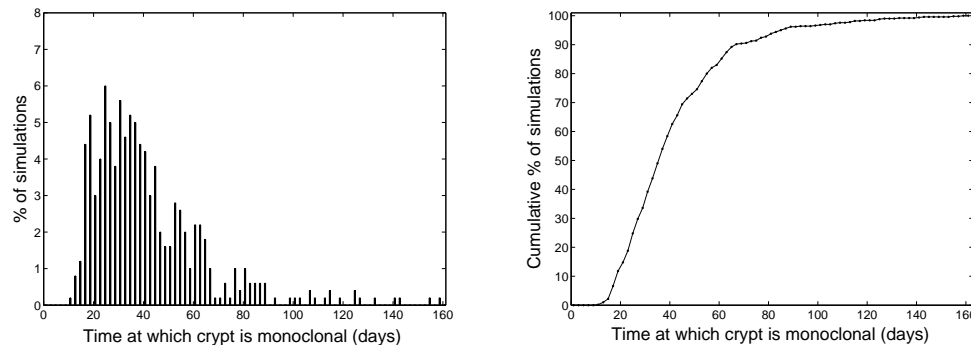
Figure 6.13: Left: the distribution, and on the right the cumulative distribution, of the time it takes for a crypt to become monoclonal. Results are from 500 simulations using the same parameter values as those used in simulations for columns three and four of Figure 6.11.

stem cells are 'immortal', rather that there is a progression in the cells which give rise to the entire population. Since the median time taken for a crypt to become monoclonal is around 960 hours a cell in one of the 'stem' positions would need to persist through around 60 generations, we see that in 250 simulations all of these ancestor cells are lost in less than 20 generations.

Wavy Columns

Prior to leaving or dominating a crypt, a labelled population in column three of Figure 6.11 may form a 'wavy column', as seen in experiments (see Figure 6.5). By visualising our simulations we observe that the crypt is a very dynamic environment; it is highly unlikely that a column would ever have regular sides within our simulation environment. The 'waves' in the sides of the columns can also correspond with groups of cells being descended from a single cell near the base of the crypt. Cells descending from a cell near the base of the crypt have roughly synchronised cell cycles, so a number of cells are born at roughly the same time (or, equivalently, height up the crypt) leading to a swell in the width of a column.

If there are n cells near the crypt base (in a 'stem cell position') and one is labelled at random there is a $1/n$ chance that this label will take over the crypt, and a $1 - 1/n$ chance that it will be swept away; there is a high probability that any single clonal population in a 'stem cell position' will be lost from the crypt.

In Figure 6.15 we present a visualisation of the loss of the penultimate population from the simulation that was shown in column 3 of Figure 6.11. We postulate that the clones which have been observed
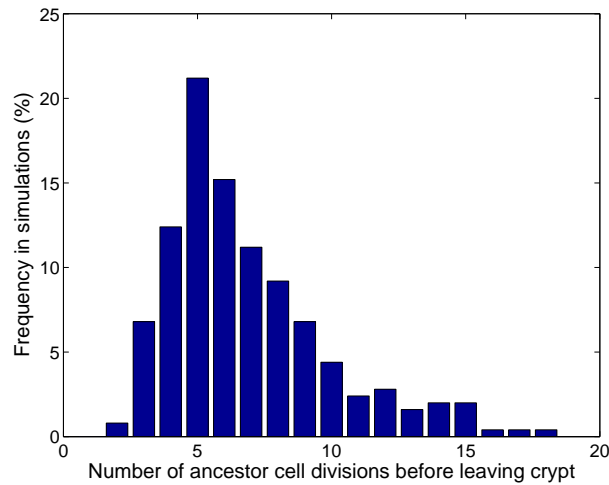
Figure 6.14: The number of divisions that the ancestor cell (which gives rise to the entire crypt population) performs before being swept out of the crypt. Results are from 250 simulations using the same parameter values as those used in the simulations of columns three and four of Figure 6.11.

starting from a height above the crypt base, are not steady populations; but are clones in the process of being swept out of the crypt (such as those in the second row of Figure 6.15). The same findings that have led Professor Wright's group to postulate a new population of stem-cells seem consistent with our observations of many more populations leaving the crypt than becoming dominant. Such stem cells occupying a higher position in the crypt also seem unlikely, given that they would have to defend their positions against a steady flow of cells emanating from the stem cells at the base of the crypt.

The main weakness in our findings is the limitation of the cylindrical 2D geometry we have been using. In reality the base of a crypt does not contain 20 cells all equally likely to become the dominant clone. There are possibly as few as four or five cells with any chance of dominating the real crypt, and they will not do so with equal probabilities; the cell directly at the base of the crypt probably has a far higher chance of becoming the dominant clone than any other cell. For this reason we expect that our 8 week timeframe for the crypt to become monoclonal is an overestimate. Conducting the same mtDNA simulations in more realistic geometries is a high priority for future work. It is notable that we can recreate all of the findings of the mtDNA experiments without having any cells explicitly behaving as 'stem cells'; all of the cells in our CHASTE simulations are simply proliferating or differentiated, the external Wnt stimulus and geometry being sufficient to drive the patterns of proliferation.
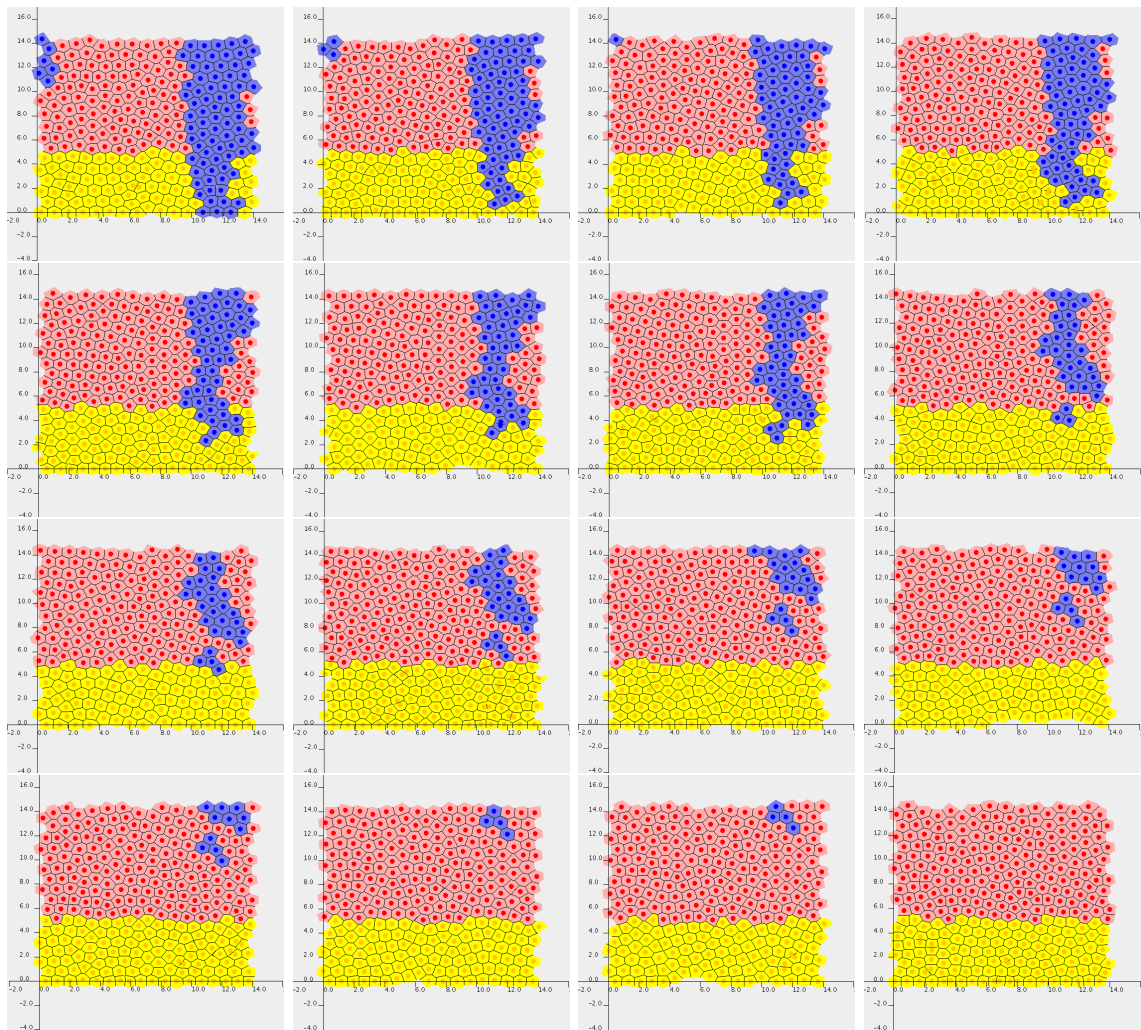
Figure 6.15: Loss of a clonal population from the crypt. Visualisation for regular intervals (over $1535 < t < 1635$ from left to right, top to bottom) for the simulation shown in columns three and four of Figure 6.11. The labelled cells are the penultimate clonal population, that which remains in the crypt for the largest amount of time apart from the dominant clone. For parameter values see Appendix A.

145

6.4.3 β-catenin expression

The van Leeuwen *et al.* (2007) Wnt signalling model predicts the amount of β-catenin distributed to the nucleus, membrane and the cytoplasm as presented in Figure 6.2. The nuclear level of β-catenin acts as a transcription factor, activating the cell-cycle model. In the context of a Wnt gradient and crypt geometry we have adapted the CHASTE visualiser to display these concentrations in the style of a GFP labelling experiment, with the intensity of a colour label depending on the concentration of the component. Figure 6.16 shows a (quasi-)steady-state crypt for each of the two hypotheses that the van Leeuwen *et al.* (2007) model tests (given in Appendix B).
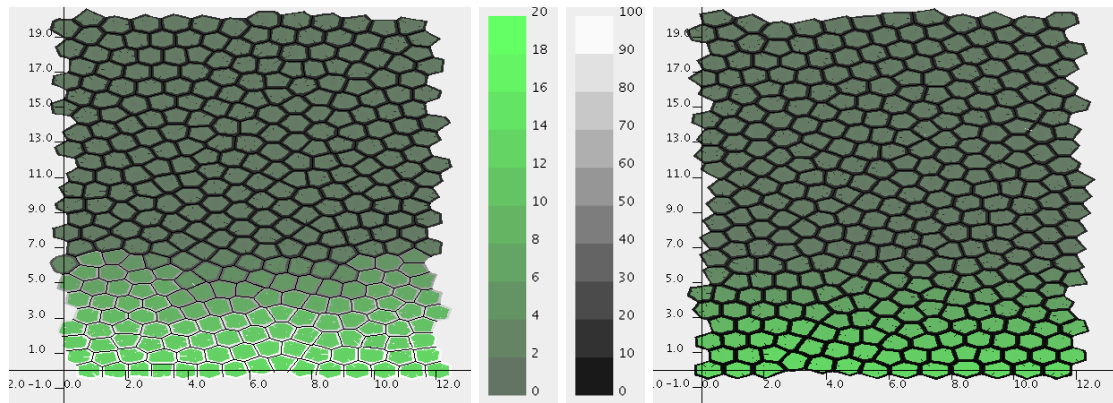
Figure 6.16: A quasi-steady simulation of van Leeuwen *et al.* (2007) under hypothesis one (left) and hypothesis two (right), with cells stained for β-catenin. The CHASTE visualiser displays the concentrations of nuclear and cytoplasmic levels of β-catenin on the green scale and membrane-bound β-catenin on the grey scale, facilitating a qualitative comparison with crypt staining or GFP-labelling experiments. For parameter values see Appendix A.

We see from Figure 6.16 that both hypotheses predict low cytoplasmic and nuclear levels of β-catenin towards the top of the crypt, with moderate membrane-bound concentrations there. However the distribution near the base of the crypt is quite different in the two cases; with high levels of membrane bound β-catenin associated with the first hypothesis, but low levels for the second hypothesis. These predictions could be compared with GFP or other labelling experiments to establish how well hypothesis one or two describe the observed results. At first glance it would appear that in reality membrane-bound levels of β-catenin remain higher than cytoplasmic and nuclear levels throughout the crypt (Shih *et al.*, 2001), suggesting that hypothesis one is more realistic (subcellular β-catenin binding is purely down to competition). This approach will also be useful as we extend the work to compare the distribution of β-catenin in healthy and early colorectal cancer tissue (Fodde & Brabletz, 2007).

6.5   Discussion

In this chapter we have used the CHASTE framework to address a number of topics relating to the function of the healthy colorectal crypt.

We have shown that there is a difference between the results of a virtual dissection and the underlying proliferative activity in a crypt simulation. This suggests that a similar difference exists between the results of crypt section experiments and the underlying proliferation in a real crypt. In particular, the taking of crypt sections appears to exaggerate how far the label has travelled, due to the packing of cells and the slicing a crypt section slightly off-axis. The difference between the virtual dissection and averaged results is smallest in what we consider to be our most realistic cell-cycle model. The process does have the unwanted effect of smoothing out all of the results; none of the cell-cycle models leads to particularly different results after the virtual dissection process.

We have coupled an external Wnt signal to cell proliferation and investigated its impact on a crypt-scale model. The initial results are encouraging and suggest that a Wnt signal could be responsible for sustaining the 'stem-cell pool', and dictating when differentiation should occur. Furthermore, we can predict the subcellular distribution of β-catenin, throughout the crypt, for different Wnt signalling models and compare these with experimental results.

Our results can explain all the findings of mtDNA experiments on a single crypt, with the rich behaviour arising simply out of the geometry and proliferative pressure of the system. Cell-cycle models being roughly synchronised, for a cell population travelling up the crypt, can help to account for the 'wavy columns'. We suggest that columns which seem to begin part-way up the crypt are actually in the process of being 'swept-out', rather than being sustained by a stem cell higher up the crypt.

Intestinal stem cells have been the subject of intense debate for well over the past ten years (Potten *et al.*, 1997; Leedham & Wright, 2007). Yet our CHASTE simulations recreate all of this behaviour without the need to model a separate population of 'stem cells'. Our simulations would suggest that cells giving rise to a population which eventually colonises the entire crypt do so simply because they are trapped at the base of a crypt and under strong proliferative signals. To replicate any of the experimental results seen to date a spatial model of the colorectal crypt does not need to have a separate population of stem cells. A separate pool of stem cells is required in some non-spatial compartmental models — this serves as a representation of the crypt geometry. We venture that considering there to be a separate population of 'stem cells' in the colon crypt is at best unhelpful, and at worst misleading, in aiding understanding of the crypt's cell population dynamics.

Our model represents the 'stemness' of cells as a continuum rather than assuming a discrete change from a stem cell to a transit cell. Thus the notions of symmetric and asymmetric stem cell division have no meaning, with the 'stemness' dependent on the external signals (in our case the Wnt concentration). Our geometry and migration captures the way in which cells can become more differentiated. This is similar approach to that taken by Roeder and collaborators in recent subcellular models for hematapoetic stem cells and their differentiation (Kirkland *et al.*, 2006; Roeder, 2006); interestingly our geometry captures the 'stemness' of the cell in much the same way, without the need for an internal variable. Future work could include adapting some of Roeder's models for differentiation (Glauche *et al.*, 2007) in order to simulate the differentiation of crypt cells into enterocytes, goblet cells and enteroendocrine cells.

Extensions of this work should focus on refining the current cylindrical 2D geometry to more closely resemble the 'test-tube' shape of a colorectal crypt. This will allow more accurate and useful predictive simulations of mtDNA clonal population experiments. By introducing mutant cells useful contributions could be made to the "where do the two hits hit?" discussion (Komarova & Wang, 2004; Leedham & Wright, 2007), shedding some light on whether the process of top-down or bottom-up mutant clone expansion is a more likely cause of colorectal cancer initiation. The code is already in a position to predict β-catenin distributions throughout the crypt within healthy and aberrant cells, which could then be tested experimentally.

CHAPTER 7

Discussion

T HE Wnt signalling pathway has long been implicated in the initiation of colorectal cancer. We have investigated some of the possible mechanisms by which Wnt signalling maintains healthy homeostasis in a colorectal crypt, and looked at the mechanisms by which mutations in the Wnt pathway may cause a cell to cycle uncontrollably.

Wnt signalling was first thought to be important in controlling the cell cycle in a crypt when it was observed that mutations in the Wnt pathway cause polyp formation (Kinzler *et al.*, 1991). In chapter 2 we performed an asymptotic analysis on the Lee *et al.* (2003) model, which is the most widely used model for the Wnt signalling pathway, being well-grounded on experimental measurements of parameter values. We exploited the fact that reaction rates and component concentrations vary by several orders of magnitude, in order to separate out the operation of the pathway onto three distinct timescales. Since β-catenin varied only on the slowest timescale we were able to reduce the entire pathway model to a single ODE, without losing any of the qualitative Wnt-dependent behaviour of β-catenin levels.

Cho *et al.* (2006) added an Axin2 feedback loop into the Lee *et al.* (2003) model, the 2006 model being the most widely used in recent publications. We performed the same asymptotic analysis on this variation of the model, reaching the same type of reduced model — comprising of a single ODE for the β-catenin levels. Again, this reduced model closely matches the behaviour of the full Cho *et al.* (2006) model. The process of the asymptotic analysis shed much light on the operation of the Wnt pathway and has made computation of the Lee *et al.* (2003) model, and its extensions to include feedback effects, far simpler.

Many of the components of the Wnt signalling pathway are localised to either the membrane or the nucleus of a cell. The Lee *et al.* (2003) model assumes that all proteins are freely mixing in the cytoplasm. Further work could include the construction of a compartmental ODE model for

the Wnt signalling pathway, with compartments representing different areas of the cell. There is much research into the control of nuclear import and export of Wnt/β-catenin pathway proteins, and the factors controlling their recruitment to the cell membrane; this should allow such a model to be constructed in the near future. The Lee *et al.* (2003) model is limited by the fact that the parameter values were established from *Xenopus* eggs *in vitro*; we would ideally gain parameter values from human crypt cells *in vivo*.

In chapter 3 we linked the simple Wnt signalling model derived in chapter 2 to an existing model of the cell cycle (Swat *et al.*, 2004), relating them via Cyclin D. We investigated the impact of mutations in the Wnt pathway on the proliferative behaviour of cells under different Wnt stimuli.

This model predicted that a single APC mutation is insufficient for cancer initiation, and that a double-hit is required; whilst a single β-catenin mutation is sufficient to significantly reduce control of the cell cycle. The observation that double APC mutants are most commonly observed in colorectal cancer, rather than a single β-catenin mutation, cannot be explained simply by the probability of such a mutation occurring or their effect on the cell cycle. This suggests that the APC mutation causes functional changes being 'selected' in the process of tumour formation. Modelling the impact of APC, and its mutant forms, on some of these other effects (such as cell adhesion, migration and the cytoskeleton) would form an interesting line of enquiry. GSK3β and other Wnt pathway components affect a similarly wide-range of processes, for which more data is available than ever before, opening up new avenues of subcellular modelling opportunities.

The model of chapter 3 could not explain results which were published last year by Sansom *et al.* (2007). In these experiments a disregulated crypt was caused by an APC knockout, yet a double knockout of APC and Myc restored the crypts to near normal. Our model could replicate the first finding, but not the second as the action of Myc was not featured in the model. In chapter 4 we constructed a new model for Wnt's control of the cell cycle featuring Myc, CDK4 and Cyclin D, with levels of Cyclin D:CDK4 complex as reporters for cell-cycle stimulation. Some parameters for this model were fixed by Sansom *et al.*'s experiments and the results of the knockout experiments can be replicated; this suggested a number of drug targets which could be used to reverse the effects of an APC mutation, with the promoter regions of Cyclin D and CDK4 being the most promising candidates. To validate our model we would like to gain some decay and dissociation rate parameters from experimental results.

There are a number of directions for future modelling linking Wnt signalling to the cell cycle. Feedback loops from cell-cycle proteins to our Wnt signalling pathway are known to exist, for example E2F1 featured in the model of chapter 3 is a Myc-promoter. The importance of such

feedback loops is not yet known and their effects could be considerable. We have also postulated the need for a secondary level of cell-cycle control via a different pathway: there is evidence that proliferation in the crypts is also dependent on non-canonical Wnt signalling or other pathways such as Erk, Delta, Notch and Hedgehog signalling.

We constructed the CHASTE software environment to run cell-based simulations of a colorectal crypt as documented in chapter 5. Working as part of a team we used principles from software-engineering to develop a large C++ code-base, a major advantage being that components common to many models do not need to be coded by each individual researcher for each implementation of a model. The code-base is fully tested so that each sub-component performs exactly the function for which it was programmed. All revisions of the code are automatically logged so that all results are replicatable. We used an 'agile' approach which splits down the workload into manageable 'iterations', with the final code structure emerging from the iterations rather than being planned from the beginning of the project. It was necessary to strike a balance between the agile approach and a more traditional planned approach to best suit the requirements of scientific computing.

In chapter 6 we have used the CHASTE framework to simulate the Meineke *et al.* (2001) model for crypt dynamics with a number of extensions. We took our crypt geometry and modelled the experimental process of taking 'crypt sections'. We then compared the results of this process with the underlying dynamics of the crypt. We found that the experiment provides a good representation of the true crypt dynamics, but the process overestimates the height at which processes occur due to polygonal packing of the cells in the crypt. We have generated a number of virtual crypt sections for different cell-cycle models, which can be compared with experimental data to reveal which cell-cycle model provides the most realistic representation of the patterns of proliferation within a crypt.

Mitochondrial DNA experiments have recently allowed experimentalists to track the progeny of a single cell within the crypt. They have found that a crypt is usually observed to be monoclonal, yet some crypts have 'wavy-columns' of labelled cells from a single ancestor whilst the rest of the crypt is filled with cells descended from different ancestors. The Meineke *et al.* (2001) model contains a population of n pinned stem cells, and so the crypt is always populated by n separate clonal populations.

We extended the Meineke *et al.* (2001) model to allow for a cell-cycle model where cells divide based upon the Wnt concentration that they are experiencing, rather than a generation number. This also removes the requirement for a population of pinned 'stem cells'. We found that a labelled population forms a 'wavy column' of cells prior to dominating or being swept out of the crypt. This process can explain all of the mitochondrial DNA experiment results that have been presented to date — in

terms of progression towards a monoclonal crypt. We suggest that cells act as 'stem cells' because of their position, rather than an inherent 'stem-cell' property. The weakness of our estimate of the time it takes for a crypt to become monoclonal is probably due to the artificial 2D cylindrical geometry we have been using. We have many cells at the base of a crypt all equally likely to become the dominant clone in the crypt. In reality the 'test-tube' geometry suggests that the cell directly at the base of the crypt has a higher probability of becoming the dominant clone. A full 3D geometry will allow far better predictions for the monoclonality timescale, as such this is a research priority.

By incorporating the van Leeuwen *et al.* (2007) subcellular Wnt signalling model into our crypt simulations we have made predictions for the distribution of β-catenin, both within a single cell and throughout the crypt, for two different hypotheses. A finding which emerged from this multiscale model came from the time it takes for β-catenin to react to a new level of Wnt stimulation. Since the cells in the crypt are constantly moving upwards towards the top of the crypt, a cell experiencing a high Wnt stimulus towards the base will maintain it for some time as it is pushed up the crypt. The model suggests that a strong Wnt stimulus around only the base of the crypt (and no Wnt stimulus elsewhere) is enough to create a gradient of nuclear β-catenin levels along the crypt axis. By comparing the quasi-steady-states of simulations with experimental data we will be able to suggest which of the model's two hypotheses is most consistent with observed distributions of β-catenin.

We are in a position to introduce cells harbouring mutations, to track the resulting populations and their success rates in dominating the crypt. We can investigate whether the inability of cells to stop proliferating affects their probability of becoming the dominant clone. There is a large discussion as to "where do the two hits hit?": for example, do both APC mutations happen in a 'stem cell' or does one happen in a stem cell and the second elsewhere? By performing sets of simulations in a realistic 3D geometry we would hope to be able to contribute a great deal to this discussion. Other members of the group are studying the effects of changing viscosity (which represents cell-substrate adhesion) on the probability of a mutant cell dominating the crypt.

We have formulated and analysed models linking an external Wnt stimulus to the cell cycle, and introduced cells with such models into a crypt-scale model. The initial results are encouraging and suggest that a Wnt stimulus is responsible for sustaining the proliferation and cell dynamics within a crypt. We are in a position to use these models to investigate the crypt dynamics which lead to the onset of colorectal cancer.

Appendix A

CHASTE Parameter Values

Table A.1 shows the geometries and cell-cycle models used in the CHASTE simulations presented in Chapter 6.

Table A.1: Parameters used in the CHASTE simulations of Chapter 6.

Figure	6.1	6.6	6.7	6.8	6.9	6.10	6.11:col 1 & 2,	col 3 & 4.	6.15	6.16
Geometry	(iii)	(i)	(i)	(i)	(i)	(i)	(iii)	(iii)	(iii)	(i)
Cell-cycle model	1	1	2	5	3	4	1	2	1	3 & 4

The geometry parameters referred to in Table A.1 are shown in Table A.2, either for the sites referred to by Sunter *et al.* (1979) as (i) or as (iii) (shown in Figure 6.3 of the main text). The cell-cycle models referred to in Table A.1 are shown in Table A.3, see section 6.2.2 for details.

The mechanics parameters used in the CHASTE simulations, which we have not varied between simulations, are shown in Table A.4. Mechanics parameters are based on Meineke *et al.* (2001), however the spring stiffness/damping constant ratio has been increased from those of Meineke *et al.* (2001) to sustain a colorectal crypt rather than the smaller small-intestinal crypt. Note that a stiffness which is too large, or damping which is too small leads to oscillations in the springs, whilst a stiffness that is too small, or damping which is too large, leads to a crypt becoming unable to maintain a quasi-steady state, with proliferation occurring faster than sloughing.

Table A.2: Parameters for the different geometries of CHASTE simulations in Chapter 6, all parameters from Sunter *et al.* (1979), crypt length adjusted for polygonal packing.

Parameter	Sunter geometry (i) value	Sunter geometry (iii) value	units
G_1 duration*	7.0	9.4	hrs
S duration	6.2	7.4	hrs
G_2 duration	1.8	1.4	hrs
M duration	0.5	0.72	hrs
Crypt width	20	14	—
Crypt length	23	15	—

* ignored by those cell cycle models using ODEs for G_1 phase.

Table A.3: Parameters for the different cell cycle models used in Chapter 6, adjusted to provide the same cell-turnover for a whole crypt of Sunter (i) geometry.

Model number	Model description	Maximum transit generations	Top of linear Wnt Concentration
1	Meineke generation-based	3	—
2	Simple Wnt-based	—	1.0
3	Van Leeuwen (2007) Hypothesis One: Swat (2004)	—	0.44
4	Van Leeuwen (2007) Hypothesis Two: Swat (2004)	—	0.61
5	Wnt ODE-based model (chapter 3)	—	0.22

Table A.4: Mechanics parameters for the CHASTE simulations of Chapter 6.

Parameter	symbol		value	units
Spring stiffness	μ	=	30	kg s^{-2}
Damping constant	η	=	1	kg s^{-1}
Timestep	Δt	=	30	s

APPENDIX B

Van Leeuwen (2007) Wnt signalling model

Two different hypotheses have been suggested to explain how β-catenin 'decides' between taking a role in cell adhesion (at the cell-membrane) or transcription (in the nucleus). In the first hypothesis the destination of β-catenin depends purely on the competition for binding partners in the different locations. In the second hypothesis, Wnt signalling causes a conformational change to the β-catenin protein, leaving it unable to perform a role in cell-adhesion.

The van Leeuwen *et al.* (2007) model for Wnt signalling takes the form of a compartmental ODE model, concentrating on the location and state of different pools of β-catenin. A schematic of the model is shown in Figure B.1. The variables shown on Figure B.1 are listed in Table B.1. β-catenin is labelled C, and can only participate in adhesion in its 'open' form, denoted by C_O. The different hypotheses are modelled by varying the rate at which β-catenin takes up its 'closed' form, C_C, through the reaction $r_{15}(W)$ in Figure B.1. This is implemented by changing from $\xi_C = 0$ for hypothesis one to $\xi_C = 5000$ for hypothesis two. The rest of the parameter values can be found in Table B.2.

The governing equations are given by the following expressions, derived from Figure B.1 using mass-action and Michaelis-Menten terms:

- APC-mediated degradation of β-catenin:

$$
\begin{aligned}
\mathrm{d}[D]/\mathrm{d}t = \quad & (1 - \sigma_D)s_D[X] - (\widehat{d}_D + \widehat{d}_{DX})[D], \\
\mathrm{d}[X]/\mathrm{d}t = \quad & s_X - (1 - \sigma_D)s_D[X] - \widehat{d}_X[X] + \widehat{d}_{DX}[D], \\
\mathrm{d}[C_U]/\mathrm{d}t = \quad & \frac{p_U[D][C_F]}{[C_F] + K_D} - d_U[C_U].
\end{aligned}
$$

Variable	Description
D	APC destruction complex
X	Axin
C_U	β-catenin marked for ubiquitination
C_O	Open form β-catenin
C_C	Closed form β-catenin
M_O	Open form mutant β-catenin
M_C	Closed form mutant β-catenin
A	Free Adhesion molecules
C_A	β-catenin:Adhesion
M_A	Mutant β-catenin:Adhesion
T	free TCF
C_{OT}	Open β-catenin:TCF
C_{CT}	Closed β-catenin:TCF
M_{OT}	Open Mutant β-catenin:TCF
M_{CT}	Closed Mutant β-catenin:TCF
Y	Wnt Target protein
W	Wnt level

Table B.1: Dependent variables in van Leeuwen *et al.*'s (2007) Wnt signalling model.
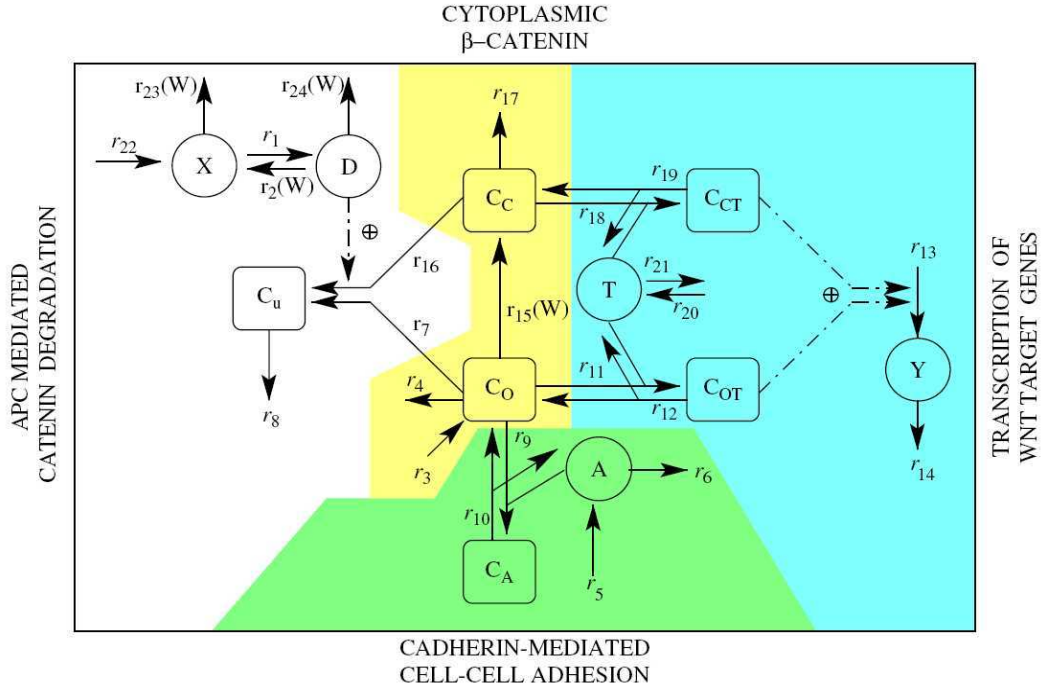
Figure B.1: Schematic of van Leeuwen *et al.*'s (2007) Wnt signalling model. Reproduced from
van Leeuwen *et al.* (2007).

- Cytoplasmic β-catenin:

$$
\begin{aligned}
\mathrm{d}[C_O]/\mathrm{d}t = \quad & (1 - \sigma_\beta)s_C + d_{CA}[C_A] + d_{CT}[C_{OT}] - (s_{CA}[A] + s_{CT}[T] + d_C)[C_O] \\
& - \frac{\widehat{p}_C[C_O]}{[C_O] + [M_O] + K_C} - \frac{p_U[D][C_O]}{[C_F] + K_D}, \\
\mathrm{d}[C_C]/\mathrm{d}t = \quad & \frac{\widehat{p}_C[C_O]}{[C_O] + [M_O] + K_C} + d_{CT}[C_{CT}] - (s_{CT}[T] + d_C)[C_C] - \frac{p_U[D][C_C]}{[C_F] + K_D}, \\
\mathrm{d}[M_O]/\mathrm{d}t = \quad & \sigma_\beta s_C + d_{CA}[M_A] + d_{CT}[M_{OT}] - (s_{CA}[A] + s_{CT}[T] + d_C)[M_O] \\
& - \frac{\widehat{p}_C[M_O]}{[C_O] + [M_O] + K_C}, \\
\mathrm{d}[M_C]/\mathrm{d}t = \quad & \frac{\widehat{p}_C[M_O]}{[C_O] + [M_O] + K_C} + d_{CT}[M_{CT}] - (s_{CT}[T] + d_C)[M_C].
\end{aligned}
$$

- Cell–cell adhesion:

$$
\begin{aligned}
\mathrm{d}[A]/\mathrm{d}t = \quad & s_A + d_{CA}([C_A] + [M_A]) - s_{CA}([C_O] + [M_O])[A] - d_A[A], \\
\mathrm{d}[C_A]/\mathrm{d}t = \quad & s_{CA}[C_O][A] - d_{CA}[C_A], \\
\mathrm{d}[M_A]/\mathrm{d}t = \quad & s_{CA}[M_O][A] - d_{CA}[M_A].
\end{aligned}
$$

• Induction of Wnt-target gene transcription:

$$\mathrm{d}[T]/\mathrm{d}t = s_T + d_{CT}([C_T] + [M_T]) - s_{CT}([C_F] + [M_F])[T] - d_T[T],$$

$$\mathrm{d}[C_{OT}]/\mathrm{d}t = s_{CT}[C_O][T] - d_{CT}[C_{OT}],$$

$$\mathrm{d}[C_{CT}]/\mathrm{d}t = s_{CT}[C_C][T] - d_{CT}[C_{CT}],$$

$$\mathrm{d}[M_{OT}]/\mathrm{d}t = s_{CT}[M_O][T] - d_{CT}[M_{OT}],$$

$$\mathrm{d}[M_{CT}]/\mathrm{d}t = s_{CT}[M_C][T] - d_{CT}[M_{CT}],$$

$$\mathrm{d}[Y]/\mathrm{d}t = \frac{s_Y([C_T] + [M_T])}{[C_T] + [M_T] + K_T} - d_Y[Y],$$

where the following substitutions have been made:

$$
\begin{aligned}
C_F &= C_C + C_O, \\
C_T &= C_{CT} + C_{OT}, \\
M_F &= M_C + M_O, \\
M_T &= M_{CT} + M_{OT}, \\
\widehat{d}_D &= D_D + \xi_D W, \\
\widehat{d}_{DX} &= D_{DX} + \xi_{DX} W, \\
\widehat{d}_X &= D_X + \xi_X W, \\
\widehat{p}_C &= p_C + \xi_C W.
\end{aligned}
$$

Mutations are handled as follows:

- $\sigma_\beta = 0 \iff$ wild-type β-catenin;

- $\sigma_\beta = 0.5 \iff$ single β-catenin mutation;

- $\sigma_D = 0 \iff$ wild-type APC;

- $\sigma_D = 0.5 \iff$ single APC mutation;

- $\sigma_D = 1 \iff$ double APC mutation.

The initial conditions for the Wnt pathway are given by the steady-state solutions, denoted by *:

$$[D^\star] = \frac{(1-\sigma_D)s_D s_X}{(1-\sigma_D)s_D \widehat{d}_D + \widehat{d}_X(\widehat{d}_D + \widehat{d}_{DX})},$$

$$[X^\star] = \frac{s_X(\widehat{d}_D + \widehat{d}_{DX})}{(1-\sigma_D)s_D \widehat{d}_D + \widehat{d}_X(\widehat{d}_D + \widehat{d}_{DX})},$$

$$[C_F^\star] = \frac{(s_C - d_C K_D - p_U[D^\star]) + \sqrt{(s_C - d_C K_D - p_U[D^\star])^2 + 4s_C d_C K_D}}{2d_C},$$

$$[C_O^\star] = \frac{s_C - \widehat{p}_c - \theta K_c + \sqrt{4s_C \theta K_c + (s_C - \widehat{p}_c - \theta K_c)^2}}{2\theta},$$

$$[C_c^\star] = [C_F^\star] - [C_o^\star],$$

$$[C_{OT}^\star] = \frac{s_{CT} s_T [C_O^\star]}{d_T d_{CT}},$$

$$[C_{CT}^\star] = \frac{s_{CT} s_T [C_C^\star]}{d_T d_{CT}},$$

$$[C_T^\star] = \frac{s_{CT} s_T [C_F^\star]}{d_T d_{CT}},$$

$$[A^\star] = \frac{s_A}{d_A},$$

$$[C_A^\star] = \frac{s_A s_{CA} [C_O^\star]}{d_A d_{CA}},$$

$$[T^\star] = \frac{s_T}{d_T},$$

$$[Y^\star] = \frac{s_{CT} s_T s_Y [C_F^\star]}{d_Y(s_{CT} s_T C_F^\star + d_{CT} d_T K_T)},$$

with $\theta = d_C + \frac{p_u[D^\star]}{[C_F^\star] + K_D}$.

s_A	=	20	nM/h	d_{CT}	=	750	h^{-1}	p_C	=	0	h^{-1}
s_{CA}	=	250	$(\mathrm{nM\ h})^{-1}$	d_D	=	5	h^{-1}	p_U	=	100	h^{-1}
s_C	=	25	nM/h	d_{DX}	=	5	h^{-1}	ξ_D	=	5	h^{-1}
s_{CT}	=	30	$(\mathrm{nM\ h})^{-1}$	d_T	=	0.4	h^{-1}	ξ_{DX}	=	5	h^{-1}
s_D	=	100	h^{-1}	d_U	=	50	h^{-1}	ξ_X	=	200	h^{-1}
s_T	=	10	nM/h	d_X	=	100	h^{-1}	d_C	=	1	h^{-1}
s_X	=	10	nM/h	d_Y	=	1	h^{-1}				
s_Y	=	10	h^{-1}	K_C	=	200	nM				
d_A	=	2	h^{-1}	K_D	=	5	nM				
d_{CA}	=	350	h^{-1}	K_T	=	50	nM				

Table B.2: Parameter values for van Leeuwen *et al.*'s (2007) Wnt signalling model.

References

S. Adhikary and M. Eilers. 2005. Transcriptional regulation and transformation by Myc proteins. *Nat. Rev. Mol. Cell Biol.*, **6**, 635–645. (doi:10.1038/nrm1703)

B.D. Aguda and Y. Tang. 1999. The kinetic origins of the restriction point in the mammalian cell cycle. *Cell Prolif.*, **32**, 321–335. (doi:10.1046/j.1365-2184.1999.3250321.x)

T. Akiyoshi, M. Nakamura, K. Koga, H. Nakashima, T. Yao, M. Tsuneyoshi, M. Tanaka and M. Katano. 2006. Gli 1, downregulated in colorectal cancers, inhibits proliferation of colon cancer cells involving Wnt signalling activation. *Gut*, **55**, 991. (doi:10.1136/gut.2005.080333)

B. Alberts, D. Bray, J. Lewis, M. Raff, K. Roberts and J.D. Watson. *Molecular Biology of the Cell*. New York: Garland Publishers, 4th edition, 2002.

C. Albuquerque, C. Breukel, R. van der Luijt, P. Fidalgo, P. Lage, F.J.M. Slors, C.N. Leitao, R. Fodde and R. Smits. 2002. The just-right signaling model: APC somatic mutations are selected based on a specific level of activation of the β-catenin signaling cascade. *Hum. Mol. Gen.*, **11**, 1549–1560. (doi:10.1093/hmg/11.13.1549)

K. Aoki and M.M. Taketo. 2007. Adenomatous polyposis coli (APC): a multi-functional tumor suppressor gene. *J. Cell Sci.*, **120**, 3327–3335. (doi:10.1242/jcs.03485)

D.J. Araten, D.W. Golde, R.H. Zhang, H.T. Thaler, L. Gargiulo, R. Notaro and L. Luzzatto. 2005. A Quantitative Measurement of the Human Somatic Mutation Rate. *Cancer Res.*, **65**, 8111–8117. (doi:10.1158/0008-5472.CAN-04-1198)

A. Asplund, Z. Guo, X. Hu, C. Wassberg and F. Ponten. 2001. Mosaic Pattern of Maternal and Paternal Keratinocyte Clones in Normal Human Epidermis Revealed by Analysis of X-Chromosome Inactivation. *J. Invest. Dermatology*, **117**, 128–131. (doi:10.1046/j.0022-202x.2001.01385.x)

J.D. Axelrod, J.R. Miller, J.M. Shulman, R.T. Moon and N. Perrimon. 1998. Differential recruitment of Dishevelled provides signaling specificity in the planar cell polarity and Wingless signaling pathways. *Gen. Dev.*, **12**, 2610–2622. (doi:10.1083/jcb.200211094)

A. Bafico, G. Lui, L. Goldin, V. Harris and S.A. Aaronson. 2004. An autocrine mechanism for constitutive Wnt pathway activation in human cancer cells. *Cancer Cell*, **6**, 497–506. (doi:10.1016/j.ccr.2004.09.032)

B. Basse, B.C. Baguley, E.S. Marshall, W.R. Joseph, B. van Brunt, G. Wake and D.J.N. Wall. 2003. A mathematical model for analysis of the cell cycle in cell lines derived from human tumors. *J. Math. Biol.*, **47**, 295–312. (doi:10.1007/s00285-003-0203-0)

E. Batlle, J.T. Henderson, H. Beghtel, M.M. van den Born, E. Sancho, G. Huls, J. Meeldijk, J. Robertson, M. van de Wetering, T. Pawson *et al.* 2002. Beta-catenin and TCF mediate cell positioning in the intestinal epithelium by controlling the expression of EphB/ephrinB. *Cell*, **111**, 251–63. (doi:10.1016/S0092-8674(02)01015-2)

J. Behrens, B.A. Jerchow, M. Wurtele, J. Grimm, C. Asbrand, R. Wirtz, M. Kuhl, D. Wedlich and W. Birchmeier. 1998. Functional Interaction of an Axin Homolog, Conductin, with β-Catenin, APC, and GSK3β. *Science*, **280**, 596–599. (doi:10.1126/science.280.5363.596)

J. Behrens, J.P. vonKries, M. Kuhl, L. Bruhn, D. Wedlich, R. Grosschedl and W. Birchmeier. 1996. Functional interaction of beta-catenin with the transcription factor LEF-1. *Nature*, **382**, 638–642. (doi:10.1038/382638a0)

E. Bell, I. Munoz-Sanjuan, C.R. Altmann, A. Vonica and A.H. Brivanlou. 2003. Cell fate specification and competence by Coco, a maternal BMP, TGFβ and Wnt inhibitor. *Development*, **130**, 1381–1389. (doi:10.1242/10.1242/dev.00344)

P. Bhanot, M. Brink, C.H. Samos, J.C. Hsieh, Y. Wang, J.P. Macke, D. Andrew, J. Nathans and R. Nusse. 1996. A new member of the frizzled family from Drosophila functions as a Wingless receptor. *Nature*, **382**, 225–230. (doi:10.1038/382225a0)

N.A. Bhowmick and E.G. Neilson. 2004. Stromal fibroblasts in cancer initiation and progression. *Nature*, **432**, 332–337. (doi:10.1038/nature03096)

M. Bienz. 2002. The subcellular destinations of APC proteins. *Nat Rev Mol Cell Biol*, **3**, 328–38. (doi:10.1038/nrm806)

M. Bienz and H. Clevers. 2000. Linking colorectal cancer to Wnt signalling. *Cell*, **103**, 311–320. (doi:10.1016/S0092-8674(00)00122-7)

B.M. Boman, J.Z. Fields, O. Bonham-Carter and O.A. Runquist. 2001. Computer Modeling Implicates Stem Cell Overproduction in Colon Cancer Initiation. *Cancer Research*, **61**, 8408–8411.

M. Bortlík, I. Vítková, M. Papežová, M. Kohoutová, A. Novotnỳ, S. Adamec, P. Chalupná and M. Lukáš. 2006. Deficiency of Adenomatous Polyposis Coli protein in sporadic colorectal adenomas and its associations with clinical phenotype and histology. *J Gastroenterol*, **12**, 3901–3905.

C. Bouchard, K. Thieke, A. Maier, R. Saffrich, J. Hanley-Hyde, W. Ansorge, S. Reed, P. Sicinski, J. Bartek

and M. Eilers. 1999. Direct induction of cyclin D2 by Myc contributes to cell cycle progression and sequestration of p27. *EMBO J.*, **18**, 5321–5333. (doi:10.1093/emboj/18.19.5321)

A.P. Bracken, M. Ciro, A. Cocito and K. Helin. 2004. E2F target genes: unraveling the biology. *Trends Biochem. Sci.*, **29**, 409–17. (doi:10.1016/j.tibs.2004.06.006)

V.H. Bustos, A. Ferrarese, A. Venerando, O. Marin, J.E. Allende and L.A. Pinna. 2006. The first armadillo repeat is involved in the recognition and regulation of beta-catenin phosphorylation by protein kinase ck1. *PNAS*, **103**, 19725–19730. (doi:10.1073/pnas.0609424104)

H.M. Byrne and M.A.J. Chaplain. 1995. Growth of nonnecrotic tumors in the presence and absence of inhibitors. *Math. Biosci.*, **130**, 151–181. (doi:10.1016/0025-5564(94)00117-3)

K.M. Cadigan and Y.I. Liu. 2006. Wnt signaling: complexity at the surface. *J. Cell Sci.*, **119**, 395–402. (doi:10.1242/jcs.02826)

H.J. Chen, C.M. Lin, C.S. Lin, R. Perez-Olle, C.L. Leung and R.K.H. Liem. 2006. The role of microtubule actin cross-linking factor 1(MACF 1) in the Wnt signaling pathway. *Genes and Development*, **20**, 1933. (doi:10.1101/gad.1411206)

W. Ching and R. Nusse. 2006. A dedicated Wnt secretion factor. *Cell*, **125**, 432–3. (doi:10.1016/j.cell.2006.04.018)

K.H. Cho, S. Baek and M.H. Sung. 2006. Wnt pathway mutations selected by optimal β-catenin signaling for tumorigenesis. *FEBS Lett.*, **580**, 3665–3670. (doi:10.1016/j.febslet.2006.05.053)

V.L. Church and P. Francis-West. 2002. Wnt signalling during limb development. *Int. J. Dev. Biol.*, **46**, 927–936.

F. Cong, L. Schweizer, M. Chamorro and H. Varmus. 2003. Requirement for a Nuclear Function of β-Catenin in Wnt Signaling. *Mol. Cell. Biol.*, **23**, 8462–8470. (doi:10.1128/MCB.23.23.8462-8470.2003)

F. Cong, L. Schweizer and H. Varmus. 2004. Wnt signals across the plasma membrane to activate the β-catenin pathway by forming oligomers containing its receptors, Frizzled and LRP. *Development*, **131**, 5103–5115. (doi:10.1242/10.1242/dev.01318)

A. Csikasz-Nagy, D. Battogtokh, K.C. Chen, B. Novak and J.J. Tyson. 2006. Analysis of a Generic Model of Eukaryotic Cell-Cycle Regulation. *Biophys. J.*, **90**, 4361. (doi:10.1529/biophysj.106.081240)

C.V. Dang, L.M.S. Resar, E. Emison, S. Kim, Q. Li, J.E. Prescott, D. Wonsey and K. Zeller. 1999. Function of the c-Myc Oncogenic Transcription Factor. *Exp. Cell Res.*, **253**, 63–77. (doi:10.1006/excr.1999.4686)

R. DasGupta, A. Kaykas, R.T. Moon and N. Perrimon. 2005. Functional genomic analysis of the Wnt-wingless signaling pathway. *Science*, **308**, 826–833. (doi:10.1126/science.1109374)

G. Davidson, W. Wu, J. Shen, J. Bilic, U. Fenger, P. Stannek, A. Glinka and C. Niehrs. 2005. Casein kinase 1 couples Wnt receptor activation to cytoplasmic signal transduction. *Nature*, **438**, 867–72. (doi:10.1038/nature04170)

L.A. DeRose and D. Padua. 1999. Techniques for the translation of MATLAB programs into Fortran 90. *ACM Transactions on Programming Languages and Systems (TOPLAS)*, **21**, 3499–3511.

J.A. Diehl, M. Cheng, M.F. Roussel and C.J. Sherr. 1998. Glycogen synthase kinase-3β regulates cyclin D1 proteolysis and subcellular localization. *Gen. Dev.*, **12**, 3499–3511.

A. d'Onofrio and I.P.M. Tomlinson. 2007. A nonlinear mathematical model of cell turnover, differentiation and tumorigenesis in the intestinal crypt. *J. Theor. Biol.*, **244**, 367–374. (doi:10.1016/j.jtbi.2006.08.022)

M. Dorie, R. Kallman and M. Coyne. 1982. Migration and internalization of cells and polystyrene microspheres in tumor cell spheroids. *Exp. Cell Res.*, **141**, 201–209. (doi:10.1016/0014-4827(82)90082-9)

M. Dorie, R. Kallman, D. Rapacchietta, D. van Antwerp and Y. Huang. 1986. Effect of cytochalasin b, nocodazole and irradiation on migration and internalization of cells and microspheres in tumor cell spheroids. *Exp. Cell Res.*, **166**, 370–378. (doi:10.1016/0014-4827(86)90483-0)

G.P. Dotto. 2000. p21 (WAF1/Cip1): more than a break to the cell cycle? *Biochim Biophys Acta*, **1471**, M43–56. (doi:10.1016/S0304-419X(00)00019-6)

D. Drasdo and S. Hoehme. 2003. Individual-based approaches to birth and death in avascular tumors. *Math. Comp. Modelling*, **37**, 1163–1175. (doi:10.1016/S0895-7177(03)00128-6)

D. Drasdo and M. Loeffler. 2001. Individual-based models to growth and folding in one-layered tissues: intestinal crypts and early development. *Nonlinear Anal.*, **47**, 245–256. (doi:10.1016/S0362-546X(01)00173-0)

C.A. Eisenberg and L.M. Eisenberg. 1999. WNT 11 promotes cardiac tissue formation of early mesoderm. *Developmental Dynamics*, **216**, 45–58. (doi:10.1002/(SICI)1097-0177(199909)216:1¡45::AID-DVDY7¿3.0.CO;2-L)

A. Eleftheriou, M. Yoshida and B.R. Henderson. 2001. Nuclear Export of Human β-Catenin Can Occur Independent of CRM1 and the Adenomatous Polyposis Coli Tumor Suppressor. *J. Biol. Chem.*, **276**, 25883–25888. (doi:10.1074/jbc.M102656200)

S. Etienne-Manneville, A. Hall, F.Q. Zhou, J. Zhou, S. Dedhar, Y.H. Wu, W.D. Snider, G.G. Gundersen, E.R. Gomes, Y. Wen *et al.* 2003. Cdc42 regulates GSK-3 beta and adenomatous. *Nature*, **421**, 753–756.

M.C. Faux, J.L. Ross, C. Meeker, T. Johns, H. Ji, R.J. Simpson, M.J. Layton and A.W. Burgess. 2004. Restoration of full-length adenomatous polyposis coli (APC) protein in a colon cancer cell line enhances cell adhesion. *J. Cell Sci.*, **117**, 427–439. (doi:10.1242/jcs.00862)

E.R. Fearon and K.M. Cadigan. 2005. Wnt Signaling Glows with RNAi. *Science*, **308**, 801–803. (doi:10.1126/science.1112622)

E.R. Fearon and B. Vogelstein. 1990. A genetic model for colorectal tumorigenesis. *Cell*, **61**, 759–67. (doi:10.1016/0092-8674(90)90186-I)

R. Fodde and T. Brabletz. 2007. Wnt/β-catenin signaling in cancer stemness and malignant behavior. *Curr. Opin. Cell Biol.*, **19**, 150–158. (doi:10.1016/j.ceb.2007.02.007)

R. Fodde, S. Greaves, U. Tepass, D.A. Calderwood, M.H. Ginsberg and H. McNeill. 2003. The multiple functions of tumour suppressors: it's all in APC. *Nature Cell Biology*, **5**, 190–192. (doi:10.1038/ncb0303-190)

R. Fodde, R. Smits and H. Clevers. 2001. APC, signal transduction and genetic instability in colorectal cancer. *Nature Rev. Can.*, **1**, 55–67. (doi:10.1038/35094067)

E. Galmozzi, F. Facchetti and CA La Porta. 2006. Cancer stem cells and therapeutic perspectives. *Curr. Med. Chem.*, **13**, 603–607. (doi:10.2174/092986706776055661)

A.L. Gartel and S.K. Radhakrishnan. 2005. Lost in Transcription: p21 Repression, Mechanisms, and Consequences. *Cancer Research*, **65**, 3980–3985. (doi:10.1158/0008-5472.CAN-04-3995)

C. Gaspar and R. Fodde. 2004. Wnt signalling/APC dosage effects in tumorigenesis and stem cell differentiation. *Int. J. Dev. Biol.*, **48**, 377–386. (doi:10.1387/ijdb.041807cg)

N. Gavert and A. Ben-Zeév. 2007. β-catenin signaling in biological control and cancer. *J. Cellu. Biochem.*, **in press**. (doi:10.1002/jcb.21505)

A. Gemin, S. Sweet, T.J. Preston and G. Singh. 2005. Regulation of the cell cycle in response to inhibition of mitochondrial generated energy. *Biochem. Biophys. Res. Comm.*, **332**, 1122–1132. (doi:10.1016/j.bbrc.2005.05.061)

A. Gerisch and M.A.J. Chaplain. 2008. Mathematical modelling of cancer cell invasion of tissue: local and non-local models and the effect of adhesion. *Journal of Theoretical Biology*, **250**, 684–704. (doi:10.1016/j.jtbi.2007.10.026)

R.H. Giles, J.H. van Ea and H. Clevers. 2003. Caught up in a Wnt storm: Wnt signalling in cancer. *BBA*, **1653**, 1–24. (doi:10.1016/S0304-419X(03)00005-2)

I. Glauche, M. Cross, M. Loeffler and I. Roeder. 2007. Lineage Specification of Hematopoietic Stem Cells: Mathematical Modeling and Biological Implications. *Stem Cells*, **25**, 1791. (doi:10.1634/stemcells.2007-0025)

J.A. Glazier and F. Graner. 1993. Simulation of the differential adhesion driven rearrangement of biological cells. *Phys. Rev. E*, **47**, 2128–2154. (doi:10.1103/PhysRevE.47.2128)

C. Grandori, S.M. Cowley, L.P. James and R.N. Eisenman. 2000. The Myc/Max/Mad network and the transcriptional control of cell behavior. *Annu. Rev. Cell Dev. Biol.*, **16**, 653–99. (doi:10.1146/annurev.cellbio.16.1.653)

F. Graner and J.A. Glazier. 1992. Simulation of biological cell sorting using a two-dimensional extended potts model. *Phys. Rev. Lett.*, **69**, 2013–2016. (doi:10.1103/PhysRevLett.69.2013)

L.C. Greaves, S.L. Preston, P.J. Tadrous, R.W. Taylor, M.J. Barron, D. Oukrif, S.J. Leedham, M. Deheragoda, P. Sasieni, M.R. Novelli *et al.* 2006. Mitochondrial DNA mutations are established in human colonic stem cells, and mutated clones expand by crypt fission. *PNAS*, **103**, 714–719. (doi:10.1073/pnas.0505903103)

H.P. Greenspan. 1972. Models for the growth of a solid tumor by diffusion. *Stud. Appl. Math.*, **51**, 317–340.

A. Gregorieff, D. Pinto, H. Begthel, O. Destree, M. KIELMAN and H. CLEVERS. 2005. Expression pattern of Wnt signaling components in the adult intestine. *Gastroenterology*, **129**, 626–38.

M. Gyllenberg and G.F. Webb. 1990. A nonlinear structured population model of tumor growth with quiescence. *J. Math. Biol.*, **28**, 671–694. (doi:10.1007/BF00160231)

M.V. Hadjihannas, M. Bruckner, B. Jerchow, W. Birchmeier, W. Dietmaier and J. Behrens. 2006. Aberrant Wnt/beta-catenin signaling can induce chromosomal instability in colon cancer. *PNAS*, **103**, 10747. (doi:10.1073/pnas.0604206103)

A.C. Hall, F.R. Lucas and P.C. Salinas. 2000. Axonal remodeling and synaptic differentiation in the cerebellum is regulated by WNT-7a signaling. *Cell*, **100**, 525–535. (doi:10.1016/S0092-8674(00)80689-3)

F. Hamada and M. Bienz. 2004. The APC tumor suppressor binds to C-terminal binding protein to divert nuclear β-catenin from TCF. *Dev. Cell*, **7**, 677–685. (doi:10.1016/j.devcel.2004.08.022)

E.K.-H. Han, S.-C. Ng, N. Arber, M. Begemann and I.B. Weinstein. 1999. Roles of cyclin D1 and related genes in growth inhibition, senescence and apoptosis. *Apoptosis*, **4**, 213–219. (doi:10.1023/A:1009618824145)

C.A. Hanson and J.R. Miller. 2005. Non-traditional roles for the Adenomatous Polyposis Coli (APC) tumor suppressor protein. *Gene*, **361**, 1–12. (doi:10.1016/j.gene.2005.07.024)

T.J. Harris and M. Peifer. 2005. Decisions, decisions: beta-catenin chooses between adhesion and transcription. *Trends Cell Biol.*, **15**, 234–7. (doi:10.1016/j.tcb.2005.03.002)

T. He *et al.* 1998. Identification of c-MYC as a Target of the APC Pathway. *Science*, **281**, 1509–1512. (doi:10.1126/science.281.5382.1509)

X. He, M. Semenov, K. Tamai and X. Zeng. 2004. LDL receptor-related proteins 5 and 6 in Wnt/β-catenin signaling: Arrows point the way. *Development*, **131**, 1663–1677. (doi:10.1242/10.1242/dev.01117)

B.R. Henderson. 2000. Nuclear-cytoplasmic shuttling of APC regulates β-catenin subcellular localization and turnover. *Nat. Cell Biol.*, **2**, 653–660. (doi:10.1038/35023605)

H. Hermeking, C. Rago, M. Schuhmacher, Q. Li, J.F. Barrett, A.J. Obaya, B.C. O'Connell, M.K. Mateyak, W. Tam, F. Kohlhuber *et al.* Identification of CDK4 as a target of c-MYC, 2000. (doi:10.1073/pnas.050586197).

L. Hinck, W.J. Nelson and J. Papkoff. 1994. Wnt-1 modulates cell-cell adhesion in mammalian cells by stabilizing β-catenin binding to the cell adhesion protein cadherin. *J. Cell Biol.*, **124**, 729–741. (doi:10.1083/jcb.124.5.729)

S.L. Holmen, S.A. Robertson, C.R. Zylstra and B.O. Williams. 2005. Wnt-independent activation of beta-catenin mediated by a Dkk1-Fz5 fusion protein. *Biochem. Biophys. Res. Comm.*, **328**, 533–9. (doi:10.1016/j.bbrc.2005.01.009)

J.C. Hsieh, L. Kodjabachian, M.L. Rebbert, A. Rattner, P.M. Smallwood, C.H. Samos, R. Nusse, I.B. Dawid and J. Nathans. 1999. A new secreted protein that binds to Wnt proteins and inhibits their activities. *Nature*, **398**, 431–436. (doi:10.1038/18899)

J. Hulit, C.G. Wang, Z.P. Li, C. Albanese, M. Rao, D. Di Vizio, S. Shah, S.W. Byers, R. Mahmood, L.H. Augenlicht, R. Russell and R.G. Pestell. 2004. Cyclin D1 genetic heterozygosity regulates colonic epithelial cell differentiation and tumor number in Apc(min) mice. *Mol. Cell. Biol.*, **24**, 7598–7611. (doi:10.1128/MCB.24.17.7598-7611.2004)

C. Hutchinson and D.M. Glover, editors. *Cell Cycle Control*. Frontiers in Molecular Biology. Oxford University Press, Oxford, 1995.

M. Ilyas. 2005. Wnt signalling and the mechanistic basis of tumour development. *J. Pathol.*, **205**, 130–144. (doi:10.1002/path.1692)

K. Inoki, H. Ouyang, T. Zhu, C. Lindvall, Y. Wang, X. Zhang, Q. Yang, C. Bennett, Y. Harada, K. Stankunas *et al.* 2006. TSC2 Integrates Wnt and Energy Signals via a Coordinated Phosphorylation by AMPK and GSK3 to Regulate Cell Growth. *Cell*, **126**, 955–968. (doi:10.1016/j.cell.2006.06.055)

T. Ishitani, S. Kishida, J. Hyodo-Miura, N. Ueno, J. Yasuda, M. Waterman, H. Shibuya, R.T. Moon, J. Ninomiya-Tsuji and K. Matsumoto. 2003. The TAK1-NLK Mitogen-Activated Protein Kinase Cascade Functions in the Wnt-5a/Ca2+ Pathway To Antagonize Wnt/β-Catenin Signaling. *Mol. Cell. Biol.*, **23**, 131–139. (doi:10.1128/MCB.23.1.131-139.2003)

I.A. Ivanova, S.J.A. D'Souza and L. Dagnino. 2005. Signalling In The Epidermis: The E2f Cell Cycle Regulatory Pathway In Epidermal Morphogenesis, Regeneration And Transformation. *Int. J. Biol. Sci.*, **1**, 87–95.

T.L. Jackson and H.M. Byrne. 2000. A mathematical model to study the effects of drug resistance and vas-

culature on the response of solid tumors to chemotherapy. *Math. Biosci.*, **164**, 17–38. (doi:10.1016/S0025-5564(99)00062-0)

E. Jho, T. Zhang, C. Domon, C. Joo, J. Freund and F. Costantini. 2002. Wnt/β-Catenin/Tcf Signaling Induces the Transcription of Axin2, a Negative Regulator of the Signaling Pathway. *Mol. Cell. Biol.*, **22**, 1172–1183. (doi:10.1128/MCB.22.4.11721183)

M.D. Johnston, C.M. Edwards, W.F. Bodmer, P.K. Maini and S.J. Chapman. 2007. Mathematical modeling of cell population dynamics in the colonic crypt and in colorectal cancer. *PNAS*, **104**, 4008. (doi:10.1073/pnas.0611179104)

S.E. Jones and C. Jomary. 2002. Secreted Frizzled-related proteins: searching for relationships and patterns. *BioEssays*, **24**, 811–820. (doi:10.1002/bies.10136)

K.B. Kaplan, A.A. Burds, J.R. Swedlow, S.S. Bekir, P.K. Sorger and I.S. Näthke. 2001. A role for the Adenomatous Polyposis Coli protein in chromosome segregation. *Nature Cell Biol.*, **3**, 429–432. (doi:10.1038/35070123)

Y. Kawasaki, R. Sato and T. Akiyama. 2003. Mutated APC and Asef are involved in the migration of colorectal tumour cells. *Nature Cell Biol.*, **5**, 1062–1070. (doi:10.1038/ncb937)

A. Kikuchi, S. Kishida, H. Yamamoto, Y.K. Choi, T.K. Kim, C.J. Kim, J.S. Lee, S.Y. Oh, H.S. Joo, D.N. Foster *et al.* 2006. Regulation of Wnt signaling by protein-protein interaction and post-translational modifications. *Exp. Mol. Med.*, **38**, 1–10.

A. Kikuchi and H. Yamamoto. 2008. Tumor formation due to abnormalities in the β-catenin-independent pathway of Wnt signaling. *Cancer Sci.*, **99**, 202–208. (doi:10.1111/j.1349-7006.2007.00675.x)

D. Kim, O. Rath, W. Kolch and K.H. Cho. 2007. A hidden oncogenic positive feedback loop caused by crosstalk between Wnt and ERK Pathways. *Oncogene*, **26**, 4571–4579. (doi:101038/sj.onc.1210230)

K. Kim, K.M. Pang, M. Evans and E.D. Hay. 2000. Overexpression of beta-Catenin Induces Apoptosis Independent of Its Transactivation Function with LEF-1 or the Involvement of Major G1 Cell Cycle Regulators. *Mol. Biol. Cell*, **11**, 3509–3523.

K.W. Kinzler, M.C. Nilbert, B. Vogelstein, T.M. Bryan, D.B. Levy, K.J. Smith, A.C. Preisinger, P. Hedge and A. Markham. 1991. Identification of a gene located at chromosome 5q21 that is mutated in colorectal cancers. *Science*, **251**, 1366–1370. (doi:10.1126/science.1848370)

MA Kirkland, PJ Quesenberry and I. Roeder. 2006. Discrete stem cells: subsets or a continuum? *Blood*, **107**, 2311–6.

M. Kishida, S. Hino, T. Michiue, H. Yamamoto, S. Kishida, A. Fukui, M. Asashima and A. Kikuchi. 2001. Synergistic Activation of the Wnt Signaling Pathway by Dvl and Casein Kinase Iε. *J. Biol. Chem.*, **276**, 33147–33155. (doi:10.1074/jbc.M103555200)

A.A. Kitazono, J.N. Fitz Gerald and S.J. Kron. 2005. Cell Cycle: Regulation by Cyclins. *Encyclopaedia of Life Sciences*. URL http://www.els.net/. John Wiley & Sons, Ltd: Chichester. (doi:10.1038/npg.els.0004024)

A.G. Knudson. 1971. Mutation and Cancer: Statistical Study of Retinoblastoma. *PNAS*, **68**, 820–823. (doi:10.1073/pnas.68.4.820)

M. Kobayashi, S. Kishida, A. Fukui, T. Michiue, Y. Miyamoto, T. Okamoto, Y. Yoneda, M. Asashima and A. Kikuchi. 2002. Nuclear localization of Duplin, a β-catenin-binding protein, is essential for its inhibitory activity on the wnt signaling pathway. *J. Bio. Chem.*, **277**, 5816–5822. (doi:10.1074/jbc.M108433200)

K.W. Kohn. 1999. Molecular Interaction Map of the Mammalian Cell Cycle Control and DNA Repair Systems. *Mol. Biol. Cell*, **10**, 2703–2734.

N.L. Komarova and P. Cheng. 2006. Epithelial tissue architecture protects against cancer. *Math Biosci*, **200**, 90–117. (doi:10.1016/j.mbs.2005.12.001)

N.L. Komarova and L. Wang. 2004. Initiation of colorectal cancer: where do the two hits hit? *Cell Cycle*, **3**, 1558–65.

K. Kozar and P. Sicinski. 2005. Cell cycle progression without cyclin D-CDK4 and cyclin D-CDK6 complexes. *Cell Cycle*, **4**, 388–391.

E. Krieghoff, J. Behrens and B. Mayr. 2006. Nucleo-cytoplasmic distribution of β-catenin is regulated by retention. *J. Cell Sci.*, **119**, 1453. (doi:10.1242/jcs.02864)

R. Kruger and R. Heinrich. 2004. Model reduction and analysis of robustness for the Wnt/β-catenin signal transduction pathway. *Gen. Inf.*, **15**, 138–148.

F. Kuphal and J. Behrens. 2006. E-cadherin modulates Wnt-dependent transcription in colorectal cancer cells but does not alter Wnt-independent gene expression in fibroblasts. *Exp. Cell. Res.*, **312**, 457–67.

LI Larsson. 2006. Distribution of E-cadherin and beta-catenin in relation to cell maturation and cell extrusion in rat and mouse small intestines. *Histochem Cell Biol.* (doi:10.1007/s00418-006-0193-2)

E. Lee, A. Salic, R. Kruger, R. Heinrich and M.W. Kirschner. 2003. The roles of APC and Axin derived from experimental and theoretical analysis of the Wnt pathway. *PLoS Biol.*, **1**, 116–132. (doi:10.1371/journal.pbio.0000010)

S. Leedham and N. Wright. 2007. Expansion of a mutated clone - from stem cell to cancer. *J. Clin. Pathol.* (doi:doi:10.1136/jcp.2006.044610)

S. Legewie, N. Blüthgen, R. Schäfer and H. Herzel. 2005. Ultrasensitization: Switch-Like Regulation of Cellular Signaling by Transcriptional Induction. *PLoS Comput Biol*, **1**. (doi:10.1371/journal.pcbi.0010054)

J.Y. Leung, F.T. Kolligs, R. Wu, Y. Zhai, R. Kuick, S. Hanash, K.R. Cho and E.R. Fearon. 2002. Activation

of AXIN2 Expression by β-Catenin-T Cell Factor, a feedback repressor pathway regulating Wnt signalling. *J. Biol. Chem.*, **277**, 21657–21665. (doi:10.1074/jbc.M200139200)

J. Liu, J. Stevens, C.A. Rote, H.J. Yost, Y. Hu, K.L. Neufeld, R.L. White and N. Matsunami. 2001. Siah-1 mediates a novel-catenin degradation pathway linking p53 to the adenomatous polyposis coli protein. *Mol. Cell*, **7**, 927–936. (doi:10.1016/S1097-2765(01)00241-6)

J. Liu, Y. Xing, T.R. Hinds, J. Zheng and W. Xu. 2006a. The Third 20 Amino Acid Repeat Is the Tightest Binding Site of APC for beta-Catenin. *J Mol Biol*, **360**, 133–144. (doi:10.1016/j.jmb.2006.04.064)

L. Liu, X. Guo, J.N. Rao, T. Zou, B.S. Marasa, J. Chen, J. Greenspon, R.A. Casero Jr and J.Y. Wang. 2006b. Polyamine-modulated c-Myc expression in normal intestinal epithelial cells regulates p21Cip1 transcription through a proximal promoter region. *Biochem. J.*, **398**, 257–267. (doi:10.1042/BJ20060217)

W. Liu, X. Dong, M. Mai, RS Seelan, K. Taniguchi, K.K. Krishnadath, K.C. Halling, J.M. Cunningham, L.A. Boardman and C. Qian. 2000. Mutations in AXIN2 cause colorectal cancer with defective mismatch repair by activating beta-catenin/TCF signalling. *Nat Genet*, **26**, 146–7. (doi:10.1038/79859)

M. Loeffler, T. Bratke, U. Paulus, YQ Li and CS Potten. 1997. Clonality and life cycles of intestinal crypts explained by a state dependent stochastic model of epithelial stem cell organization. *J Theor Biol*, **186**, 41–54. (doi:10.1006/jtbi.1996.0340)

M. Loeffler, CS Potten, U. Paulus, J. Glatzer and S. Chwalinski. 1988. Intestinal crypt proliferation. II. Computer modelling of mitotic index data provides further evidence for lateral and vertical cell migration in the absence of mitotic activity. *Cell Tissue Kinet*, **21**, 247–58.

M. Loeffler, R. Stein, HE Wichmann, CS Potten, P. Kaur and S. Chwalinski. 1986. Intestinal cell proliferation. I. A comprehensive model of steady-state proliferation in the crypt. *Cell Tissue Kinet*, **19**, 627–45.

C.Y. Logan and R. Nusse. 2004. The Wnt signaling pathway in development and disease. *Annu. Rev. Cell Dev. Biol.*, **20**, 781–810. (doi:10.1146/annurev.cellbio.20.010403.113126)

M. Lüchtenborg, M.P. Weijenberg, G.M.J.M. Roemen, A.P. de Bruïne, P.A. van den Brandt, M.H.F.M. Lentjes, M. Brink, M. van Engeland, R.A. Goldbohm and A.F.P.M. de Goeij. 2004. APC mutations in sporadic colorectal carcinomas from The Netherlands Cohort Study. *Carcinogenesis*, **27**, 1219–1226. (doi:10.1093/carcin/bgh117)

A. Lugli, I. Zlobec, P. Minoo, K. Baker, L. Tornillo, L. Terracciano and J.R. Jass. 2007. Prognostic significance of the wnt signalling pathway molecules APC, β-catenin and E-cadherin in colorectal cancer – a tissue microarray-based analysis. *Histopathology*, **50**, 453464. (doi:10.1111/j.1365-2559.2007.02620.x)

B. Lustig, B. Jerchow, M. Sachs, S. Weiler, T. Pietsch, U. Karsten, M. van de Wetering, H. Clevers, P.M. Schlag, W. Birchmeier *et al.* 2002. Negative Feedback Loop of Wnt Signaling through Upregu-

lation of Conductin/Axin2 in Colorectal and Liver Tumors. *Molecular and Cellular Biology*, **22**, 1184. (doi:10.1128/MCB.22.4.1184-1193.2002)

H.H. Luu, R. Zhang, R.C. Haydon, E. Rayburn, Q. Kang, W. Si, J.K. Park, H. Wang, Y. Peng, W. Jiang *et al.* 2004. Wnt/beta-catenin signaling pathway as a novel cancer drug target. *Curr Cancer Drug Targets*, **4**, 653–671.

H.T. Lynch and A. de la Chapelle. 2003. Hereditary Colorectal Cancer. *N. Engl. J. Med.*, **348**, 919–932. (doi:10.1056/NEJMra012242)

D.G. Mallet and L.G. De Pillis. 2006. A cellular automata model of tumor–immune system interactions. *J. Theor. Biol.*, **239**, 334–350. (doi:10.1016/j.jtbi.2005.08.002)

J. Mao, J. Wang, B. Liu, W. Pan, G.H. Farr III, C. Flynn, H. Yuan, S. Takada, D. Kimelman, L. Li *et al.* 2001. Low-density lipoprotein receptor-related protein-5 binds to Axin and regulates the canonical Wnt signaling pathway. *Mol Cell*, **7**, 801–9. (doi:10.1016/S1097-2765(01)00224-6)

E. Marshman, C. Booth, C.S. Potten *et al.* 2002. The intestinal epithelial stem cell. *BioEssays*, **24**, 91–98. (doi:10.1002/bies.10028)

SI Matsuzawa and J.C. Reed. 2001. Siah-1, SIP, and Ebi collaborate in a novel pathway for beta-catenin degradation linked to p53 responses. *Mol. Cell*, **7**, 915–926. (doi:10.1016/S1097-2765(01)00242-8)

P. Maye, J. Zheng, L. Li and D. Wu. 2004. Multiple Mechanisms for Wnt11-mediated Repression of the Canonical Wnt Signaling Pathway. *J. Biol. Chem.*, **279**, 24659–24665. (doi:10.1074/jbc.M311724200)

S.A. McDonald, S.L. Preston, L.C. Greaves, S.J. Leedham, M.A. Lovell, J.A. Jankowski, D.M. Turnbull and N.A. Wright. 2006. Clonal Expansion in the Human Gut: Mitochondrial DNA Mutations Show Us the Way. *Cell Cycle*, **5**, 808–811.

F.A. Meineke, C.S. Potten and M. Loeffler. 2001. Cell migration and organization in the intestinal crypt using a lattice-free model. *Cell Prolif.*, **34**, 253–266. (doi:10.1046/j.0960-7722.2001.00216.x)

F. Michor, Y. Iwasa, C. Lengauer and M.A. Nowak. 2005. Dynamics of colorectal cancer. *Semin. Cancer Biol.*, **15**, 484–93. (doi:10.1016/j.semcancer.2005.06.005)

P.L. Miliani de Marval, E. Macias, R. Rounbehler, P. Sicinski, H. Kiyokawa, D.G. Johnson, C.J. Conti and M.L. Rodriguez-Puebla. 2004. Lack of Cyclin-Dependent Kinase 4 Inhibits c-myc Tumorigenic Activities in Epithelial Tissues. *Mol. Cell. Biol.*, **24**, 7538–7547. (doi:10.1128/MCB.24.17.7538-7547.2004)

L. Mirabelli-Primdahl, R. Gryfe, H. Kim, A. Millar, C. Luceri, D. Dale, E. Holowaty, B. Bapat, S. Gallinger and M. Redston. 1999. β-Catenin Mutations Are Specific for Colorectal Carcinomas with Microsatellite Instability but Occur in Endometrial Carcinomas Irrespective of Mutator Pathway 1. *Cancer Res.*, **59**, 3346–3351.

M.M. Mogensen, J.B. Tucker, J.B. Mackie, A.R. Prescott and I.S. Näthke. 2002. The adenomatous polyposis coli protein unambiguously localizes to microtubule plus ends and is involved in establishing parallel arrays of microtubule bundles in highly polarized epithelial cells. *J. Cell Biol.*, **157**, 1041–1048. (doi:10.1083/jcb.200203001)

K.A. Moore and I.R. Lemischka. 2006. Stem Cells and Their Niches. *Science*, **311**, 1880–1885. (doi:10.1126/science.1110542)

P.J. Morin, A.B. Sparks, V. Korinek, N. Barker, H. Clevers, B. Vogelstein and K.W. Kinzler. 1997. Activation of beta-catenin-Tcf signaling in colon cancer by mutations in beta-catenin or APC. *Science*, **275**, 1752–3. (doi:10.1126/science.275.5307.1787)

M.J. Murphy, A. Wilson and A. Trumpp. 2005. More than just proliferation: Myc function in stem cells. *Trends Cell Biol*, **15**, 128–37. (doi:10.1016/j.tcb.2005.01.008)

H. Nagase and Y. Nakamura. 1993. Mutations of the *apc* (Adenomatous Polyposis Coli) gene. *Hum. Mutat.*, **2**, 425–434. (doi:10.1002/humu.1380020602)

T. Nakamura, K. Tsuchiya and M. Watanabe. 2007. Crosstalk between Wnt and Notch signaling in intestinal epithelial cell fate decision. *J. Gastroenterology*, **42**, 705–710. (doi:10.1007/s00535-007-2087-z)

I.S. Näthke. 2004. The Adenomatous Polyposis Coli protein: the Achilles heel of the gut epithelium. *Annu. Rev. Cell Dev. Biol.*, **20**, 337–366. (doi:10.1146/annurev.cellbio.20.012103.094541)

I.S. Näthke. 2005. Relationship between the role of the adenomatous polyposis coli protein in colon cancer and its contribution to cytoskeletal regulation. *Biochem. Soc. Trans*, **33**, 694–697. (doi:10.1042/BST0330694)

I.S. Näthke. 2006. Cytoskeleton out of the cupboard: colon cancer and cytoskeletal changes induced by loss of APC. *Nat. Rev. Cancer*, **66**, 967–974. (doi:10.1038/nrc2010)

W.J. Nelson and R. Nusse. 2004. Convergence of Wnt, β-catenin, and Cadherin pathways. *Science*, **303**, 1483–1487. (doi:10.1126/science.1094291)

D. Noble. 1960. Cardiac action and pacemaker potentials based on the Hodgkin-Huxley equations. *Nature*, **188**, 111. (doi:10.1038/188495b0)

D. Noble. 2007. From the Hodgkin-Huxley axon to the virtual heart. *The Journal of Physiology*, **580**, 15. (doi:10.1113/jphysiol.2006.119370)

B. Novak and J.J. Tyson. 2004. A model for restriction point control of the mammalian cell cycle. *J. Theor. Biol.*, **230**, 563–579. (doi:10.1016/j.jtbi.2004.04.039)

M.A. Nowak, F. Michor, N.L. Komarova and Y. Iwasa. 2004. Evolutionary dynamics of tumor suppressor gene inactivation. *PNAS*, **101**, 10635–10638. (doi:10.1073/pnas.0400747101)

R. Nusse. 2005. Cell biology: relays at the membrane. *Nature*, **438**, 747–9. (doi:10.1038/438747a)

R. Nusse. The Wnt Homepage. Website, 2007. URL http://www.stanford.edu/~rnusse/.

M.N. Obeyesekere, E.S. Knudsen, J.Y.J. Wang and S.O. Zimmerman. 1997. A mathematical model of the regulation of the G_1 phase of $Rb^{+/+}$ and $Rb^{-/-}$ mouse embryonic fibroblasts and an osteosarcoma cell line. *Cell Prolif.*, **30**, 171–194. (doi:10.1046/j.1365-2184.1997.00078.x)

M.N. Obeyesekere and S.O. Zimmerman. 1999. A model of cell cycle behaviour dominated by kinetics of a pathway stimulated by growth factors. *Bull. Math. Biol.*, **61**, 917–934. (doi:10.1006/bulm.1999.0118)

A. Okabe, B. Boots and K. Sughihara. *Spatial Tesselations: Concepts and Aplpications of Voronoi Diagrams.* John Wiley & Sons, Chichester, 2nd edition, 2000.

K.A. ODonnell, E.A. Wentzel, K.I. Zeller, C.V. Dang and J.T. Mendell. 2005. c-Myc-regulated microRNAs modulate E2F1 expression. *Nature*, **435**, 839–843. (doi:10.1038/nature03677)

J. Papkoff, B. Rubinfeld, B. Schryver and P. Polakis. 1996. Wnt-1 regulates free pools of catenins and stabilizes APC-catenin complexes. *Mol. Cell. Biol.*, **16**, 2128–2134.

G.A. Penman, L. Leung and I.S. Näthke. 2005. The adenomatous polyposis coli protein (APC) exists in two distinct soluble complexes with different functions. *J. Cell Sci.*, **118**, 4741–4750. (doi:10.1242/jcs.02589)

G.J. Pettet, C.P. Please, M.J. Tindall and D.L.S. McElwain. 2001. The migration of cells in multicell tumor spheroids. *Bull. Math. Biol.*, **63**, 231–257. (doi:10.1006/bulm.2000.0217)

S. Piccolo, E. Agius, L. Leyns, S. Bhattacharyya, H. Grunz, T. Bouwmeester and EM De Robertis. 1999. The head inducer Cerberus is a multifunctional antagonist of Nodal, BMP and Wnt signals. *Nature*, **397**, 707–10. (doi:10.1038/17820)

D. Pinto and H. Clevers. 2005. Wnt control of stem cells and differentiation in the intestinal epithelium. *Exp. Cell Res.*, **306**, 357–363. (doi:10.1016/j.yexcr.2005.02.022)

P. Polakis. 2000. Wnt signalling and cancer. *Genes and Dev.*, **14**, 1837–1854. (doi:10.1101/gad.14.15.1837)

E.M. Porter, C.L. Bevins, D. Ghosh and T. Ganz. 2002. The multifaceted Paneth cell. *Cellular and Molecular Life Sciences (CMLS)*, **59**, 156–170. (doi:10.1007/s00018-002-8412-z)

C.S. Potten, C. Booth and D.M. Pritchard. 1997. The intestinal epithelial stem cell: the mucosal governor. *Int. J. Exp. Path.*, **78**, 219–243. (doi:10.1046/j.1365-2613.1997.280362.x)

C.S. Potten and M. Loeffler. 1987. A comprehensive model of the crypts of the small intestine of the mouse provides insight into the mechanisms of cell migration and the proliferation hierarchy. *J Theor Biol*, **127**, 381–91. (doi:10.1016/S0022-5193(87)80136-4)

S.M. Powell, N. Zilz, Y. Beazer-Barclay, T.M. Bryan, S.R. Hamilton, S.N. Thibodeau, B. Vogelstein and K.W. Kinzler. 1992. APC mutations occur early during colorectal tumorigenesis. *Nature*, **359**, 235–237. (doi:10.1038/359235a0)

F. Radtke and H. Clevers. 2005. Self-Renewal and Cancer of the Gut: Two Sides of a Coin. *Science*, **307**, 1904–1909. (doi:10.1126/science.1104815)

T. Reya and H. Clevers. 2005. Wnt signalling in stem cells and cancer. *Nature*, **434**, 843–850. (doi:10.1038/nature03319)

R.A. Rimerman, A. Gellert-Randleman and J.A. Diehl. 2000. Wnt1 and MEK1 cooperate to promote Cyclin D1 accumulation and cellular transformation. *J. Biol. Chem.*, **275**, 14736–14742. (doi:10.1074/jbc.M910241199)

I. Roeder. 2006. Quantitative stem cell biology: computational studies in the hematopoietic system. *Current Opinion in Hematology*, **13**, 222.

M.H. Ross, G.I. Kaye and W. Pawlina. *Histology: A Text & Atlas.* Lippincott Williams & Wilkins, Philadelphia, 2003.

A.J. Rowan, H. Lamlum and M. Ilyas. 2000. APC mutations in sporadic colorectal tumors: a mutational 'hotspot' and interdependence of the 'two hits'. *PNAS*, **97**, 3352–3357. (doi:10.1073/pnas.97.7.3352)

B. Rubinfeld, B. Souza, I. Albert, O. Muller, S.H. Chamberlain, F.R. Masiarz, S. Munemitsu and P. Polakis. 1993. Association of the APC gene product with β-catenin. *Science*, **262**, 1731–1734. (doi:10.1126/science.8259518)

C. Sakanaka, J.B. Weiss and L.T. Williams. 1998. Bridging of β-catenin and glycogen synthase kinase-3β by Axin and inhibition of β-catenin-mediated transcription. *PNAS*, **95**, 3020–3023. (doi:10.1073/pnas.95.6.3020)

P. C. Salinas. 2007. Modulation of the microtubule cytoskeleton: a role for a divergent canonical Wnt pathway. *TRENDS Cell Biol.*, **17**, 333–342. (doi:10.1016/j.tcb.2007.07.003)

W.S. Samowitz, M.D. Powers, L.N. Spirio, F. Nollet, F. van Roy and M.L. Slattery. 1999. *β-catenin* mutations are more frequent in small colorectal adenomas than in larger adenomas and invasive carcinomas. *Cancer Res.*, **59**, 1442–1444.

E. Sancho, E. Batlle and H. Clevers. 2004. Signalling pathways in intestinal development and cancer. *Annu. Rev. Cell Dev. Biol.*, **20**, 695–723. (doi:10.1146/annurev.cellbio.20.010403.092805)

J.A. Sanders and P.A. Gruppuso. 2006. Coordinated regulation of c-Myc and Max in rat liver development. *Amer. J. Phys. - Gastro. Liver Phys.*, **290**, 145–155. (doi:10.1152/ajpgi.00545.2004)

O.J. Sansom, V.S. Meniel, V. Muncan, T.J. Phesse, J.A. Wilkins, K.R. Reed, J.K. Vass, D. Athineos, H. Clevers and A.R. Clarke. 2007. *Myc* deletion rescues Apc deficiency in the small intestine. *Nature*, **446**, 676–679. (doi:10.1038/nature05674)

O.J. Sansom, K.R. Reed, A.J. Hayes, H. Ireland, H. Brinkmann, I.P. Newton, E. Batlle, P. Simon-Assmann, H. Clevers, I.S. Nathke, A.R Clarke and D.J. Winton. 2004. Loss of Apc in vivo immedi-

ately perturbs Wnt signaling, differentiation, and migration. *Genes and Development*, **18**, 1385–1390. (doi:10.1101/gad.287404)

O.J. Sansom, K.R. Reed, M. van de Wetering, V. Muncan, D.J. Winton, H. Clevers and A.R. Clarke. 2005. Cyclin D1 is not an immediate target of β-catenin following APC loss in the intestine. *J. Biol. Chem.*, **280**, 28463–28467. (doi:10.1074/jbc.M500191200)

N. Savill and J.A. Sherratt. 2003. Control of epidermal stem cell clusters by Notch-mediated lateral induction. *Developmental Biology*, **258**, 141–153. (doi:10.1016/S0012-1606(03)00107-6)

J. Schneikert, A. Grohmann and J. Behrens. 2007. Truncated APC regulates the transcriptional activity of β-catenin in a cell cycle dependent manner. *Hum. Mol. Gen.*, **16**, 199–209. (doi:10.1093/hmg/ddl464)

T. Schwarz-Romond, C. Metcalfe and M. Bienz. 2007. Dynamic recruitment of axin by Dishevelled protein assemblies. *J. Cell Sci.*, **120**, 2402–2412. (doi:10.1242/jcs.002956)

J.H. Sellin, S. Umar, J. Xiao and A.P. Morris. 2001. Increased β-Catenin Expression and Nuclear Translocation Accompany Cellular Hyperproliferation in Vivo. *Cancer Research*, **61**, 2899–2906.

T. Senda, A. Iizuka-Kogo, T. Onouchi and A. Shimomura. 2007. Adenomatous polyposis coli (APC) plays multiple roles in the intestinal and colorectal epithelia. *J. Med. Mol. Morph.*, **40**, 68–81. (doi:10.1007/s00795-006-0352-5)

L.C. Sheldahl, D.C. Slusarski, P. Pandur, J.R. Miller, M. Kuhl and R.T. Moon. 2003. Dishevelled activates Ca2+ flux, PKC, and CamKII in vertebrate embryosL. C. Sheldahl's present address is Department of Cell and Developmental Biology, Oregon Health Sciences University, Portland, OR 97201. *J. Cell Biol.*, **161**, 769–777. (doi:10.1083/jcb.200211094)

C.J. Sherr and J.M. Roberts. 1999. CDK inhibitors: positive and negative regulators of G1-phase progression. *Genes & Dev.*, **13**, 1501–1512. (doi:10.1101/gad.13.12.1501)

J.R. Shewchuk. Triangle: Engineering a 2D Quality Mesh Generator and Delaunay Triangulator. In M.C. Lin and D. Manocha, editors, *Applied Computational Geometry: Towards Geometric Engineering*, volume 1148 of *Lecture Notes in Computer Science*, pages 203–222. Springer-Verlag, 1996.

I.M. Shih, T.L. Wang, G. Traverso, K. Romans, S.R. Hamilton, S. Ben-Sasson, K.W. Kinzler and B. Vogelstein. 2001. Top-down morphogenesis of colorectal tumors. *PNAS*, **98**, 2640–2645. (doi:10.1073/pnas.051629398)

M. Shtutman, J. Zhurinsky, I. Simcha, C. Albanese, M. DAmico, R. Pestell and A. Ben-Zeev. 1999. The cyclin D1 gene is a target of the β-catenin/LEF-1 pathway. *PNAS*, **96**, 5522–5527. (doi:10.1073/pnas.96.10.5522)

J. Sierra, T. Yoshida, C.A. Joazeiro and K.A. Jones. 2006. The APC tumor suppressor counteracts beta-catenin activation and H 3 K 4 methylation at Wnt target genes. *Genes & Dev.*, **20**, 586. (doi:10.1101/gad.1385806)

R. Städeli, R. Hoffmans and K. Basler. 2006. Transcription under the control of nuclear Arm/β-catenin. *Curr. Biol.*, **16**, R378–R385. (doi:10.1016/j.cub.2006.04.019)

T.S. Stappenbeck, M.H. Wong, J.R. Saam, I.U. Mysorekar and J.I. Gordon. 1998. Notes from some crypt watchers: regulation of renewal in the mouse intestinal epithelium. *Curr. Opin. Cell Biol.*, **10**, 702–709. (doi:10.1016/S0955-0674(98)80110-5)

D. Strutt. 2003. Frizzled signalling and cell polarisation in Drosophila and vertebrates. *Dev.*, **130**, 4501–4513. (doi:10.1242/10.1242/dev.00695)

J.P. Sunter, D.R. Appleton, M.S. De Rodriguez, N.A. Wright and A.J. Watson. 1979. A comparison of cell proliferation at different sites within the large bowel of the mouse. *J. Anat.*, **129**, 833–42.

M. Swat, A. Kel and H. Herzel. 2004. Bifurcation analysis of the regulatory modules of the mammalian G_1/S transition. *Bioinformatics*, **20**, 1506–1511. (doi:10.1093/bioinformatics/bth110)

K. Tago, T. Nakamura, M. Nishita, J. Hyodo, S. Nagai, Y. Murata, S. Adachi, S. Ohwada, Y. Morishita, H. Shibuya *et al.* 2000. Inhibition of Wnt signaling by ICAT, a novel β-catenin-interacting protein. *Gen. Dev.*, **14**, 1741–1749.

J. Taipale and P.A. Beachy. 2001. The Hedgehog and Wnt signalling pathways in cancer. *Nature*, **411**, 349–354. (doi:10.1038/35077219)

C.M. Takacs, J.R. Baird, E.G. Hughes, S.S. Kent, H. Benchabane, R. Paik and Y. Ahmed. 2008. Dual Positive and Negative Regulation of Wingless Signaling by Adenomatous Polyposis Coli. *Science*, **319**, 333–336. (doi:10.1126/science.1151232)

Y. Takahashi, J.B. Rayman and B.D. Dynlacht. 2000. Analysis of promoter binding by the E2F and pRB families in vivo: distinct E2F proteins mediate activation and repression. *Genes & Development*, **14**, 804–816. (doi:10.1101/gad.14.7.804)

K. Tamai, M. Semenov, Y. Kato, R. Spokony, C. Liu, Y. Katsuyama, F. Hess, JP Saint-Jeannet and X. He. 2000. LDL-receptor-related proteins in Wnt signal transduction. *Nature*, **407**, 530–535. (doi:10.1038/35035117)

R.W. Taylor, M.J. Barron, G.M. Borthwick, A. Gospel, P.F. Chinnery, D.C. Samuels, G.A. Taylor, S.M. Plusa, S.J. Needham, L.C. Greaves, T.B.L. Kirkwood and D.M. Turnbull. 2003. Mitochondrial DNA mutations in human colonic crypt stem cells. *J. Clin. Invest.*, **112**, 1351–1360. (doi:10.1172/JCI19435)

O. Tetsu and F. McCormick. 1999. β-catenin regulates expression of cyclin D1 in colon carcinoma cells. *Nature*, **398**, 422–426. (doi:10.1038/18884)

N.S. Tolwinski and E. Wieschaus. 2004. Rethinking WNT signaling. *Trends Genet.*, **20**, 177–81. (doi:10.1016/j.tig.2004.02.003)

I. Tomlinson and W. Bodmer. 1999. Selection, the mutation rate and cancer: Ensuring that the tail does not wag the dog. *Nature Medicine*, **5**, 11–12. (doi:10.1038/4687)

I.P.M. Tomlinson and W.F. Bodmer. 1995. Failure of Programmed Cell Death and Differentiation as Causes of Tumors: Some Simple Mathematical Models. *PNAS*, **92**, 11130–11134. (doi:10.1073/pnas.92.24.11130)

L. Topol, X. Jiang, H. Choi, L. Garrett-Beal, P.J. Carolan and Y. Yang. 2003. Wnt-5a inhibits the canonical Wnt pathway by promoting GSK-3independent β-catenin degradation. *J. Cell Biol.*, pages 899–908. (doi:10.1083/jcb.200303158)

F.M. Townsley, A. Cliffe and M. Bienz. 2004. Pygopus and Legless target Armadillo/β-catenin to the nucleus to enable its transcriptional co-activator function. *Nat. Cell Biol.*, **6**, 626–633. (doi:10.1038/ncb1141)

J.J. Tyson and B. Novak. 2001. Regulation of the eukaryotic cell cycle: Molecular antagonism, hysteresis and irreversible transitions. *J. Theor. Biol.*, **210**, 249–263. (doi:10.1006/jtbi.2001.2293)

F. Ulrich, M. Krieg, E.M. Schötz, V. Link, I. Castanon, V. Schnabel, A. Taubenberger, D. Mueller, P.H. Puech and C.P. Heisenberg. 2005. Wnt11 Functions in Gastrulation by Controlling Cell Cohesion through Rab5c and E-Cadherin. *Dev. Cell*, **9**, 555–564. (doi:10.1016/j.devcel.2005.08.011)

G.R. van den Brink and J.C.H. Hardwick. 2006. Hedgehog Wnteraction in colorectal cancer. *Gut*, **55**, 912. (doi:10.1136/gut.2005.085902)

I.M.M. van Leeuwen, H.M. Byrne, O.E. Jensen and J.R. King. 2006. Crypt dynamics and colorectal cancer: advances in mathematical modelling. *Cell Prolif.*, **39**, 157–181. (doi:10.1111/j.1365-2184.2006.00378.x)

I.M.M. van Leeuwen, H.M. Byrne, O.E. Jensen and J.R. King. 2007. Elucidating the interactions between the adhesive and transcriptional functions of β-catenin in normal and cancerous cells. *J. Theor. Biol.*, **247**, 77–102. (doi:10.1016/j.jtbi.2007.01.019)

M.T. Veeman, J.D. Axelrod and R.T. Moon. 2003. A second canon. Functions and mechanisms of beta-catenin-independent Wnt signaling. *Dev. Cell*, **5**, 367–377. (doi:10.1016/S1534-5807(03)00266-1)

H.L. Wang, J. Wang, S. Xiao, R. Haydon, D. Stobier, T. He, M. Bissonnette and J. Hart. 2002a. Elevated protein expression of Cyclin D1 and FRA-1 but decreased expression of c-Myc in human colorectal adenocarcinomas overexpressing β-catenin. *Int. J. Cancer*, **101**, 301–310. (doi:10.1002/ijc.10630)

T.L. Wang, C. Rago, N. Silliman, J. Ptak, S. Markowitz, J.K.V. Willson, G. Parmigiani, K.W. Kinzler, B. Vogelstein and V.E. Velculescu. 2002b. Prevalence of somatic alterations in the colorectal cancer cell genome. *PNAS*, **99**, 3076–3080. (doi:10.1073/pnas.261714699)

M. Wanzel, S. Herold and M. Eilers. 2003. Transcriptional repression by Myc. *TRENDS in Cell Biol.*, **13**, 146–150. (doi:10.1016/S0962-8924(03)00003-5)

H.S. Wasan, H.S. Park, K.C. Liu, N.K. Mandir, A. Winnett, P. Sasieni, W.F. Bodmer, R.A. Goodlad and N.A. Wright. 1998. APC in the regulation of intestinal crypt fission. *J. Pathol.*, **185**, 246–255.

C. Wawra, M. Kühl and H.A. Kestler. 2007. Extended analyses of the Wnt/β-catenin pathway: Robustness and oscillatory behaviour. *FEBS Letters*, **581**, 4043–4048. (doi:10.1016/j.febslet.2007.07.043)

M. Wehrli, ST Dougan, K. Caldwell, L. O'Keefe, S. Schwartz, D. Vaizel-Ohayon, E. Schejter, A. Tomlinson and S. DiNardo. 2000. arrow encodes an LDL-receptor-related protein essential for Wingless signalling. *Nature*, **407**, 527–30. (doi:10.1038/35035110)

G. Weidinger and R.T. Moon. 2003. When Wnts antagonize Wnts. *J. Cell Biol.*, **162**, 753–755. (doi:10.1083/jcb.200307181)

W.C. Weinberg and M.F. Denning. 2002. $P21^{WAF1}$ Control of Epithelial Cell Cycle and Cell Fate. *Crit. Rev. Oral Biol. Med.*, **13**, 453.

K. Willert and K.A. Jones. 2006. Wnt signaling: is the party in the nucleus? *Gen. Dev.*, **20**, 1394. (doi:10.1101/gad.1424006)

R. Winklbauer, A. Medina, RK Swain and H. Steinbeisser. 2001. Frizzled-7 signalling controls tissue separation during Xenopus gastrulation. *Nature*, **413**, 856–60. (doi:10.1038/35101621)

J. H. Xiao, C. Ghosn, C. Hinchman, C. Forbes, J. Wang, N. Snider, A. Cordrey, Y. Zhao and R.A.S. Chandraratna. 2003. Adenomatous polyposis coli (APC)-independent regulation of beta-catenin degradation via a retinoid X receptor-mediated pathway. *J. Bio. Chem.*, **278**, 29954–62. (doi:10.1074/jbc.M304761200)

Y. Xiong and Y. Kotake. 2006. No exit strategy? No problem: APC inhibits β-catenin inside the nucleus. *Gen. Dev.*, **20**, 637. (doi:10.1101/gad.1413206)

R.Y. Yang, W.J. Bie, A. Haegebarth and A.L. Tyner. 2006. Differential regulation of D-type cyclins in the mouse intestine. *Cell Cycle*, **5**, 180–183.

L. Zeng, F. Fagotto, T. Zhang, W. Hsu, T.J. Vasicek, W.L. Perry, J.J. Lee, S.M. Tilghman, B.M. Gumbiner and F. Costantini. 1997. The mouse Fused locus encodes Axin, an inhibitor of the Wnt signaling pathway that regulates embryonic axis formation. *Cell*, **90**, 181–192.

X. Zeng, H. Huang, K. Tamai, X. Zhang, Y. Harada, C. Yokota, K. Almeida, J. Wang, B. Doble, J. Woodgett, A. Wynshaw-Boris, J. Hsieh and X He. 2008. Initiation of Wnt signaling: control of Wnt coreceptor Lrp6 phosphorylation/activation via frizzled, dishevelled and axin functions. *Development*, **135**, 367–375. (doi:10.1242/dev.013540)

X. Zeng, K. Tamai, B. Doble, S. Li, H. Huang, R. Habas, H. Okamura, J. Woodgett and X. He. 2005. A dual-kinase mechanism for Wnt co-receptor phosphorylation and activation. *Nature*, **438**, 873–877. (doi:10.1038/nature04185)

F. Zhang, R.L. White and K.L. Neufeld. 2001. Cell Density and Phosphorylation Control the Subcellular Localization of Adenomatous Polyposis Coli Protein. *Mol. Cell. Biol.*, **21**, 8143–8156. (doi:10.1128/MCB.21.23.8143-8156.2001)

J. Zumbrunn, K. Kinoshita, A.A. Hyman and I.S. Näthke. 2001. Binding of the adenomatous polyposis coli protein to microtubules increases microtubule stability and is regulated by GSK3β phosphorylation. *Curr. Biol.*, **11**, 44–49. (doi:10.1016/S0960-9822(01)00002-1)